Durability and performance of South African recycled granulates in unbound (sub)base pavement layers

Thomas Aelen

Technische Universiteit Delft

TU Delft Delft University of Technology

UNIVERSITEIT STELLENBOSCH UNIVERSITY

Challenge the future

Durability and performance of South African recycled granulates in unbound (sub)base pavement layers

Thomas Aelen

in partial fulfillment of the requirements for the degree of

Master of Science

in Structural Engineering

at the Delft University of Technology,

to be defended publicly on Friday February 22, 2019 at 4:00 PM.

Student number:	1533746	
Thesis committee:	Prof.dr.ir. S.M.J.G. Erkens	TU Delft
	Prof.dr.ir. K.J. Jenkins	Stellenbosch University
	Dr.ir. C. van der Veen	TU Delft
	Ir. C.E. Rudman	Stellenbosch University
	Ir. L.J.M. Houben	TU Delft

ABSTRACT

Recycled granular materials such as Recycled Concrete Aggregate (RCA) and Recycled Crushed Masonry (RCM) are widely used in The Netherlands as base layers in asphalt pavements. The lack of natural resources and the growing amounts of demolition waste made that the Dutch industries in the early 1980s started to explore the possibilities to use construction debris in road construction. Recently, the application of recycled materials in pavement structures has also found traction in South Africa. Due to differences in pavement design, however, the mechanical and environmental exposure of these materials will be more severe than in the Netherlands. This results in different challenges with respect to (long term) performance and material durability. Understanding the potential durability issues and the way durability affects pavement performance is crucial to successfully implement these materials in South African pavements.

This research, conducted at Stellenbosch University, South Africa, involves laboratory testing to investigate the performance and durability aspects of recycled aggregates. By means of triaxial testing before and after durability simulation, it is aimed to address the extent of potential material breakdown and the influence this has on performance. Tests are conducted on RCA, RCM, MG65 and MG30. The latter two refer to a mixture of RCA and RCM, with a mass percentage RCA of 65% and 35%, respectively. In addition to the recycled materials, a commonly used crushed rock of G2 quality is tested as well to serve as benchmark. Monotonic triaxial tests, to obtain the shear parameters, are performed on all materials except the pure RCM. Permanent deformation triaxial tests, to gain understanding of the long term response to cyclic loading, are performed on RCA and MG65. Specimens are tested under different confinement and deviator stress levels. For the durability simulation, the South African Durability Mill (DMI) is used. The DMI enables durability testing of the full grading under soaked and dry conditions. After the tests, the milled specimens are sieved out to obtain the change in grading.

The most important findings regarding granulate durability include that the breakdown in recycled materials is significant in comparison with the G2. Mainly the largest particle fractions are affected. Furthermore, for these particular resources of recycled granulates, the RCA suffers more breakdown than the RCM. The breakdown in the blends decreases with increasing masonry content, implying that the RCA is the most prone to mechanical damage. Considering the monotonic triaxial tests, substantial values of shear parameters are measured in all materials. The highest cohesion is measured in the MG30, while the highest internal angles of friction are measured in the pure RCA. The shear parameters in the recycled materials are in all cases higher than those for the G2. Differences in failure type (brittle versus plastic) are observed as well. Durability milling results in a small increase of the internal angle of friction and in a moderate decrease of cohesion. The latter is the most governing for the material's compressive strength after milling, as this is decreased in all milled specimens. Still, the shear parameters of the milled specimens remain relatively high. In the permanent deformation triaxial tests, a decrease of performance can be observed in both the RCA and MG65. Delayed shear failure is observed in milled specimens tested at a deviator stress ratio (DSR) higher than 30%. Although the number of permanent deformation tests performed in this research is limited, 30% DSR seems the upper limit with respect to cyclic loading. This points out that monotonic triaxial testing alone is not sufficient for an adequate material characterization. A small linear elastic pavement analysis based on the tested materials, however, shows that the occuring DSR levels in a reference pavement caused by standard axles of 80 kN do not exceed 20% DSR, proving the potential of these materials for further studies.

Figure 1: Lab crew. From left to right: Rowen, Gaven, Colin, Thomas & Eric

PREFACE

This thesis forms a part of the ongoing research into recycled demolition waste materials in the South African pavement industry. It is conducted in collaboration with Stellenbosch University and includes several laboratory tests on recycled concrete and masonry granulates. The potential of recycled granulates being used as (sub)base course layers is currently heavily researched and it will probably not take long until these materials are implemented in practice. Delivering a contribution to this has been a great pleasure. Not only on an educational level this was a very learnful experience, but also on a personal level. Working in a foreign country, with a foreign culture, comes with some challenges but can also be highly rewarding. And that was definately the case for me.

This work could not be establised without all the help I recieved during its course. First of all, I want to thank Antonia Mazibuko and Elaine Goosen for being the best office mates I could wish for. I really enjoyed the time we spend together and want to thank them for showing me around in their home country. I also want to thank Elaine, together with Herman Kasper Gilissen, for checking the spelling of this thesis.

Then, I want to show my gratitude to Sandra Erkens for being the chair of my thesis comittee and for her trust to send me overseas. Cor van der Veen I want to thank for his advises through the final stages of this research. Another big thanks goes to my daily supervisor Lambert Houben, who was involved from the very beginning and explored the possibilities for doing my thesis in South Africa. The fact that his door is always open for questions and that he intensively read through all my work is highly appreciated.

My South African supervisors Kim Jenkins and Chantal Rudman I want to thank for their guidance and hospitality. They made me feel very welcome in my new pavement family and were always available for help and advice. I very much enjoyed their enthousiasm about appearantly simple, but hard to comprehend waste materials. This made our meetings fun and challenging. Especially figuring out the right testing order and managing all laboratory logistics were satisfying exercises for the mind.

In the laboratory, I recieved great help from Riaan Briedenhann, Gaven Williams, Colin Isaacs, Eric Nojewu, Rowen Gideons and Margaret[1]. Their contribution to this research and all other research before mine may not be underestimated. Riaan made sure all equipment in the lab worked properly and kept calling for service even when one of the ovens broke down for the fourth time. Gaven showed me how to work with the lab equipment and managed that the resourced materials were crushed and sieved on time. Eric sieved all crushed materials (±1850kg!) in the required particle fractions. Special thanks goes to Colin and Rowen, who assisted me for several months and washed and sieved all processed materials. Together, they obtained 93 gradings for the purpose of this research.

A final big thanks goes to my family for all their support and for making this thesis and my stay in South Africa literally possible.

Thomas Aelen
Delft, February 2019

[1] Margaret is actually a machine but deserves some credits. She rolled 174 material drums of 25 kg each in a total running time of 14.5 hours.

CONTENTS

NOMENCLATURE

Materials

G2	Graded Crushed Stone G2, high quality South African basecourse material
RCA	Recycled Concrete Aggregate
RCM	Recycled Crushed Masonry
MG30	Mixed Granulate: 30% RCA, 70% RCM (% by mass)
MG50	Mixed Granulate: 50% RCA, 50% RCM (% by mass)
MG65	Mixed Granulate: 65% RCA, 35% RCM (% by mass)
MG80	Mixed Granulate: 80% RCA, 20% RCM (% by mass)

Abbreviations

AASHTO	American Association of State Highway and Transportation Officials
ASR	Absolute Stress Ratio [%]
CBR	Californian Bearing Ratio
DD	Dry Density
DMI	Durability Mill Index
DSR	Deviator Stress Ratio
FMC	Field Moisture Content
FP	Fineness Product
G20C	20 mm scalped+added grading
HMA	Hot Mix Asphalt
HMC	Hygroscopic Moisture Content
LVDT	Linear Variable Differential Transformer
MC	Moisture Content
MDD	Maximum Dry Density
OMC	Optimum Moisture Content
PD	Permanent Deformation
PI	Plasticity Index
SANRAL	South African National Roads Agency Limited
SAPEM	South African Pavement Engineering Manual

Grading abbreviations by Van Niekerk

AL	Average Limit, the average of the upper and the lower limit
CO	Continuous, contains a high amount of fines (0 - 2 mm) and course material (8 - 40 mm)
FL	Füller, theoretically ideal Füller curve with n = 0.45
LL	Lower Limit, the coursest allowable grading
UL	Upper Limit, the finest allowable grading
UN	Uniform, the opposite of CO, contains a high amount of the fraction 2 - 8 mm

Symbols

ϵ_1	Axial strain [%,-]
ϵ_p	Permanent strain [%,-]
ϕ	Internal angle of friction [°]
σ_0	Reference stress [1 kPa]
$\sigma_{1,f}$	Vertical absolute failure stress [kPa]
σ_1	Major principle stress [kPa]
σ_3	Minor principle stress / confinement stress [kPa]
$\sigma_{d,f}$	Vertical deviator failure stress [kPa]
σ_{xx}	Normal stress in the x-direction of a rotated plane [kPa]
σ_{xy}	Shear stress in the y-direction, acting on the plane perpendicular to x-direction [kPa]
σ_{yx}	Shear stress in the x-direction, acting on the plane perpendicular to y-direction [kPa]
σ_{yy}	Normal stress in the y-direction of a rotated plane [kPa]
τ_f	Failure shear stress [kPa]
θ	Sum of principle stresses ($\sigma_1 + 2{\cdot}\sigma_3$) [kPa]
θ_0	Reference stress [1 kPa]
c	Cohesion [kPa]
C_c	Coefficient of curvature [-]
C_u	Coefficient of uniformity [-]
MB	Material Breakdown [%]
Mr	Resilient modulus [MPa]
Mr*	Approximated resilient modulus [MPa]
N	Number of load cycles [-]
R^2	Coefficient of determination [-]
v	Poisson's ratio [-]
w	Dissipated energy per cycle per unit of volume [kPa]

Sample terminology

INITIAL	Non tested reference material
DMIS	Durability mill, scalped+added graded
DMIF	Durability mill, full graded
MONO	Unmilled monotonic triaxial test
PERM	Unmilled permanent deformation triaxial test
S	Scalped+added graded (G20C)
F	Full graded
M	Monotonic test
PD	Permanent deformation test
DB	Dry ball mill
WB	Wet ball mill
W	Wet mill

Units

kg	Kilo gram
mm	Milimeter
μm	Micrometer
kN	Kilo Newton
Pa	Pascal [N/m^2]
kPa	Kilo Pascal [kN/m^2]
MPa	Mega Pascal [N/mm^2]

List of Figures

List of Tables

1

INTRODUCTION

Recycled crushed granulates are widely used in the Netherlands as road base- and subbase materials. The lack of natural resources and the increasing environmental awareness about the growing amounts of demolition waste, made that Dutch industries in the early 1980s started to explore the possibilities to use recycled aggregates as road base and subbase [6]. Since then, a significant amount of research has been carried out into the structural performance of Recycled Concrete Aggregate (RCA), Recycled Crushed Masonry (RCM) and Mixed Granulates (MG). Multiple studies and practical experience proved the applicability of these materials, and led that they are nowadays commonly being used as pavement base course materials. Besides the Netherlands, various other countries such as Germany, Great Britain and the United Arab Emirates recognized the potential of recycled granulates and succesfully implemented them in their road infrastructure [3].

Recently, research into the use of recycled aggregates has also started in South Africa. Due to the fact that high quality natural resources are slowly depleting and the demand for new construction materials continues to rise, alternative materials need to be found. Considering the wide availablity of demolition waste and the economical and environmental benefits of recycling, recycled aggregates might form a good solution. Therefore, the South African road authorities and industries set up a working group to develop guidelines for the use of these materials in practice. Several topics into the structural properties of recycled aggregates are currently researched at Stellenbosch University. The durability aspects however, have only been addressed to a limited extent. Durability describes the particle resistance against crushing and abrasion and forms an important aspect in South African pavement design. Material disintegration and decomposition can significantly affect pavement performance and lead to early failure. Research into the durability properties of recycled aggregates and the way particle breakdown influences performance is therefore crucial.

1.1. DIFFERENCES BETWEEN SOUTH AFRICAN AND DUTCH PAVEMENT DESIGN

The importance of granulate durability in the South African context can be explained by considering the differences between Dutch and South African pavement design. Figure 1.1 shows the layer structure of a typical Dutch highway and the South African N1 highway in the Western Cape province. In the Netherlands, weak subgrade conditions (i.e. clay and peat) and high intensity heavy traffic require substantial layer thicknesses. The structural capacity is mainly provided by the asphalt, which has high load spreading abilities and is able to follow uneven subsoil settlements. The top layers are supported by a recycled granulate base of around 250 mm and a sand subbase of at least 1000 mm. Besides further spreading of the traffic loads to the subgrade, a thick subbase layer is applied for two reasons: Firstly, the mass of the sand is used to initiate primary settlements. By placing the subbase layer some time before the rest of the pavement is constructed, initial settlements may already be resolved. Secondly, due to high groundwater levels, it often occurs that capillary water enters the subbase. As a requirement, frost penetration may not reach the capillary

water (the structure may never become completely frozen), to avoid excess moisture during thaw [13]. Especially in the western regions of The Netherlands, total construction heights of more than 1.5 m are not uncommon.

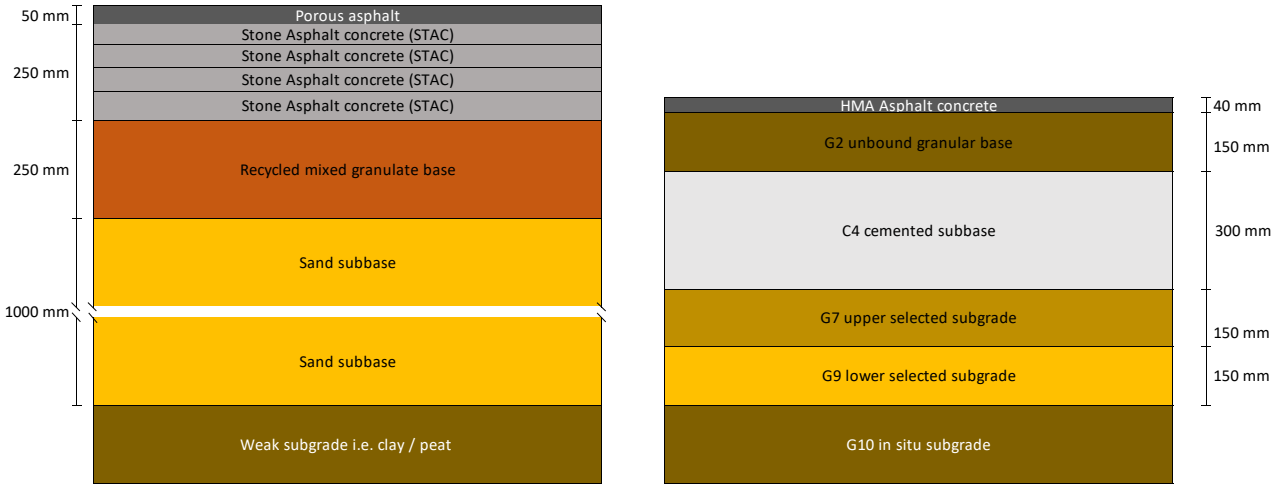

Figure 1.1: Layer structure of typical Dutch and South African highways **Left:** The Netherlands **Right:** South Africa

The South African design philosophy is slightly different. Lighter traffic conditions and better quality subgrades require a less thick structure. Although the former is subjected to change due to the developing economy [3], the traffic intensity is still considerably smaller in comparison with the western part of the Netherlands. The surface layer of the South African N1 either consists of a relatively thin asphalt layer (i.e. 40 mm) or a seal. In the latter case, the surface layer has no load spreading capacity and mainly serves for driving comfort, skid resistance and to prevent water infiltrating the structure. A granular base of high quality crushed stone in combination with a cemented subbase forms the most important structural component. Often, a granular base is placed above a cemented subbase in order to prevent reflection cracks propagating to the surface layer. The quality of the granulates is classified in ranges from G1 to G10. For each class, requirements for material type, grading, Atterberg Limits and bearing strength (CBR) are specified. An overview of the material classification system from G1 up to G6 can be found in Appendix A. Higher class numbers represent lower quality materials, and are usually located in the lower layers of the pavement structure. This can also be seen in the structure under consideration, where the quality of the (selected) subgrade layers decreases with increasing depth. Although the in situ G10 subgrade is of the lowest distinghuished quality, this subgrade has still a considerably higher bearing capacity than the peat / clay subsoils in the Netherlands. Due to this, higher compaction rates can be achieved which improve the quality of the layers.

As mentioned before, durability is defined as the grain particle resistance against wearing crushing over time. While the recycled granulates in The Netherlands are covered by a thick asphalt layer, the granulates in South Africa are closely located to the surface. The materials experience higher stresses which make them more likely to suffer from abbrasion and crushing. Together with that, small cracks in the seal or asphalt immediatly expose the materials to environmental conditions. Changes in moisture content due to rain water inflow can cause severe material distress and make them more prone to damage. Therefore, base course materials in highways are always of the highest quality chrushed rock, i.e. G1 and G2. Durability requirements in terms of particle crushing strength are specified as well as the materials need to withstand harsh moisture and stress conditions. For recycled materials to be used in South African base course layers, not only a comparable bearing capacity is required, but also should the loss of performance due to material degradation stay within reasonable limits. It is therefore important to research possible extent of material damage, and the influence of this damage on performance. Sound judgement can then be made by comparing the overall performance and the degrated performance with commonly used G1 or G2 materials.

1.2. OBJECTIVES

The primary aim of this research is to establish insight into the relationship between potential material breakdown and the change of performance of recycled aggregates. By means of triaxial testing before and after durability degradation simulation, it is aimed to find the extent of material breakdown and the way this affects performance (Figure 1.2). Both the shear parameters and the response to long term cyclic loading are addressed. Durability simulation is conducted with the Durability Mill, a common South African test apparatus to test granulate durability. Several combinations of recycled materials are composed, with the masonry content serving as the main variable. Furthermore, a comparison with a reference material is included as part of benchmarking recycled aggregates against typical South African base course materials. The following four topics are addressed:

- The durability parameters of RCA, RCM and MG by means of durability milling (see 2.6.1). The durability mill simulates particle degradation and gives insight in the extent of potential (mechanical) breakdown.
- The relationship between durability milling and change in performance by means of triaxial testing before and after durability milling. This provides understanding of how particle change (grading and form) affects the performance parameters.
- The influence of masonry content on material degradation and performance.
- A comparison of how recycled materials relate to a well known, similar tested reference material. Benchmarking against typical South African base course granulates, i.e. a G2 material, enables sound judgement of the material durability.

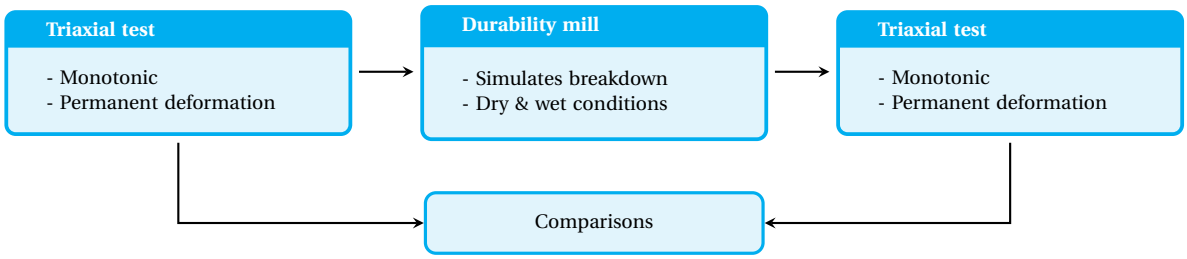

Figure 1.2: Testing principle

This study can be considered as a first step in addressing the mechanical durability aspects of recycled aggregates. It forms part of the process to develop durability guidelines for the use of these materials in practice. It is recognized that several research questions stay open after this project. For instance, this new way of combining durability testing with triaxial testing must still be correlated to what happens in the field. It does also not include the quality spread of the concrete and masonry granulates. The influence of brick quality on performance is definitely important to investigate, but as the South-African masonry resources mainly consist of industrial processed bricks and the first applications of the recycled materials are likely to be done in urban areas where industrial processed bricks form the main resources, this will not yet be addressed in this early stage of research. Nevertheless, this research gives some useful insights, benchmarks and recommendations for the future use of these materials.

1.3. PROJECT OVERVIEW

A laboratory testing program is developed which combines triaxial testing with durability milling. Figure 1.3 shows an overview of the testing plan, output parameters and comparisons to be made. Both monotonic and permanent

deformation triaxial tests are included. Since the durability mill addresses particle degradation, sieve analysis forms a large part of this research. Gradings before and after durability simulation are compared to study the impact of the durability mill. Both dry and soaked conditions are tested. The research behind the durability mill is discussed in Section 2.6.1. More detailed information about the experimental set up can be found in Chapter 3.

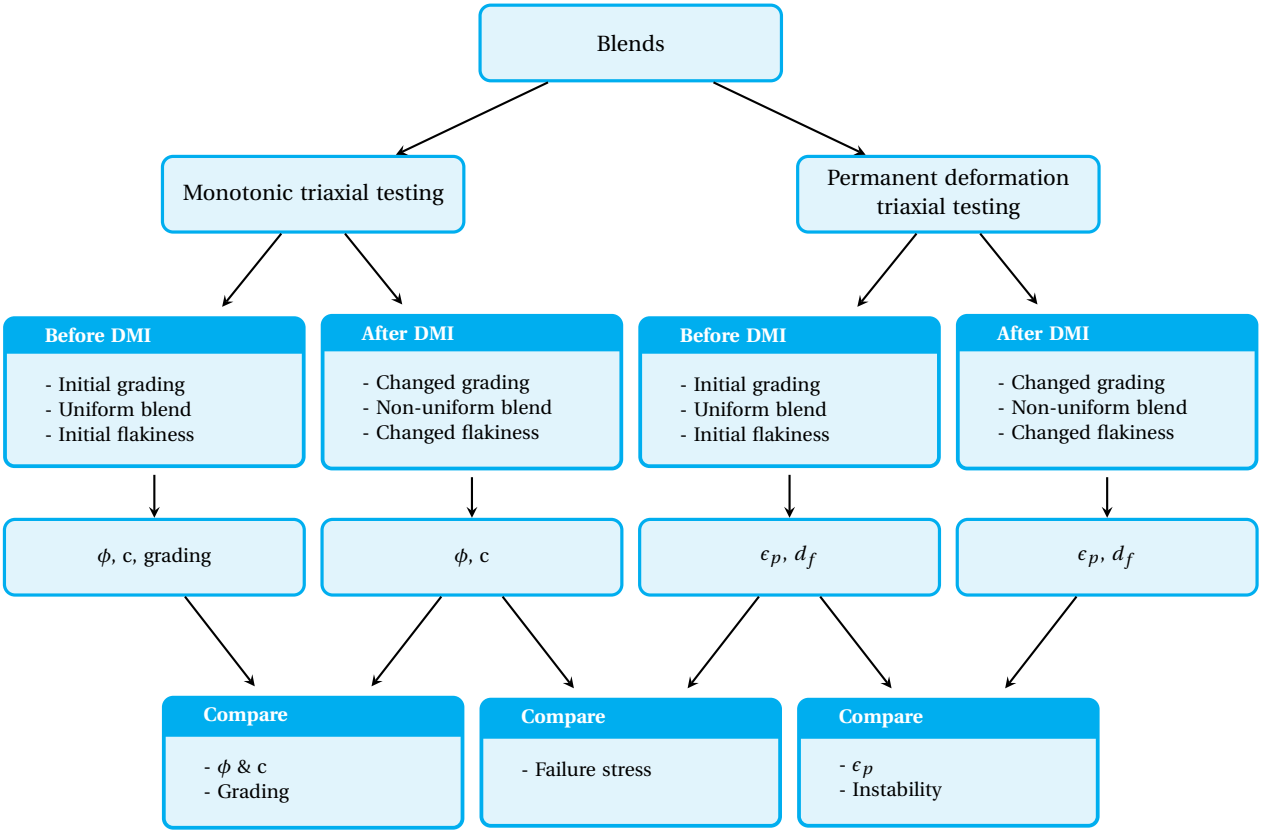

Figure 1.3: Combining durability and performance testing

1.4. THESIS OUTLINE

The outline of this report is as follows: Firstly, in Chapter 2, the theoretical background is discussed. The theories presented here are applied in the processing of the laboratory test results and form the fundamentals of this research. Then, in Chapter 3, the experimental design and methodologies are explained. All test procedures are briefly discussed and some overal points of attention with respect to sample preparation are highlighted. Chapter 4 contains the results and provides a first level analysis of the obtained findings. Limits regarding loading capacity and comparisons with other work are incorporated in this chapter as well. In Chapter 5, an in depth analysis of the triaxial test results is presented. The main focus considers the permanent deformation triaxial test results, and whether unstable behavior can be predicted in the beginning stages of the test. The analysis of the results ends with a small pavement assesment. In this assesment, it is aimed to acquire a first impression of stress levels occuring in a reference pavement, and how these relate to the obtained stress limits. Finally, in Chapter 6, the most important conclusions are summarised and some recommendations for future work are given.

2

THEORETICAL BACKGROUND

2.1. INTRODUCTION

This chapter provides the theoretical background of this research. The theories presented here are used widely and form the basis of this study. Emphasis is placed on the theories supporting the triaxial test apparatus and the modelling of the measured behavior. In the past, extensive research has substantially improved the understanding of the complex behavior of unbound granulates. This includes research by Van Niekerk [14], who carried out an study into recycled materials and investigated influence factors such as grading, composition and degree of compaction. Werkmeister [28] focussed on permanent deformation behavior and researched the applicability of the shakedown theory. In this research, a number of references is made to their findings. The chapter starts with an explanation of the performance properties of unbound granular materials. Then, soil stresses and the fundamentals of triaxial testing are discussed. Thereafter, the most common forms of triaxial testing applied in pavement engineering are presented. Finally, granulate durability and durability testing with the durability mill are adressed.

2.2. PERFORMANCE PROPERTIES OF UNBOUND GRANULATES

Three important performance aspects of unbound pavement layers are resistance against shearing (failure behavior), load spreading capacity (stiffness) and resistance against rutting (permanent deformation). Although material characterisation methods such as Californian Bearing Ratio (CBR) testing, Atterberg Limit testing and Proctor testing are internationally known and relatively easy to perform, they are not directly related to field performance. The need exists to better adress these performance properties which led to the development of the triaxial test for road (sub)base course materials. The triaxial test aims to closely simulate a field conditions, and is nowadays accepted as the most accurate way to test the performance properties of unbound granulates [28].

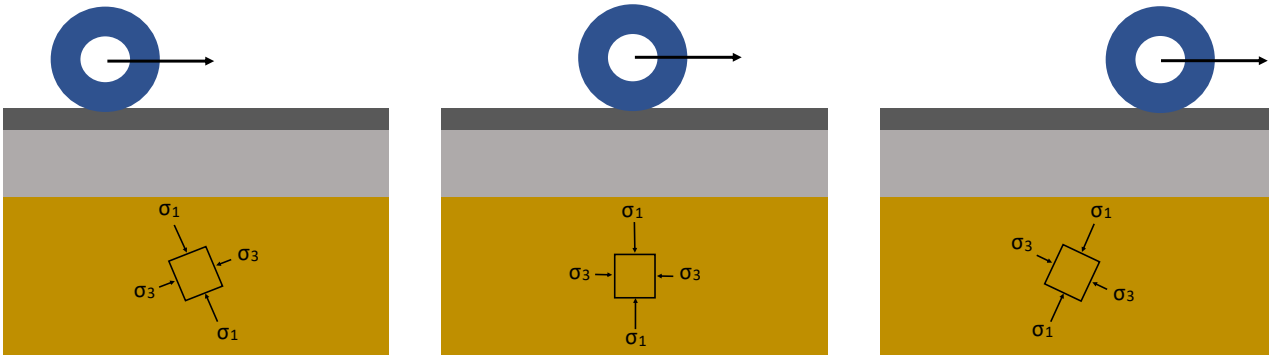

Figure 2.1: Principle stress directions changing with moving wheel load

2.2.1. SOIL STRESSES

At any given moment, the stress state in a soil element can be expressed in terms of shear and (compressive) normal stresses. Figure 2.2 considers a small two dimensional element in a pavement structure. The wheel introduces a vertical load which is transferred through the structure to the subgrade. In a stable situation, the stresses acting on the element balance each other out due to force and moment equilibrium. Regardless of the orientation of the element, equilibrium is maintained. It can be shown that an element orientation exists at which the shear stresses are zero. The corresponding normal stresses are referred to as the principle stresses σ_1 and σ_3. The principle stresses are the maximum and minimum occuring normal stresses, and act in the principle stress directions. By using geometry rules, the stress state in each orientation can be expressed in terms of principle stresses and the angle of the plane under consideration with respect to the principle stress directions (α). Elaboration results in the following set of equations:

$$\sigma_{xx} = \sigma_1 \sin^2 \alpha + \sigma_3 \cos^2 \alpha \tag{2.1}$$

$$\sigma_{yy} = \sigma_1 \cos^2 \alpha + \sigma_3 \sin^2 \alpha \tag{2.2}$$

$$\sigma_{xy} = \sigma_{yx} = \sigma_1 \sin(\alpha)\cos(\alpha) - \sigma_3 \sin(\alpha)\cos(\alpha) \tag{2.3}$$

Where σ_{xx}, σ_{yy}, σ_{xy}, σ_{yx} are the normal and shear stresses acting in the rotated plane as displayed in Figure 2.2. In a static situation, where a point directly under a load is considered, the vertical load corresponds with the first principle stress (σ_1). The third and second principle stresses (σ_3 and σ_2) work in the perpendicular directions and are confinement reactions of the vertical loading. In practice, wheel loads are not static but move along with the vehicle. This causes the principle stress directions to change continuously. An illustration of this is presented in Figure 2.1.

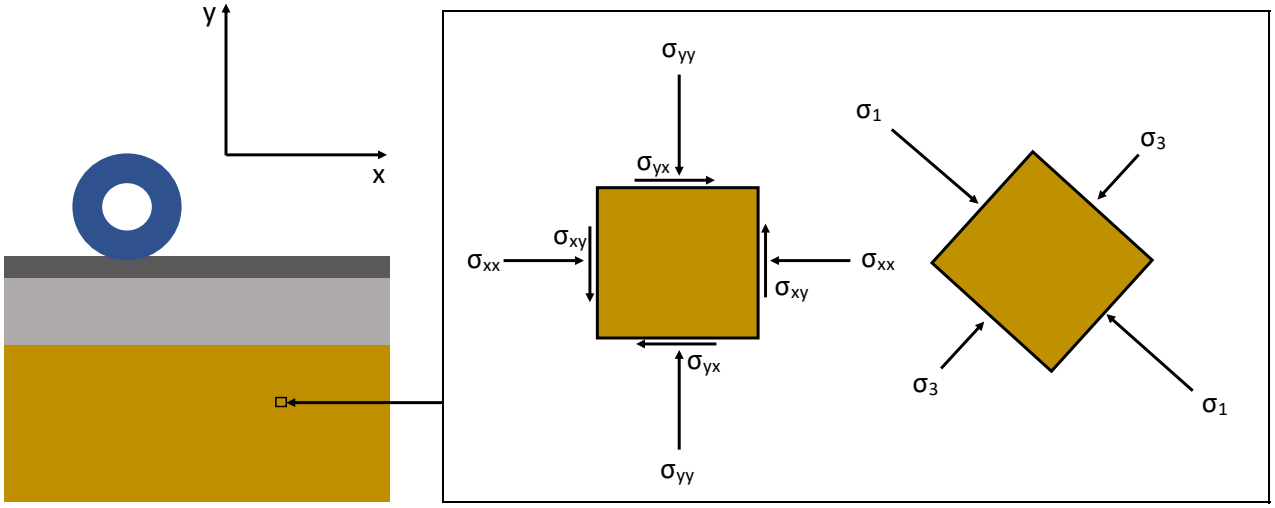

Figure 2.2: Stresses in a two dimensional element

2.2.2. TRIAXIAL TESTING

The triaxial test is developed to simulate stress conditions in the field as accurate as possible. The main principle of the test is that it loads a specimen in the three principle, perpendicular stress directions. Besides a vertical load (σ_1), two (equal) horizontal stress components acting in the radial direction ($\sigma_2 = \sigma_3$) are present as well to serve as confinement. Confinement stress is applied by a medium, i.e. water or air, in a cell enclosing the specimen. A

membrane wrapped around the specimen ensures a pressure difference between the specimen and the confinement medium. Figure 2.3 shows a schematic view of the triaxial set-up and the triaxial test machine at Stellenbosch University, respectively. As an alternative, confinement stress can be established by applying an underpressure in the specimen. In this case, air is sucked out of the specimen creating a partial vacuum. This type of triaxial test is carried out by Van Niekerk [14]. It is a less expensive set-up in comparison with the overpressure cell, but has the main disadvantage that confinement stress levels are limited to about 80 kPa. Together with that, small variations in sample packing and porosity cause a non-uniform stress distribution over the sample height. The overpressure cell set-up is more expensive but does not have these disadvantages.

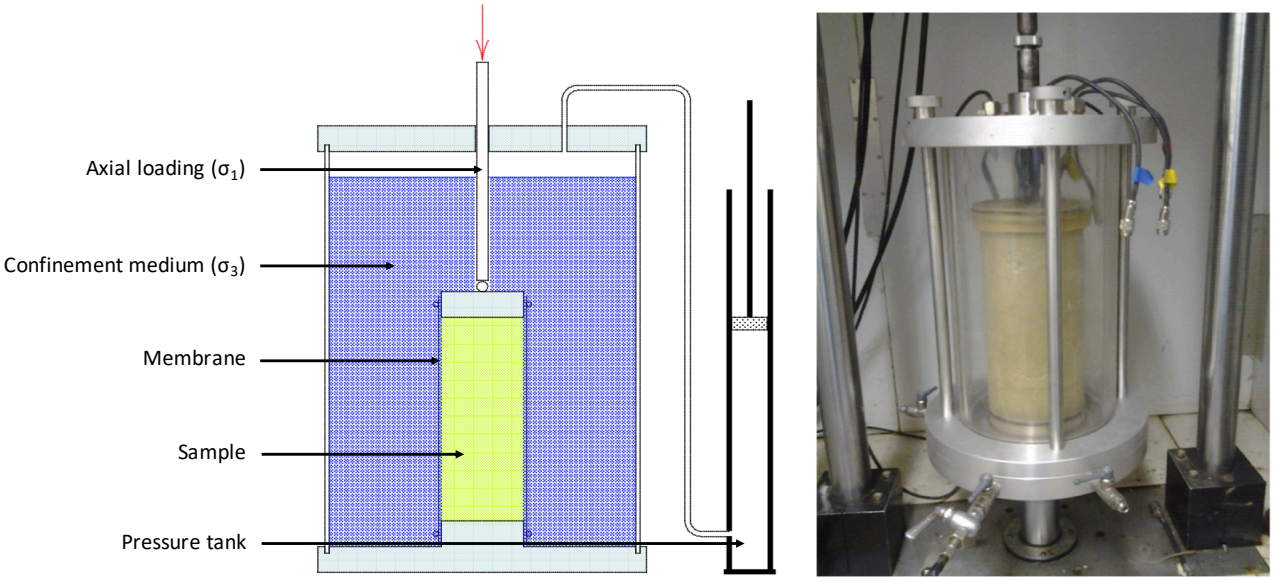

Figure 2.3: Triaxial test set-up **Left:** Triaxial test set-up [27] **Right:** Triaxial cell at Stellenbosch University [29]

Some advanced triaxial test machines are able to incorporate the change of principle stress direction explained in the previous section [28]. Sometimes it is also possible to apply a dynamic, stress dependent confinement stress. The most common triaxial tests however are carried out with a constant confinement stress and no change of principle stress directions. To obtain uniform stress distributions within specimens, the specimen should be of adequate size. For soils and clayey materials, the required specimen diameter is 38 mm [27]. Unbound granulates consist of larger aggregates (up to 37.5 mm in South Africa and 40 mm in The Netherlands) and therefore require a larger specimen diameter. A diameter of at least 5 or 6 times the maximum particle size is advised [9]. Common dimensions for large scale triaxial testing (d_{max} = 40 mm) are 300 x 600 mm. Common dimensions for small scale triaxial testing (d_{max} = 20 mm) are 150 x 300 mm or 100 x 200 mm. The height is usually twice the specimen diameter. Too high specimens carry unnecesary mass and can become prone to buckling. Too small specimens may not obtain a uniform stress state due to frictional effects of the bottom and top plates. In geotechnical engineering, triaxial tests are mainly carried out on soils and clayey materials and involve consolidation stages. In road engineering, the primary use of the triaxial test considers unbound granulates. The three most common triaxial testing types for unbound granulates in road engineering are:

- Monotonic triaxial testing;
- Resilient modulus triaxial testing;
- Permanent deformation triaxial testing.

Each type adresses different performance aspects. The monotic triaxial test determines the shear properties (failure behavior), the resilient modulus triaxial test adresses the stiffness response and the permanent deformation triaxial

test gains understanding in the long term behavior. In the following sections, the three types of triaxial testing are discussed in more detail.

2.3. UNBOUND GRANULATE FAILURE BEHAVIOR

In the discussion about failure behavior of soils and unbound granulates, it is important to describe what is actually meant with failure. Since these materials cannot take up tensile forces and rely heavily on supporting conditions, their failure behavior is less straight forward than that of other materials. In general, failure is regarded as the occurence of irreversible deformations such that bearing capacity is lost. Due to (too large) shear forces, soil bodies can slide over each other causing large deformations and loss of capacity to support the structure on top of them. Determining if and when this happens is one of the fundamentals of soil structure design. Crushing of individual particles can happen as well and of course influences failure behavior, but this phenomina is rather a durability aspect than a failure type (see Section 2.6).

2.3.1. MOHR-COULOMB THEORY

One of the methods to decribe the failure behavior of soils and coarse granulates is the Mohr-Coulomb theory. The starting point of this theory is that at a certain surface in the soil, the combination of shear and normal stresses is such that shearing in the materials occurs. As an example one can think of a block with weight W resting on a slope with angle α, illustrated in Figure 2.4. Force equilibrium exists where the normal force equals N = W cos α and the shear force equals T = W sin α. Sliding occurs when T $\geq$ N·C$_f$, with C$_f$ a material dependent friction coeficient. This can also be written as: W sin $\alpha \geq$ W cos $\alpha \cdot$ C$_f$, or, tan $\alpha \geq$ C$_f$. In other words, when the slope angle becomes so large that its tangent is larger than the friction coeffient, the block will slide down. Charles-Augustin de Coulomb used this anology in 1776 to formulate failure criteria for a soil body [27]:

$$\tau_f = c + \sigma \tan\phi \tag{2.4}$$

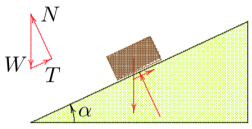

Figure 2.4: Block on a slope [27]

Where τ_f represents the failure shear stress and σ the acting normal stress on a certain plane in a soil. ϕ and c are material parameters and stand for the internal angle of friction and the cohesion respectively. Cohesion is present when there is resistance to shearing even when there is no normal force present. This is usually the case for clayey materials, which can form cohesive bonds. Sands on the other hand have very little or no cohesion at all. The cohesion and friction angle, also called the shear parameters, are influenced by a variety of different factors and are not a constant material property. Variables such as grading, moisture content, density, and loading history all play an important role in the material shear strength. Referring to the element stress state discussed in Section 2.2.1, it is now aimed to check whether there are planes existing in the element for which the condition of Equation 2.4 is met. To do so, the stress state for each element orientation is be plotted by making use of Equation 2.1. Normal stresses are displayed on the x-axis and the shear stresses on the y-axis. The obtained circles are the so called Mohr circles (Figure 2.5). The failure criteria from Equation 2.4 can be plotted as well. This linear relation between the normal

stress and the shear stress is known as the failure envelope. When the combination of principle stresses is such that the circle touches the failure envelope, force equilibrium cannot be maintained and shearing occurs. The former equations can be rewritten in a form where the maximum absolute principle stress is expressed a function of the shear parameters and the confinement stress:

$$\sigma_{1,f} = \frac{(1+\sin\phi)\sigma_3 + 2c\cdot\cos\phi}{1-\sin\phi} \tag{2.5}$$

The Mohr-Coulomb failure model is fairly accurate in describing shear failure in soils and other granulate materials. However, soil properties such as moisture content, grading and density might change over time, causing significant changes in the shear parameters. Loading history also plays an imporant role. Besides changes in density, (over)loading can break cohesive bonds (for example due to self cementation in recycled materials) causing an irreversible decrease in shear strength.

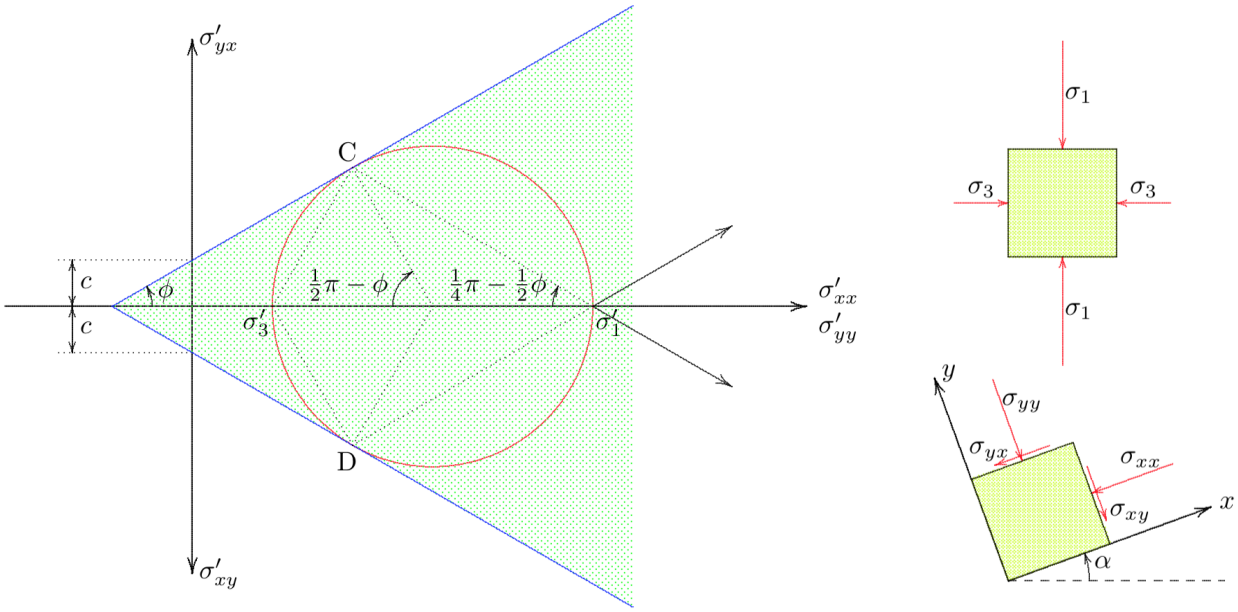

Figure 2.5: Mohr-Coulomb failure criterion [27]

2.3.2. MONOTONIC TRIAXIAL TESTING

Monotonic triaxial testing is performed to research the failure behavior of soils and unbound granulates. It is a destructive test meaning that the samples will be loaded up to failure. In theory, a minimum of two similar composed samples are needed to find the shear parameters, but most standards require at least three or more tests to obtain reliable results. The maximum resisting force is recorded as $\sigma_{1,f}$. By testing the samples at different confinement stresses, the corresponding Mohr circles can be plotted. The shear parameters are then determined by linear curve fitting of Equation 2.5. The coefficient of determination (R^2) describes the accuracy of the fitted failure envelope. A perfect fit is obtained when $R^2 = 1$:

$$R^2 = 1 - \frac{SS_{res}}{SS_{tot}} \qquad SS_{res} = \sum_{i=1}^{N}(\tau_i - \eta_i)^2 \qquad SS_{tot} = \sum_{i=1}^{N}(\tau_i - \overline{\tau})^2 \tag{2.6}$$

Where:

R^2 = Coefficient of determination [-]

SS_{res} = Residual sum of squares [kPa^2]

SS_{tot} = Total sum of squares [kPa^2]

τ_i = Measured failure shear stress for test i [kPa]

η_i = Modelled failure shear stress for test i [kPa]

$\overline{\tau}$ = Mean measured failure shear stress [kPa]

N = number of tests [-]

The obtained force-displacement curve can be used for further analysis and contains information about the type of failure (brittle or plastic). The slope gives an estimation of the material stiffness at the tested confinement. However, since soil stiffness is stress dependent, it would take a considerable number of specimens to acquire enough data for an accurate determination. Especially for bigger granulates this is problematic because of the labour intensive preparation of specimens. More common practice is to perform resilient modulus triaxial testing, which is non-destructive and requires only one specimen to obtain the stiffness parameters.

2.3.3. FACTORS INFLUENCING SHEAR PARAMETERS

Van Niekerk [14] studied the influence of composition, grading and degree of compaction on the shear parameters. For practical reasons, the specimens used in monotonic triaxial testing were already subjected to a permanent deformation test. To exclude the effects of loading history as much as possible, only specimens which gained limited permanent deformations were selected. A summary of the obtained results on MG65 is presented in Figure 2.6. A summary of the grading abbreviations used by Van Niekerk can be found in Appendix B. The degree of compaction is expressed as percentage standard Proctor density. The figure shows a general increase in both cohesion and friction angle with increasing compaction. Especially the cohesion at 103% DOC increased tremendiously for all gradings. Higher cohesion levels are also measured in the finer graded specimens. The friction angle of the average limit graded specimens appears to be higher than in the upper and lower limit graded specimens. Van Niekerk recognized that the measured friction angles are on the low side for granular materials, and attributed this effect to particle wear occurring in the preceeding permanent deformation tests.

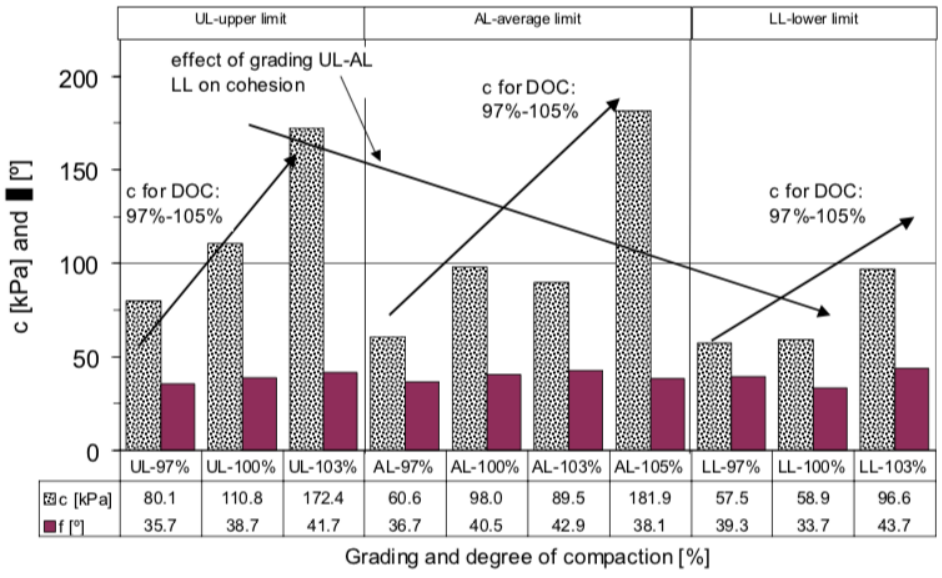

Figure 2.6: Influence factors on shear parameters [14]. DOC is expressed as percentage standard Proctor density

Another important factor influencing the shear parameters is moisture content. Following on the Mohr-Coulomb theory, soil stress is the sum of effective stress and pore water pressure. Effective stress is the portion of the total stress taken up by the grain particles. Since water can only resist normal stress, all shear stresses must be effective stress. Excessive pore water pressures reduce the effective normal stress, which in turn reduces the maximum shear stress a soil body can withstand (Equation 2.4). Pore water pressure thus affects the shear strength, while total occuring shear stress is unaffected. It also works the other way around. Negative pore water pressures (suction), increase the effective normal stress and the shear strength. Alemgena [1] showed that for dry to moderate moisture conditions (while maintaining equal DOC), the cohesion increases with increasing moisture content. In moderate to wet conditions, a significant loss of cohesion was found (Figure 2.7). Alemgena conluded that the increase of cohesion went up to optimum moisture content (explained in Section 3.2.2), and that all above will cause a significant reduction.

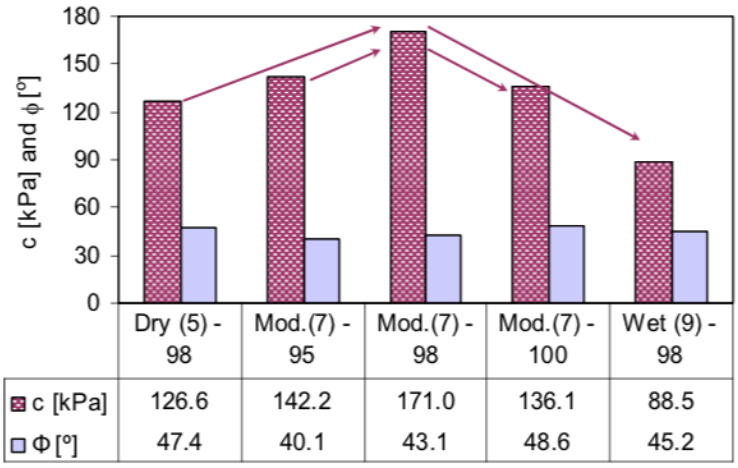

Figure 2.7: Influence factors on shear parameters [1]. (MC[%]) - DOC[%]. DOC is expressed as percentage standard Proctor density

2.4. UNBOUND GRANULATE STIFFNESS

The main function of (sub)base layers, and actually the main function of a road, is spreading loads such that they can be carried by the underlying layers. To what extent this happens is highly dependent on the layer stiffness. Stiff materials have high load spreading capacitiy and vice versa. In contrast to conventional construction materials such as concrete and steel, the elastic modulus of unbound granulates is not a constant property. Besides composition and environmental conditions, stress conditions direcly influence the stiffness response. Due to this stress dependency, the elastic modulus is expressed as "resilient modulus", denoted as Mr, instead of Youngs modulus. At low stress levels, stiffness increases with increasing stress (strain hardening) [9]. The particle packing and interlock increases causing more resistance to deformation. At stress levels near failure, stiffness will significantly decrease and eventually become zero when failure is reached (strain softening). The occuring strains in cyclic loaded unbound granulates have an elastic and a permanent component. The elastic strain is the recoverable, resilient strain. The permanent strain is not recoverable and results in permanent deformation. The resilient modulus is now defined as the slope of the recoverable stress - strain path, illustrated in Figure 2.8. The figure shows a typically observed hysteresis loop. The area enclosed by the curve represents the energy dissipation. Permanent deformations can occur at very small stress and strain levels [28]. At increasing load cycles and low stress levels however, the accumulation of permanent deformation decreases which results in a primary elastic response. Measuring this response at varying confinement and deviator stress levels is done to obtain of the stress dependent resilient modulus.

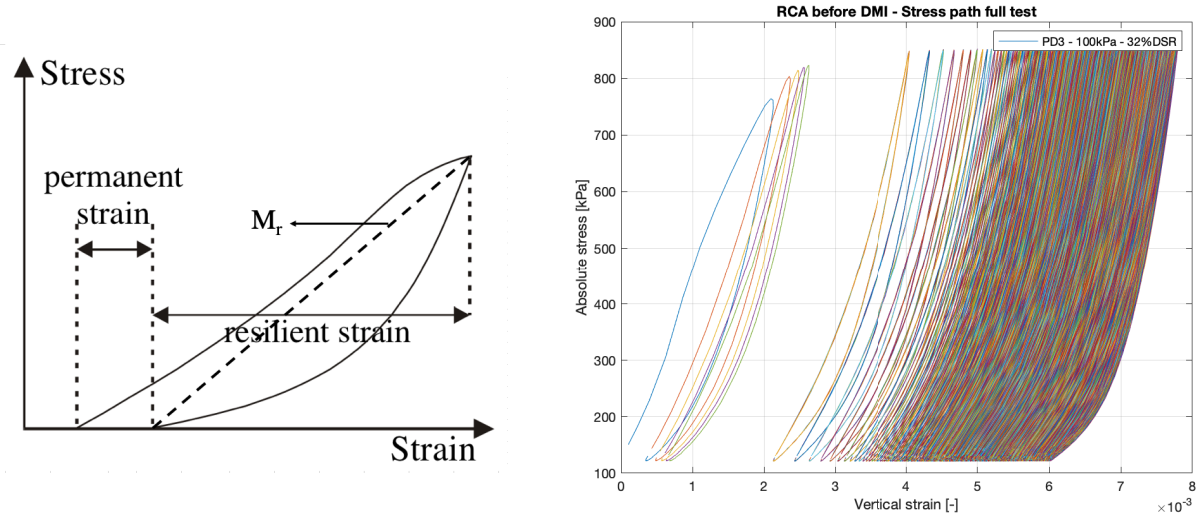

Figure 2.8: Cyclic loading: Stress - strain cycles [28]

2.4.1. RESILIENT MODULUS TRIAXIAL TESTING

Resilient modulus triaxial testing is perfomed to obtain the stiffness behavior of soils and unbound granulates. It is a cyclic, non-destructive test which measures the resilient moduli at varying combinations of confinement and deviator stress levels. Stress levels and the number of load cycles are kept low to ensure that the effects of loading history on the specimen are limited. In this case one specimen can be used to test all desired stress combinations. Van Niekerk [14] for instance, who extensively researched unbound (recycled) materials, used the following regime in his study:

- σ_3 = 12 kPa, σ_1 / σ_3 = 2, 3, 4, ... , 8;
- σ_3 = 24 kPa, σ_1 / σ_3 = 2, 3, 4, ... , 8;
- σ_3 = 36 kPa, σ_1 / σ_3 = 2, 3, 4, ... , 8;
- σ_3 = 48 kPa, σ_1 / σ_3 = 2, 3, 4, ... , 8;
- σ_3 = 60 kPa, σ_1 / σ_3 = 2, 3, 4, ... , 8;
- σ_3 = 72 kPa, σ_1 / σ_3 = 2, 3, 4, ... , 8;

The stress combinations are tested with increasing order of confinement stress. After each increase of confinement, the specimen should be allowed to consolidate for 15-20 minutes before running a new test [14]. The specimen is equiped with axial and radial LVDTs to measure the occuring displacements. The LVDTs are placed over one third of the height in the middle of the specimen to exclude the effects of friction at the top and bottom plates. Each stress combination is tested for 50 or 100 cycles at 1 Hz [14]. An example of the triaxial specimen set-up and cyclic loading is presented in Figure 2.9. A resting phase follows each cycle. A constant static load is present to simulate the weight of the parent structure. For the last ten cycles, displacements measured by the LVDTs are recorded. The axial loads and confinement stresses are recorded as well. The resilient modulus corresponding to each regime is then calculated as the average axial (vertical) stress over the average axial strain (σ_1/ϵ_1). By plotting the obtained values against the sum of principle stresses θ ($\theta = \sigma_1 + 2{\cdot}\sigma_3$), the stiffness behavior can usually be fitted well with the widely used Mr - θ model:

$$M_r = k_1 \left(\frac{\theta}{\theta_0} \right)^{k_2} \tag{2.7}$$

Where:

Mr = Resilient modulus [MPa]

θ = Sum of principle stresses ($\sigma_1 + \sigma_2 + \sigma_3$) [kPa]

θ_0 = Reference stress [1 kPa]

k_1 = model coefficient [MPa]

k_2 = model coefficient [-]

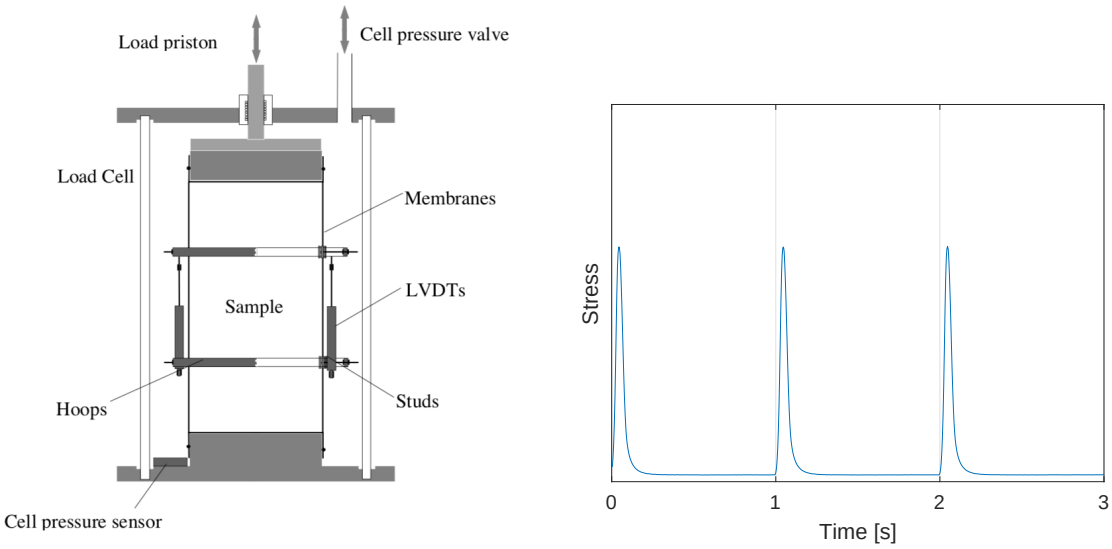

Figure 2.9: Resilient modulus triaxial testing: **Left:** Triaxial setup [28] **Right:** Loading diagram

As can be seen in Van Niekerk's [14] results in Figure 2.11, the Mr - θ model fits the data well for "mild" stress regimes. In this case, that is when the cyclic vertical stress is considerably lower than the monotonic failure stress ($\sigma_1/\sigma_{1,f}$ < 0.5), the strain hardening behavior at low stress levels is modelled fairly accurate. For more severe stress regimes however, when $\sigma_1/\sigma_{1,f}$ goes up to even 0.9, the model starts to deviate. It predicts an increase of stiffness with increasing stress, while tests results clearly show the opposite behavior. Another remark on the Mr - θ model is that it does not differentiate between confinement and vertical stress. Two different combinations of σ_1 and σ_3 can result in the same resilient modulus, while not taking into account their individual contributions. This is physically incorrect. Therefore, other models have been developed in the past which include a strain softening component at higher stress levels and/or discriminate between principle stress contributions. Huurman [10] for instance showed that his model given in Equation 2.8 is actually very suitable for sandy materials. For granular materials, van Niekerk [14] slightly modified this model and applied it on his results (Equation 2.9). Altough still fundamentally incorrect, it gives a better approximation of the resilient modulus at higher stress regimens than the Mr - θ model.

$$M_r = k_5 \left(\frac{\sigma_3}{\sigma_0} \right)^{k_6} \left(1 - k_7 \left(\frac{\sigma_1}{\sigma_{1,f}} \right)^{k_8} \right) \tag{2.8}$$

$$M_r = k_5 \left(\frac{\theta}{\theta_0} \right)^{k_8} \left(1 - k_7 \left(\frac{\sigma_1}{\sigma_{1,f}} \right)^{k_8} \right) \tag{2.9}$$

Where:

Mr	= Resilient modulus [MPa]
σ_1	= Absolute vertical stress [kPa]
$\sigma_{1,f}$	= Absolute failure stress, at corresponding confinement stress [kPa]
σ_3	= Confinement stress [kPa]
θ	= Sum of principle stresses ($\sigma_1 + \sigma_2 + \sigma_3$) [kPa]
σ_0, θ_0	= Reference stress [1 kPa]
k_5	= model coefficient [MPa]
k_6, k_7, k_8	= model coefficients [-]

The former equations have been modified by Jenkins [11], who used relative stress conditions instead of absolute stress conditions. Instead of the absolute stress ratio, ASR = $\sigma_1/\sigma_{1,f}$, he used the deviator stress ratio, DSR = $\sigma_d/\sigma_{d,f}$. Here σ_d is the applied deviator stress (the difference between the major and minor principle stress (σ_1 - σ_3)) and $\sigma_{d,f}$ the maximum deviator stress the specimen can withstand.

2.4.2. FACTORS INFLUENCING UNBOUND GRANULAR STIFFNESS

Stress conditions are one of the most important factors influencing stiffness response. Besides that, other variables such as moisture conditions, compaction, composition, grading and particle shape play a role to a greater or lesser extent. Van Niekerk aimed to demonstrate the influence of degree of compaction, grading and moisture content, on the resilient behavior. He found an overal increase of stiffness with increasing DOC (see Figure2.10. With respect to moisture content, he found an overal increase of the resilient modulus for under saturated materials. Over saturation caused the stiffness, similar as the shear parameters, to decrease drastically. The influences of grading on the stiffness response appears to be of influence but to a lesser extent, although well graded materials are correlated with higher stiffness parameters than uniform gradings [15].

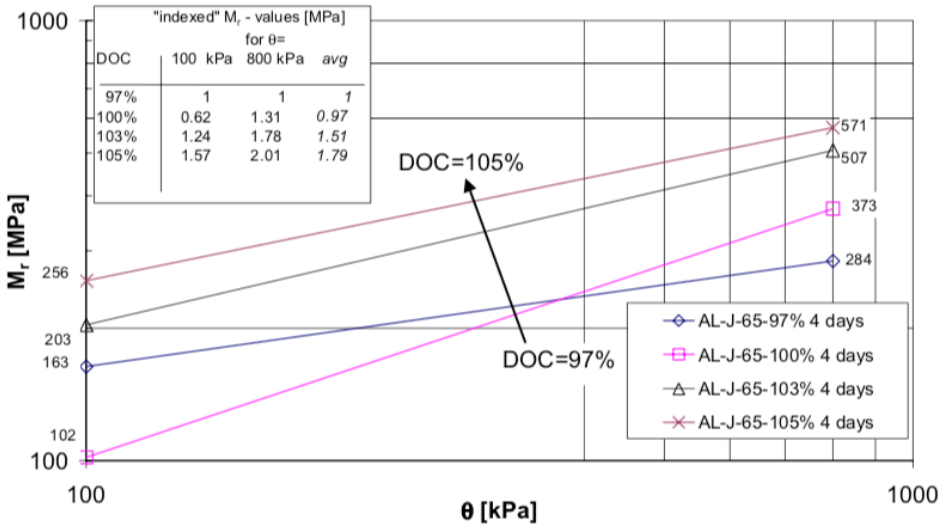

Figure 2.10: Resilient modulus comparisons: Influence of DOC (% standard Proctor density) on resilient behavior [14]

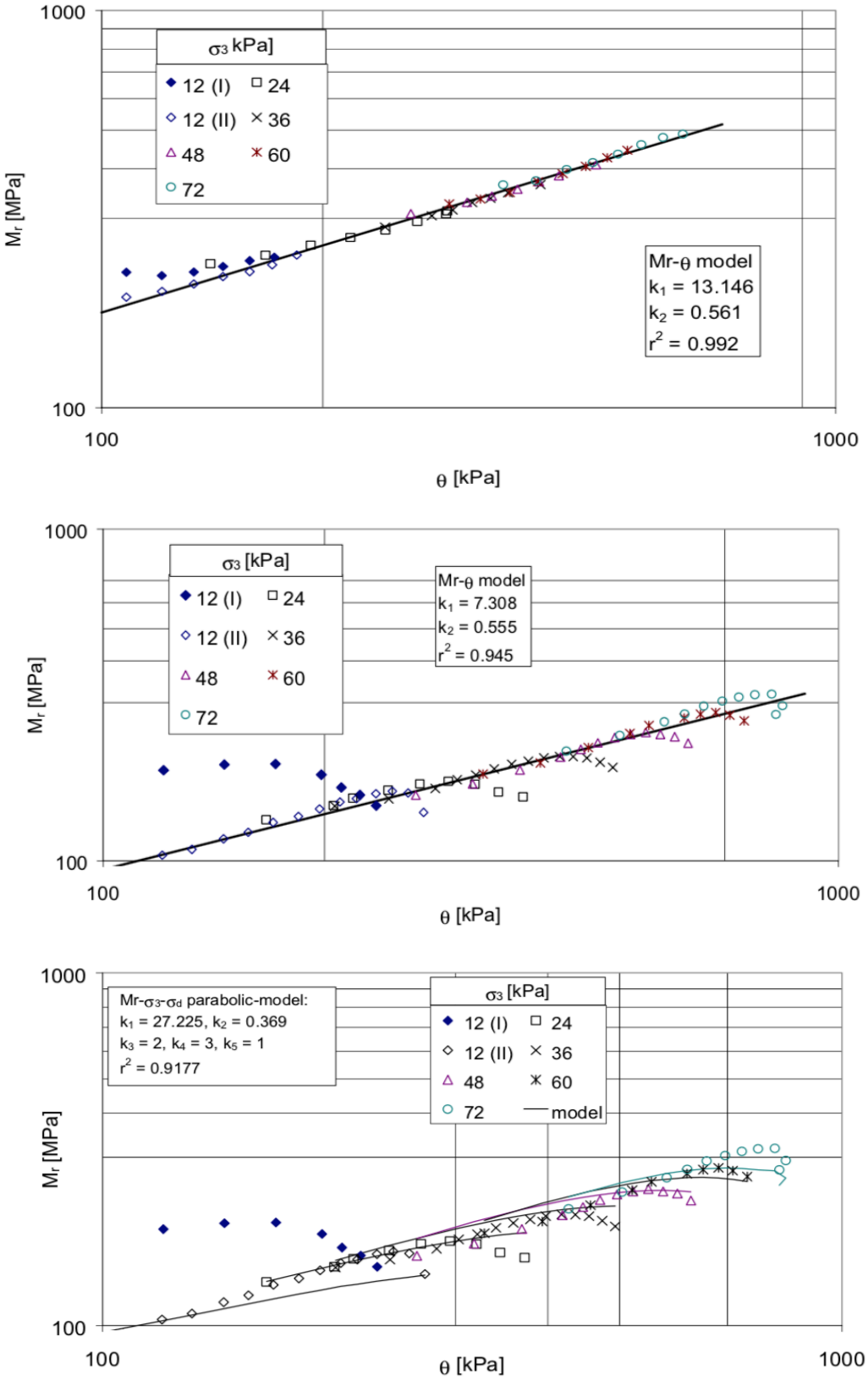

Figure 2.11: Resilient modulus test results by van Niekerk [14] **Top:** Mr - θ model at "mild" stress regime **Middle:** Mr - θ model at "severe" stress regime **Bottom** Adjusted Huurman model 2.9

2.5. UNBOUND GRANULATE PERMANENT DEFORMATIONS

As mentioned in Section 2.4, a part of the strains occuring when soils and unbound granulate materials are subjected to cyclic loading is permanent and irreversable. Accumulation of permanent strains after repetitive loading can cause significant deformations in a road structure (rutting) with potential loss of functionality. Resistance against permanent deformation is therefore an important performance parameter of (sub)base materials. It is believed that permanent deformations mainly occur due to re-orientation of grain particles [28]. When stressed, individual particles can slide or roll over each other resulting in rearrangement of the grain matrix. To what extent this happens is determined by the inter particle friction, which is in turn influenced by stress conditions, particle shape, grading, density, moisture content and loading history [1]. Stress conditions in combination with the number of load cycles have a major influence on the long term behavior. At low (deviator) stress levels, permanent deformations are usually limited. The change of permanent strain per cycle decreases with increasing load cycles until a purely elastic response is reached. Higher stress levels on the other hand can lead to progressive increase of permanent strains resulting in failure. This is also referred to as delayed shear failure. A typical representation of stable and unstable responses is illustrated in Figure 2.12.

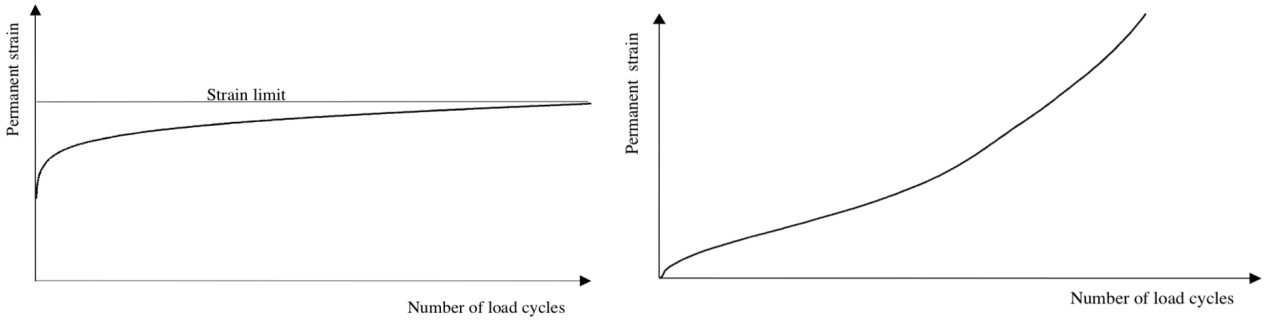

Figure 2.12: Permanent deformation behavior [28] **Left:** Stable, limited permanent strains **Right:** Unstable, progressive increase of permanent strains

Predicting whether or not unstable behavior occurs is intensively studied over the years but remains an extremely complex task [28]. For design purposes, it would be very usefull to know if, and after how many load cycles instablity can be expected. For instance, materials can show stable behavior in the beginning stages of the test, but still become unstable after a sufficient number of load cycles. This is shown in Figure 2.13. Furthermore, the aspect of variability within specimens (no specimen is the same) may not be underestimated. Especially when testing long term behavior, small imperfections can lead to substantial differences in results.

2.5.1. PERMANENT DEFORMATION TRIAXIAL TESTING

In the permanent deformation triaxial test, a specimen is loaded for a significant number of load cycles at a constant stress level. Although most standards limit the maximum required number of load cycles to 100,000, it is not uncommon to test up to 1,000,000 cycles for reseach purposes. It is a non-destructive test, but a specimen can only be used once because of permanent changes of the specimen integrity. Similar as in the resilient modulus test, see section 2.4.1, radial and axial LVDT's measure the occuring displacements. Stress levels are expressed as the ratio of (deviator) stress over the (deviator) failure stress ($\sigma_1/\sigma_{1,f}$, or $\sigma_d/\sigma_{d,f}$). Due to the large number of load cycles and the fact that at least three different stress levels need to be tested to obtain an accurate picture of the permanent deformation behavior [9], permanent deformation triaxial testing is time consuming. Nevertheless, permanent deformation tests give valuable insights in the long term behavior. In the past, several researchers have

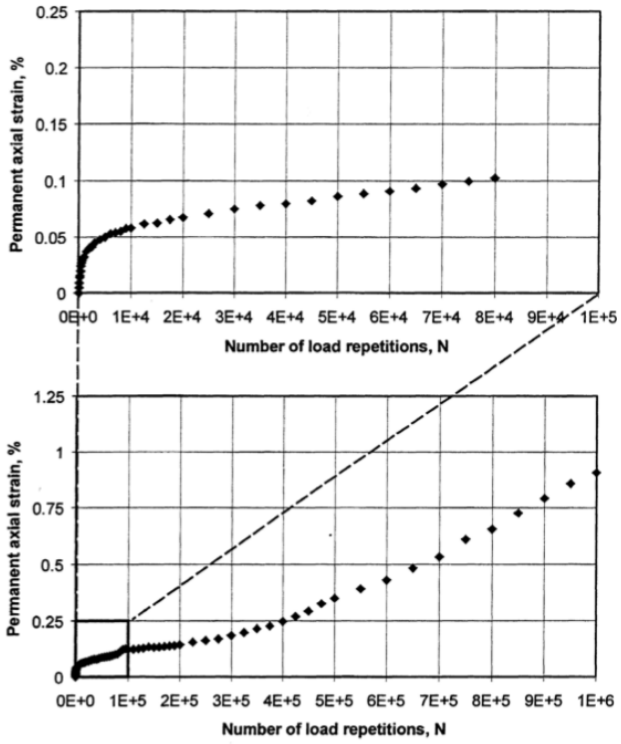

Figure 2.13: Permanent deformation testing [28] **Top:** Stable, after 80,000 load cycles **Bottom:** Unstable, after 1,000,000 load cycles

aimed to mathematically describe the permanent strain in terms of stress levels and number of load cycles. Sweere [25] for instance, suggested that the relation between permanent deformation and the number of load cycles should be approached as follows:

$$\epsilon_p = a \cdot N^b \tag{2.10}$$

Where:

ϵ_p = Permanent strain [10^{-4}]
N = Number of load cycles [-]
a, b = Model coefficients [-]

Huurman [10] extended this relationship with a term to describe unstable behavior:

$$\epsilon_p = A \cdot \left(\frac{N}{1000}\right)^B + C \cdot \left(e^{D \cdot \frac{N}{1000}} - 1\right) \tag{2.11}$$

Where:

ϵ_p = Permanent strain [%]
N = Number of load cycles [-]
A, C = Model coefficients [%]
B, D = Model coefficients [-]

The model parameters A, B, C and D are stress dependent. In case of stable behavior, model parameters C and D are zero. The following expressions, which contain stress components, showed to correlate well with obtained results:

$$A = a_1 \left(\frac{\sigma_d}{\sigma_{d,f}}\right)^{a_2} \qquad B = b_1 \left(\frac{\sigma_d}{\sigma_{d,f}}\right)^{b_2} \qquad C = c_1 \left(\frac{\sigma_d}{\sigma_{d,f}}\right)^{c_2} \qquad D = d_1 \left(\frac{\sigma_d}{\sigma_{d,f}}\right)^{d_2} \tag{2.12}$$

Where:

σ_d	= Deviator stress [kPa]
$\sigma_{d,f}$	= Deviator failure stress [kPa]
a_1, c_1	= Model parameters [%]
a_2, b_1, b_2, c_2, d_1, d_2	= Model coefficients [-]

2.5.2. SHAKEDOWN THEORY

In pavement design, it is aimed to limit permanent deformations in (sub)base layers as much as possible. In the ideal situation, only purely resilient deformations occur. Since this is practically impossible, pavements should be designed such that permanent deformations stay within an acceptable, controleable, limit. Several researchers in past have studied permanent deformations and identified the two different responses to loading illustrated in Figure 2.12. A widely accepted hypothesis is that there exists a certain stress level at which the response switches from stable to unstable [28]. Identifying this stress level and ensuring that the stresses in the pavement structure do not exceed this critical level is of great importance. To acquire better understanding of the material response under cyclic loading, the shakedown concept used to describe conventional building materials is adapted for unbound granulates. The original shakedown theory distinguishes four different responses to repeated loading, which are illustrated in Figure 2.14:

- **Purely elastic.** In this case, no permanent deformations or yields occur. The response is purely elastic starting from the first cycle.
- **Elastic shakedown.** Here, plastic deformations occur to a limited extent. The final response however is purely elastic. It is said that the material has "shaken down". The maximum stress at which elastic shakedown is still achievable is denoted as the elastic shakedown limit.
- **Plastic shakedown.** In this case, the plastic deformations are larger in comparison with the elastic shakedown. A stable resilient response is reached in the end, with no further accumulation of permanent strains. The materal however maintains to absorb a certain amount of energy at each cycle. The maximum stress level at which plastic shakedown can occur is referred to as the plastic shakedown limit.
- **Incremental collapse / ratchetting.** When the stresses are too high to reach a stable response, ratchetting may occur. Permanent strains caused by yielding accumulate progressively and lead ultimately to failure.

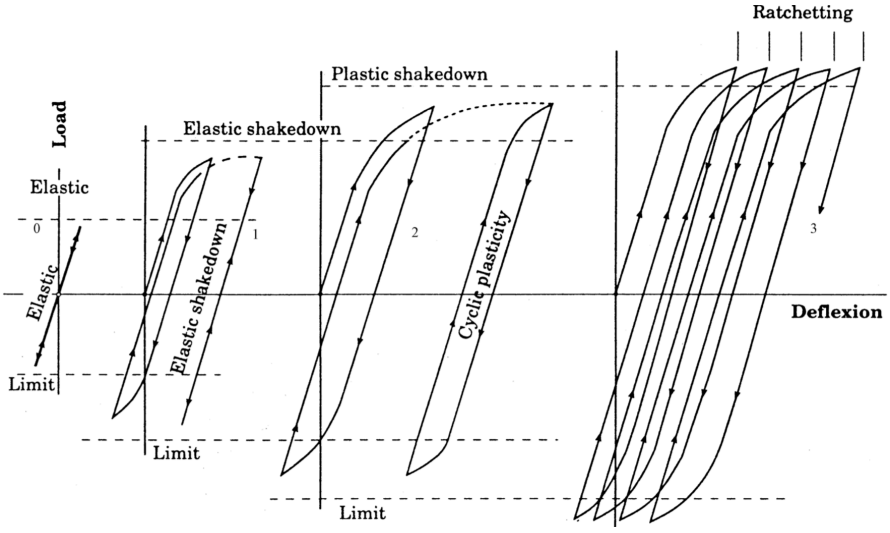

Figure 2.14: Shakedown principle for materials subjected to compressive - tensile load cycles [28]

In unbound granulates, a purely elastic response is never achieved [28]. Elastic shakedown might occur but only at very low stress levels. Besides that, they hardly can take any tensile stresses. Therefore, the shakedown theory as adapted in road engineering considers slightly different shakedown limits. Three ranges, illustrated in Figure 2.15, are distinguised:

- **Range A - Plastic shakedown.** Shakedown range A corresponds with plastic shakedown. It represents stable behavior. In the beginning of the test, a post compaction phase introduces relatively large permanent deformations. The strain rate however decreases considerably. After a finite number of load cycles, a purely resilient response is observed with no further accumulation of permanent strains.
- **Range B - Plastic creep.** Shakedown range B is the intermittent stage between range A and range C. After post compaction, the strain rate decreases towards a low but constant level. The accumulation of permanent strains continues almost linearly. After a significant number of load cycles, the strain rate slowly starts to increase which ultimately leads to failure. For a limited number of load cycles, the response might appear to be stable. At higher number of load cycles however, instability occurs. Figure 2.13 shows an example of typical range B behavior.
- **Range C - Incremental collapse.** Shakedown range C represents a progressive accumulation of permanent strains which quickly leads to collapse. In the very beginning stages of the test, the response might show similarities with the responses of range A and range B. The course of the curve however can be regarded as a "compressed" version of shakedown range B. A typical example of range C behavior is presented in Figure 5.5.

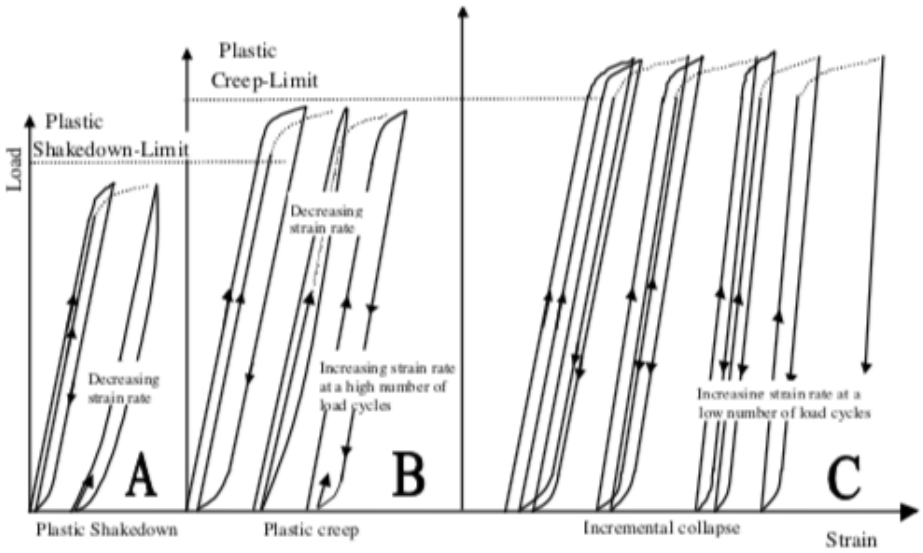

Figure 2.15: Shakedown principle adapted for granular materials subjected to compressive load cycles [28]

In practice, full plastic shakedown is desired. Range B is undesireable since collapse might occur in an early stage. Shakedown range C should be avoided at all times. The classification of responses can be made fairly accurate once the complete picture of a response (i.e. N > 1,000,000) is available. From there, the shakedown limits of the particular specimens can be derived. In most cases, however, tests are only conducted up to a limited number of load cycles. Distinguishing the different shakedown limits in the early stages of a test is desirable but can be difficult. To overcome this, Werkmeister proposed a set of boundary conditions which predict the shakedown range before cycle 5000 (see Section 5.1.3). The boundaries are somewhat subjective, but proved to function well in her results.

2.6. GRANULATE DURABILITY

Granular durability is commonly defined as the material resistance against crushing, attrition and abbrasion. Due to repetitive loading and environmental effects, particles wear out during their service life. This affects grading, texture roughness and grain shape, which in turn influences performance. In South Africa, problems regarding material detoriation during service life are known for many years [16]. Despite a variety of available durability tests, in field durability issues have often questioned the reliability of these tests. As a result, confidence in the durability of local available materials is hard to establish, leading to the import of 'better' materials with a known quality from further away. This significantly increases pavement costs. Paige-Green [16] recognized the shortcomings of the existing durability tests, and found that conflicting results between the tests appear to be the norm rather than the exeption. He concluded that no single South African durability test identifies potential durability issues of basic crystaline rocks satisfactorily, and that more than one type of test is required to ensure durablity of a material. One of methods which has according to Paige-Green significant potential is the "Durability Mill". The Durability Mill Index test, or DMI test, is based on the Texas Ball Mill from the Texas Highways Department [20] and has, compared to other aggregate durability tests such as the 10% FACT test and the Aggregate Impact Value (AIV) test the main advantage that it considers the complete grading instead of only a single particle size [17]. The outcome parameter of the durability mill, the Durability Mill Index, gives an indication of the degradation potential of the material and the generation of plastic fines. Limits of the durability mill index are used in the South-African National Standards to specify aggregate suitability. A brief summary of the background of the test is given below.

2.6.1. DURABILITY MILL

The durability mill is developed in the late 1980's by L.R. Sampson and F. Netterberg [20]. There was a need for a new, alternative aggregate durability test, which simulated more closely material degradation caused by traffic action. At several distressed roads, samples were taken from both sound and distressed wheel track areas. A common observation was that in almost all cases the Plasticity Index and the amount of fines was significantly higher in the distressed samples (see Table 2.1). The ratio of field moisture content over the (initial) optimum moisure content (FMC/OMC) appeared to be always higher in the distressed areas. A good correlation was found between the Fineness Product (FP, the product of the plasticity index and the mass percentage fines passing the 425 μm sieve) and the performance of the roads. From 77 field measurements, it was found that materials with a fineness product below 100% are likely to perform well. As this gets higher, the performance decreases. Values above 150% are almost all times related to poor performance. See also Figure 2.17. This finding resulted in the development of af test which expressed the potential material breakdown in terms of PI and degradation (grading). The test should also consider the whole grading and include a soaked state test. The durability mill test, shown in Figure 2.16, suited all these demands. The basic principle is that it simulates particle breakdown by milling material in a steel drum with steel balls under several conditions. To verify the test, the fineness products of distressed samples were compared with the fineness products of undisturbed, center lines samples which had undergone a DM simulation (the undisturbed center line samples where considered to be the best representation for the initial applied base course). Results between the two revealed very good agreement. The durability mill test showed the importance of grading, as significant differences where found between same, but differently graded materials.

In the Durability Mill Index test, a specimen with a known grading is divided into four subsamples [23]. The first subsample serves as reference sample, and is not milled in the durability mill. The other three samples are tested under the following conditions: Dry with steel balls, soaked with steel balls and soaked without steel balls. Each sample is milled for 10 minutes at an angular velocity of 1 rotation per second. After the test, the specimens are

Figure 2.16: Double barrel durability mill at Stellenbosch University

Table 2.1: Comparison of results from sound and distressed outer wheel track areas of similar basecourse material [20]

Site	Material	Condition	PI[1] [%]	P425[2] [%]	P075[1] [%]	Finess product[3] [%]	Soaked[4] CBR 2.5 mm [%]	FMC/OMC [-]
Hanover to Richmond	Beaufort	Sound	5	17	9	85	91	0.62
(9 / 8)	Sandstone	Distressed	8	25	17	200	74	0.90
Hanover to De Aar	Dolerite	Sound	6	20	8	120	107	0.62
(17 / 2)		Distressed	10	30	15	300	60	0.71
Port Alfred to East London	Tillite	Sound	4	21	7	84	89	0.62
(45 / 3)		Distressed	8	21	8	168	62	0.85

1. Mean of four results. P075 = percentage passing 0.075 mm sieve
2. Mean of two results. P425 = percentage passing 0.425 mm sieve
3. Fineness product = P425 x PI
4. At 98 % MAASTHO compaction
5. Inner wheel track in this case only

sieved and the fines (passing 425μm) are retained. The output parameter of the Durability Mill, the Durability Mill Index (DMI), is now defined as the product of the maximum mass percentage passing the 425μm sieve and the maximum Plasticity Index of the retrieved fines:

$$DMI_{0.425} = Max(p_{0.425}) \cdot Max(PI_{0.425}) \tag{2.13}$$

An important note on the verification of the durability mill is that only plastic materials are considered. According to the definition, the Plasticity Index greatly influences the Durability Mill Index. Since the recycled granulates RCA and RCM are known to be non-plastic (PI = 1), the DMI for these materials is in all cases lower than 100%. Following the quality judgement in Figure 2.17, this would imply that non-plastic materials will always be classified as sound, no matter the amount of breakdown. It can therefore be argued that the definition of the Durability Mill Index, as prescribed by the standards, is not suitable for non-plastic materials. This was also recognized by Sampson and Netterberg, which as an additional durability requirement suggested that the maximum mass percentage passing the 425μm sieve should not exceed 35%. Further research into the use of the durability mill for non-plastic materials was recommended but never conducted. In this research, DMI values are calculated but not used for further comparisons. The results of the durability mill are interpretated as potential mechanical breakdown, as the change in grading is considered the relevant outcome.

2.7. CHAPTER SUMMARY

In this chapter, the most relevant background theories supporting this research are discussed. Unbound granular failure behavior, stiffness and permanent deformation behavior are briefly explained. The corresponding triaxial testing methods are currently regarded as the most accurate ways to simulate the behavior of unbound granulates in pavement structures. Over the years, models have been developed to mathematically describe the complex behavior of unbound granular materials. Although shortcomings still exist, the models fairly accurate describe the observed response. Predicting delayed shear failure after repetitive cyclic loading is intensively studied but still not fully understood. The shakedown theory applied by Werkmeister however might serve as tool to identify long term behavior in the beginning stages of the test. The applicability of this theory is therefore be checked with the permanent deformation triaxial tests results obtained in this research. As a final remark, it is noticed that the current calculation of the Durability Mill Index is most likely not sufficient to describe the durability of non-plastic (recycled) materials. Therefore, not the DMI values but the mechanical degradation potential (change in grading) is emphasized during the course of this research.

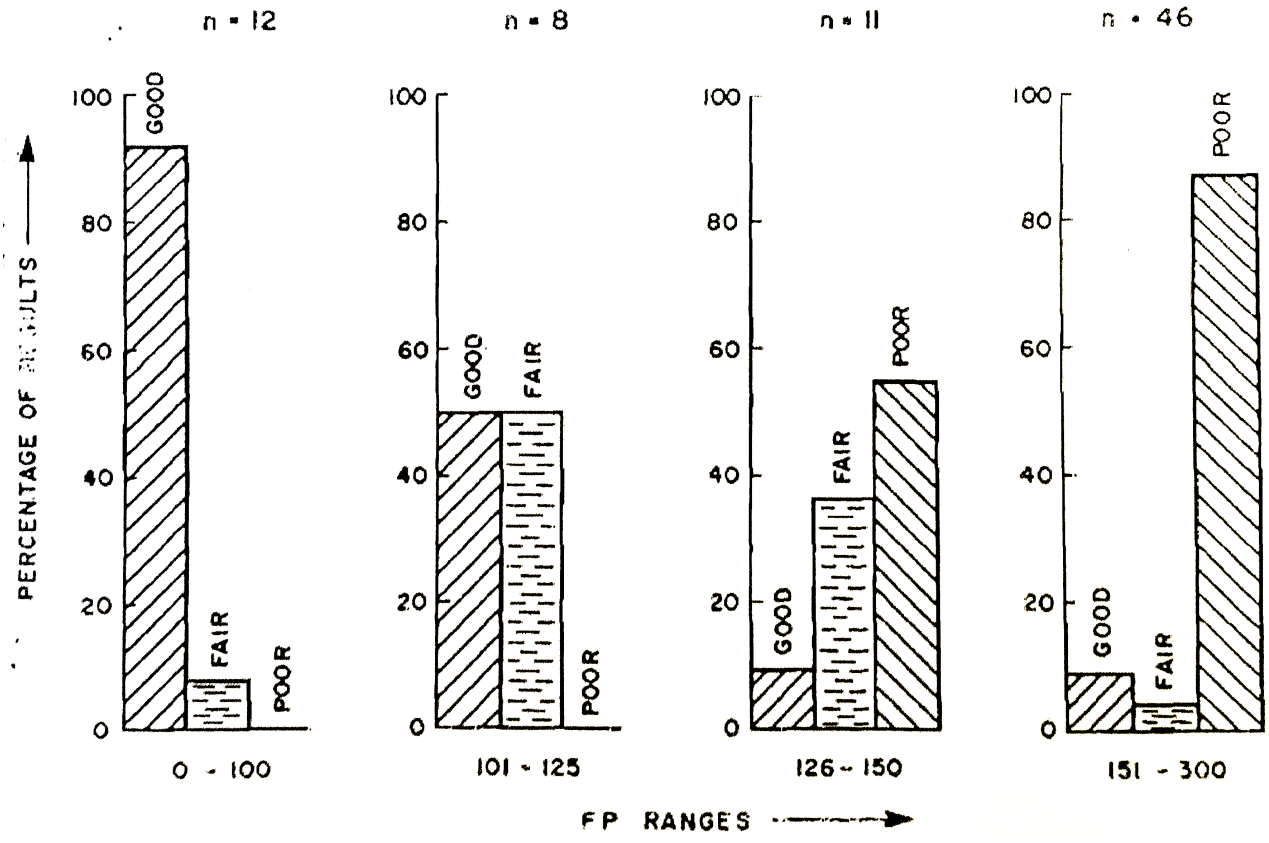

Figure 2.17: Performance-related results at different ranges of FP for basecourse in the outer wheel track [20]

3

METHODOLOGY

This chapter briefly discusses the set-up of the research, testing scale and test procedures followed. Emphasis is placed on the triaxial sample preparation, since no conventional South African standard is available. Some overall points of attention are reported which have shown to increase consistency between specimens and therefore improve confidence in the results. Preliminary test results needed beforehand, such as optimum moisture content and maximum dry density, are also presented in this chapter.

3.1. EXPERIMENTAL PLAN

A summary of the experimental plan, testing scale, sample composition, grading and testing conditions is given in Table 3.1. The contents of the table is explained in more detail in the following paragraphs.

Table 3.1: Scale and test overview

Scale overview

	Durability mill	Monotonic triaxial test		Permanent deformation triaxial test	
		Before DMI	After DMI	Before DMI	After DMI
Output	DMI, Grading	ϕ, c	ϕ, c	ε_p , d_f, Grading	ε_p , d_f
Composition	5	4	4	2	2
Grading	1	1	1	1	1
Moisture content	-	1	1	1	1
Degree of compaction	-	1	1	1	1
Tests per specimen	3	6	6	3	3
Total tests	**15**	**24**	**24**	**6**	**6**

Test overview

	Durability mill	Monotonic triaxial test		Permanent deformation triaxial test	
		Before DMI	After DMI	Before DMI	After DMI
Output	DMI, Grading	ϕ , c , grading	ϕ , c	ε_p , d_f	ε_p , d_f
Composition	G2, RCA, RCM, MG65, MG30	G2, RCA, MG65, MG30	G2, RCA, MG65, MG30	RCA, MG65	RCA, MG65
Grading	G2 scalped+added	G2 scalped+added	Output DMI	G2 scalped+added	Output DMI
Moisture content	-	OMC	OMC initial material	OMC	OMC initial material
Degree of compaction (Vibratory hammer SU)	-	97%	97% initial material	97%	97% initial material
Confinement stress	-	2 x 50 kPa 2 x 100 kPa 2 x 150 kPa	2 x 50 kPa 2 x 100 kPa 2 x 150 kPa	100 kPa	100 kPa
Deviator stress ratio ($\sigma_d/\sigma_{d,f}$)	-	-	-	1 x 25% milled material 1 x 30% milled material 1 x 35% milled material	1 x 25% 1 x 30% 1 x 35%
Total tests	**15**	**24**	**24**	**6**	**6**

Nomenclature:
DMI: Durability Mill Index
RCA: Recycled Concrete Aggregate
RCM: Recycled Crushed Masonry
MG65: Mixed Granulates, 65%RCA - 35%RCM
MG30: Mixed Granulates, 30%RCA - 70%RCM

3.1.1. MATERIALS

The materials considered in this research are RCA (Recycled Concrete Aggregate), RCM (Recycled Crushed Masonry), two blends of mixed granulates and a South African G2 material. The latter is a widely used South African base course material and added as reference. The blends are composed and refered to as follows, with the number indicating the mass percentage concrete:

- MG65: 65% RCA, 35% RCM (% by mass);
- MG30: 30% RCA, 70% RCM (% by mass);

Initially, three blends corresponding to Van Niekerk (MG50, MG65 and MG80, [14]) were to be tested, but due to time considerations MG50 was omitted. When the first triaxial results of the RCA and MG65 became available, it was decided to rather test a blend outside the practical range (for instance in the Netherlands, the percentage RCA should at least be 50% [5]), to gain a better understanding of the influence of masonry content. Therefore MG80 is changed to MG30, where the mass percentage interval of concrete between the RCA and the two blends is maintained constant at 35%.

All five compositions are tested in the durability mill. However, only a selected number of compositions are subjected to permanent deformation testing. Considering the amount of time, permanent deformation tests are only carried out on the pure RCA and MG65. For the monotic triaxial tests, all compositions are tested except the pure RCM. The influence of masonry content on performance is definitely important, but the performance of pure RCM is considered less relevant.

Figure 3.1: Recycled granulates **Left:** RCA & RCM particle fractions **Right:** Composition of a MG65 sample

3.1.2. GRADING

The initial grading for all materials is derived from the average grading of a G2 material. It is based on good packing and particle interlock, and in line with what is currently used in other RCA research performed at Stellenbosch University. Because of the triaxial specimen size of 300 x 152 mm, testing the full grading is not possible (see Section 2.2.2. Particles larger than 20 mm are therefore removed (scalped) and replaced (added) with an equal mass of particles from the largest remaining fraction (14 mm - 20 mm). This "20 mm scalped+added" grading, or "G20C" grading, gives a better representation of the full grading compared to just scalping, as it equals the full grading curve until the largest fraction (See also Table 3.2). It is shown that this grading also gives the best approximation of the

performance, when compared to the large size triaxial specimen (600 x 300 mm) containing the full grading [29]. In the durability mill, only the G20C grading is tested. The original plan stated that DMI testing of the full graded specimens would be considered as well. However, when it became clear that sieving was one of the more time consuming aspects of the laboratory work, it appeared to be not realistic to take this into account as well. Note that the design grading is based on the new sieve sizes prescribed by the South African National Standards (SANS) [21].

Table 3.2: Design grading - G2 average & G2 average 20 mm scalped+added

Lab sieves	Average G2		Average G2 - 20mmS&A	
[mm]	Retained [%]	Passing [%]	Retained [%]	Passing [%]
37.5	0	100	0	100
28	11	89	0	100
20	23	78	0	100
14	33	67	33	67
5	56	45	56	45
2	69	32	69	32
0.425	83	18	83	18
0.075	92	8	92	8
Pan	100	0	100	0

In Figure 3.2, the grading curve boundaries prescribed by the standards for a G2 material are presented. The average G2 grading and the 20 mm scalped+added grading are plotted as well. For the blends, the mass ratio RCA/RCM will be present in all fractions, meaning that both RCA and RCM start with the same grading curve. It is expected that this ratio will change after durability mill simulation, as the RCA and the RCM will probably break down differently.

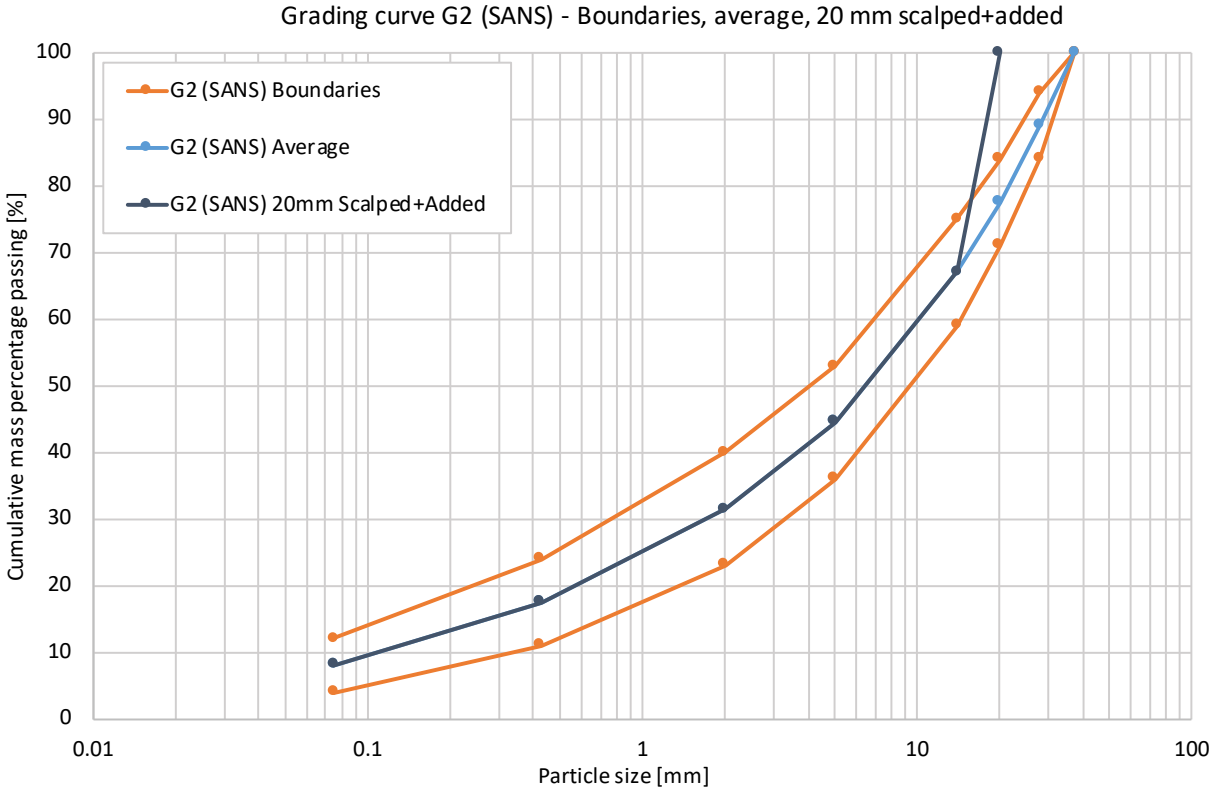

Figure 3.2: Design grading - Average G2, average G2 20 mm scalped+added (G20C) and G2 boundaries

3.1.3. RESOURCES

Figure 3.3 shows the 14 - 20 mm fractions of the G2, RCA and RCM used in this study. The recycled aggregates need to be crushed beforehand. This is done with a laboratory jaw crusher. All materials are then sieved out dry in the separate particle fractions according to the design grading (see Table 3.2). Note that these are only the fractions prescribed for a G2 grading, and that the standards actually distinguishes also particle fractions in between [22]. Therefore, reference gradings with the full sieve set are performed on the untested materials to determine the actual grading of the designed samples (3.2.3). The gradings obtained after testing are all carried out with the full sieve set as well.

Figure 3.3: Material fractions 14 mm **Left:** G2 **Middle:** RCA **Right:** RCM

G2 BASECOURSE MATERIAL

The G2 material used in this research is of a is a continuously graded crushed rock of Hornfels geology and originates from a quarry in Tygerberg, South Africa. The name G2 rather refers to the material quality and not to the type of rock alone. The South African road autorities (SANRAL) ranks granular, gravel and sandy materials into ten different categories. G1 is the highest available quality, G10 the lowest. Requirements exist for grading, particle shape, Atterberg Limits, crushing strength and bearing strength (CBR). An extract of the classification system from the South African pavement engineering manual[21] for G1 up to G6 is included in Appendix A.

RECYCLED CONCRETE AGGREGATE (RCA)

The Recycled Concrete aggregate is sourced from a concrete pavement between Borcherds Quarry and Swartklip interchange in Cape Town (National Route 2). Originally, this road was a Jointed Unreinforced Concrete Pavement (JCP) constructed between 1971 and 1972. Not long after construction, akali silica reactions caused excessive expansion in the concrete slabs resulting in severe cracking at the contraction joints. Measures were taken in 1986 to reduce further crack development and the most heavily damaged joints were replaced with new concrete. The measures proved succesfull, as no major maintenance was carried out until 2016, when it was identified that the pavement had deteriorated to such an extent that it qualified for an investigation. This ultimately led to the scheduling of periodic maintenance to extent the service life of the road for ten years.

RECYCLES CRUSHED MASONRY (RCM)

The Recycled Crushed Masonry originates from industrial processed bricks. The exact quarry and manufacturer are unknown. Formerly, the masonry was used in an experimental set-up in the water laboratory of Stellenbosch University. After breaking down the experiment, the materials were left to dry and subsequently crushed with the laboratory jaw crusher.

QUANTITIES

Table 3.3 shows the total amount of materials used in this research. The dry mass of the triaxial specimen is a rounded value based on the sample volume and a raw approximation of the dry density.

Table 3.3: Estimated amount of materials used

		G2	RCA	RCM	MG65	MG30	Total
Preliminary testing							
Dry mass per reference sieving	[kg]	3.75	3.75	3.75	3.75	3.75	
Number of reference sievings	[-]	6	3	6	3	3	
Mass per OMC measurement - vib.mod	[kg]	25	25	0	25	25	
Total mass preliminary testing	**[kg]**	**48**	**36**	**23**	**36**	**36**	**179**
Performance testing							
Dry mass per unmilled specimen	[kg]	15	13	-	13	12	
Dry mass per milled specimen	[kg]	15	15	-	15	15	
Number of unmilled triaxial specimens	[-]	6	9	-	9	6	
Number of milled triaxial specimens	[-]	6	9	-	9	6	
Number of trial / extra triaxial specimen	[-]	0	3	-	0	0	
Total mass performance testing	**[kg]**	**180**	**291**	**-**	**252**	**162**	**885**
Durability testing							
Dry mass per DMI test (contains 3 drums)	[kg]	11.25	11.25	11.25	11.25	11.25	
Number of DMI specimen	[-]	6	3	3	3	3	
Number of trial / extra DMI specimen	[-]	0	0	0	0	0	
Total mass durability testing	**[kg]**	**68**	**34**	**34**	**34**	**34**	**203**
Estimated mass per composition	**[kg]**	**295**	**361**	**56**	**322**	**232**	**1266**
Estimated mass per material	**[kg]**	**295**	**640**	**331**	-	-	**1266**

3.1.4. DURABILITY TESTING

The durability mill is used to determine the extent of material breakdown and for preparing the materials for the simulated triaxial tests. Three DMI tests are performed per material composition. Each test contains a dry ball mill, a wet ball mill and a wet mill, meaning that nine drums are milled per material. Samples are composed according to the 20 mm scalped+added (G20C) grading. The Durability Mill Index (DMI) is then determined according to the procedure described in Chapter 3.3. In addition to what the standards prescribe, samples coming out of the durability mill are sieved out to obtain the full grading. For the preparation of the material for triaxial testing after durability simulation, it is chosen to mill 100% according to the wet ball mill procedure (see Section 3.3). It is believed that wet ball milling creates the worst case conditions for simulating material durability, and that this will result in the most particle breakdown. Later on, the results however show that this is not always the case, and that for the blends dry milling even causes slightly more degradation. This is discussed in more detail in Section 4.2.1).

3.1.5. PERFORMANCE TESTING

Performance testing is carried out on small scale specimens of 300 x 152.5 mm by both monotonic and permanent deformation triaxial testing. The resilient properties are not included considering time limitations. The angle of

internal friction and cohesion are obtained by monotonic triaxial testing with varying confinement stress. Tests are performed before and after durability milling to see how the durability simulation affects the shear parameters. For the permanent deformation tests, the same set-up is used. In this case, however, the specimens are loaded dynamically up to 250,000 load repetitions. The development of permanent strain is then plotted against the number of load cycles. Comparisons are made between permanent deformation behavior before and after durability milling, and between the materials. Due to time limitations, only a limited amount of permanent deformation tests are included in this research. After permanent deformation testing, intact specimens of the unmilled batches have been subjected to a monotonic triaxial test and sieved out. The resulting grading and failure stress are then compared with the durability milled monotonic triaxial tests.

All triaxial specimens are compacted to 97% degree of compaction at optimum moisture content. Determination of the maximum dry density and optimum moisture content is not carried out by Proctor compaction, but by compaction with the (heavier) vibratory compacter (see Section 3.4.4). Doing so leads to a better representation of field compaction, and is consistent with the way the triaxial specimens are compacted. Due to an expected change in grading after durability milling, the maximum dry density and optimum moisture content have most likely changed as well. This however is not taken into account, and the milled specimens are designed with the same dry density and moisture content as the unmilled specimens. Modified Proctor testing to relate the vibratory densities to was considered, but, due to lack of time, not performed. The triaxial specimens coming out of the triaxial machine have been broken down and placed in the oven. After drying, the actual moisture content and dry density are recorded and compared to the target values.

MONOTONIC TRIAXIAL TESTING CONDITIONS

Before durability mill simulation, six monotonic triaxial tests are performed per material. Tests are performed under confinement stresses of 50 kPa, 100 kPa and 150 kPa, two for each confinement. See also Table 3.1. After testing, three of these unmilled (initial) specimens have been sieved out to see how compaction and shearing has degraded the material. This initial degradation is then compared with the durability mill results. After durability simulation, an additional six monotic triaxial tests are performed under similar conditions.

PERFORMANENT DEFORMATION TRIAXIAL TESTING CONDITIONS

Permanent deformation tests are carried out on RCA and MG65. Six tests are performed per material; three before durability simulation and three after durability simulation. The confinement stress is kept constant for all tests at 100 kPa. This is a representative average value of what can typically be found in South African basecourse layers. The loading depends on the applied deviator stress ratio (the ratio of deviator stress over the failure deviator stress $\sigma_d/\sigma_{d,f}$, also denoted as DSR, where $\sigma_{d,f}$ is the failure deviator stress measured in the first set of the monotonic triaxial tests). For comparability, the loading levels before and after durability simulation are kept equal. The deviator stress ratios are therefore taken at 25%, 30% and 35% based on the milled materials. This means that the milled and unmilled specimens are loaded equally, but have different deviator stress ratios. The applied number of load cycles is 250,000. Kotze [12] concluded in his study that the number of load cycles required by most international standards is too little to obtain an accurate understanding of the long term behavior. Models predicting long term behavior based on only a limited number of load cycles (i.e. N = 10,000) significantly deviated from the results in case the specimens were tested longer. Together with this, although some models are able to describe unstable behavior, none can actually predict it. If instability does not occur in the modelled range, the models will not describe eventual failure later on. In practice, it is often observed that initially stable specimens become unstable at a later stage (Figure 2.13). For these two reasons, a higher number of load repetitions is preferred. In South Africa, the required number of load cycles is at least 100,000 [21]. In this research however, it is chosen to even test up to 250,000 cycles. The South African Pavement Design Method furthermore prescribes a load frequency of 1 Hz, which means that it takes 2.5 days

per permanent deformation test to complete. After the permanent deformation test, the specimens are subjected by a monotonic test to see if the shear strength is influenced by density increase and/or particle wear.

3.1.6. TESTING PROCESS

Due to the variety of tests, required test sequence, oven capacty and running time of the permanent deformation tests, it is of importance to develop process schemes to make testing efficient. Only one material is considered at the time. Doing so has the following advantages:

- Testing one material at the time reduces the risk of accidentally mixing up blends or results and ensures higher confindence in the quality of testing.
- In case of unforseen circumstances or extreme delays, it is possible to leave one blend out. (This was the case when it became clear that there was too little time to test a third blend.)
- Less storage space is needed as not all blends and milled materials are needed at the same time.
- Less repetitive work due to an equal distribution of the different tests.

Two different testing procedures can be distinguished, depending on whether permanent deformation triaxial testing is included or not. Figures 3.4 and 3.5 show the two processes. The processes are divided into phases to clarify the testing order. The arrows connecting the tests represent the flow of materials. Both processes are explained in more detail in the following paragraphs. Since the loading levels of the permanent deformation triaxial tests are based on the failure stress of the milled 100 kPa monotonic triaxials tests, it is necessary to start with milling of the materials. Although this is not required for the materials containing only monotonic triaxial tests, the same approach is adapted for consistency.

PROCESS 1 - MONOTONIC TRIAXIAL TESTING WITH DURABILITY MILL SIMULATION

This testing process considers the materials G2 and MG30 (Figure 3.4). First, the (original) materials are milled in batches of 3.75 kg in order to prepare them for the milled monotonic triaxial tests. All materials are simulated according to the wet ball mill procedure described in Section 3.3. Considering oven space, three specimens can be milled at the time. This means that milling and triaxial testing is done in batches of three and that this loop is repeated twice. While drying out the milled materials, the optimum moisture content and hygroscopic moisture content is determined. After phase one, DMI tests are performed on nine 20 mm scalpled+added (G20C) graded samples and sieved out. The six unmilled monotonic triaxial specimens are then prepared and tested. Finally, after sieving, plasticity index tests are performed on the fines extracted from the DMI tests and reference samples. In total this process consists of twelve monotonic triaxial tests and three DMI tests. The total testing time is approximately three weeks.

PROCESS 2 - MONOTONIC AND PERMANENT DEFORMATION TRIAXIAL TESTING WITH DURABILITY MILL SIMULATION

This testing process considers the materials RCA and MG65 (Figure 3.5). It is equal to the testing process containing only monotonic triaxial tests, except that six permanent deformation tests are added. Milling and triaxial testing are again performed in batches of three; one permanent deformation specimen and two monotonic specimens at a time. The failure stress from the 100 kPa monotonic tests serve as input for the loading level of the permanent deformation tests. In total this process consists of twelve monotonic triaxial tests, six permanent deformation triaxial tests and three DMI tests. The total testing time is approximately three weeks.

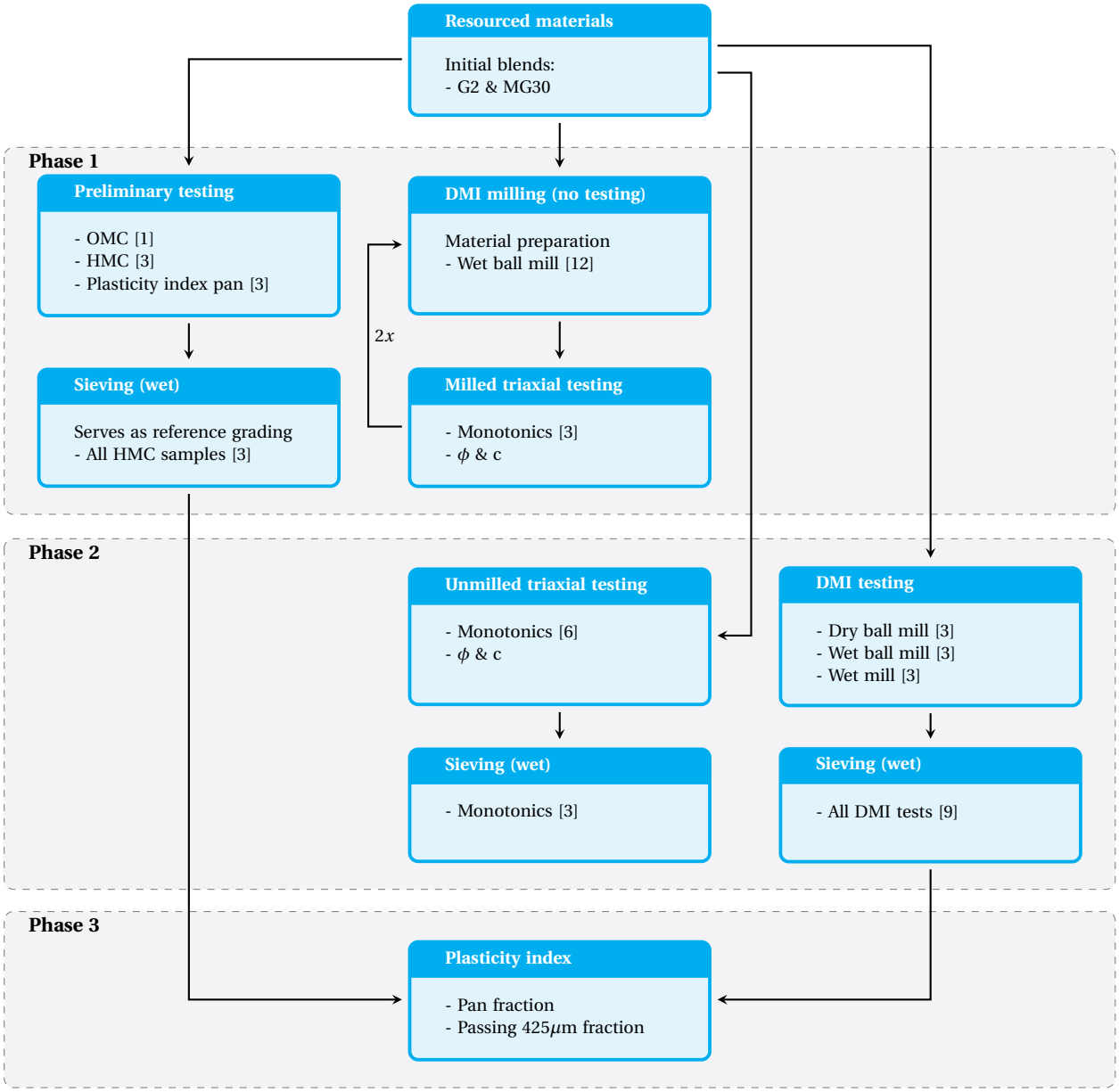

Figure 3.4: Testing process without permanent deformation tests. Performed on G2 and MG30

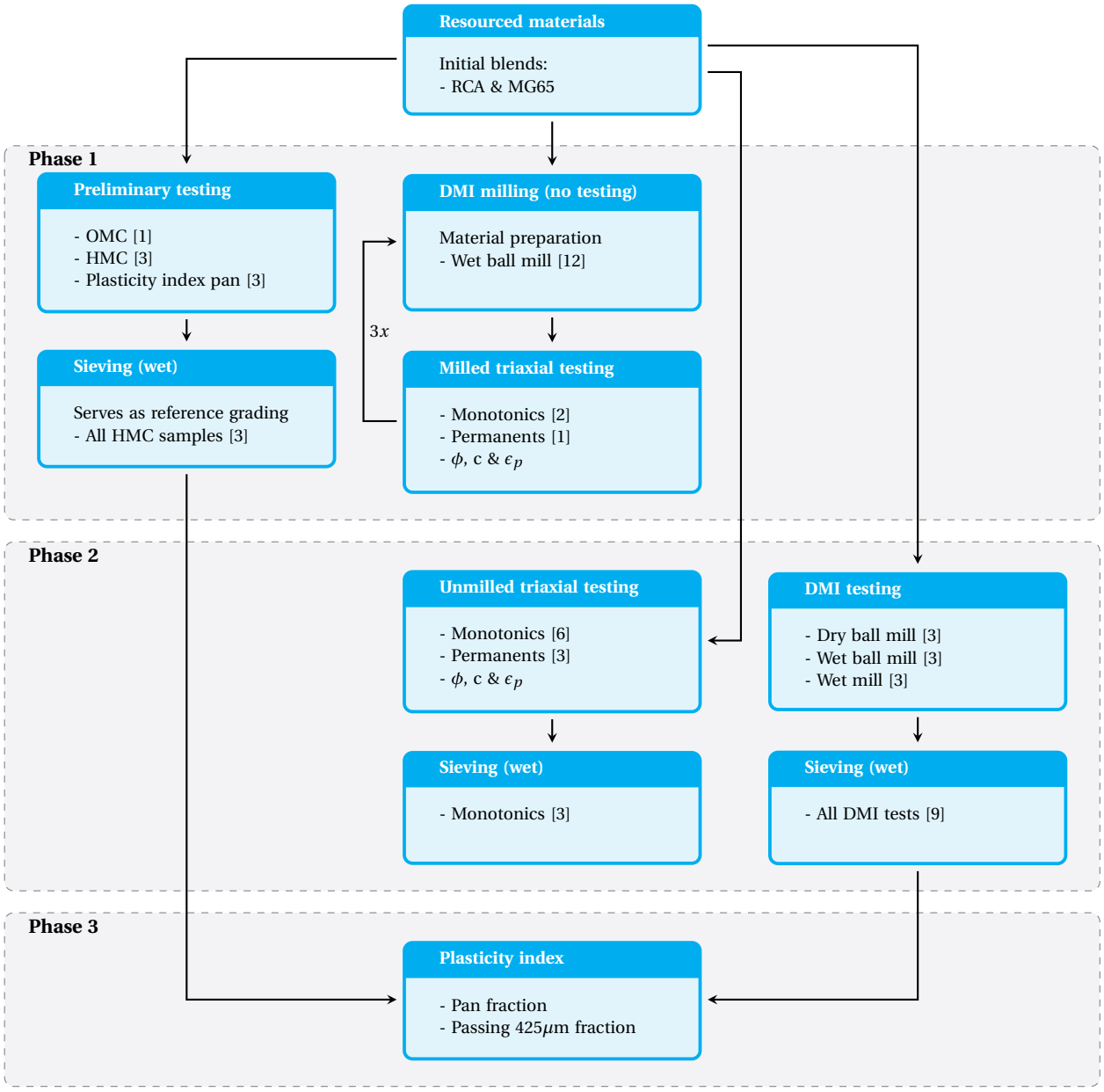

Figure 3.5: Testing process with permanent deformation tests. Performed on RCA and MG65

3.2. PRELIMINARY TESTING

3.2.1. HYGROSCOPIC MOISTURE CONTENT

The hygroscopic moisture content, also denoted as HMC, is the moisture content of the aggregate particles under air dried conditions. It is influenced by material type and local humidity. The hygroscopic moisture content is of importance for triaxial sample preparation as it influences the amount of water which must be added to reach the target moisture content. It is determined on the reference samples from section 3.2.3 before sieving by weighing the materials before and after 24 hours oven drying. The (hygroscopic) moisture content is then calculated by dividing the mass of the evaporated water by the dry mass of the aggregates. Table 3.4 shows the results for all reference samples. The average of the samples serve as the reference hygroscopic moisture content for the material under consideration. It can be seen form the table that the RCA attracts the most moisture, decreasing almost linear with increasing masonry content.

Table 3.4: Hygroscopic moisture content of the reference samples

Material	ID	Air dry sample [g]	Oven dry sample [g]	Mass water [g]	Hygroscopic MC [%]	Average MC [%]
G2	G2-INITIAL-S1	3751	3742	9	0.24	**0.24**
	G2-INITIAL-S2	3751	3742	9	0.24	
	G2-INITIAL-S3	3751	3742	9	0.24	
RCA	RCA-INITIAL-S4	3754	3680	74	2.01	**2.05**
	RCA-INITIAL-S5	3754	3675	79	2.15	
	RCA-INITIAL-S6	3753	3678	75	2.04	
	RCA-INITIAL-S7	3752	3678	74	2.01	
RCM	RCM-INITIAL-S1	3754	3738	16	0.43	**0.43**
	RCM-INITIAL-S2	3753	3738	15	0.40	
	RCM-INITIAL-S3	3753	3736	17	0.46	
MG65	MG65-INITIAL-S1	3753	3695	58	1.57	**1.57**
	MG65-INITIAL-S2	3752	3694	58	1.57	
	MG65-INITIAL-S3	3754	3696	58	1.57	
MG30	MG30-INITIAL-S1	3753	3716	37	1.00	**0.97**
	MG30-INITIAL-S2	3753	3717	36	0.97	
	MG30-INITIAL-S3	3754	3719	35	0.94	

3.2.2. OPTIMUM MOISTURE CONTENT

Density has a significant influence on the mechanical behavior of unbound granulates. In general, it is aimed to achieve the highest density as possible, as this greatly improves performance. The maximum achievable dry density (MDD) depends on the compaction energy and the moisture content. At a certain moisture content (with constant compaction energy), the dry density reaches a maximum. The moisture content at this maximum is referred to as the optimum moisture content (OMC). Finding the optimum moisture content and the corresponding dry density is usually done with a (modified) Proctor or AASHTO test. In this case however, the vibratory compactor method is used. This method is widely used within Stellenbosch University and is in principle equal to the Proctor and AASHTO test. The main difference is that specimens are compacted with the vibratory compator instead of a falling weight, resulting in a greater compaction energy. This gives gives a better indication of achievable densities of the triaxial samples (since the same compactor is used) and is a much closer representation of field compaction. The vibratory compactor, shown in Figure 3.12, is discussed in more detail in Section 3.4.4.

Determining the optimum moisture content is carried out by weighing and mixing a 5 kg sample with a certain target amount of moisture. The sample is then compacted in two layers, with a compaction time of 60 seconds per layer. After demolding, the mass and height (at four points) are measured. The specimen is broken down, placed in the oven and dried for at least 24 hours. With the wet mass, dry mass and height known, the actual moisture content and dry density can be calculated. This process is repeated with increasing moisture content to obtain the moisture content - dry density plot. A regression line is then drawn through the points to indicate the MDD and OMC. Figure 3.6 and Table 3.5 present the results of the OMC tests for all materials. The design moisture content is taken as a rounded value of the optimum moisture content. For the RCA and MG30, a slightly lower value was chosen because the materials appeared to be too wet and less workable at OMC. Especially for MG30 the moisture content could be chosen lower without significantly influencing the maximum achievable dry density. The design dry density is taken as 97% of the maximum dry density. Coincidently and erroneously, the design degree of compaction for the pure RCA is 100% instead of 97%. This is marked in red. More detailed results of the OMC tests per specimen can be found in Appendix C.1.

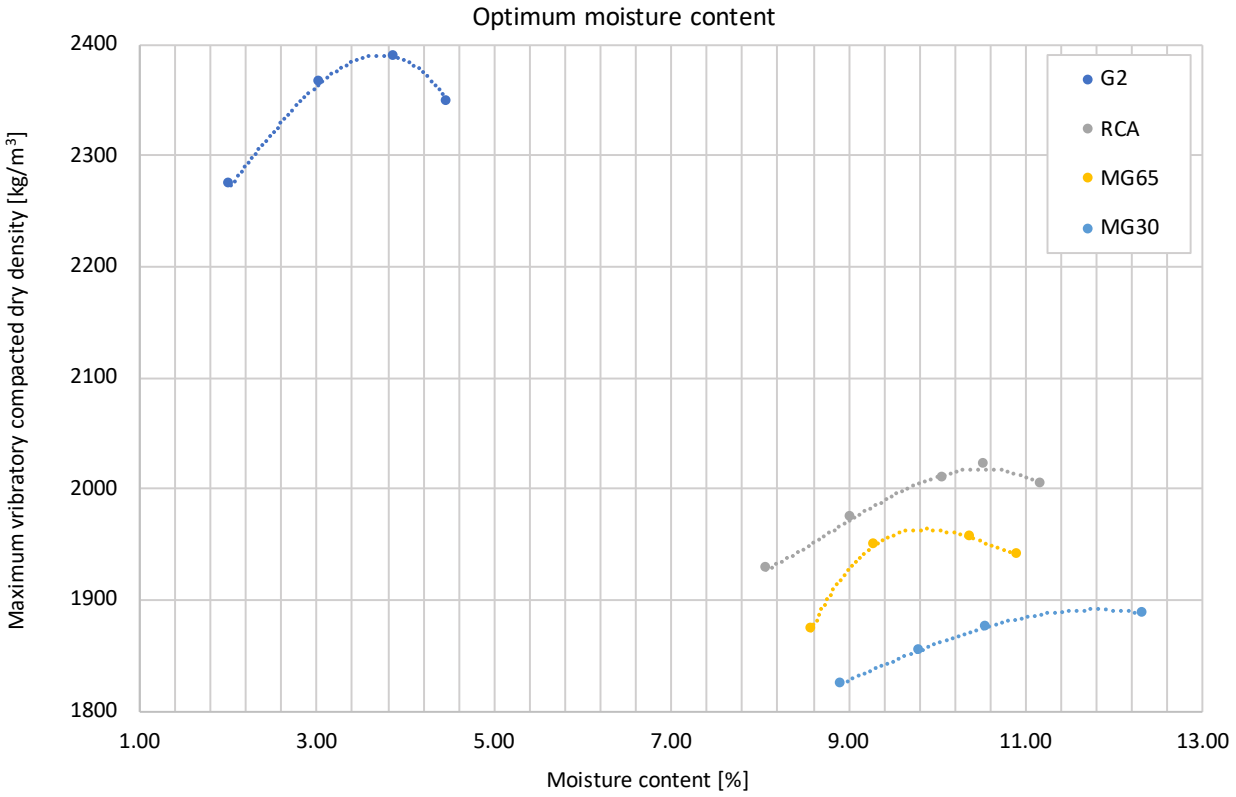

Figure 3.6: Optimum moisture content test results for G2, RCA, MG65 and MG30

Table 3.5: Design moisture content and dry density

Material	Optimum moisture content [%]	Maximum dry density [kg/m^2]	Design degree of compaction [%]	Design moisture content [%]	Design dry density [kg/m^2]
G2	3.72	2390	97	3.70	2318
RCA	10.52	2018	100	10.00	2018
MG65	9.86	1964	97	10.00	1905
MG30	11.50	1890	97	10.50	1833

3.2.3. REFENCE GRADING

The reference gradings are the actual gradings of the weighed-off samples. As the design grading considers only six of the twelve sievable fractions, the exact particle distribution is not known. In addition it is noted that all materials (especially G2) are covered with dust, meaning that the pan fraction is actually slightly higher than designed for. It is important to know the exact grading, so three samples of 3.75 kg per material have been sieved without any testing. The average of the three then serves as reference grading for the material under consideration. Table 3.6 and Figure 3.7 show the actual grading curves compared to their design grading curves. Apart from the G2, which contains more fines, they appear to be comparable.

Table 3.6: Particle distributions of the reference samples: Cumulative mass percentage passing

Sieve [mm]	Particle fraction [mm]	Design grading [%]	G2-INITIAL-S [%]	RCA-INITIAL-S [%]	RCM-INITIAL-S [%]	MG65-INITIAL-S [%]	MG30-INITIAL-S [%]
37.5	> 37.5	100	100.0	100.0	100.0	100.0	100.0
28	37.5 - 28	100	100.0	100.0	100.0	100.0	100.0
20	28 - 20	100	100.0	100.0	100.0	100.0	100.0
14	20 - 14	67	68.5	68.9	68.1	67.4	70.4
10	14 - 10	Not defined	58.1	57.0	60.3	59.7	62.4
7.1	10 - 7.1	Not defined	51.4	48.4	52.9	52.1	53.0
5	7.1 - 5	45	44.9	44.4	45.2	44.1	45.2
2	5 - 2	32	32.3	31.8	32.1	31.0	32.3
1	2 - 1	Not defined	26.7	25.4	24.9	24.3	25.0
0.6	1 - 0.6	Not defined	23.7	21.1	20.6	19.9	20.9
0.425	0.6 - 0.425	18	21.7	18.0	18.3	17.6	18.5
0.3	0.425 - 0.3	Not defined	19.3	15.6	15.9	14.9	16.2
0.15	0.3 - 0.15	Not defined	14.3	10.6	11.7	10.8	12.1
0.075	0.15 - 0.075	8	11.3	8.9	9.0	8.8	9.6
Pan	< 0.075 (pan)	0	0.0	0.0	0.0	0.0	0.0

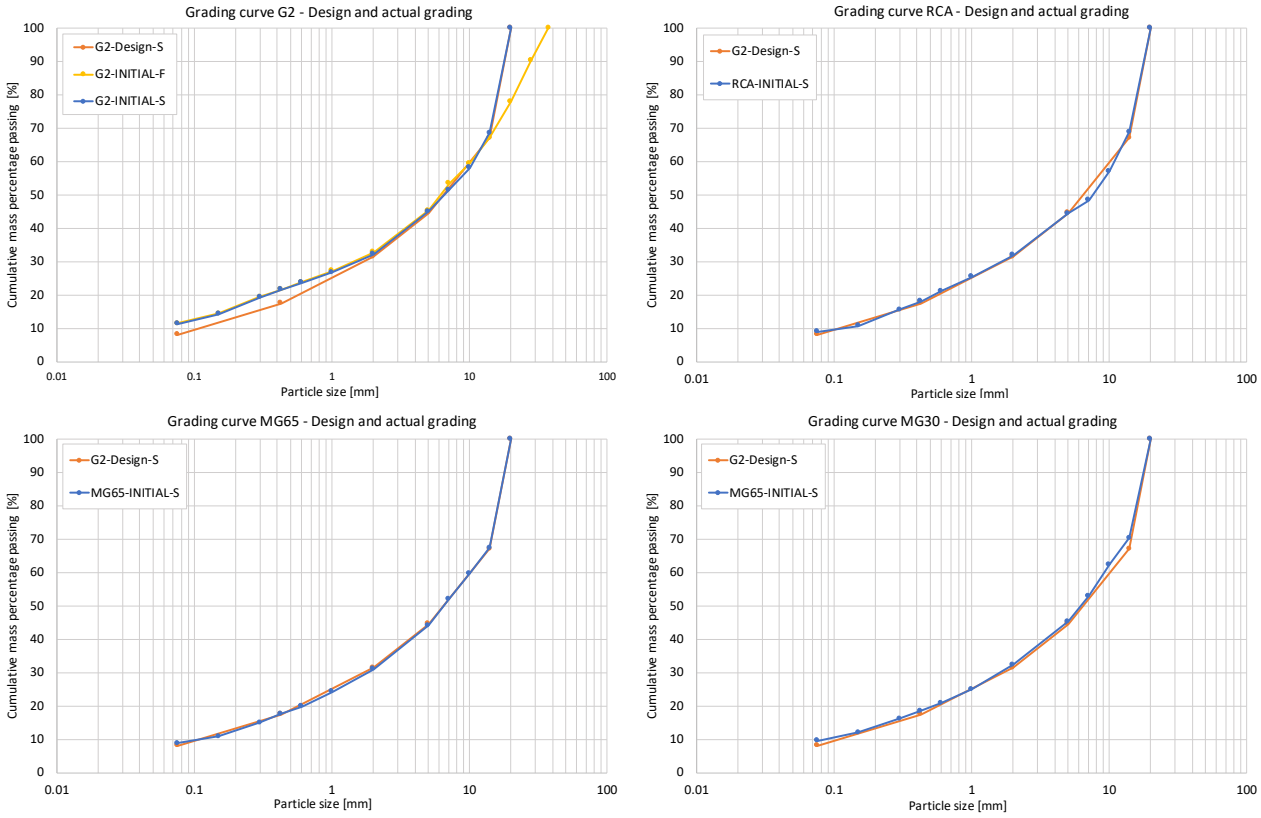

Figure 3.7: Inital (reference) grading curves compared with the design grading

3.3. DURABILITY MILL TESTING

According to the South African standards [23], durability milling is performed by extracting four subsamples of 3.75 kg each from a material sample of at least 16 kg. The grading is supposed to be known. The first subsample serves as reference sample and is not tested in the durability mill. The other three samples are tested under the following conditions:

- Dry Ball Mill: Dry specimen with steel balls;
- Wet Ball Mill: Soaked specimen with excess water and steel balls;
- Wet Mill: Soaked specimen with excess water without steel balls.

In this case, the three 3.75 kg subsamples are composed directly from the material batches. The reference specimens described in Section 3.2.3 serve as the fourth reference subsample. One test in the durability mill takes 10 minutes at a speed of 60 rotations per minute. The total amount of water in the drums for the latter two milling methods should be 2.5 iters. It appeares convenient to use 2 liters for soaking, and the remaining half for washing. After the test, the materials are washed out the drums and sieved. Figure 3.8 shows the double barrel durability mill at Stellenbosch University and the buckets in line for sieving. Although the standard prescribes sieving out only the particles passing the 425 μm sieve, it is chosen for this research to perform a full sieving in order to compare the grading before and after milling. For all four subsamples, the mass percentage and the plasticity index of the materials passing the 425 μm sieve is measured. The Durability Mill Index is then calculated as the product of the maximum measured plasticity index and the maximum measured percentage fines passing the 425 μm sieve. A remark on the procedure is that it is expected that the recycled materials actually do not contain plastic fines. This implies that the plasticity index is 1, and that the durability mill index is always below 100%. The materials would then always be regarded as sound, no matter the amount of breakdown. To compensate for this, Sampsom and Netterberg [20] suggest as extra requirement for non-plastic materials that the increase of fines should not exceed 15%, and the total amount should never exceed 35%. This suggestion is however based on only one test. Since the recycled materials probably hardly contain any plastic fines, durability is tested and expressed as a mechanical degradation potential only. The durabily mill index values are calculated but the change in grading rather than these numbers will be emphasized. Figure 3.9 shows the different steps of durability milling.

Figure 3.8: Left: Double barrel durability mill at Stellenbosch University **Right:** Buckets in line for sieving

3.4. TRIAXIAL TESTING - SAMPLE PREPARATION

Preparing the triaxial samples is a delicate process which, if not carried out properly, can result in significant inconsistencies in the results. Since the behavior of unbound materials is influenced by many variables, controlling every single aspect is impossible. It is aimed to reduce human errors as much as possible and prepare the samples consistently with respect to each other. Due to inexperience in the beginning, however, the first batch of monotic triaxial specimens (six unmilled G2 specimens) are made slightly different compared to the rest. Considerable inconsistencies in the results of this batch point out the importance of properly assembled specimens. This section is a step by step description of how the specimens are made. Attention is paid to details and some overall important aspects to considere are decribed in Section 3.4.5.

3.4.1. SPECIMEN COMPOSITION

With the blend ratio, grading, dry density, geometry and moisture content defined, a recipe for mix design can be made. Table 3.7 shows the design and composition parameters used for small scale triaxial specimens (300 mm x 152.5 mm). The composition parameters are only needed for unmilled specimens. An extra 2 kg oven dry mass is added to compensate for losses and the determination of the mixing moisture content. A calculation of the required amount of water is added as well because of the hygroscopic moisture content of the air dry resourced materials. With the composition air dry mass known, the mass to be weighed per fraction can be calculated. The exact make up of all unmilled specimens can be found in Appendix D. For the milled specimens, there is always enough material available to account for losses and moisture content determination since 15 kg (four DMI drums) get milled per specimen. This is because the DMI standards prescribe a mass of 3.75 kg per test, and at least four drums are needed to obtain enough materials for one specimen. The dried milled materials come directly out of the oven and carry no moisture, meaning that the required amount of water can be calculated directly.

Table 3.7: Recipe table for small scale (300 mm x 152.5 mm) triaxial specimens

Triaxial specimen design		**G2**	**RCA**	**MG65**	**MG30**
Maximum dry density	[kg/m^3]	2390	2018	1964	1890
OMC	[%]	3.70	10.50	9.90	11.50
Design specimen dry density	[kg/m^3]	2318	2018	1905	1833
Design specimen MC	[%]	3.70	10.00	10.00	10.50
Design specimen dry mass	[kg]	12.703	11.058	10.439	10.047
Design specimen water mass	[kg]	0.470	1.106	1.044	1.055
Design specimen bulk density	[kg/m^3]	2404	2220	2096	2026
Total specimen mass	**[kg]**	**13.173**	**12.164**	**11.483**	**11.102**
Divide in 5 bags of:	**[kg]**	**2.635**	**2.433**	**2.297**	**2.220**

Triaxial specimen composition		**G2**	**RCA**	**MG65**	**MG30**
Composition dry mass	[kg]	14.703	13.058	12.439	12.047
Composition water mass	[kg]	0.544	1.306	1.244	1.265
Material air-dry MC	[%]	0.24	2.05	1.2	0.97
Mass water to be added	[kg]	0.509	1.038	1.095	1.148
Composition air-dry mass	[kg]	**14.739**	**13.326**	**12.588**	**12.163**
Total composition mass	[kg]	**15.247**	**14.364**	**13.683**	**13.312**

A remark on the recipe tables is that a calculation error was found after testing. This resulted in that the unmilled MG65 triaxial specimens are actually composed with 62% RCA and 38% RCM. The milled triaxial and DMI specimens are made correctly. Despite the RCA/RCM ratio difference before and after milling, the two will still be compared with each other as the influence is expected to be negligible.

3.4.2. MILLED VS UNMILLED

Two types of triaxial specimens are made during this research. One containing initial (recycled) granulates and one containing durability milled (recycled) granulates. The materials used for the initial specimens can be weighed and mixed directly. Preparing the materials for the milled specimens is more elaborate. Firstly, the materials need to be weighed in four batches of 3.75 kg (since four drums are needed to obtain enough materials for one specimen, see Section 3.4.1). In this research, the wet ball mill DMI procedure (see 3.3) is followed, meaning that the materials need to soak for one hour before milling. After soaking, the materials are carefully washed into the drums and milled with the six steel balls for 10 minutes similar as the durability mill test. After milling, the drums are washed out in large mixing bowls while containing all the water with the fines. Finally, the bowls are stored in the ovens and dried out. In one day it is possible to perform twelve millings, implying that materials for three triaxial specimens can be prepared per day.

Figure 3.9: Durability milling: Soaking of the materials and loading, milling and washing out the drums

Figure 3.10: Drying process **Left:** Pre drying if oven capacity is exceeded **Middle:** Milled materials before drying **Right:** Milled materials after drying

3.4.3. MIXING

Mixing is done with the mixer shown in Figure 3.12. Once the mixer is rotating, the required amount of water is added and the aggregates are mixed for a couple of minutes until no dry spots are visible. A shovel is used to scrape the edges and the bottom of the mixing drum to provide a proper mixture. The triaxial specimens are constructed in five layers. After mixing, five bags are weighed each containing one fifth of the design triaxial specimen mass as shown in Figure 3.11. The remaining material is placed in the oven to determine the mixing moisture content.

Figure 3.11: Weighing aggregates after mixing in five equal portions

3.4.4. COMPACTING

The triaxial specimens are compacted with the Wirtgen WLV1 vibratory compacter shown in Figure 3.12. It exerts an operation mass of 170 kg with a frequency of 1,900 revolutions per minute (±32 Hz). The compactor has the ability to compact multiple layers, regulated by a time or height measurement. The density can be controlled by compacting a certain mass until a specified height is reached. The compactor is set up such that it compacts five layers each to

a thickness of one fifth of the specimen height, with a maximum compaction time of 60 seconds. If the optimum moisture content and maximum dry density are determined correctly (see Section 3.2.2), the compaction time will not reach 60 seconds. Compaction takes place in a steel mold which is greased with baking lubricant "Spray 'n' Cook". After the mold is placed on the base plate and clamped with a collar, the first bag of materials is carefully placed into the mold. A spatula is used to distribute the fines along the edges and after that the first layer can be compacted. Once the layer thinkness is reached, the machine shuts down automatically. Before placing the next layer, the surface is made rough with a scarifier to provide layer interlock (Figure 3.12). This process is repeated until all layers are compacted. The final layer is covered with a piece of paper. When all layers are compacted, the specimen is carefully demolded, tagged, sealed and stored for curing. A curing time of 24 hours is used for all specimens. Because recycled aggregates have some self-cementing properties, the time between preparing and testing should be equal between all samples to make a reasonable comparison.

Figure 3.12: Left: Mixer **Middle:** Compaction apparatus **Right:** Mold & scarifier

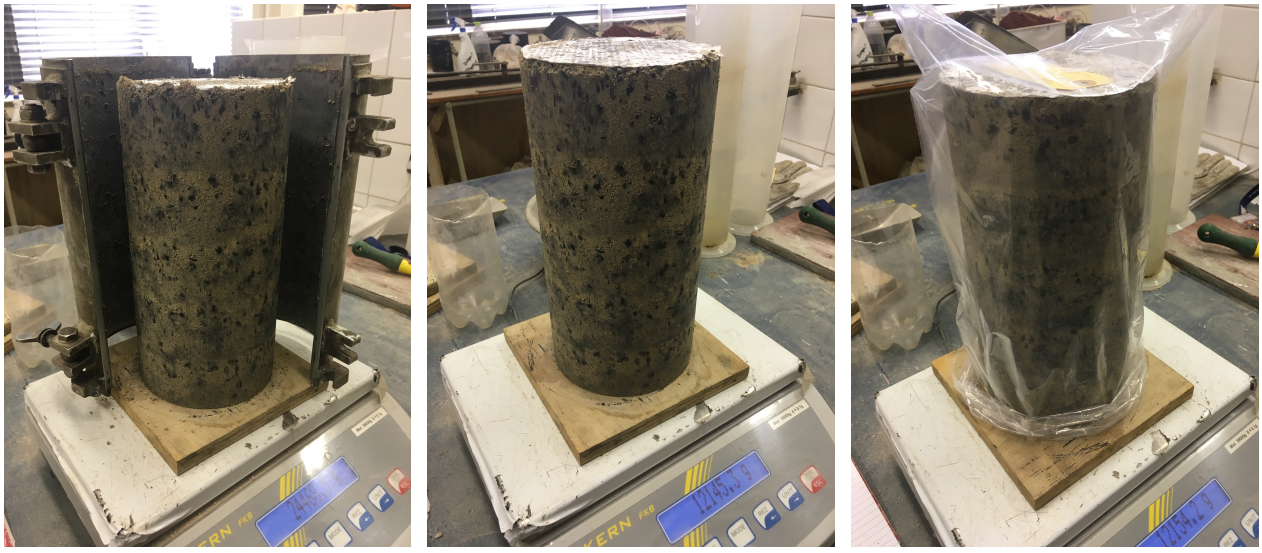

Figure 3.13: Demolding and sealing of a specimen

3.4.5. DETAILS OF SIGNIFICANCE

The way triaxial specimens are prepared can have a significant influence on the results. This section highlights some details which are believed to be of importance to obtain consistency between specimens. The first batch of unmilled G2 samples were made without taking the following points into consideration, resulting in very odd results (see also Section 4.3):

- To avoid segregation after mixing, the materials are shovelled into the plastic bags directly from the mixing pan (see Figure 3.11). Furthermore, mixed materials should be placed carefully (not dropped) into the mold.
- Once the material is placed in the mold, the edges are scraped quickly with a spatula to distribute the fines on the sides (Figure 3.14).
- Only the scarefier must be used for creating interlock between layers. Drills or other tools can cause damage to the already compacted layers.
- A smooth top surface is obtained by scraping stuck materials from the compaction head before compacting the last layer.
- The base plate on which the specimen gets compacted should be even. Screwholes or other disturbances cause the specimen to wobble. It is unclear how much influence this has on the results, but it is best to rule out all uncertainties (Figure 3.14).

Figure 3.14: Specimen detailing **Left:** Without scraping the edges with the spatula **Right:** Uneven compaction plate

3.4.6. MEMBRANES

In order to apply confinement stress on the triaxial samples, the specimens must be sealed with a membrane. Membranes are made manually by pouring liquid latex into a basin, and bringing it in contact with a slowly rotating mold. While the mold rotates through the latex, one must blow on the bubbles to prevent the accumulation of local weakspots. Once a smooth surface is obtained, the latex bath is slowly released from the mold. The remaining latex is then removed from the basin and the rotating mold is left to dry for at least 8 hours. This process is repeated until the desired membrane thickness is reached. Too few layers result in a fragile membrane, risking rupture or leaks while testing. Too many layers result in a very stiff membrane, which could add an extra unknown confinement stress to the sample. In general it is accepted that the membranes add a small amount of confinement stress, but by making the membranes not too thick it is assumed this can be neglected. Three layer membranes are found to be the most convenient in terms of workability, but the four layer membranes last significantly longer. It is therefore decided to perform the triaxial tests with the four layer membranes. Based on the drying time, it takes two days to produce one membrane. Figure 3.15 shows the set-up for membrane production, just after applying a layer.

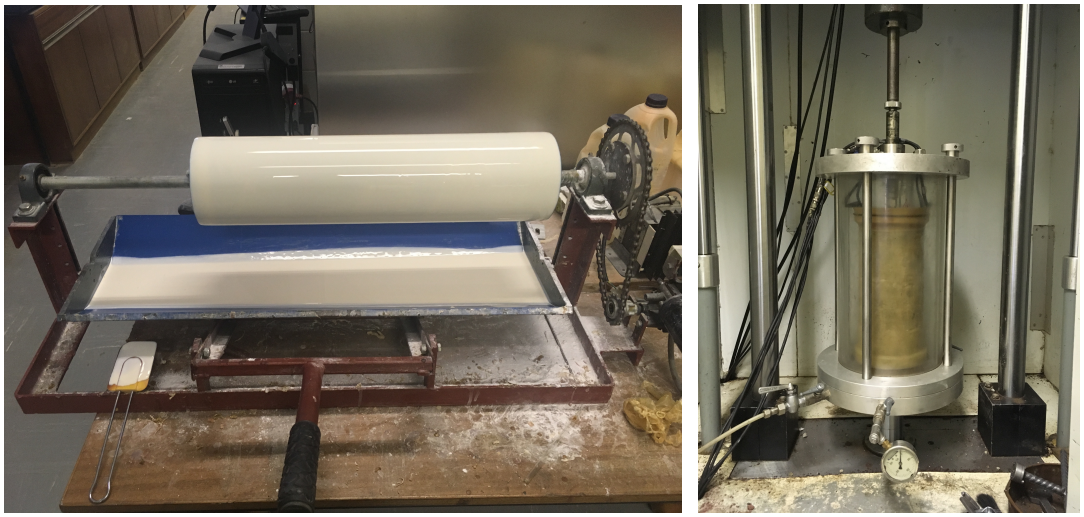

Figure 3.15: Left: Set-up for membrane production **Right:** Triaxial testing machine

3.5. TRIAXIAL TESTING - TEST EXECUTION

The triaxial test set-up at Stellenbosch University, shown in Figure 3.15, is of the type Material Testing System (MTS 810, model 318.10). The machine works with an overpressure cell to provide confinement, and is capable of both force and displacement controlled tests. Confinement stress is applied manually. The ramp at the top is fixed and equipped with a force measurement cell. Displacements are applied from the bottom. Although it is possible to mount LVDTs over one third of the sample height to measure lateral and radial displacements, deformations are only measured with the actuator LVDT. The reason for this is the risk of damage to the side LVDTs at large displacements and specimen failure. Measuring deformations with the actuator LVDT is less accurate than measuring with the side LVDTs, as frictional effects of the top and bottom plates introduce local non-uniform stress distributions. However, since relative trends are considered more important than absolute values, this will still give reasonable results. When the side LVDTs are not used, setting up the monotonic and permanent deformation tests is similar. Small differences can be noticed between researchers in the test set-up. In this research, the following stepwise approaches are used for membrane placement and triaxial set-up. Figures 3.16 and 3.17 illustrate the corresponding steps, respectively:

MEMBRANE PLACEMENT

- The plastic seal is removed from the specimen and the height is measured at four points (the average serves as the height for density calculations). The specimen is then placed on a bottom plate with a wooden block underneath it.
- A latex membrane is checked for holes and wrapped around a steel cylinder specially made for membrane placement. The cylinder has a hose attached to its side such that the membrane can be in- or deflated once mounted. First, the membrane is inflated and checked again for leakage. Then, if it does not leak, the membrane is deflated as much as possible and placed around the sample. By removing the vacuum the membrane will inflate again and wrap itself around the specimen.
- The lower part of the membrane is gently pulled down over the bottom plate and folded back such that the wooden block is completely free. The top part of the membrane is pulled up and the cylinder is removed.
- The top part of the membrane is folded down over the sample in order to place the top plate. Then, the membrane is pulled up over the top plate and folded back again. The specimen is now ready to be placed in the triaxial machine.

Figure 3.16: Membrane attachment

TRIAXIAL SETUP

- The triaxial sample is placed on the center of the machine's base plate. The membrane is then pulled down at the bottom such that it covers a part of the base plate. Rubber O-rings are placed at the top and bottom plate after which the sample is fixed for monotonic triaxial testing. For permanent deformation triaxial testing, the top and bottom plates are covered with an extra piece of latex and an extra set of rubber O-rings. This is an additional measure for dynamic testing to prevent air slipping into the specimen.

- Once the specimen is fixed to the base plate, the cell can be placed. Grease is used between all elements to make the cell air tight. The last part of the cell, the triaxial head, carries the pin which loads the specimen. The pin must touch the sample exactly in the middle of the top plate where a small notch is located. Often the pin and the notch are not perfectly aligned causing the specimen to wobble. If this happens, the specimen has to be shifted slightly until no eccentricity can be observed. Once the pin and the sample are aligned, the cell can be bolted together.

- After tightening, the cell is moved up to its starting position using the MTS software. Then, the top ramp is lowered until it touches the triaxial head pin. The ramp gets locked and does not move while testing. It is very important that after lowering the ramp the cell is not moved anymore, as this can crush the sample immediatly.

- Finally, confinement stress is applied. Small leakage of air is unavoidable (for instance around the head-pin) but no air should leak trough the edges of the cell elements. Significant leakage can be observed clearly and points out that the cell is not properly assembled. Furthermore, the membrane has to be 'sucked' onto the sample as this indicates pressure difference between the cell and the specimen. Once there is no observed leakage outside the cell or inside the membrane, the test is ready to start.

3.5.1. LOADING

All specimens in the monotonic triaxial test are loaded by a constant displacement of 3 mm (1 % strain) per minute. The force is measured and logged together with the displacement values. Loading stops automatically after a displacement of 15 mm or when only 20% residual strength is left. Usually the former is the governing condition, resulting in a testing time of five minutes. A maximum displacement of 15 mm appeared to be enough for all specimens to reach their peak strength.

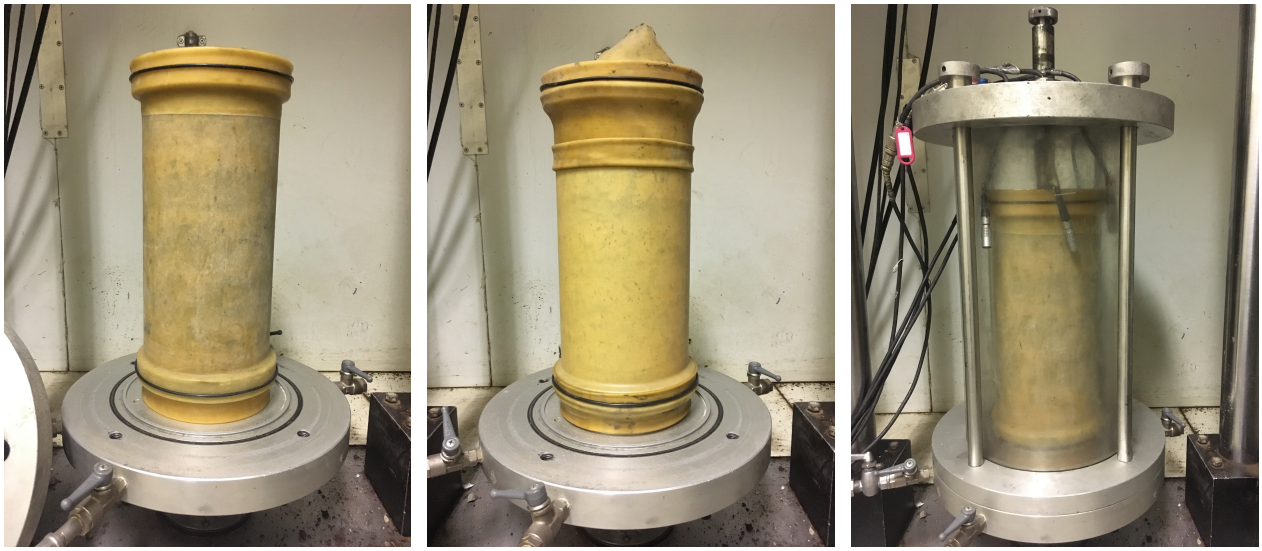

Figure 3.17: Triaxial set-up **Left:** Monotonic triaxial sample **Middle:** Permanent deformation triaxial sample **Right:** Triaxial cell

Permanent deformation testing is performed under cyclic loading conditions as shown in Figure 3.18. The specimens are loaded up to 250,000 load cycles at 1 Hz, taking 2.5 days per test to complete. A deviator seating load of 0.4 kN (21.9 kPa) is applied in all tests. The peak load differs per material and is dependent on the average deviator failure stress of the corresponding 100 kPa milled monotonic triaxial tests. Although the deviator failure stress differs between the milled and unmilled specimens, it is decided to apply the same loading to all samples within a material in order to make a fair comparison. Table 4.7 shows the applied loading per test. A conditioning phase of 500 cycles of 5 kN (273.7 kPa) preceeds the actual test. Significant permanent deformation already occurs during this phase. When comparing absolute deformations with other research, one must be aware whether or not the conditioning phase is included in the final results. In this research, permanent deformation results do not include the conditioning phase, meaning that the zero measurement is taken directly after the last cycle of the condition phase.

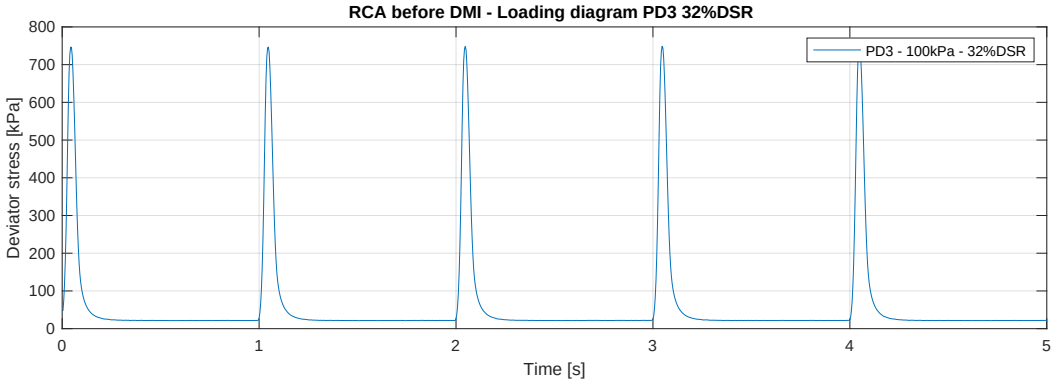

Figure 3.18: Permanent deformation triaxial test loading diagram

A drawback of the triaxial set-up is that the confinement stress cannot be controlled automatically. It is set to a certain value in the beginning of the test by manually opening a pressure valve. Small leakage of air out of the cell is unavoidable and present from the start. As long as this leakage is constant, the confinement stress is maintained well. When the cell moves upwards in the monotonic test however, leakage around the pin might fluctuate and cause changes in confinement stress. The set-up does not compensate for this, which sometimes results in an increase or decrease of confinement stress up to 10 kPa.

3.6. SIEVING

This research includes a large scale sieving program to address the particle breakdown in the DMI and triaxial specimens. Since the understanding of material degradation of forms a large part of this study, the sievings have to be carried out as accurate as possible. Therefore, wet sievings are performed instead of dry sievings. Wet sievings are more elaborate and time consuming compared to their dry counterpart, but they are also more accurate. The difference between the two is the addition of a washing and a drying step. After soaking the materials for at least 24 hours, the aggregates are carefully washed through the finest sieve (75 μm). Doing so removes the pan fraction from the sample and prevents it from clogging together with other particles. After washing, the remaining materials are dried in the oven and weighed. The difference between the oven dry mass before and after washing then determines the mass of the pan fraction. Normally, the pan fraction is flushed away through the basin, but since the fines generated by DMI milling are needed for the determination of the Plasticity Index, all the water used for washing is retained and dried out as well. This causes a significant bottleneck in the testing process as large quantities of water has to be evaporatored in limited oven space.[1] Figure 3.19 shows the vibratory sieve tower used in this research. The dried aggregates without the pan fraction are added at the top and sieved for 30 minutes. After sieving, the mass of each retained fraction is weighed and recorded. The sieve sizes are in conformity with the new South African National Standards [21], i.e. 28 mm, 20 mm, 14 mm, 10 mm, 7.1 mm, 5 mm, 2 mm, 1 mm, 600 μm, 425 μm, 300 μm, 150 μm, 75 μm and pan, respectively.

Figure 3.19: Left: Washing of the aggregates **Right:** Vibrating sieve tower

The scale of sieving is rather extensive. During the testing stage it became clear that it would be unrealistic to do all the initially planned sievings, and therefore DMI testing of the full graded specimens is only completed on the G2 material. An overview of the sieving work per material per test is presented in Table 3.8.

Table 3.8: Number of sievings performed per material

Number of sievings	G2	RCA	RCM	MG65	MG30	Total
Initial material full graded (reference samples)	3	3	0	0	0	6
Initial material scalped+added graded (reference samples)	3	3	3	3	3	15
After full graded DMI testing	9	0	0	0	0	9
After scalped+added graded DMI testing	9	9	9	9	9	45
After initial monotonic triaxial tests	3	3	0	3	3	12
After initial permanent deformation triaxial tests	0	3	0	3	0	6
Total	**27**	**21**	**12**	**18**	**15**	**93**

[1] At a later stage, when it became clear that both the milled RCA and milled RCM did not contain any plastic fines (and thus the blends would not either), retaining the fines was discontinued.

3.7. PLASTICITY INDEX

The Plasticity Index, or PI, is a part of the Atterberg Limits and quantifies the ability of a soil to retain moisture. It is defined as the difference between the Liquid Limit and the Plastic Limit. Clayey materials are known to have a high Plasticity Index, while sands have a very low or even no PI at all. The Plastic Limit and Liquid Limit tests are performed on the fines (passing 425 μm) of the durability milled materials. It is recognized that the results of the tests may vary along different researchers as they require some subjective jugdements. Together with that, different ways are decribed to obtain the Liquid Limit (it can be determined with the cone penetrometer or the Casagrande Cup). The Atterberg limit tests as they are carried out in this research are briefly discussed below.

LIQUID LIMIT

The Liquid Limit is determined using the Casagrade Cup shown in Figure 3.20. A material sample is thoroughy mixed with a certain amount of water until a consistent mixture is obtained. Then the material is placed in the cup, smoothed out and given five blows at a rate of two blows per second. The falling height of the cup should be one centimeter. After the blows, a V-groove to the bottom is cut through the sample (dividing it in two equal halfs) and again 25 blows are given. The Liquid Limit is reached when after 25 blows the two halfs touch each other for over a length of about one centimeter. If this is more, it means that material is too wet and that more dry material needs to be added to the sample. If this is less, or the parts do not touch at all, the material is too dry and more water is needed. The corresponding moisture content of the sample at the Liquid Limit is then defined as the Liquid Limit of the material. If the Liquid Limit cannot be determined, that is when sample appears to be too wet in the Casagrande Cup but crumbles when adding more dry material, the material does not have any water retaining capacity and is recorded as non-plastic.

PLASTIC LIMIT

The Plastic Limit is usually determined after the Liquid Limit. If the material under consideration appears to be non-plastic, this test cannot be performed. From the leftover material in the Casagrande Cup (not all is used to determine the moisture content), rolls of about three millimeter thick are made by hand. The Plastic Limit is reached when the rolls are just about to crack at three millimeter thickness. If they are still consistent, the material needs to be molded and rolled again to evaporate more water. When more or less 20 g of material is rolled, the moisture content is determined to obtain the Plastic Limit. Figure 3.20 shows the rolls and blocks of the Atterberg Limit tests after drying.

Figure 3.20: Left: PI test equipment **Right:** Tested samples for Liquid and Plastic Limits

3.8. CHAPTER SUMMARY

In this chapter, all relevant details regarding the set up of this research, are discussed. The experimental design and laboratory logistics are explained, as well as the execution and sample preparation of all tests. The preliminary tests results show that the hygroscopic moisture content is the highest in the RCA, and decreases linearly with increasing masonry content. The hygroscopic moisture content of the G2 materials is very little, and mainly concentrates in the finest fraction. Regarding the determination of the optimum moisture content, the highest dry densities are measured in the G2. This does not necesserily mean that a better packing is achieved, but it is mainly the result of the higher specific mass of the G2 granulates. In the recycled materials, it appears harder to find the maximum dry density, as the corresponding moisture content - dry density curves are more flat. This was also recognized by Van Niekerk [15], who performed Proctor tests on the recycles materials and did not find a clear optimum. Nevertheless, by using the vibratory hammer, optimum moisture contents and the corresponding maximum dry densities can still be determined. The referece gradings show that only the finest fractions of the G2 slighty deviates from the design grading. All other compositions almost exactly follow the design grading curve. The difference in the G2 is most likely caused by the fines sticking to the larger particles. In all fractions, the granular particles are covered with dust before weighing, implying that slightly more fines are present in the tested samples. A final remark considers specimen detailing. It is noticed that the variability between specimens can be greatly reduced by paying attention to a number of small details listed in Section 3.4.5. Especially measures to ensure an optimum distribution of particles are believed to be of great importance.

4

RESULTS

In this chapter an overview of the test results is presented. More detailed results such as specimen compositions and gradings can be found in Appendices E to H. Firstly, the outcomes of the durability millings are discussed. This section contains the results of the sievings and the plasticity index tests and combines them to obtain the Durability Mill Index values. As mentioned previously, the Durability Mill Index may not be the foremost method to classify recycled materials with a lack of plastic fines. Therefore mechanical breakdown (i.e. full grading change) is also investigated. The durability aspects are succeeded by the monotonic and permanent deformation triaxial test results. For the processing and modelling of the triaxial test results, extensive use is made of MATLAB. Several scripts have been developed for managing the large datafiles generated by permanent deformation testing. Especially for data fitting and modelling MATLAB proves to be very useful. The scripts are written in a generic way, such that they can serve as a tool for other researchers working with this specific triaxial test machine.

4.1. SAMPLE TERMINOLOGY

All tested specimens are labelled according to the same terminology. This is needed during the testing phase, as specimens can get lost or mixed up easily in the rather complex logistics of this research. The same name structure is kept for the presentation and modelling of the results. A specimen name consists of three parts: The first part decribes the tested material and the middle and the last part combined the type of testing. The name ends with a batch number. Table 4.1 explains all abbreviations. For instance, sample "MG65-DMIT-M3" stands for mixed granulates blend MG65 (65% RCA, 35% RCM), which is monotonic triaxial tested after durability milling and carries the batch number 3.

Table 4.1: Sample terminology

	Material
G2	G2 Base Course
RCA	Recycled Concrete Aggregate
RCM	Recycled Crushed Masonry
MG65	Mixed Granulate (65% RCA, 35% RCM)
MG30	Mixed Granulate (30% RCA, 70% RCM)

	Testing type
INITIAL	Non tested reference material
DMIS	Durability mill, scalped+added graded (G20C)
DMIF	Durability mill, full graded
DMIT	Durability milled triaxial test
MONO	Unmilled monotonic triaxial test
PERM	Unmilled permanent deformation triaxial test

	Additional information
S	Scalped+added graded (G20C)
F	Full graded
M	Monotonic test
PD	Permanent deformation test
DB	Dry ball mill
WB	Wet ball mill
W	Wet mill

4.2. DURABILITY MILLING

4.2.1. SIEVE RESULTS

All durability milled samples have been sieved out after testing. The obtained grading curves are shown in Figure 4.1 and contain the initial grading, dry ball mill, wet ball mill and wet mill sieve results per material. The grading curves are the average of three milled samples, with the exception for RCA dry ball mill, RCA wet mill, RCM dry ball mill and

MG65 wet ball mill. These are averages of two. The first sample got lost in the testing process and the latter three didn't match a reasonable mass balance (significant differences in total mass before and after sieving were obtained). A list containing the recorded losses per sieving and excluded specimens can be found in Appendix E.16. Appendix E further contains all sieve tables and grading curves obtained, including the grading curves of the specimens sieved after monotonic triaxial testing. DMI results of the full graded G2 materials, which are obtained before discontinuing the full graded materials, are included in this appendix as well.

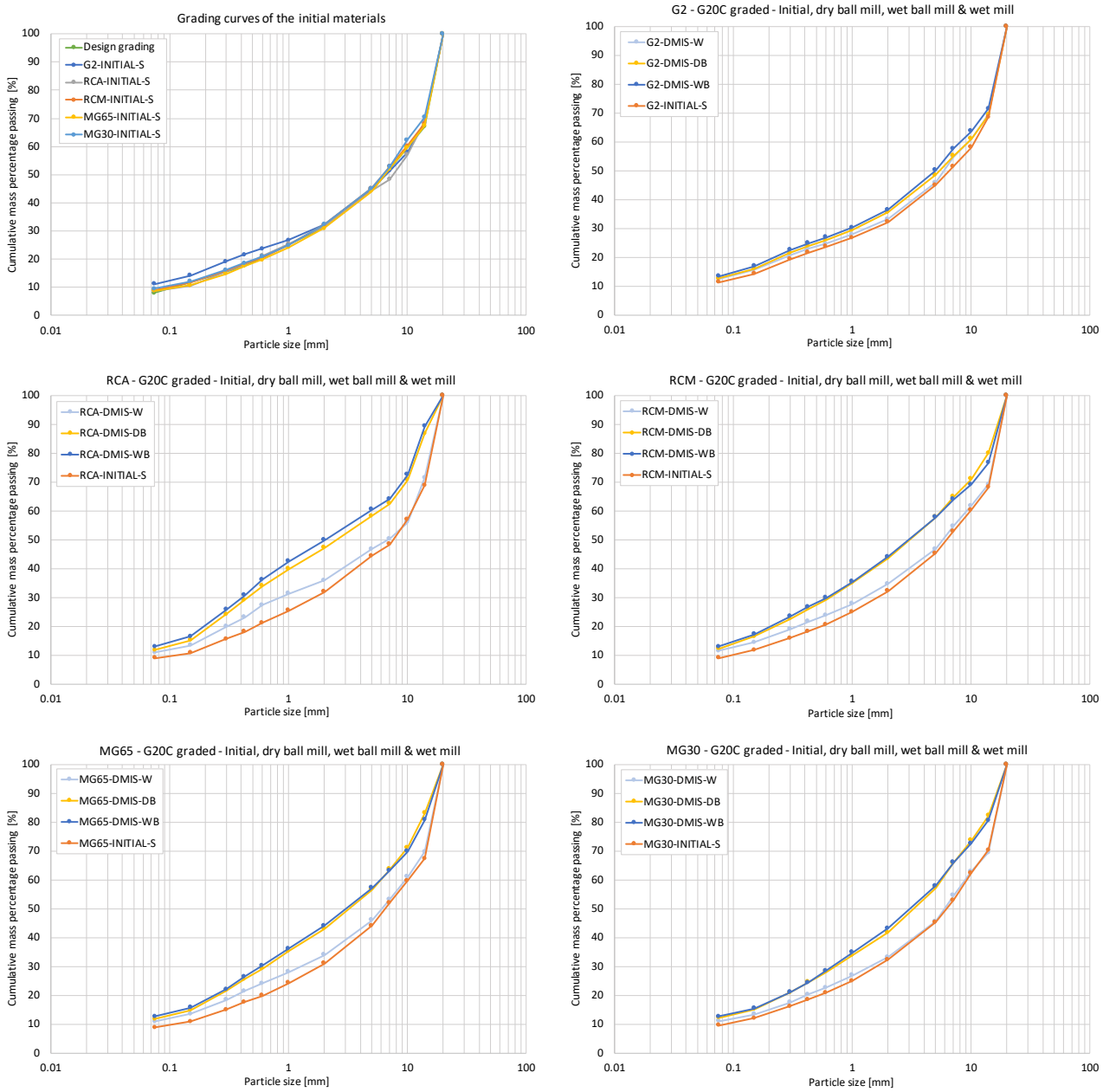

Figure 4.1: Sieve results after durability milling: Dry ball mill, wet ball mill & wet mill per material

It can be seen from the gradings that dry ball milling and wet ball milling cause the most particle breakdown in all materials. The difference between these two testing types appears to be rather small, and disproves the initial assumption that wet ball milling always creates the worst durabilty simulation conditions. Especially for the materials containing masonry, dry ball milling results in almost similar amounts of material breakdown. Another

finding is the significant difference in grading curve change between the recycled materials and the reference G2. This was expected beforehand, since it is known that recycled materials are much more prone to crushing than natural rocks such as G2. What is suprising however, is that the pure RCA appears to be more severely damaged than the pure RCM. Together with that, the blends show less change in grading in comparison with the pure RCA, indicating that RCA is more susceptible to particle breakdown than RCM. A more detailed discussion of the inter particle breadown can be found in Section 4.2.4.

4.2.2. PLASTICITY INDEX

Plasticity Index tests are done on the reclaimed fines of G2, RCA and RCM. The pan fractions of the milled and unmilled RCA and RCM did not contain any plastic fines (the determination of the liquid limit was not possible), and therefore it is concluded that the blends do not contain plastic fines either. Furthermore, if the pan fractions are non-plastic, it is assumed that the rest of the fines (passing 0.425 mm) is non-plastic as well. This results that all recycled materials are reported with PI = 1. The results of the Plastic Index tests for G2, which do contain some degree of plasticity, are presented in Table 4.2. Three tests are performed on only the pan fraction of the wet ball milled G2 materials to indicate the difference between the two fractions. Due to time limitations, only one PI test is carried on the wet milled materials and no PI tests of the unmilled reference samples are performed. It is assumed that the PI of the reference samples is the same or less than the PI of the wet ball milled samples (PI = 3).

Table 4.2: Plasticity Index test results

Sample	Fraction	Liquid Limit [%]	Plastic Limit [%]	Plastcity Index [%]	Average PI [%]
G2-DMIS-DB1	Passing 0.425 mm	16.5	12.9	3.6	**3**
G2-DMIS-DB2		15.4	12.0	3.4	
G2-DMIS-DB3		16.0	12.9	3.1	
G2-DMIS-WB1	Passing 0.425 mm	16.4	13.2	3.3	**3**
G2-DMIS-WB2		16.8	13.9	2.9	
G2-DMIS-WB3		15.3	13.2	2.1	
G2-DMIS-W1	Passing 0.425 mm	15.8	12.8	2.9	**3**
G2-DMIS-W2		-	-	-	
G2-DMIS-W3		-	-	-	
G2-DMIS-WB1	Pan	22.9	18.1	4.8	**6**
G2-DMIS-WB2		25.4	20.4	5.1	
G2-DMIS-WB3		25.8	18.6	7.2	

4.2.3. DURABILITY MILL INDEX

The Durability Mill Index is defined as the product of the maximum mass percentage fines and the maximum plasticity index measured in the four different subsamples (one reference sample, dry ball mill, wet ball mill and wet mill). The standards [23] distinguishes two types of DMI, depending on which part of the fines are considered:

$$DMI_{0.425} = Max(p_{0.425}) \cdot Max(PI_{0.425}) \tag{4.1}$$

$$DMI_{0.075} = Max(p_{0.075}) \cdot Max(PI_{0.075}) \tag{4.2}$$

Where p_i represents the mass percentage passing sieve i. In this case, $DMI_{0.425}$ is considered. This means that the full fraction of fines is taken into account which is in accordance with the fundamental research of the DMI test [20]. The calculated DMI values are presented in Table 4.3. The mass percentage passing the 0.425 mm sieve is the average of three DMI millings, with the same exceptions of the ones listed in 4.2.1. According to the findings of Sampson

and Netterberg displayed in Figure 2.17, sound behavior can be expected when the Durability Mill Index lies below 100. This is the case for all tested materials. As an extra requirement for non-plastic materials, it was suggested that the total mass percentage fines may not exceed 35%, with a maximum increase of 15%. The recycled materials also meet these criteria and would therefore be classified as durable. Caution however is advised with this conclusion. The research behind these extra criteria is very limited (n=1) and due to the absence of plastic fines, non-plastic materials would always classify as sound regardles the amount of material breakdown. In this case, the recycled materials score even better than the G2 materials although the material breakdown is significantly more severe. The question arises whether this is realistic, and whether the Durability Mill Index, as defined in the standards, is actually applicable for non-plastic materials. Verification of the DMI test with non-plastic materials should be done in order to draw justified conclusions. Together with that, a verification of the DMI test with recycled materials is advised to indicate if the measured breakdown is indeed comparable with what happens in the field.

Table 4.3: Durability Mill Index results

Material	Milling type [-]	Passing 0.425mm [%]	Increase 0.425mm [%]	Plasticity Index [%]	DMI 0.425mm [-]
G2	Dry ball	23.9	2.3	3	
	Wet ball	24.8	3.1	3	**74**
	Wet ball	22.9	1.2	3	
RCA	Dry ball	29.2	11.1	1	
	Wet ball	30.6	12.6	1	**31**
	Wet ball	23.1	5.0	1	
RCM	Dry ball	26.0	7.8	1	
	Wet ball	26.8	8.5	1	**27**
	Wet ball	21.6	3.4	1	
MG65	Dry ball	25.6	8.1	1	
	Wet ball	26.4	8.8	1	**26**
	Wet ball	21.5	3.9	1	
MG30	Dry ball	24.5	6.0	1	
	Wet ball	24.4	5.9	1	**25**
	Wet ball	20.3	1.7	1	

4.2.4. MATERIAL BREAKDOWN

Due to the debatable nature of the Durability Mill Index for non-plastic materials, purely mechanical breakdown in terms of grading change is considered as well. Broken down particles distribute itself over smaller sieves causing an increase in these fractions. By summing up the percentage positive (or negative) change per fraction, it is possible to quantify the total amount of breakdown with a single value and to compare this between materials. The latter is mathematically decribed in Equation 4.3. The results are presented in Table 4.4 and Figure 4.2. Note that the material breakdown value does not discriminate between the severity of breakdown. Particles can break once, ending up one sieve below, or get fully crushed and end up as fines. The method does not differentiate between the two and will record the same breakdown. Therefore, the mass percentage increase of the fines (passing 425 μm) is plotted as well. In combination with the total material breakdown, this gives an indication of the severity of damage since the bigger particles need to be crushed or break more than once to end up as fines.

$$MB = \frac{1}{2}\sum_{i=1}^{N} |g_i - dg_i| \tag{4.3}$$

Where:

MB = Total material breakdown [%]

g_i = Particle fraction of the initial material between sieve i and sieve i-1 [%]

dg_i = Particle fraction of the degraded material at sieve i [%]

N = Total number of sieves used [-]

Table 4.4: Breakdown per material for dry ball mill, wet ball mill, wet mill and after monotonic triaxial testing

	Dry ball mill		Wet ball mill		Wet mill		After monotonic triaxial testing	
	Breakdown [%]	Fines increase [%]	Breakdown [%]	Fines increase [%]	Breakdown [%]	Fines increase [%]	Breakdown [%]	Fines increase [%]
G2	3.7	2.3	6.3	3.1	4.0	1.2	3.0	0.5
RCA	20.0	11.1	22.8	12.6	9.8	3.4	15.3	5.9
MG65	16.7	8.1	16.4	8.8	5.3	3.9	15.2	2.4
MG30	13.5	6.0	13.1	5.9	4.2	1.7	11.1	2.8
RCM	13.8	7.8	12.5	8.5	3.6	3.4	-	-

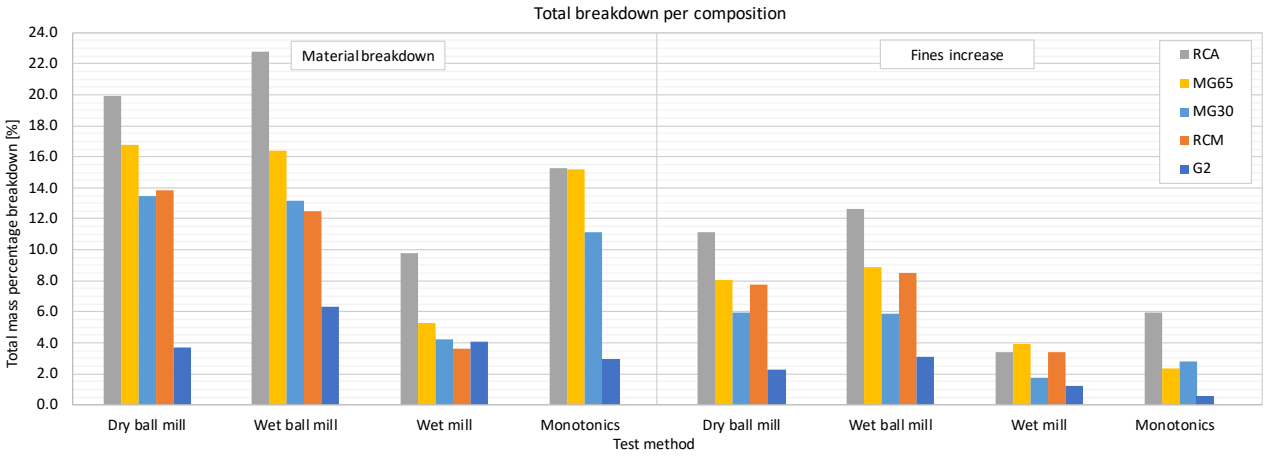

Figure 4.2: Breakdown and fines increase per material for dry ball mill, wet ball mill, wet mill and after monotonic triaxial testing

It can be seen from Figure 4.2 that the G2 suffers the least breakdown in all of the tests. When only comparing the recycled materials, the most breakdown seems to happen in the RCA, and not in the RCM as was expected. In the wet ball mill and wet mill tests, breakdown even decreases with increasing masonry content, justifying the conclusion that RCA is indeed more susceptible to breakdown than RCM. The most likely reason for this is that the cement binding the concrete aggregates is weaker than the crushed masonry particles. Just as can be seen in the gradings of Figure 4.1, the difference between dry ball milling and wet ball milling is very small for the materials containing masonry. When considering the grading change after unmilled monotonic triaxial testing, significant breakdown of the larger fractions is observed. This is an unexpected finding, and suggests that compaction breakdown is a significant part of the total breakdown. Since only the unmilled triaxial specimens have been sieved out, the exact grading difference between the milled and unmilled triaxial specimens is not known. It is however assumed that the order of magnitude of material breakdown caused by compaction before and after durability milling is the same. In that case, the change of performance can be assigned to the effects of durability milling alone. Together with this, compaction breakdown is unavoidable and always present in the field. Therefore, the measured performance parameters can be related to the initial, starting grading before compaction. Afterwards, it would be advisable to sieve out the milled triaxial specimens as well to obtain the exact grading difference between the milled and unmilled triaxial specimens and to validate this assumption. More detailed information about the grading curve change per fraction can be found in Appendix F.

In addition to the total material breakdown, the change of the seperate particle fractions can be considered as well. Figure 4.3 presents the cumulative mass percentage passing the 14 mm and the 0.425 mm fractions for all testing types. The differences between the broken down and initial materials are displayed above the charts. Considering the 14 mm fraction, similar trends as in Figure 4.2 are observed. In this case, it appears that all materials containing masonry are worse of in dry ball milling. The pure RCA and the G2 suffer more breakdown by wet ball milling. When comparing the change of the 14 mm particle fraction with the the total material breakdown (Figure 4.2), it can be seen that the majority of the grading change happens within the largest fraction. Other fractions suffer breakdown as well, but also 'gain' new particles form sieves above. For all materials tested according the wet ball mill and the

dry ball mill procedure, it appears that the largest fraction is the most affected. This observation could be of interest in case the DMI is revisited for non-plastic materials, as it shows the impact of the durability mill in a much clearer way than the current, prescribed by the standard, 0.425 mm fraction.

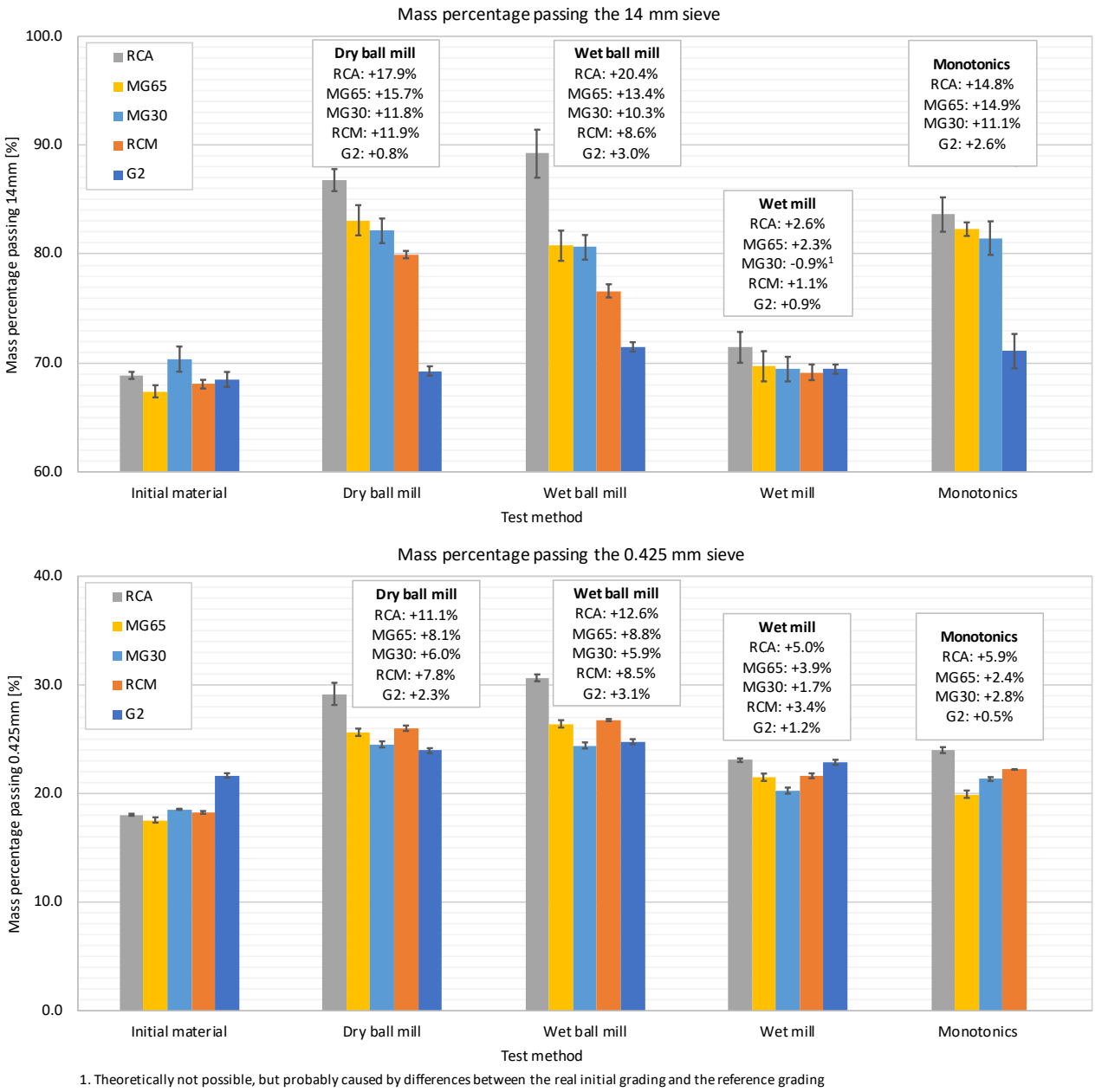

Figure 4.3: Material breakdown per fraction **Top:** Passing 14 mm sieve **Bottom:** Passing 0.425 mm sieve

Other posibilities to quantify particle breakdown could involve the change of total particle surface or the difference between the cumulative mass percentage passing particle distributions. The latter can be seen as the surface enclosed by the initial and broken down grading curves, with each particle size equally weighed as 1. The advance of this method is that is accounts for the severity of particle breakdown. Particles which are crushed to fines pass more sieves and therefore contribute more to the obtained number (i.e. surface). An extension which involves particle diameter or surface (and thus discriminates between fraction size) can be made as well. While not elaborated in this work, this method might give interesting insights for future analysis.

4.3. MONOTONIC TRIAXIAL TESTING

The results of the monotonic triaxial tests are summarized in Table 4.5. It contains the sample properties and failure loads of all specimens. Apart from the first batch of unmilled G2 samples, the results clearly show the influence of the confinement stress on the failure load. In almost all cases, the moisture content measured after testing is lower than the moisture content measured after mixing. The main reason for this decrease is evaporation during overnight curing. It is observed that the bags sealing the specimens become wet and filled with water droplets. Other reasons for this drop in moisture content are water absorption by the wooden bottom plate and paper top layer. It is also observed that the moisture content after mixing is most of the time higher than the design moisture content. It is possible that the remaining material after mixing, on which the moisture content is determined, contains slightly more fine particles than the specimens and thus absorb more water.

Table 4.5: Monotonic triaxial test results

Test	Specimen ID	Target MC [%]	Target DD [kg/m^2]	Mixing MC [%]	Specimen MC [%]	Dry density [kg/m^2]	Confinement stress [kPa]	Absolute failure load [kN]	Absolute failure stress [kPa]
G2 before DMI	G2-MONO-M1	3.7	2318	-	3.23	2310	50	23.97	1312
	G2-MONO-M2			-	3.29	2321	100	20.39	1117
	G2-MONO-M3			-	3.31	2322	150	33.23	1819
	G2-MONO-M4			-	3.20	2320	50	19.12	1047
	G2-MONO-M5			-	3.22	2315	100	33.92	1857
	G2-MONO-M6			-	3.23	2324	150	37.62	2059
G2 after DMI	G2-DMIT-M1	3.7	2318	4.07	3.07	2317	50	23.45	1284
	G2-DMIT-M2			3.84	3.15	2319	100	28.65	1568
	G2-DMIT-M3			3.80	3.04	2329	150	37.59	2058
	G2-DMIT-M4			3.66	3.09	2318	50	22.36	1224
	G2-DMIT-M5			3.99	3.20	2335	100	27.21	1490
	G2-DMIT-M6			4.34	3.09	2345	150	37.73	2065
RCA before DMI	RCA-MONO-M1	10	2018	10.16	9.95	2015	50	34.97	1914
	RCA-MONO-M2			10.51	9.95	2023	100	44.86	2456
	RCA-MONO-M3			10.65	10.19	2009	150	52.24	2860
	RCA-MONO-M4			10.56	10.16	2007	50	36.91	2021
	RCA-MONO-M5			10.62	10.16	2013	100	48.09	2633
	RCA-MONO-M6			9.92	10.03	2011	150	56.61	3099
RCA after DMI	RCA-DMIT-M1	10	2018	10.56	8.87	2015	50	34.66	1897
	RCA-DMIT-M2			10.31	9.83	2010	100	40.79	2233
	RCA-DMIT-M3			10.51	9.47	2019	150	51.20	2803
	RCA-DMIT-M4			10.57	9.56	2020	0	19.71	1079
	RCA-DMIT-M5			9.96	9.56	2013	100	43.16	2363
	RCA-DMIT-M6			10.57	9.29	2023	150	51.81	2836
MG65 before DMI	MG65-MONO-M1	10	1905	10.70	9.09	1915	50	43.11	2360
	MG65-MONO-M2			10.49	9.48	1904	100	49.17	2692
	MG65-MONO-M3			10.52	9.33	1909	150	58.21	3187
	MG65-MONO-M4			10.42	9.26	1910	50	45.29	2479
	MG65-MONO-M5			10.23	9.20	1909	100	52.79	2890
	MG65-MONO-M6			10.29	9.29	1909	150	59.59	3262
MG65 after DMI	MG65-DMIT-M1	10	1905	10.13	9.41	1897	50	32.13	1759
	MG65-DMIT-M2			10.22	9.53	1905	100	41.08	2249
	MG65-DMIT-M3			10.45	9.41	1907	150	47.46	2599
	MG65-DMIT-M4			10.08	9.41	1895	50	31.16	1706
	MG65-DMIT-M5			10.01	9.50	1906	100	41.65	2280
	MG65-DMIT-M6			10.17	Unknown	Unknown	150	49.39	2704
MG30 before DMI	MG30-MONO-M1	10.5	1833	11.06	10.09	1842	50	44.42	2432
	MG30-MONO-M2			11.00	9.92	1845	0	36.68	2008
	MG30-MONO-M3			11.03	9.93	1845	150	62.99	3448
	MG30-MONO-M4			10.67	9.98	1847	50	46.55	2548
	MG30-MONO-M5			10.84	9.98	1842	100	53.43	2925
	MG30-MONO-M6			10.72	9.68	1849	150	62.19	3405
MG30 after DMI	MG30-DMIT-M1	10.5	1833	10.70	9.35	1856	50	41.24	2258
	MG30-DMIT-M2			10.77	9.86	1849	100	49.14	2690
	MG30-DMIT-M3			10.85	9.68	1852	150	59.82	3275
	MG30-DMIT-M4			10.79	9.95	1847	50	41.09	2250
	MG30-DMIT-M5			10.72	Unknown	Unknown	100	48.66	2664
	MG30-DMIT-M6			10.87	Unknown	Unknown	150	57.29	3136

A remark on Table 4.5 is that specimen "RCA-DMIT-M4" and specimen "MG30-MONO-M2" are reported with zero confinement stress. It was not intented to test these specimens on zero confinement, but after unexpected premature failure, the membranes were checked and both showed small ruptures. Therefore, zero pressure difference between the triaxial cell and the specimen is assumed. The results justify this assumption. For all recycled materials, it is found that milling causes a slight increase in friction angle and a moderate drop in the cohesion. Overall, no drastic changes in shear properties are observed between the milled and unmilled materials (Figure 4.7).

4.3.1. FAILURE BEHAVIOR

The triaxial test machine applies a controlled displacement of 3 mm per minute and measures the resisting force of the specimen. At a certain point the rate of which the force develops starts to reduce. This indicates that the specimen has started to fail. After the peak strength is reached, the resisting force gradually decreases. The test is stopped after a total vertical displacement of 15 mm is reached. Figure 4.4 shows the force - displacement curves of G2 and MG65 after durability milling. The force - displacement curves of all tests can be found in Appendix G.

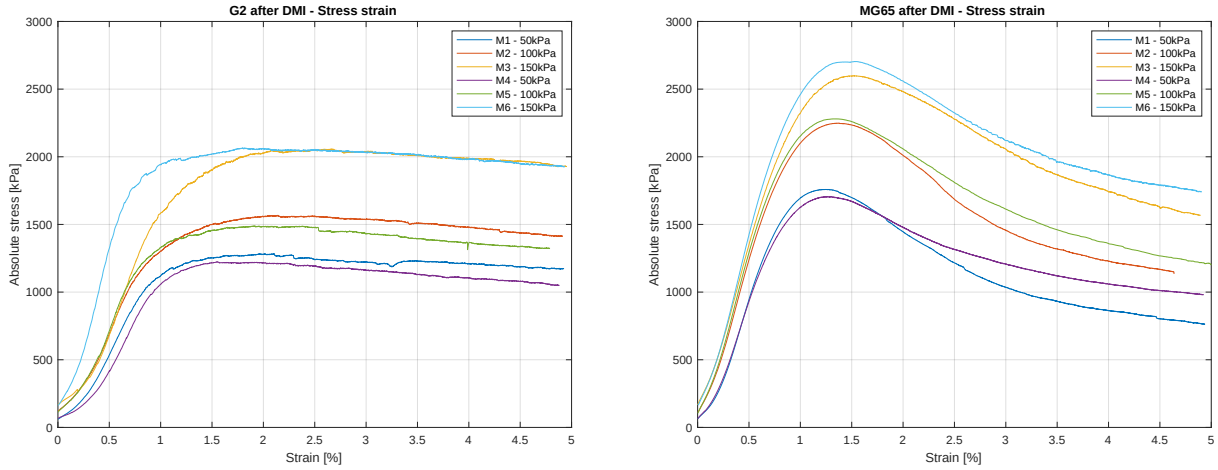

Figure 4.4: Monotonic triaxial test results for G2 and MG65 after durability milling

Figure 4.5: Typical shear failure observed in recycled aggregates

Different failure modes are observed between the G2 and the recycled materials. In all G2 samples, a more plastic type of failure occurs, meaning that after reaching the peak strength only little decrease in resisting force is measured. The recycled materials show more brittle behavior, with a clear drop in resisting force after reaching the peak strength. The different failure mechanisms can also be noticed when observing the specimens after testing. Typical shear cracking in the recycled aggregate specimens associated with brittle failure are presented in Figure 4.5. The G2 specimens do not show these shear planes, but rather develop a dilatation of the middle part as displacement further increases. An explanation for this difference can be that when failure occures, the recycled material particles (and conglomerates of particles) tend to break and shear, while the stronger G2 particles roll over each other and/or redistribute themselves. The latter explains the observed dilatation and the remaining of strength in the G2 specimens. Considering the differences in cohesion between the G2 and the recycled materials, it makes sense that more brittle behavior is observed in the recycled aggregates. Highly cohesive granulates act stiff and are generally associated with brittle failure.

4.3.2. SHEAR PARAMETERS

With the failure loads known, the shear properties of each material batch can be estimated by linear curve fitting of Equation 2.4 (see also the Mohr-Coulomb theory explained in Section 2.3.1). A visualisation of the Mohr-Coulomb circles with corresponding failure envelope for the mixed granulate MG65 is shown in Figure 4.6. The Mohr-Coulomb graphs of the other materials can be found in Appendix G. In Table 4.6, the friction angle, cohesion and coefficient of determination (R^2) of all batches are presented. Apart from the first batch of unmilled G2 materials, the coëfficient of determination values are very close to 1, implying consistency within the results. Although the results of the unmilled G2 materials are very inconsistent, the shear angle and cohesion fall within realistic ranges compared to the findings of Rudman (c = 245.5 kPa & 176.4 kPa , ϕ = 47.7° & 50.9°) [19] and Van Zyl (c = 109.47 kPa, ϕ = 50°) [29]. It is therefore decided not to redo the tests and continue with these values.

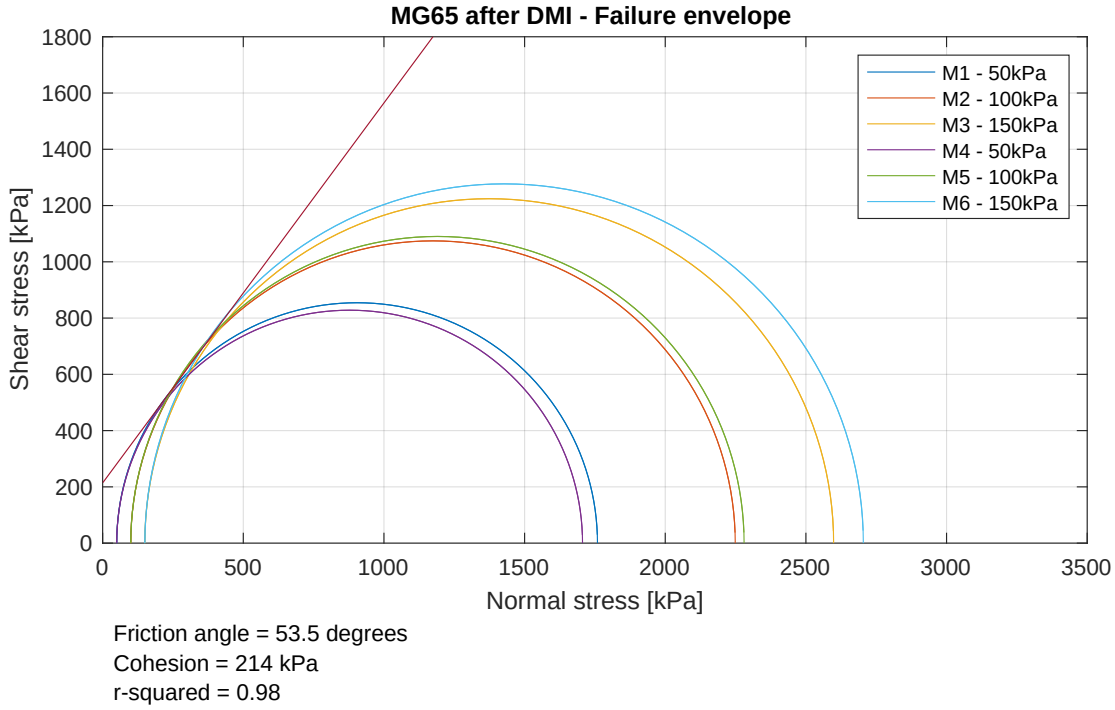

Figure 4.6: Mohr circles for milled MG65 after monotonic triaxial testing

Table 4.6: Shear properties of the tested materials

Material	Friction angle [°]	Cohesion [kPa]	R^2 [-]
G2 before DMI	50.1	141	0.63
G2 after DMI	51.2	142	0.96
RCA before DMI	55.1	233	0.95
RCA after DMI	56.6	178	0.98
MG65 before DMI	51.2	354	0.95
MG65 after DMI	53.5	214	0.98
MG30 before DMI	53.9	328	0.99
MG30 after DMI	54.1	285	0.99

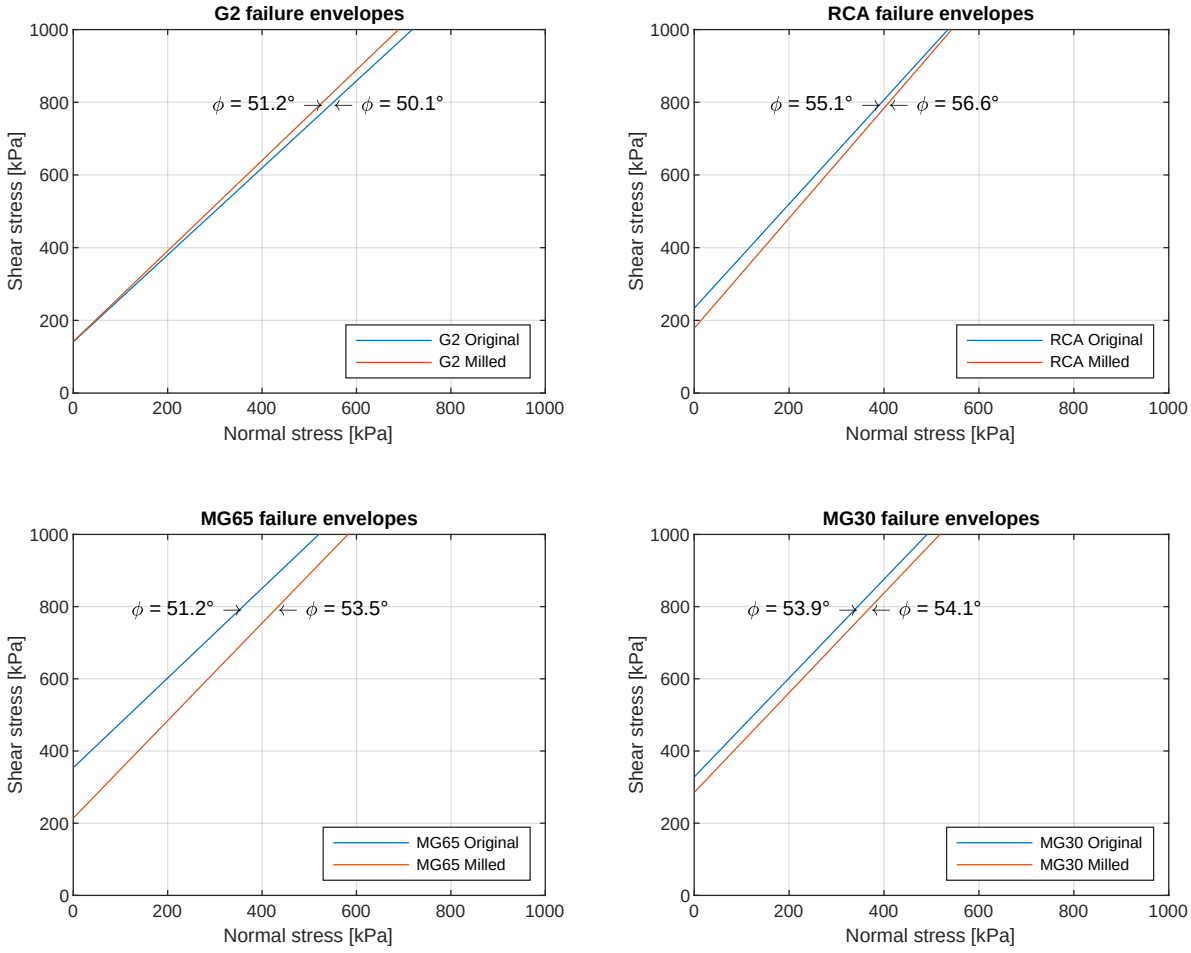

Figure 4.7: Comparison of failure envelopes within materials

All recycled materials, milled and unmilled, have equal or higher internal angles of friction compared to the G2 materials. Cohesion is in all cases significantly higher in the recycled materials. A recalculation of the failure loads based on the shear parameters is made for all materials at 100 kPa confinement (Figure 4.8). For the recycled materials, durability milling always causes a decrease in absolute compressive strength when compared in realistic ranges of confinement stress. This observation is attributed to the decrease in cohesion. The increase in friction angle would cause the difference between milled and unmilled specimens to decrease with increasing confinement stress, but, it is only at very high confinement stresses that the absolute compressive strength is expected to be equal or even higher after durability milling. The decrease in cohesion might be caused by increased water absorption and lower degree of compaction in the milled specimens. The milled samples contain broken down

particles and thus experience an increase of total particle surface. Since the moisture content is kept equal between the milled and unmilled specimens, the milled samples appear more dry, with a possible loss of cohesion. This phenomina is also observed at the mixing and compaction stage, where the milled specimens were significantly dryer than the unmilled ones. Furthermore, the required compaction time for the milled specimens was almost always less than the compaction time needed to compact the unmilled specimens. This implies that although the dry density is kept equal, the maximum dry density of the milled specimens is higher and thus the degree of compaction at testing lower. Afterwards a more fair comparison could be made should both milled and unmilled specimens be tested at their own specific optimum moisture content and maximum dry density. The durability milled specimens would then have a slightly higher density and moisture content, which is reasonable for the field conditions at the end of surface life. Other reasons for the decrease of cohesion could be loss of surface roughness and the fact that the amount of larger particles in the grain skeleton is reduced. It is recognized that the recycled materials have some self-cementing properties. The latent cement in the RCA can react with the added water and form strong cohesive bonds. However, since the curing time of the specimens is 24 hours, the effects of self-cementation are nihil. Bredenkamp [3] tested pure RCA specimens with a curing time of a month to study the influence of self-cementation. The specimens appeared to be bonded so well that the triaxial machine was unable to reach its peak strength.

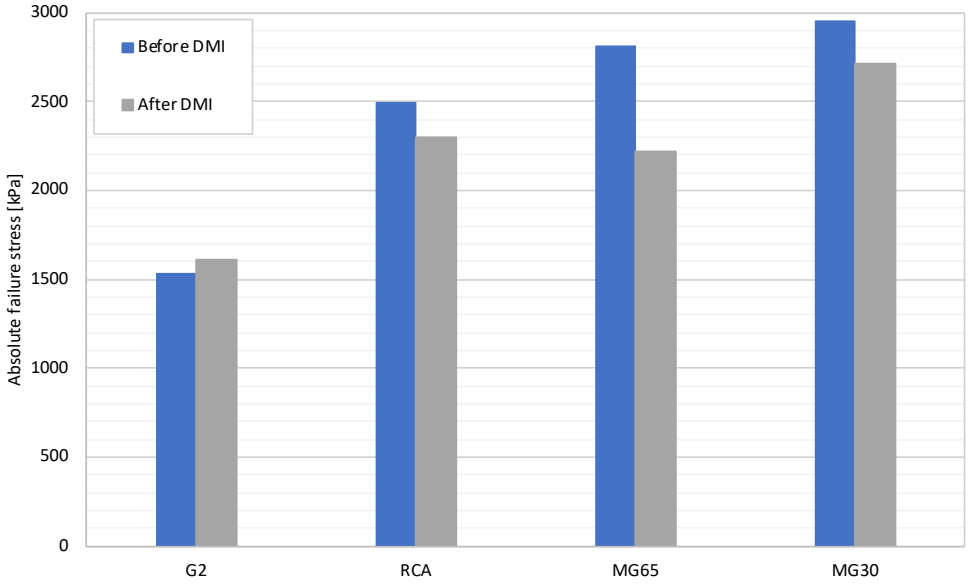

Figure 4.8: Absolute compressive strength modelled with Mohr-Coulomb at 100 kPa confinement stress

Another observation is that the absolute strength of the unmilled materials seems to improve with masonry content. This was not expected but may be caused by similar reasons as why more breakdown is observed in the RCA. It is believed that at failure, shearing happens within the recycled particles (the particles actually break) which causes a brittle type of failure. The results from the DMI show that the RCA breaks down more than RCM, suggesting that the masonry particles are stronger than the mortar binding the RCA and possibly less prone to shear cracking. Another reason for the increase in strength might be the fact that less compaction damage is observed in samples with increased masonry content (although not always significant). It is found that the majority of the compaction breakdown happens in the largest fraction, thus the grain skeleton of the masonry containing samples is probably kept more intact than the pure RCA ones. For the milled recycled materials, no such relationship could be observed. It is unclear why MG65 experiences such a significant loss of cohesion (and thus in absolute strength) when compared to MG30 or pure RCA.

It is tried to see whether an empirical relationship exists between the change in grading and the change in cohesion. The change of the shear angles are nihil and therefore not taken into account. The considered parameters are material breakdown (as defined in Section 4.2.4), the coefficient of uniformity (C_u), the coefficient of curvature C_c) and the cohesion. The results of this exercise can be found in Appendix F.11. Although it is clear that durability milling causes a reduction of cohesion and that the RCA is more prone to breakdown than RCM, no distict relationship between breakdown and the shear parameters could be found.

A final remark is that for G2, the cohesion is almost unchanged after durability milling. The compressive strength even improves after durability milling. It is believed that this could be the result of the poor preparation of the first batch of unmilled samples. It is expected that the cohesion (and thus the compressive strength) of the milled G2 samples should be slightly lower than the unmilled ones. However, due to only little breakdown in the G2 materials these differences are not expected to be significant.

4.3.3. COMPARISONS WITH OTHER RESEARCH

The shear parameters of the unmilled specimens can be compared with other research. When considering the pure RCA there are good correlations with the findings of Bredenkamp [3] and Rudman [19]. Bredenkamp used exactly the same source of concrete and found a cohesion of 274 kPa and an interal angle of friction of 54.6°. Rudman (Figure 4.9, right) found 252 kPa and 51°, respectively. Both recognised the high cohesion levels in comparison with other research, and attributed it to the age and processing steps of this relatively newly crushed concrete. Apart from the RCA tested by Rudman, Figure 4.9 (right) also containes the shear parameters of some blends obtained by Barisanga [2]. When comparing the unmilled MG65 with the 70C:30M [80-102] (the closest resemblance, although it is unknown how 102% modified AASHTO density relates to the 97% vibratory compaction), very good agreement is found. MG30 and 30C:70M [80-102] do show similar friction angles but differ noticably in cohesion. Older research done by Van Niekerk [14] shows more contradictions. In here, both the cohesion and friction angle are found to be significantly different in comparison with the blends tested by Barisanga and in this study (Figure 4.9, left). Differences in specimen size, application of confinement, density, grading, degree of compaction and material processing however make these results less comparable. Furthermore, Van Niekerk's finding that cohesion increases with increasing RCA content also conflicts with the results presented here. A rise in compressive strength with increasing RCA content was measured by Van Niekerk, while in this research it appears to be the other way around (Figure 4.8).

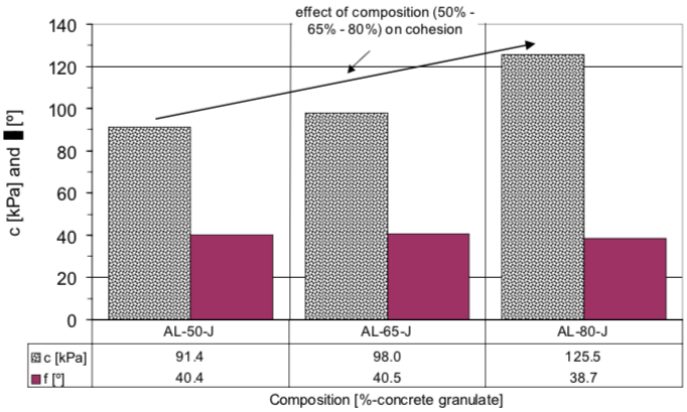

Material Type	Cohesion	Friction Angle	R^2
Tulip Concrete 1 Day	166	53.3	0.99
New Concrete 1 Day	252.1	51	0.99
New Concrete 1 Month	317.6	61	0.99
Hornfels G2	245.5	47.7	0.98
Hornfels G2	176.43	50.9	0.96
70C:30M [70_100]	223	45.4	0.997
70C:30M [80_100]	266	48.72	0.993
70C:30M [70_102]	314	48.4	0.919
70C:30M [80_102]	313	51.3	0.992
30C:70M [70_100]	286	42.5	0.97
30C:70M [80_100]	171.5	50.3	0.956
30C:70M [70_102]	257	48.4	0.998
30C:70M [80_102]	203	53.6	0.992

Figure 4.9: Left: Shear parameters of mixed granules as a function of composition by Van Niekerk [14]. Specimens are tested after PD testing (4-days) **Right:** Cohesion [kPa] and friction angle [°] of G2 and several recycled (mixed) granulates [19]. **Nomenclature:** (RCA:RCM)[%OMC_%modAASHTO]

4.4. PERMANENT DEFORMATION TRIAXIAL TESTING

Similar to the previous section, a summary of the permanent deformation tests is given in Table 4.7. Permanent deformation tests are conducted on RCA and MG65, both milled and unmilled. All specimens are tested for 250,000 cycles with a confinement stress of 100 kPa. The failure loads used to calculate the applied deviator loading are based on the mean measured strength of the corresponding unmilled monotonic triaxial tests. This means that the deviator stress ratios between the milled and unmilled specimens are different, but that the absolute loading is the same. The difference in deviator stress ratios can also be interpretated as an indicator of disadvantage for the milled specimens. A recalculation of the deviator stress ratios based on the modelled failure loads at 100 kPa (which are obtained from the shear parameters) is included in the table as well. The absolute failure load in the last column represents the remaining monotonic strength after testing. For specimen "RCA-DMIT-PD3" no absolute failure load could be obtained as a result of early failure after 153,000 cycles.

Table 4.7: Permanent deformation triaxial test results

Test	Specimen ID	Target MC [%]	Target DD [kg/m^2]	Mixing MC [%]	Specimen MC [%]	Dry mass [kg]	Height [mm]	Dry density [kg/m^2]
RCA before DMI	RCA-PERM-PD1	10	2018	10.59	9.87	11.019	302.00	1998
	RCA-PERM-PD2			10.64	9.83	11.023	298.00	2025
	RCA-PERM-PD3			10.60	9.49	11.060	299.50	2022
RCA after DMI	RCA-DMIT-PD1	10	2018	10.26	9.50	11.042	299.75	2017
	RCA-DMIT-PD2			10.64	9.14	11.083	300.25	2021
	RCA-DMIT-PD3			10.65	9.26	11.058	306.50	1975
MG65 before DMI	MG65-PERM-PD1	10	1905	10.59	9.31	10.402	297.75	1913
	MG65-PERM-PD2			10.24	8.93	10.435	298.25	1916
	MG65-PERM-PD3			10.19	9.29	10.398	298.00	1910
MG65 after DMI	MG65-DMIT-PD1	10	1905	10.31	9.35	10.395	298.25	1908
	MG65-DMIT-PD2			10.66	9.23	10.409	298.50	1909
	MG65-DMIT-PD3			10.34	9.32	10.394	300.25	1895

		Triaxial test loading conditions						
Test	Specimen ID	Confinement [kPa]	Target DSR [%]	Static deviator failure stress [kPa]	Applied deviator load [kN]	Applied deviator stress [kPa]	Actual DSR [%]	Absolute residual strength [kPa]
RCA before DMI	RCA-PERM-PD1	100	25	2395	9.98	546	22.82	2251
	RCA-PERM-PD2	100	30		11.98	656	27.39	2418
	RCA-PERM-PD3	100	35		13.98	765	31.96	2791
RCA after DMI	RCA-DMIT-PD1	100	25	2198	9.98	546	24.87	2360
	RCA-DMIT-PD2	100	30		11.98	656	29.85	2312
	RCA-DMIT-PD3	100	35		13.98	765	34.83	Failed in PD test
MG65 before DMI	MG65-PERM-PD1	100	25	2717	9.93	544	20.01	2268
	MG65-PERM-PD2	100	30		11.88	650	23.94	2239
	MG65-PERM-PD3	100	35		13.88	760	27.98	2674
MG65 after DMI	MG65-DMIT-PD1	100	25	2118	9.93	544	25.68	1814
	MG65-DMIT-PD2	100	30		11.88	650	30.72	2091
	MG65-DMIT-PD3	100	35		13.88	760	35.89	2075

The permanent deformation test results are plotted in Figure 4.10. A conditioning phase of 500 cycles with a cyclic deviator loading of 5 kN (273.7 kPa) preceeds all tests. It is important to note that the permanent deformation occuring during this phase is not taken into account, and that the zero measurement is taken immediatly after conditioning. The triaxial test machine records the force and displacement data of the first five of every 1000 load cycles. In other research performed at Stellenbosch University it is commonly believed that the machine records the last five cycles per 1000 cycles, but when comparing the measured displacements between the last cycle of the conditioning phase and the first five cycles recorded in the test, it can be concluded that these cycles must folow up each other (an interval of 995 cycles seems unrealistic when looking at the measured displacements). The

permanent deformation values are then derived from the displacement data as the average strain between 0.3s and 0.9s of each load cycle, when the loading is in its static 'resting' phase of 0.4 kN (21.9 kPa). It is recognized that small specimen imperfections and anomalities can significantly influence the permanent deformation results [14]. Since every test is performed only once, its statistical uncertainty should be taken into account. The curves however show typical permanent deformation behavior, with large permanent strains in the beginning of the test stabilizing after further increase of load cycles. In all cases, the development of permanent deformation gets larger with increasing deviator stress ratio. Unstable behavior can be observed in the milled RCA and milled MG65 at deviator stress ratios of 34.83% and 35.89%, respectively. The results imply that the DSR for these materials may not exceed ±30% to avoid instability. This is low, and remarkable in comparison with the relatively high shear parameters. Together with this, specimens which show stable behavior in the range up to 250,000 load cycles might still become unstable when tested up to 1,000,000 or even more load cycles. When considering specimen RCA-PERM-PD3 for instance, instability in a later stage is expected because of the relatively high strain rate (the slope of the PD curve). For design purposes, it would be very useful to know at what degree of loading instability occurs. The prediction of unstable behavior has been intensively studied over the years but remains an extremely complex task. In the next chapter the permanent deformation results are further analyzed. The Shakedown theory as suggested by Werkmeister [28] is applied to see whether or not instability could be expected based on the behavior in the early stages of the test. In conjuction with this, (stress dependent) modelling and dissipated energy calculations are performed to see if any predicions can be made regarding unstable behavior.

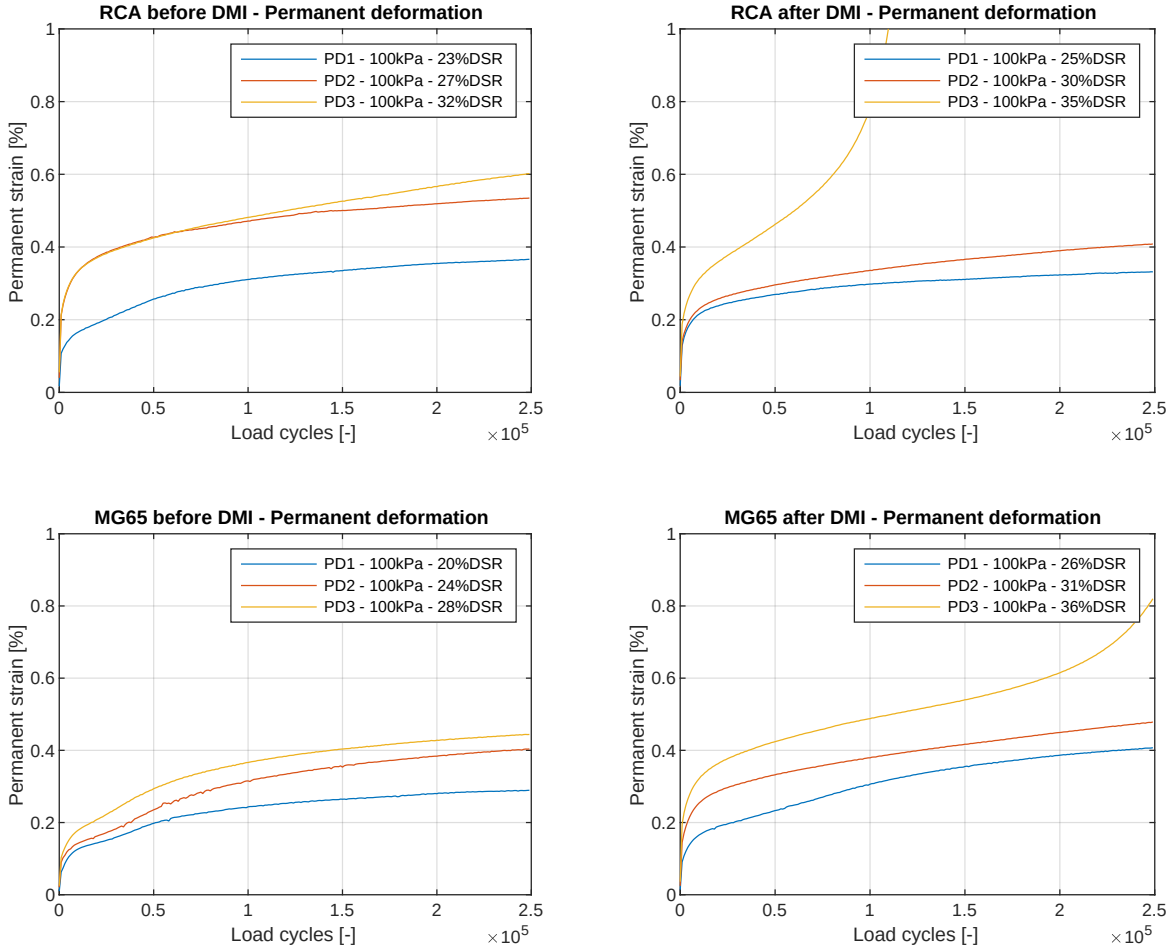

Figure 4.10: Permanent deformation triaxial test results

4.4.1. REMAINING STRENGTH

The force-displacement curves of the monotonic triaxial tests done after permanent deformation testing can be found in Appendix H. A comparison between the monotonic failure loads measured after permanent deformation testing and those modelled based on the shear parameters is plotted in Figure 4.11. The absolute strength seems to decrease in the MG65 blend after permanent deformation testing, but, no clear relationship could be observed in the RCA materials. A decrease of the compressive strength is expected in general due to particle wear. In contrast, permanent deformation testing can also result in an increase of density which improves the compressive strength. This can be seen when comparing the monotonic failure loads of the specimens tested at 545 kPa and 760 kPa. The latter always appears higher, which may be attributed to a greater increase in density. Furthermore, when considering specimen MG65-DMIT-PD3 (tested at 760 kPa deviator stress), it can be seen that the residual strength is still in the same range as to the other two milled MG65 specimens. This is a noticeable observation since the specimen has already started to fail. It suggests that the monotonic failure stress was higher in the earlier stages of the test, with similar pattern as the residual strength measured in RCA before DMI.

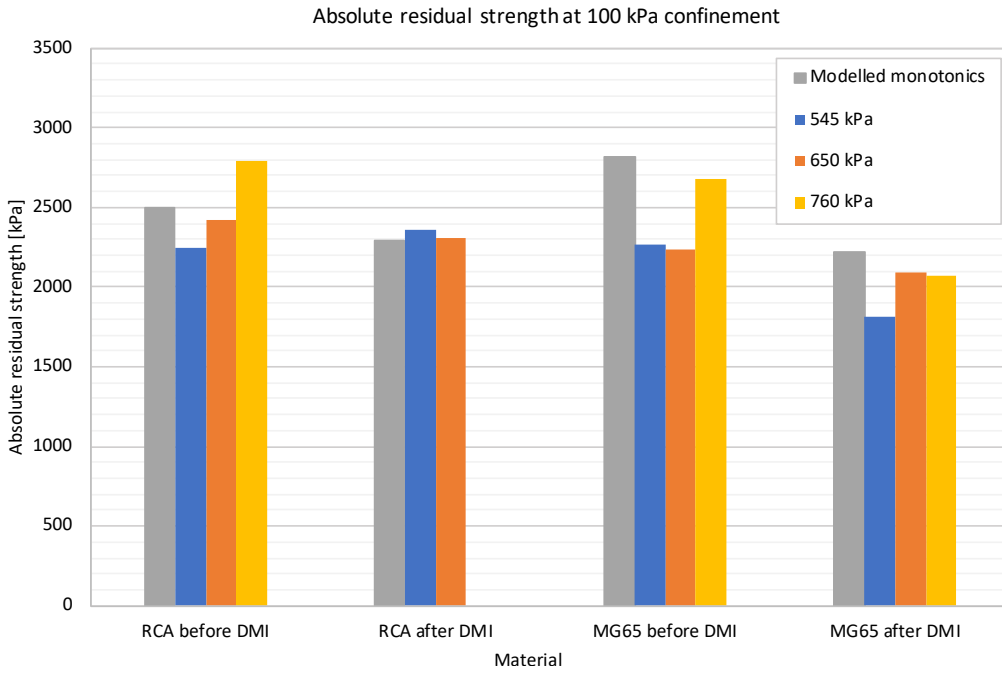

Figure 4.11: Comparisons of monotonic triaxial test results after permanent deformation triaxial testing

4.4.2. COMPARISONS WITH OTHER RESEARCH

In terms of RCA resource and triaxial testing method the findings in this research are best to be compared with Bredenkamp [3]. Bredenkamp also studied the effects of a durability simulation on the performance parameters of RCA and used the exact same source of RCA and the same triaxial test set-up. Instead of simulating mechanical durability with the durability mill, Bredenkamp focussed on chemical breakdown. By exposing the RCA in a water bath of 40°C for 14 days, it was aimed to induce self-cementation within the material. Monotonic and permanent deformation triaxial tests were performed before and after exposing. The shear parameters of the exposed materials showed more variability but did not differ significantly from the unexposed ones. The permanent deformation results, on the other hand, did show significant differences. Independent of confinement stress, all exposed samples

tested at a DSR of 27% became unstable. The unexposed specimens showed instability starting at 37% DSR. Similar as in this research, instability already occured at relatively low DSR levels while the shear parameters are high. The general conclusion of Bredenkamp that the shear parameters alone are not sufficient to obtain a justified characterisation of the material behavior is therefore agreed. The permanent deformation results of Bredenkamps unexposed, original material (which is comparable with the unmilled RCA materials in this research) are shown in Figure 4.12. In the stable specimens, the absolute accumulated strains at the end of the tests are in all cases around 0.5% to 1.0% higher than the ones obtained in this research. It is assumed that Bredenkamp included the permanent deformation occuring in the conditioning phase in her results as well while this is not the case in this study. The specimens are tested at 37%, 45% and in a single case at 50% DSR with varying confinement stress. When considering the specimens tested at 100 kPa, three of the four specimens became unstable. It is unclear why the tests executed at 45% DSR shows rapid unstable behavior in the first batch and remains stable in the second batch, but it can be concluded that a DSR of 37% is too high for the materials. Interestingly, the permanent deformations appear to decrease with lower confinement stress at equal DSR levels. Bredenkamp argued that this might be caused due to breaking of self-cemented bonds by confinement pressure. However, it is questionable if the effects of self-cementation are already measurable in specimens which have only been cured for 24 hours.

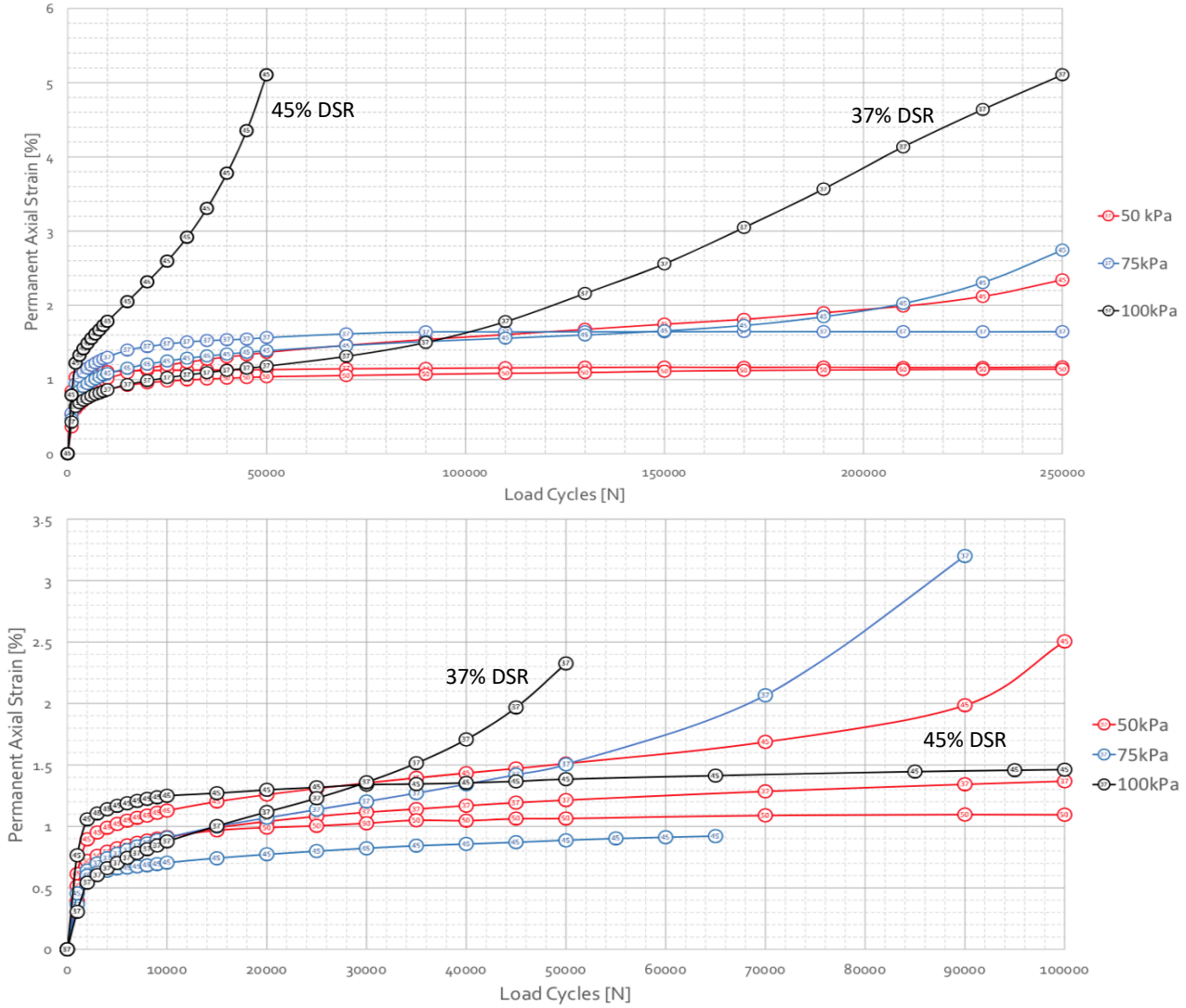

Figure 4.12: Permanent deformation triaxial test results of Bredenkamp [3]

Regarding the mixed granulates, Van Niekerk [14] performed several permanent deformation tests on MG65. Specimens of 600 mm x 300 mm were tested at three different stress ratios with a constant confinement stress of 12 kPa. The grading and the degree of compaction served as variables. The results were then modelled with the equations developed by Huurman (see Section 2.5). With the model parameters known, Van Niekerk calculated the absolute stress ratios ($\sigma_1/\sigma_{f,1}$) corresponding to the following permanent strain ranges:

- Negligible, i.e. ϵ_p = 1% at N = 1,000,000;
- Moderate, i.e. ϵ_p = 5% at N = 1,000,000;
- Excessive, i.e. ϵ_p = 10% at N = 50,000;

Excessive permanent strain, i.e. 10% after 50,000 load cycles, can also be interpretated as instability or failure. Figure 4.13 shows the results of the exercise for five different gradings at DOC = 100% (DD = 1735 kg/m^3). MC was for all specimens kept on 8%. Thresshold stress ratios were determined dependent on the lowest stress ratios of which the criteria above are met. It was found that for stress ratios lower than 25%, the permanent strains fell always in the neglible range. For stress ratios lower than 38%, the permanent strains would never exceed the moderate range. The governing grading for both thressholds is the coursest, lower limit grading (see Section 2.1 for the definition of the used gradings). The other gradings show a more discrete behavior, with very small differences in stress levels between the negligible and excessive permanent strain ranges. This corresponds with the findings in this research, where the behavior is either stable, with very limited permanent strains, or unstable, with rapid progressing permanent strains. The permanent strains in stable specimens never exceeded 0.6% after 250,000 cycles. Higher permanent strain levels were only observed in unstable specimens.

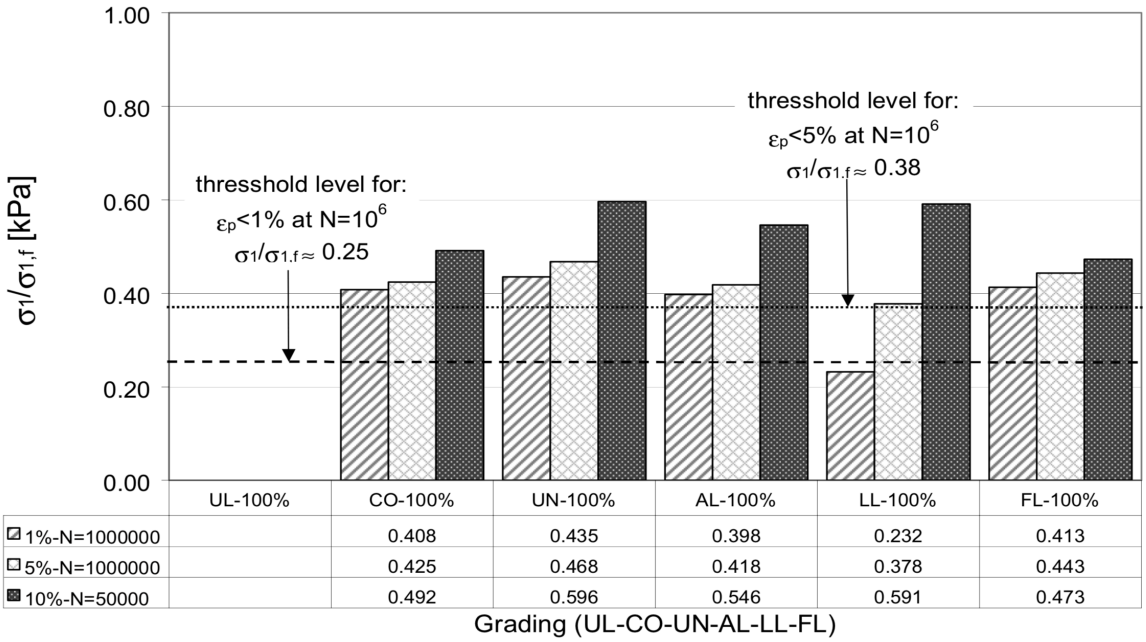

Figure 4.13: Backcalculation of absolute stress ratios for ϵ_p = 1% and 5% after N = 10e^6 and ϵ_p = 10% after N = 5e^5 [14]

Due to differences in grading, density, moisture content, specimen size and triaxial set-up, the concluded 'thresshold' of maximum 30% DSR cannot directly be compared with the thresshold of 25% ASR (Absolute Stress Ratio) obtained by Van Niekerk. Together with that, the absolute and relative stress levels at which both materials are tested differ significantly. However, when considering the model corresponding to AL-100% (average grading,

the closest resemblance of the grading used in this research), a rough comparison between the obtained results can be made. The model predicts 1% and 5% permanent strain after 1,000,000 load cycles at absolute stress ratios of 39.8% (38.3% DSR) and 41.8% (40.3% DSR), respectively. Although not tested, it is expected that instability would occur if these stress levels were applied in this research (the pure RCA tested by Bredenkamp showed that this is actually the case). The model suggests that the materials tested by Van Niekerk can withstand cyclic loading better. This is especially true when taking into account that the specimen dry densities of Van Niekerk are considerably lower than the dry densities used in this research (1905 kg/m^3 v.s. 1735 kg/m^3). By using the model parameters for AL-100% (r^2 = 0.997), it is possible to relate the findings of Van Niekerk at the same deviatoric stress levels as used in this research. A comparison between the obtained results for MG65 before DMI and the predicted permanent deformations by Van Niekerks model is shown in Figure 4.14. A possible reason for these considerable differences can the difference in processing. The materials used in this study underwent only one jaw-crushing step, while the materials in work of Van Niekerk were subjected to two (primary and jaw) crushing steps. Multiple processing steps may break of weak (mortar) bonds better and result in a higher quality end product. In further studies, it is worthwile to investigate different steps of processing to acquire the most optimal materials. Another explanation for the observed differences relates to differences in absolute stress levels. Although some researchers argue that DSR levels can be used as an independent measure to decribe stress states in a material [14], it is very likely that differences in confinement stress (12 kPa versus 100 kPa) plays an important role here.

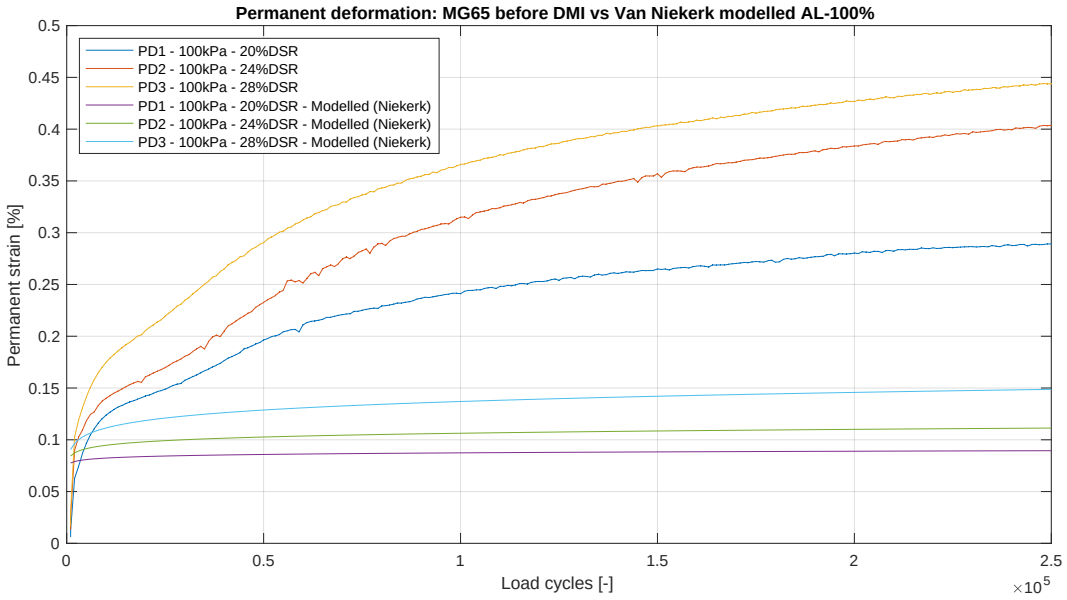

Figure 4.14: Permanent deformations: MG65 vs Van Niekerk modelled AL-100%

4.5. CHAPTER SUMMARY & CONCLUSIONS

This chapter contains the acquired test results and a first analysis of the observed material behavior. Where possible, comparisons with other work are made. To optimize comparisons with other tests conducted at Stellenbosch University, the MATLAB tools to read out this specific triaxial machine can be used in further studies. Especially for finding Huurman's parameters and filtering relevant data from the large datafiles, these scripts may be very usefull. From the obtained results, the following conclusions can be drawn:

DURABILITY TESTING

- Durability milling causes the most degradation in the pure RCA. The G2 is the least affected. In general, it appears that breakdown reduces with increasing masonry content. This leads to the hypothesis that the mortar binding the concrete aggregates is the weakest part in the mixed materials. It is recognized that the quality of the concrete and masonry granulates may play an imporant rol. The variability of the resources should be studied to verify if this finding also holds in general.
- For the G2 and the RCA, wet ball milling causes the most severe breakdown. For the materials containing masonry, dry ball milling results in slightly more degradation than wet ball milling. Wet milling is in all cases the least damaging durability mill procedure. For non-plastic materials, wet milling seems unnecessary.
- The Durability Mill Index, as prescribed by the standards [23], is not a good measure to quantify durability of non-plastic materials. In the calculation, non-plastic materials will practically always be classified as sound, regardless of the amount of breakdown. In this research, the recycled materials rank higher than the G2 while the degradation is much more severe.
- Significant breakdown is measured in specimens sieved out after monotonic triaxial testing. This implies that the vibratory compactor already damages the material. It is likely that a similar amount of damage also occurs should these materials be applied in practice. The breakdown affects mainly the largest, 14 mm, particle fraction.

PERFORMANCE TESTING

- Substantial values of the shear parameters, especially cohesion, are observed in the recycled materials. The highest cohesion is measured in the unmilled MG30, the highest internal angle of friction is measured in the unmilled RCA. For the unmilled recycled materials, it appears that the cohesion increases with increasing masonry content.
- The effect of durability milling on the performance of G2 is limited. In the recycled materials, wet ball milling causes a small increase in the internal angle of friction and a moderate decrease of cohesion. The latter is of the biggest influence with respect to the material's compressive strength, as all specimens have become weaker after durability milling.
- Different types of monotonic failure can be observed between the G2 and the recyled materials. In the G2, the specimens show a plastic type of failure. After reaching the peak strength, the resisting force maintains relatively high and a dilatation of the middle part of the specimen can be observed. The recycled materials show a more brittle type of failure. After reaching the peak strength, a shear plane is developed and the resisting force quickly reduces. It is only after considerable strains ($\epsilon > 5\%$) that the resisting strength of the G2 materials is higher than that of the recycled materials.
- Monotonic triaxial testing alone is not sufficient for an adequate material characterisation. The permanent deformation results show that although the shear parameters indicate sound behavior, delayed shear failure may still occur. Even at low DSR levels, long term stability is not guaranteed.
- The permanent deformations occuring in stable specimens are limited to less than 1 percent. Instability is measured in the milled specimens tested at DSR > 30%. For this reason, 30% DSR is concluded as the limit stress level at which stable behavior (up to 250,000 load cycles) may be expected.

5

RESULT ANALYSIS

This chapter provides an in depth analysation of the obtained triaxial test results. The main focus lies on the permanent deformation behavior. It is aimed to study the influence of durability milling and to see whether eventual instability can be predicted in the early stages of the tests. As a starting point, the permanent deformation test results are modelled with the equations provided by Huurman [10]. From there, the strain rates (the change of permanent strain accumulation per load cycle) are calculated and the applicability of the shakedown theory proposed by Werkmeister [28] is checked. In addition to that, the dissipated energy and stiffness response curves with respect to the number of load cycles are analysed, to see if any predictions with regarding durability issues and instability can be made. The chapter finalises with a small pavement assesment to obtain a first insight in the expected stress levels in a reference pavement. These stress levels are then compared with the boundary limits, obtained in the previous chapter, to enable sound judgement. The Matlab scripts mentioned in Chapter 4 form the basis of all calculations and illustrations. Enlarged figures of the presented graphs can be found in Appendix G and Appendix H.

5.1. PERMANENT DEFORMATION TRIAXIAL TESTING

5.1.1. PERMANENT DEFORMATION MODELLING

The permanent deformation triaxial test results are modelled using Equation 5.1 developed by Huurman [10]. Determination of the parameters A, B, C, D is done by iteration. Per parameter, the chosen starting value are -0.2, -0.1, 0, 0.1 and 0.2 (in total 5^5 = 3125 combinations of starting values are evaluated per test). The parameters corresponding to the best fit are recorded and presented in Table 5.1. Although only the milled specimens PD3 develop unstable behavior, all twelve test results are modelled including the second term of the equation as this results in a better fit. The unstable specimens are modelled until maximum strain of 2.0%. The test results of RCA-DMIT-PD3 includes records up to 7.0%, but taking this into account in the model disturbs the accuracy of the fit in the more important initial phase of the test.

$$\epsilon_p = A \cdot \left(\frac{N}{1000}\right)^B + C \cdot \left(e^{D \cdot \frac{N}{1000}} - 1\right) \tag{5.1}$$

Where:

ϵ_p	= Permanent strain [%]
N	= Number of load cycles [-]
A, B, C, D	= Model parameters [%, -]

Table 5.1: Permanent deformation model parameters for stress independent Huurman modelling

Test	Specimen ID	A [%]	B [-]	C [%]	D [-]	$\sum d^2$	R^2
RCA before DMI	RCA-PERM-PD1	0.0983	0.1595	-0.1305	-0.0161	0.0020	0.9979
	RCA-PERM-PD2	0.2123	0.1990	0.1266	-0.0063	0.0018	0.9983
	RCA-PERM-PD3	0.2127	0.2253	0.1372	-0.0207	0.0004	0.9998
RCA after DMI	RCA-DMIT-PD1	0.1014	0.1735	-0.0698	-0.3033	0.0011	0.9973
	RCA-DMIT-PD2	0.1463	0.2109	0.0589	-0.0203	0.0004	0.9995
	RCA-DMIT-PD3	0.1588	0.2769	0.0001	0.0760	0.0219	0.9985
MG65 before DMI	MG65-PERM-PD1	0.0670	0.1831	-0.1072	-0.0163	0.0021	0.9969
	MG65-PERM-PD2	0.0836	0.1025	-0.2757	-0.0104	0.0043	0.9975
	MG65-PERM-PD3	0.0997	0.1641	-0.2020	-0.0143	0.0018	0.9990
MG65 after DMI	MG65-DMIT-PD1	0.1047	0.2815	0.0790	-0.0675	0.0046	0.9970
	MG65-DMIT-PD2	0.1512	0.2497	0.1229	-0.0161	0.0005	0.9996
	MG65-DMIT-PD3	0.2044	0.1877	0.0003	0.0273	0.0026	0.9993

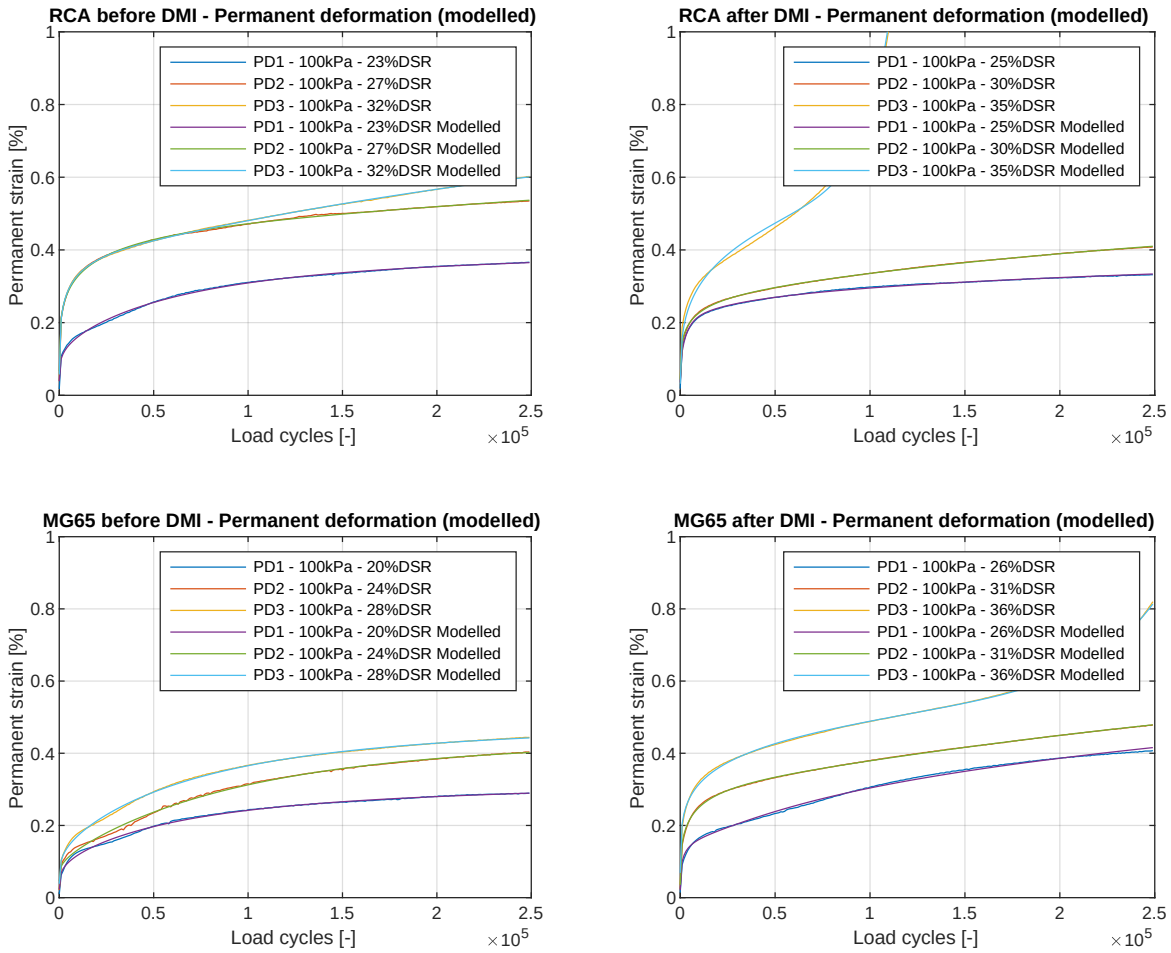

Figure 5.1: Stress independent modelling of permanent deformation triaxial test results (all tests)

As can be seen in the table, the models fit the data very well. The graphs corresponding to the models are presented in Figure 5.1. Considering the overlap in the unmilled RCA-PERM-PD2 and RCA-PERM-PD3, and the relatively wide gap between RCA-PERM-PD1 and RCA-PERM-PD3, it is believed that the permanent deformations occuring in the

beginning of RCA-PERM-PD2 are incidentally on the high side. It is expected that the curve for this test will shift downwards in case the test is repeated. The model parameters A, B, C and D are stress dependent and defined as follows:

$$A = a_1 \left(\frac{\sigma_d}{\sigma_{d,f}} \right)^{a_2} \qquad B = b_1 \left(\frac{\sigma_d}{\sigma_{d,f}} \right)^{b_2} \qquad C = c_1 \left(\frac{\sigma_d}{\sigma_{d,f}} \right)^{c_2} \qquad D = d_1 \left(\frac{\sigma_d}{\sigma_{d,f}} \right)^{d_2} \tag{5.2}$$

Where:

A, B, C, D = Model parameters [-]
σ_d = Vertical deviator stress [kPa] [-]
$\sigma_{d,f}$ = Vertical deviator failure stress [kPa]

With A, B, C, D and the deviator stress ratios known, it is tried to apply another curve fitting iteration step to obtain the parameters a, b c and d. It appeared very difficult, however, to achieve good results with materials containing both stable and unstable behavior. Stress dependent modelling in the range where the behavior is stable (up to 30% DSR), on the other hand, is possible. In this case, only the first term of Equation 5.1 is used. The corresponding parameters a_1, a_2, b_1 and b_2 are obtained by performing two iteration steps. Firstly, the parameters A and B are determined from the measured results similar as in the "full" model. A and B then serve as input for another curve fitting step to find the best fit for a_1, a_2, b_1 and b_2. The starting values for A and B range from -0.5 up to 0.5 with intervals of 0.1 (in total $11^2 = 121$ combinations of starting values). The starting values for a_1, a_2, b_1 and b_2 range from -2.5 up to 2.5, again with intervals of 0.1 (in total $51^2 = 2601$ combinations of starting values). Table 5.2 contains the results of the stress dependent modelling. The corresponding curves are presented in Figure 5.2. The obtained parameters can be used to calculate permanent deformations for the materials up to 250,000 load cycles in stress ranges below 30% DSR. An exception exists for MG65 before DMI, which is valid for stress ranges below 25% DSR. Care should be taken when extrapolating the model. Although the models fit well with the data, it can be seen in most curves that the strain rate at cycle 250,000 is different from the measurements. Although it is unknown what happens after 250,000 cycles, this is an indication that the model will start to deviate from the test results. Another point to consider is the fact that the obtained parameters are based on only two specimens per material. More permanent deformation tests should be carried out in order to gain a higher accuracy.

Table 5.2: Permanent deformation model parameters for stress dependent Huurman modelling (up to 30% DSR)

Material	a_1 [%]	a_2 [-]	b_1 [-]	b_2 [-]	$\sum d^2$	R^2
RCA before DMI	112.5222	4.7650	0.0049	-2.6362	0.0188	0.9909
RCA after DMI	0.0827	-0.4481	1.3505	1.6256	0.0089	0.9926
MG65 before DMI	0.0304	-0.5187	2.6154	1.4274	0.0305	0.9874
MG65 after DMI	22.5390	4.2551	0.0113	-2.4659	0.0244	0.9912

5.1.2. STRAIN RATE

The strain rate is defined as the change of accumulated permanent strains per load cycle. Due to noise and the non-continuous nature of the permanent deformation measurements, a numerical calculation based on the measured data did not lead to workable results. Therefore, the strain rate is calculated analytical based on the stress independent models derrived in the previous section. Taking the first derivative of Equation 5.1 with respect to the number of load cycles leads to:

$$\frac{d\epsilon_p}{dN} = \frac{A \cdot B}{1000} \cdot \left(\frac{N}{1000} \right)^{B-1} + \frac{C \cdot D}{1000} \cdot e^{D \cdot \frac{N}{1000}} = \frac{A \cdot B}{N} \cdot \left(\frac{N}{1000} \right)^{B} + \frac{C \cdot D}{1000} \cdot e^{D \cdot \frac{N}{1000}} \tag{5.3}$$

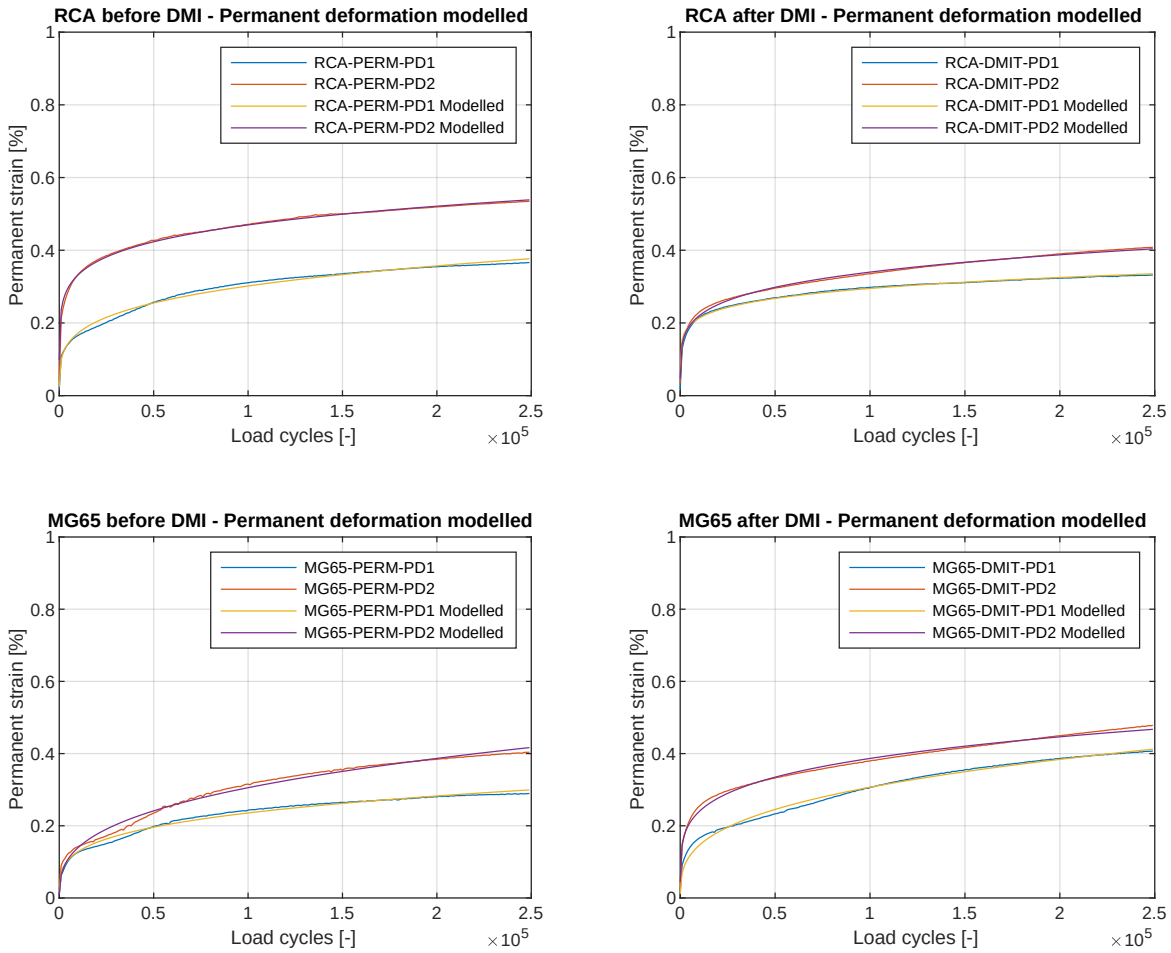

Figure 5.2: Stress dependent modelling of permanent deformation triaxial test results (up to 30% DSR)

Where $\frac{d\epsilon_p}{dN}$ [%] represents the strain rate at cycle N. The corresponding graphs are presented in Figure 5.3. It can be seen from the curves that the strain rates decrease rapidly in the beginning stages of the test. In the stable specimens, the decrease continues until reaching almost zero. Zero strain rate implies no accumulation of permanent strain and a fully resilient response. Instability can be recognized when the gradient of the curve becomes positive. In this case, the accumulation of permanent strain does not further decrease with increasing load cycles, and indicates that specimen has started to fail. This holds for the milled RCA and the milled MG65, tested at 35% DSR and 36% DSR, respectively. For the milled RCA, the onset of failure is after 53,000 cycles. For the milled MG65, the onset of failure is after 120,000 cycles. The disadvantage of durability milling is represented by the change of relative stress levels. The absolute stress levels are kept the same to gain a better understanding of the influence of durability milling and to simulate unchanged traffic loading conditions. In the MG65, the strain rates of the unmilled samples are smaller and have steeper negative gradients at the end of the test compared to the milled samples. Although less clearly, a similar pattern can be observed in the RCA.

Another common representation of the strain rate is in combination with the permanent deformation. Figure 5.4 shows the strain rate plotted against the permanent strain. Again, differences due to durability milling are clearly visible in the MG65. Steep negative slopes at the end of the test, as can be seen in all unmilled MG65 specimens, indicate a stable response. It is expected that these specimens would stay in the stable range when tested longer. The strain rates of the milled MG65 PD1 and PD2 are also fairly small, but considering the gradient of the curves

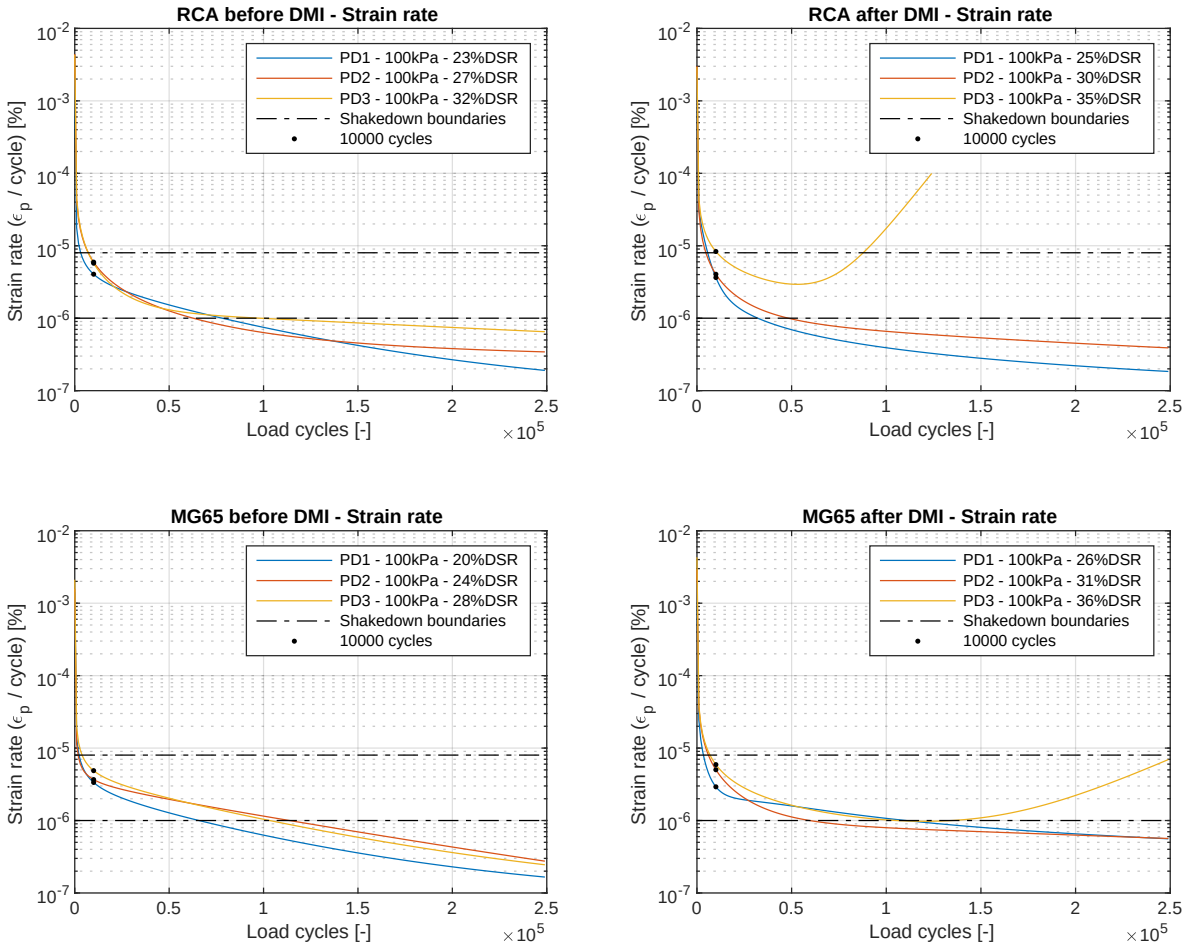

Figure 5.3: Strain rates of modelled permanent deformation triaxial test results

at the end of the test, it is expected that instability will occur sooner in these specimens when compared to their unmilled counterpart. Caution however is advised when extrapolating this data. Absolute conclusions about what will happen after 250,000 cycles cannot be drawn. Overall, the MG65 seems perform better initially, but is affected more by durability milling. In correspondence with the findings from the monotonic triaxial tests (represented by the DSR levels), the milled MG65 experiences a bigger drop in compressive strength in comparison with the RCA (see Figure 4.8). This is however in contrast to the change in grading found after durability milling. According to the obtained gradings, the MG65 suffers less damage than the RCA. It is unclear why the change in performance parameters is more severe than the RCA, while the degradation is less.

5.1.3. SHAKEDOWN LIMITS

The shakedown ranges in which the tested materials fall are determined for two sets of shakedown limits. Werkmeister [28] considered the difference between the accumulated permanent strain at cycle 5000 and cycle 3000, and proposed the following boundaries:

- Range A: $\epsilon_{p,5000} - \epsilon_{p,3000} < 0.045 \cdot 10^{-3}$
- Range B: $0.045 \cdot 10^{-3} < \epsilon_{p,5000} - \epsilon_{p,3000} < 0.4 \cdot 10^{-3}$
- Range C: $0.4 \cdot 10^{-3} < \epsilon_{p,5000} - \epsilon_{p,3000}$

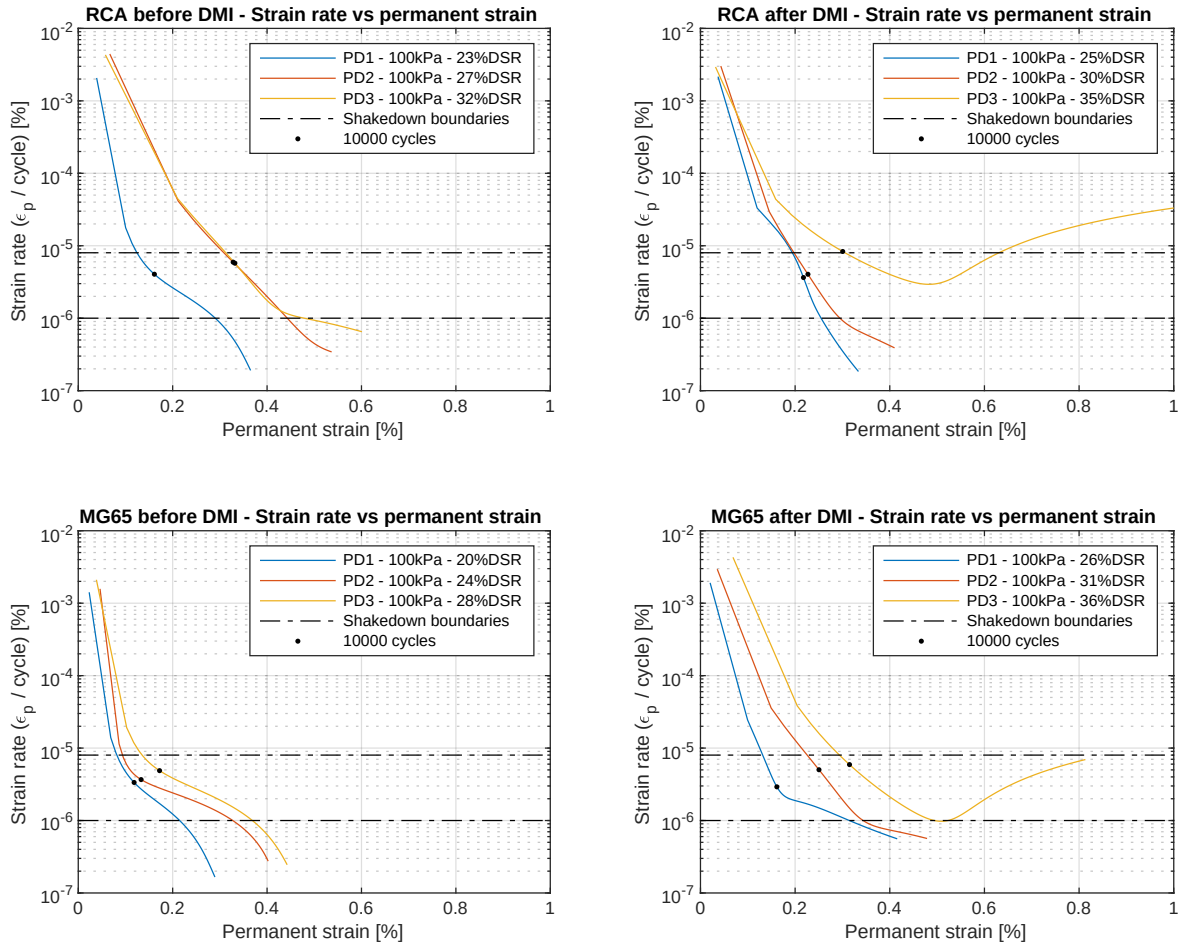

Figure 5.4: Strain rates versus permanent deformation of modelled permanent deformation triaxial test results

A slightly different approach, applied by Tao [26] but referenced as Werkmeister, is to consider the strain rate at cycle 10,000:

- Range A: $\frac{d\epsilon_p}{dN} < 1{\cdot}10^{-6}$
- Range B: $1{\cdot}10^{-6} < \frac{d\epsilon_p}{dN} < 8{\cdot}10^{-6}$
- Range C: $8{\cdot}10^{-6} < \frac{d\epsilon_p}{dN}$

The latter is graphically visualised in Figure 5.4 and Figure 5.3. The results for both sets of shakedown calculations are presented in Table 5.3. It can be seen that the first set of limits, denoted as Werkmeister, classifies all tests in range B. The second set, denoted as Tao, classifies all but one test in range B. This is a noticeable outcome since the responses between the specimens are considerably different. In correspondence with the definition of range B, however, the accumulation of plastic strains does indeed never become zero. This implies that plastic shakedown does not happen within 250,000 cycles, and therefore it is believed that range A behavior does not occur in the materials as tested in this study (even not in the unmilled MG65 materials). The methods differ in the classification of specimen RCA-DMIT-PD3. According to the boundaries adapted by Tao, the response of this sample if of range C. The boundaries applied by Werkmeister classify the response as range B. Range C behavior involves progressive strain accumulation and incremental collapse after a relatively small number of load cycles. Range B behavior shows a stable response in the beginning but may lead to failure after a more significant number of load cycles. No clear

formulation exists whether the onset of failure after 53,000 cycles should still be regarded as incremental collapse, but following the analogy of Figure 5.5, it seems more reasonable to classify RCA-DMIT-PD3 as range B instead of range C. This difference, however, is not considered very relevant since the response is a boundary case in both methods. The other specimens, including the unstable specimen MG65-DMIT-PD3, are believed to be classified correcty as range B in both cases.

Concluding on the above, shakedown range B embraces a wide variaty of responses. In practice, range A response is desired and range C response should be avoided at all times. Range B is much more unpredictable, but this does not automatically imply that all responses in this range are detrimental. Based on the obtained permanent deformation and strain rate curves, it is very likely that unmilled recycled granulates loaded below 30% DSR can withstand a significant number of load cycles before collapsing. Permanent deformation testing up to 1,000,000 load cycles is therefore adviced to gain a better understanding of the long term endurance. Together with that, permanent deformation tests conducted on G2 materials should be analysed for shakedown limits to serve as benchmark. It is the author's belief that, based on the proposed limits and test results, range B may also frequently occur in conventional, widely used materials tested under similar conditions.

Table 5.3: Shakedown limits of the permanent deformation triaxial test results

General	Final permanent deformation [%]	Shakedown limit Werkmeister	Shakedown limit Tao	Failure [-]	Instability [-]
RCA-PERM-PD1	0.37	B	B	No	No
RCA-PERM-PD2	0.53	B	B	No	No
RCA-PERM-PD3	0.60	B	B	No	No
RCA-DMIT-PD1	0.33	B	B	No	No
RCA-DMIT-PD2	0.41	B	B	No	No
RCA-DMIT-PD3	7.25	B	C	Yes	Yes
MG65-PERM-PD1	0.29	B	B	No	No
MG65-PERM-PD2	0.40	B	B	No	No
MG65-PERM-PD3	0.44	B	B	No	No
MG65-DMIT-PD1	0.41	B	B	No	No
MG65-DMIT-PD2	0.48	B	B	No	No
MG65-DMIT-PD3	0.82	B	B	No	Yes

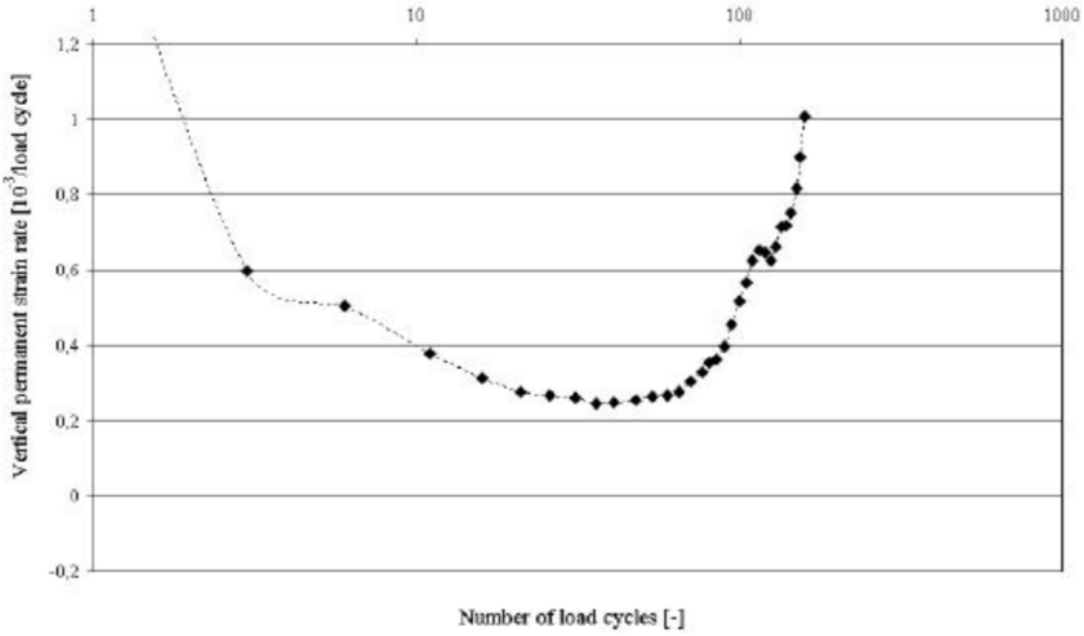

Figure 5.5: Example of shakedown range C according to Werkmeister [28]

5.1.4. DISSIPATED ENERGY

The dissipated energy per unit of volume can be estimated by calculating the area under the stress hysteresis loop. The triaxial machine records the the first five of every 1000 cycles. Every cycle consists of 256 axial force and axial displacement measurements. A typical obtained stress - strain path is shown in Figure 5.6, which contains the recorded data of MG65 after DMI tested at 36% DSR. The accumulation of permanent strain is clearly visible as the horizontal shift of the stress - strain loop. In this particular case, the gap between the cycles decreases in the beginning stage of the test, and increases towards the end. This corresponds with the observed strain rate in Figure 5.3, where progressive accumulation of permanent strain at the end indicates that the specimen has started to fail. The area enclosed by the loops represent the dissipated energy. It can be approximated by the quadrature rule proposed by Green [8]:

$$w = \int \sigma_i \, d\epsilon_i = \int (\sigma_1 \, d\epsilon_a + 2\sigma_3 \, d\epsilon_h) = \int [\sigma_d \, d\epsilon_a + \sigma_3(1-2v) \, d\epsilon_a] \tag{5.4}$$

$$\approx \frac{1}{2} \sum_{i=1}^{N-1} (\sigma_{d,i} + \sigma_{d,i+1})(\epsilon_{a,i+1} - \epsilon_{a,i}) + \frac{1}{2}(1-2v) \sum_{i=1}^{N-1} 2\sigma_3(\epsilon_{a,i+1} - \epsilon_{a,i}) \tag{5.5}$$

Where:

w	= Dissipated energy per cycle per unit of volume [kPa]
v	= Poisson's ratio [-]
σ_i	= Stress corresponding to the i-th point of the stress - strain cycle [kPa]
σ_1	= Major principle stress [kPa]
σ_3	= Minor principle stress [kPa]
$\sigma_{d,i}$	= Major deviatoric stress corresponding to the i-th point of the stress - strain cycle [kPa]
$d\epsilon_i$	= Strain increment corresponding to the i-th point of the stress - strain cycle [-]
$d\epsilon_{a,i}$	= Axial strain increment corresponding to the i-th point of the stress - strain cycle [-]
$d\epsilon_a$	= Axial strain increment [-]
$d\epsilon_h$	= Radial strain increment [-]
$\epsilon_{a,i}$	= Axial strain corresponding to the i-th point of the stress - strain cycle [-]
N	= Number of datapoints in stress - strain loop [-]

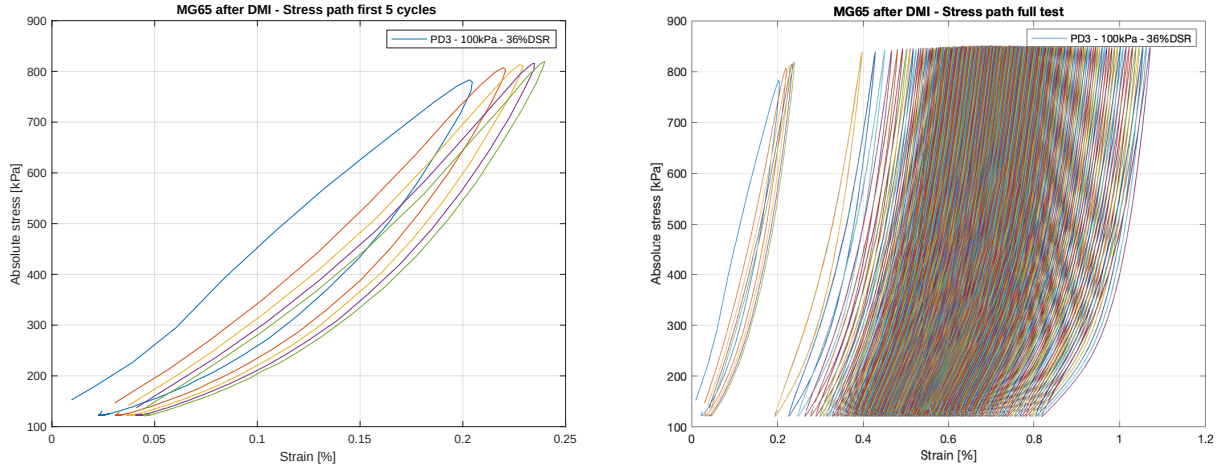

Figure 5.6: Recorded stress strain path of MG65 after DMI **Left:** First five cycles **Right:** Full test

Implementing Equation 5.4 on the obtained measurements leads to the dissipated energy curves presented in Figure 5.7. A Poisson's ratio of 0.35 is assumed for all materials. The curves are somewhat irregular, but clear trends can be observed. It appears that Huurman's model to describe permanent deformations also works well to describe the dissipated energy. By fitting of Equation 5.1 to the dissipated energy data (similar as done in Section 5.1.1), the model parameters A, B, C and D can be determined. The results of this exercise are presented in Table 5.4. Although the R^2 values are lower in comparison with the permanent deformation fittings, it can be seen from the graphs that the model follows the trend satisfactorily.

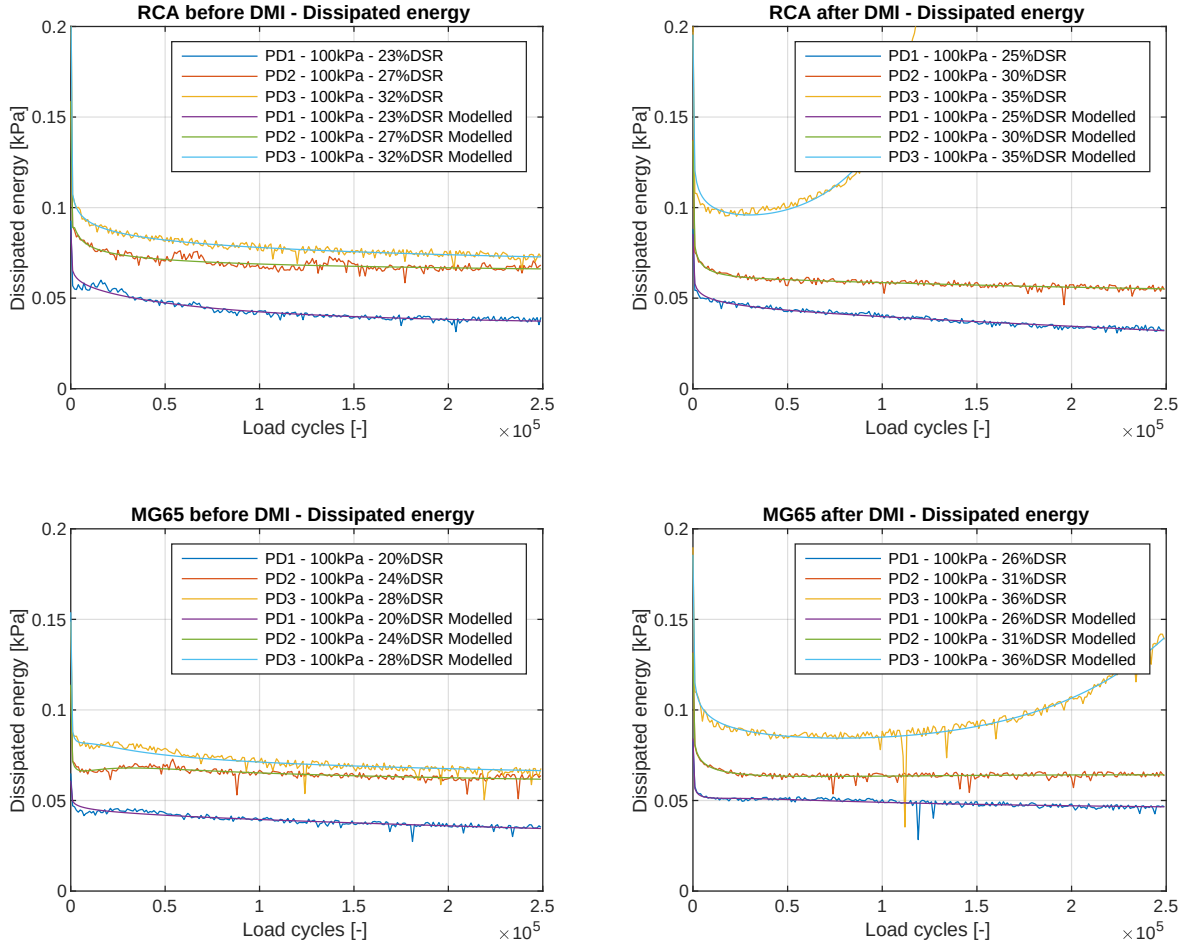

Figure 5.7: Dissipated energy per load cycle of the permanent deformation triaxial test results

The trends of the dissipated energy curves are very similar to the strain rates. At the start of the test, the dissipated energy is relatively high due to sliding and rearrangement of particles (post compaction). This gets less as the number of load cycles increases, and corresponds to a decrease in strain rate. A stable response can be observed when the gradient of the dissipated energy curve is (close to) zero. In this case, the energy dissipation is constant. All energy is converted into heat via particle friction and, to a limited extent, particle attrition [28]. Instability can be observed when the gradient is positive. In this case, more and more energy is dissolved into sliding, rolling and (frictional) damage of particles. Similar as for the strain rate, the onset of failure can be indentified when the gradient of the dissipated energy curve becomes zero. For RCA after DMI this at 30,000 cycles and for MG65 after DMI this at 78,000 cycles. Considering the onset of failure obtained from the strain rate curves in Section 5.1.2, it appears that the dissipated energy indicates instability earlier than the strain rate. The differences are 23,000 cycles 42,000 cycles, respectively. A remark on this finding is that the gradient of the dissipated energy can be slightly

positive in the beginning stages of the test, and alternates to a negative value later on. This can be observed in MG65-PERM-PD2, which shows a positive gradient in the beginning but does not become unstable. Therefore, indicating failure based on the dissipated energy rate alone might not be sufficient. Overall, more testing is required to obtain a better understanding of the relationship between strain rate and dissipated energy and to validate the finding that dissipated energy might be an earlier indicator for instability.

Table 5.4: Dissipated energy model parameters for stress independent Huurman modelling

Test	Specimen ID	A [kPa]	B [-]	C [kPa]	D [-]	$\sum d^2$	R^2
RCA before DMI	RCA-PERM-PD1	0.0654	-0.0511	0.0124	-0.0136	0.0007	0.9331
	RCA-PERM-PD2	0.0412	-0.2317	-0.0547	-2.0811	0.0010	0.9188
	RCA-PERM-PD3	0.1831	-0.0380	0.0757	-10.0000	0.0007	0.9774
RCA after DMI	RCA-DMIT-PD1	0.0581	-0.0665	-0.0175	0.0015	0.0003	0.9668
	RCA-DMIT-PD2	0.0787	-0.0955	-0.0087	-0.0237	0.0005	0.9494
	RCA-DMIT-PD3	0.1204	-0.0835	0.0043	0.0268	0.0011	0.9706
MG65 before DMI	MG65-PERM-PD1	0.0496	-0.0353	0.0421	-0.0006	0.0005	0.8589
	MG65-PERM-PD2	0.0705	-0.0827	-0.0171	-0.0658	0.0008	0.8154
	MG65-PERM-PD3	0.0856	-0.1010	-0.0174	-0.1506	0.0016	0.8896
MG65 after DMI	MG65-DMIT-PD1	0.0562	-0.0697	-0.0083	-0.0567	0.0007	0.7450
	MG65-DMIT-PD2	0.0811	-0.0832	-0.0151	-0.0078	0.0006	0.9015
	MG65-DMIT-PD3	0.1151	-0.0823	0.0020	0.0143	0.0042	0.9337

5.1.5. DISSIPATED ENERGY APPLICATION

The dissipated energy as calculated in the previous section is applied by Tao [26], who investigated its potential for the determination of the shakedown limits. Tao [26] recognized that the shakedown boundaries proposed by Werkmeister [28] are subjective, and suggested a more objective approach based on energy dissipation. The starting point of this method is to plot the relation between the strain rate and the dissipated energy. Figure 5.8 shows the results of a multistage permanent deformation test on crushed limestone. The corresponding strain rate versus dissipated energy relationship is presented as well. The test consists of five stages of 10,000 cycles. After each stage, the vertical stress is increased and the confinement stress is decreased. In the final stage, the confinement stress is set to zero. The vertical stress is such that failure occurs.

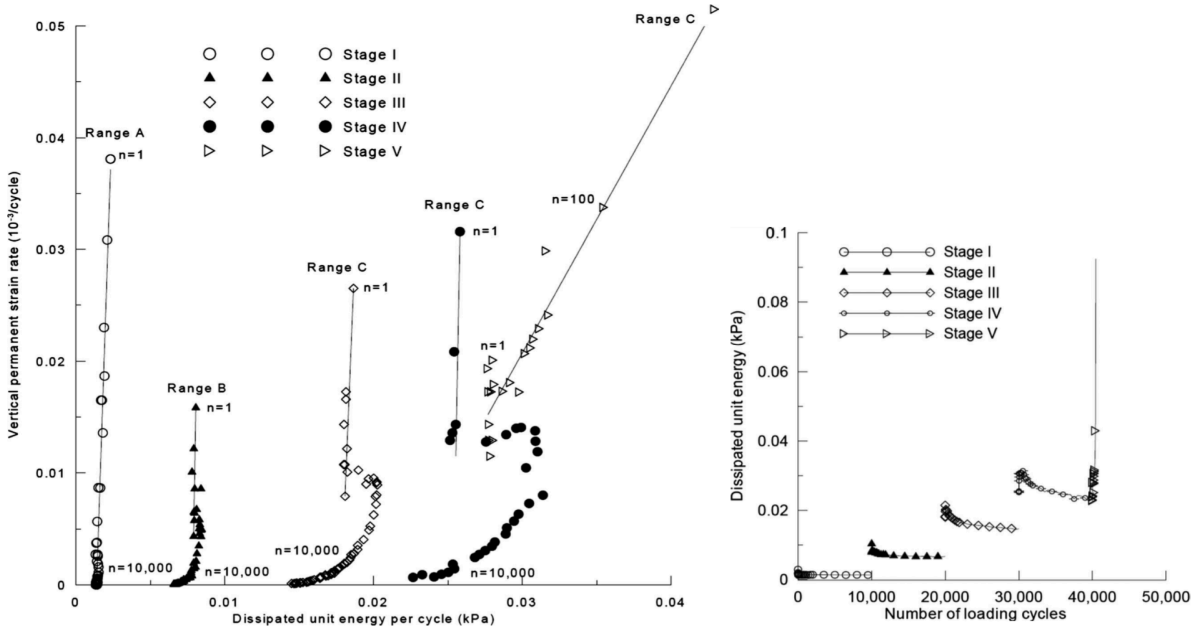

Figure 5.8: Application of the dissipated energy concept by Tao [26], based on multistage triaxial tests on crushed limestone.

Per stage, two phases can be distinguished. The first linear phase represents the rapid decrease of strain rate in the beginning of the test. Since the strain rate decreases much faster than the dissipated energy, this phase implies that the portion of the dissipated energy causing permanent deformations becomes less and less. The second, nonlinear phase, shows that while the strain rate gradually continues to decrease, the portion of the dissipated energy causing damage to the specimen starts to increase[1]. It can be seen from the figure that as the stress level increases, the nonlinear part of the curve gets dominant. According to Tao, shakedown range A can be identified when the linear phase is dominant. When the nonlinear phase is dominant, range C is identified. Range B corresponds to the case when both phases are equally present. It is tried to repoduce this method with limited succes. The results are presented in Figure 5.9. The added value is questioned because of the following aspects:

- **Repeatability.** Obtaining the graphs from Figure 5.9 requires both the permanent deformation as the dissipated energy curves to be continous (i.e. modelled). Directly plotting the meaured values results in erratic, chaotic graphs. Despite the modelling, the trend of the results are only to a small extent comparable to the findings of Tao. The derivation of the shakedown limits from these graphs did not succeed.
- **Shakedown Boundaries.** No boundaries are derived / suggested for an objective classification of the shakedown ranges. Identifiying which phase is most dominant is therefore still a subjective measure. The reasoning behind the classification of stage II and stage III is relevant but not provided.

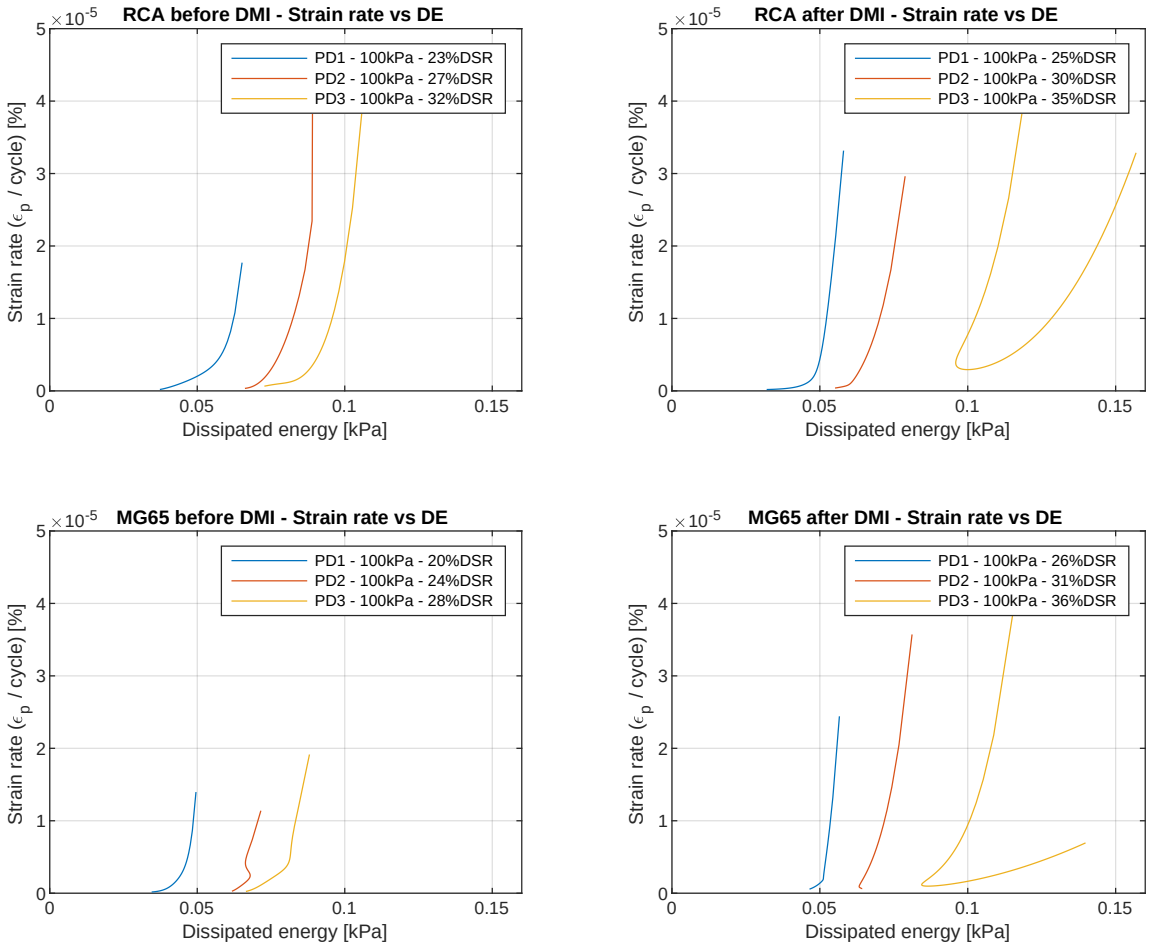

Figure 5.9: Strain rate in relation with the dissipated energy

[1]The reasoning behind the second, nonlinear, phase is debatable. It can be seen that in most cases the dissipated energy first increases and then decreases. Only if the dissipated energy decreases more than the strain rate, it can be argued that the portion of dissipated energy causing damage to the specimen increases.

5.1.6. STIFFNESS RESPONSE

As discussed in Section 2.4.1, the stiffness response of unbound granulates is stress dependent. It is described by the resilient modulus (Mr). Although resilient modulus triaxial tests are not conducted in this research, it is possible to gain insight in the stiffness response by considering the permanent deformation triaxial test results. Analogous to resilient modulus triaxial testing, the approximated resilient modulus (Mr^*) at the particular stress levels tested is found by deriving the slope of the hystersis loop (Figure 2.9). Since the hysteresis loops are recorded for the full permanent deformation test, the course of the stiffness response with respect to the number of load cycles can be plotted. This is illustrated in Figure 5.10. It should be noted that Mr^* differs from Mr since the strain response is measured over the full height of the specimen. This includes frictional influences of the top and bottom plate, making it a different determination. Together with that, Mr^* is only based on tests with a confinement stress of 100 kPa, while Mr is usually determined for various combinations of stress levels.

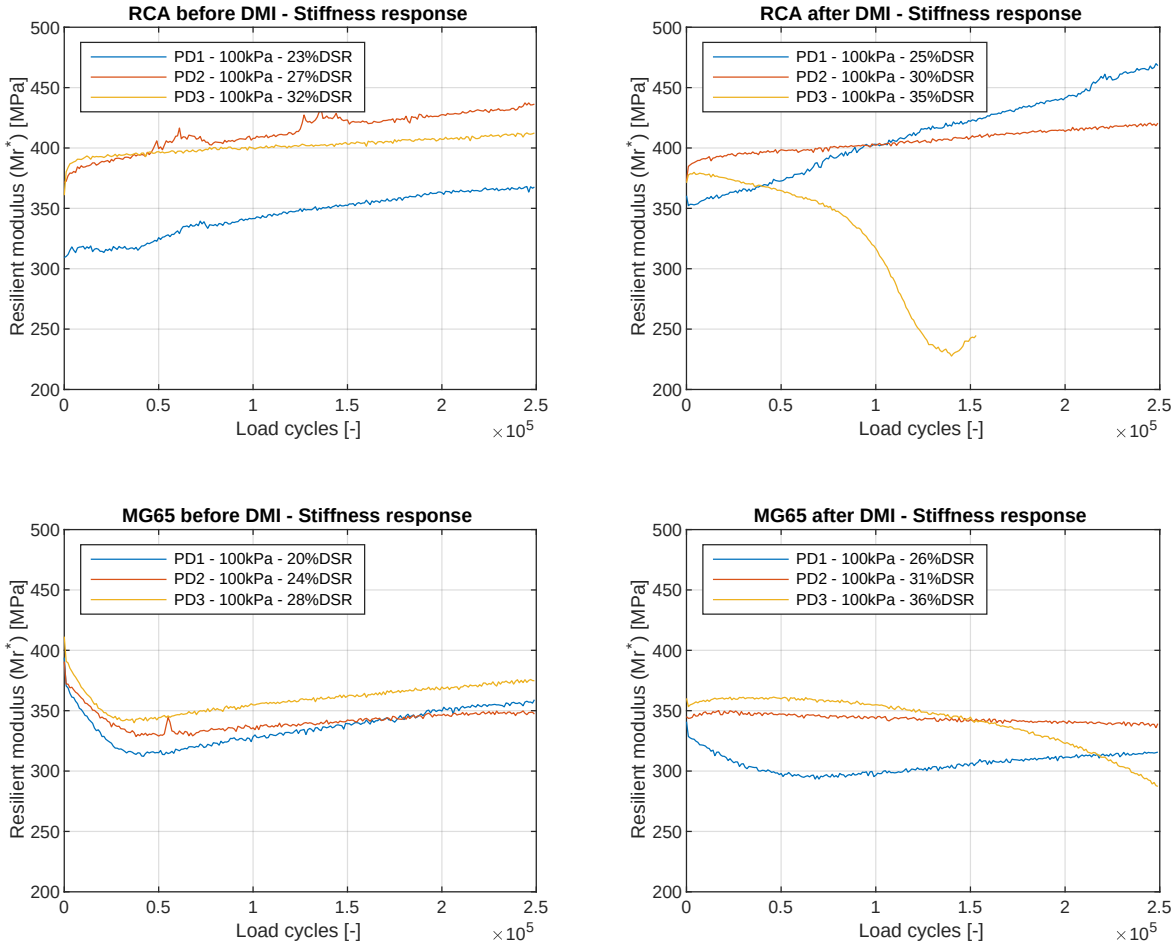

Figure 5.10: Stiffness response of permanent deformation triaxial test results

Figure 5.10 shows that the stiffness response is not constant, but changes over the duration of the test. The resilient modulus of all stable specimens tend to increase towards the end of the test. In most cases, higher deviator stress ratios correspond with higher stiffness (strain hardering), but this does not hold for later stages of the test. The unstable specimens, RCA-DMIT-PD3 and MG65-DMIT-PD3 are clearly visible by a rapid, progressive decrease of stiffness, with both having a negative slope and negative curvature. Interestingly, the onset of this trend in the

milled RCA is already visible in the very beginning stages (N < 10,000) of the test. In the milled MG65, the onset of instability is less clear but still happens before 25,000 load cycles. In both cases, the approximated resilient modulus seems to predict instability earlier than the corresponding strain rate or dissipated energy curves. The unstable specimens characterize themselves by having both a negative slope and a negative curvature. The stiffness of some stable specimens (for instance the unmilled MG65 specimens) decreases in the beginning stages of the test, but stabilise later on. The direction of the curvature now seems to indicate if either stable or unstable behavior can be expected. In the beginning stages of the test however, its direction may not yet be clear and alternate around zero. Together with this, specimen MG65-DMIT-PD2 shows in a very small extend also a negative slope and negative curvature, but does not become unstable. Concluding on the obtained observations, the stiffness response may be a very early indicator of instability, but also seems less reliable. More permanent deformation test results should be analysed to verify whether this is the case or not.

Regarding the influence of durability milling, it can be seen that in most cases (but not all) the stiffness has decreased in the milled specimens. This corresponds with the observed decrease in cohesion. To gain a better understanding of the influence of DSR and durability milling on the stiffness response of the materials, the resilient modulus of cycle 10,000 and the average resilient modulus between cycle 1,000 and 10,000 are considered. Together with this, the resilient modulus of cycle 100 of the conditioning phase and the average resilient modulus of the full conditioning phase are considered. The former is the closest representative of the resilient modulus as determined in the resilient modulus triaxial test. The loading in the condition phase is relatively small (around 12% DSR) and no loading history is present. The resilient moduli of the four points considered are presented in Table 5.5.

Table 5.5: Approximated resilient moduli in permanent deformation triaxial testing at 100 kPa

		Conditioning phase			Testing phase		
Test	**Specimen ID**	**DSR** [%]	**Mr^*_{100}** [MPa]	**$Mr^*_{average}$** [MPa]	**DSR** [%]	**Mr^*_{10000}** [MPa]	**$Mr^*_{average}$** [MPa]
RCA before DMI	RCA-PERM-PD1	11.5	261	262	22.82	319	316
	RCA-PERM-PD2		331	332	27.39	384	380
	RCA-PERM-PD3		298	299	31.96	391	388
RCA after DMI	RCA-DMIT-PD1	12.53	328	327	24.87	358	354
	RCA-DMIT-PD2		313	314	29.85	391	389
	RCA-DMIT-PD3		298	298	34.83	378	379
MG65 before DMI	MG65-PERM-PD1	10.14	353	345	20.01	349	359
	MG65-PERM-PD2		324	322	23.94	359	366
	MG65-PERM-PD3		341	337	27.98	368	379
MG65 after DMI	MG65-DMIT-PD1	13.01	312	310	25.68	321	324
	MG65-DMIT-PD2		299	297	30.72	349	346
	MG65-DMIT-PD3		304	301	35.89	357	357

It can be seen from the table that the approximated resilient moduli of the single point and the average do not differ significantly. Furthermore, the resilient moduli in the conditioning phase are always lower than the resilient moduli in the testing phase. This corresponds with the strain hardering behavior mentioned in Section 2.4. In Figure 5.11, the average approximated resilient modulus ($Mr^*_{average}$) is expressed as a function of deviator stress ratio. Four datapoints are considered per material. The first point represents the average of the three conditioning phase resilient moduli. The other three points correspond with the three tested resilient moduli.

In the MG65 materials, a linear trend can be observed between the four points. A linear estimation is also carried out for the RCA, but with less accurate results. The corresponding model and model parameters are given in Equation 5.6 and Table 5.6. The obtained model parameters can be used as a reference in other research, but should not be regarded as design values. The influence of durability milling in the MG65 is cleary visible as a slight but constant reduction of stiffness of 40 MPa. The influence of durability milling on the stiffness of the RCA is less obvious. It

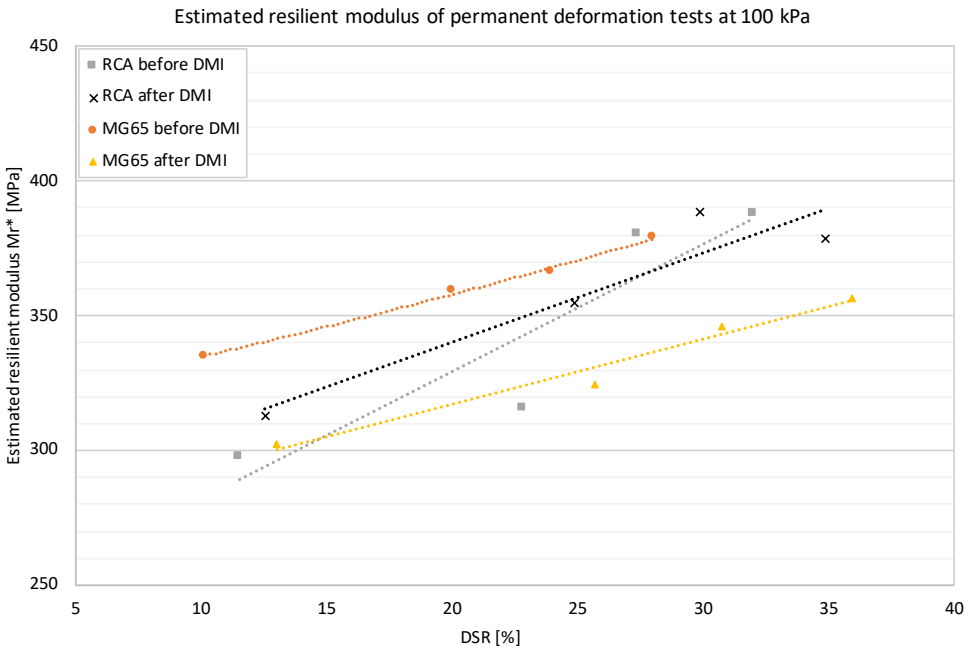

Figure 5.11: Estimation of the resilient modulus obtained from permanent deformation triaxial testing

appears, however, that similar as can be seen in the monotonic triaxial test results, the MG65 is more affected by durability milling than the RCA. Overall, the differences in approximated resilient moduli between the four series lie within 40 MPa. As the number of datapoints per material is only 4, this difference is not considered significant.

$$Mr^* = A \cdot DSR + B \tag{5.6}$$

Where:

Mr* = Approximated resilient modulus [MPa]

DSR = Deviator stress ratio [%]

A, B = Material parameters [MPa]

Table 5.6: Approximated resilient moduli at 100 kPa confinement stress

	A [MPa]	B [MPa]	R^2 [-]
RCA before DMI	4.72	235	0.83
RCA after DMI	3.31	274	0.89
MG65 before DMI	2.42	310	0.99
MG65 after DMI	2.40	269	0.97

5.2. MONOTONIC TRIAXIAL TESTING

5.2.1. MONOTONIC STIFFNESS

Besides the approximated resilient modulus, discussed in Section 5.1.6, an estimation of the specimen stiffness can also be derived from the monotonic test results. For each specimen, a linear regression line is fitted on the datapoints between 20% and 60% of the failure stress. This is illustrated in Figure 5.14. The slope of the regression line represents the material stiffness at the corresponding confinement stress. As mentioned in Section 2.4.1, the stiffness of soils and unbound granulates is stress dependent. Not only the confinement stress influences the stiffness response, but also the vertical stress. Nevertheless, the slope of the stress - strain curves obtained from monotonic triaxial testing can serve as an indication of the expected material stiffness at the particular confinement stress tested. The results of this exercise for all specimens can be found in Appendix G.3. Figure G.10 and Table G.4 present the average values for each confinement. The average is based on two tests per confinement stress. Incidentally, only one test was available due to membrane rupture of the second specimen (see Section 4.3). This is the case for the milled RCA tested at 50 kPa and the unmilled MG30 tested at 100 kPa.

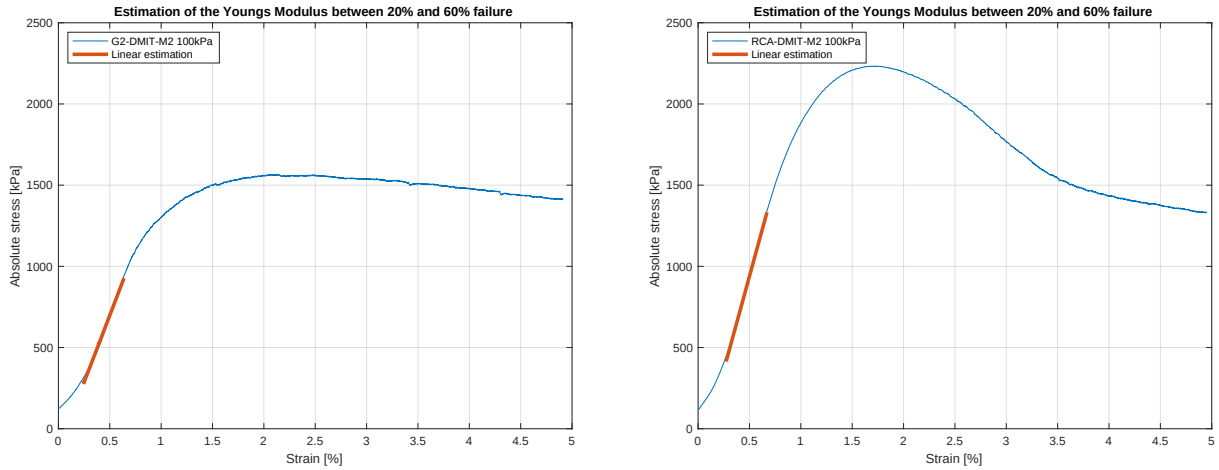

Figure 5.12: Linear estimation of the Youngs modulus between 20% and 60% of the failure stress **Left:** Milled G2 **Right:** Milled RCA

The influence of confinement stress on the stiffness is clearly visible in the unmilled materials. Higher levels of confinement stress are generally associated with an increase of stiffness, which is also observed here. With the exception for RCA tested at 50 kPa, a similar pattern can be recognized in the milled specimens. The G2 materials appear to be the least stiff, and experience a small increase in stiffness after durability milling. As mentioned in Section 4.3.2, it is believed that the cohesion of the unmilled specimens is actually slightly higher than what the results show. This also implies that the unmilled materials are expected to respond a little more stiff than what is found here. The difference in stiffness before and after DMI however is rather small, and in line with the previous findings that the change in grading and the change of shear parameters are hardly influenced by durability milling. More drastic changes in stiffness can be seen in the blends. The blends appear to be the most stiff, but also experience the most losses. Especially in MG65, the stiffness decreases with almost 100 MPa regardless of confinement stress. The observation that both the biggest change in stiffness and the biggest loss of cohesion are found in the same materials corresponds with the fact that cohesion and stiffness are closely related. The pure RCA on the other hand, which also suffers some loss of cohesion due to durability milling, appears not to lose any stiffness.

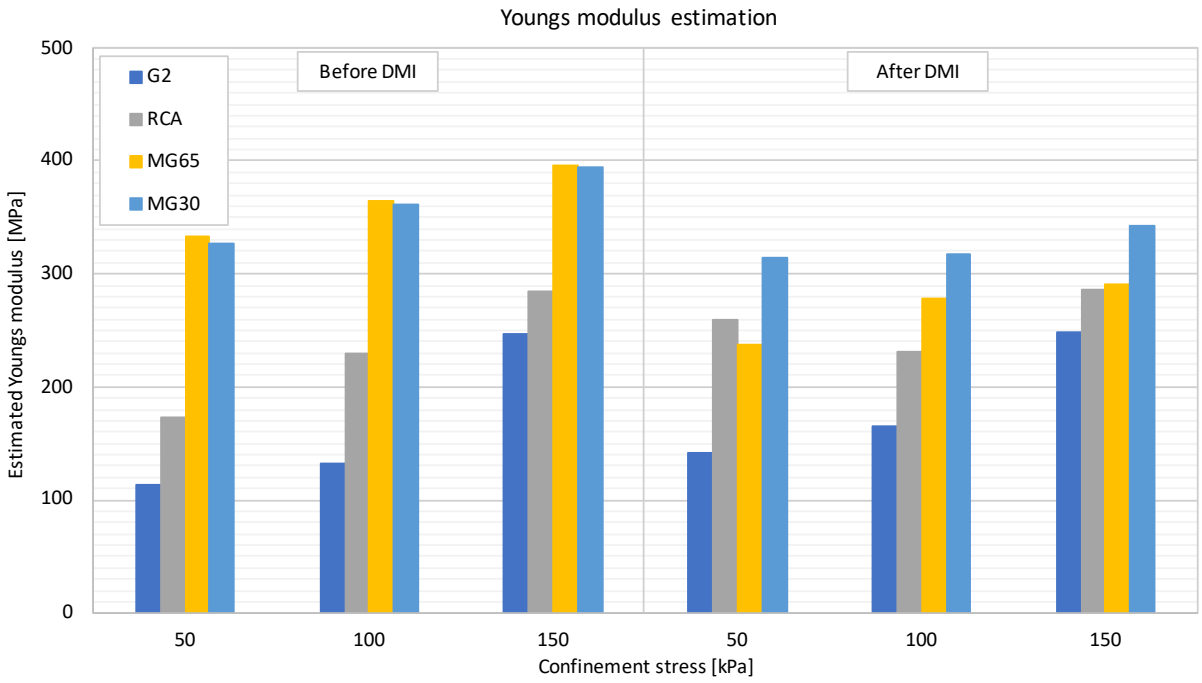

Figure 5.13: Average estimated Youngs moduli obtained after monotonic triaxial testing

Table 5.7: Average linear estimated Youngs moduli obtained after monotonic triaxial testing

		Before DMI			After DMI		
Confinement stress	[kPa]	50	100	150	50	100	150
G2	[MPa]	113	132	246	142	165	249
RCA	[MPa]	173	229	284	259	231	286
MG65	[MPa]	333	365	396	237	278	291
MG30	[MPa]	326	362	394	314	318	342

5.2.2. DISSIPATED ENERGY

The dissipated energy in the monotonic triaxial tests is calculated according to Equation 5.4. The approach is similar as for the permanent deformation triaxial tests, where the area under the stress - strain path is considered. Three points are distinguished:

- The dissipated energy of the full test (up to 4% strain);
- The dissipated energy up to failure;
- The dissipated energy between failure and 95% residual strength.

The dissipated energy of the full test encloses the area under the stress - strain curve until 4% strain. A visualisation of the other two dissipated energy levels is given in Figure 5.14. The results of the calculations for all specimens can be found in Appendix G.3. Similar as for the stiffness, the average dissipated energy of two tests per confinement stress is taken for the dissipated energy up to failure. The same exceptions apply as in the previous section, where the results for the milled RCA tested at 50 kPa and the unmilled MG30 tested at 100 kPa are only based on one test. The average dissipated energy levels up to failure are presented in Figure 5.15 and Table 5.8.

The influence of confinement stress on the energy dissipation is clearly visible. In the unmilled results, an interesting difference can be observed between the G2 and RCA on the one hand, and MG65 and MG30 on the other hand. It appears that although the compressive strength of G2 and RCA is lower in comparison with the blends, more energy

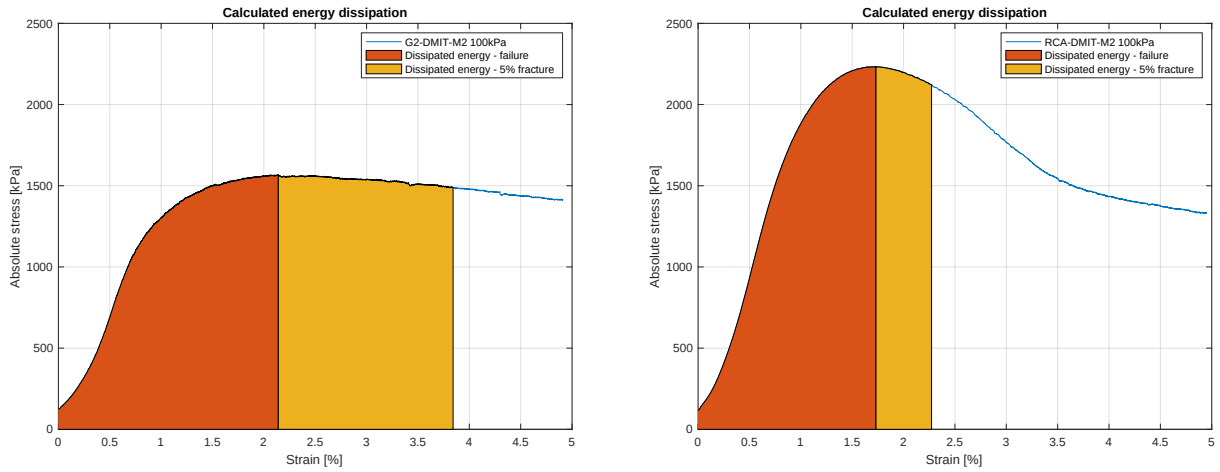

Figure 5.14: Considered levels of dissipated energy **Left:** Milled G2 **Right:** Milled RCA

is required to reach failure. Reason for this is that these materials are less stiff and have more deformation capacity before reaching their peak strength (see Figure 5.14). In all materials, durability milling causes the required failure energy to drop. This is mainly due to a decrease in absolute strength. Differences between the G2 and RCA with respect to the blends are still noticeable, although less obvious.

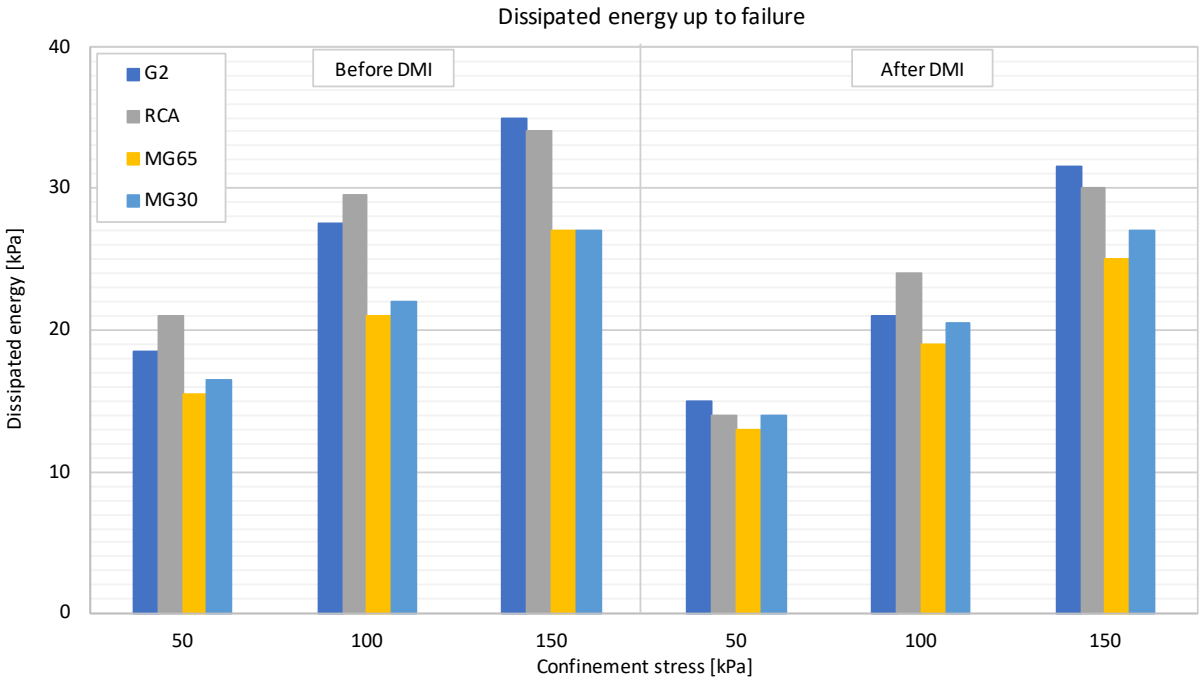

Figure 5.15: Average energy dissipation up to failure after monotonic triaxial testing

Table 5.8: Average energy dissipation up to failure after monotonic triaxial testing

		Before DMI			After DMI		
Confinement stress	[kPa]	50	100	150	50	100	150
G2	[kPa]	19	28	35	15	21	32
RCA	[kPa]	21	30	34	14	24	30
MG65	[kPa]	16	21	27	13	19	25
MG30	[kPa]	17	22	27	14	21	27

When considering the energy dissipation after reaching the maximum stress, clear differences can be noticed between the G2 and the recycled materials. Figure 5.16 and Table 5.9 present the 5% fracture energy as the ratio of the failure energy. This ratio is relatively high for the G2 because of its plastic nature. The resisting force of the recycled materials quickly reduces after reaching the maximum, while the resisting force of the G2 materials remains close to the peak value. In most G2 specimens, the resisting forced stays even above 90% of the peak strength for the remaining duration of the test. In Section 4.3.1, it is explained that this plastic failure behavior is probably caused by sliding and rolling of particles. It is believed that when this happens, the particles push each other away resulting in the observed dillatation. After rearranging, a new equilibrium is formed with no significant loss of strength. In the recycled materials, a different mechanism can be distinguished. The rough surface and sharp edges of the recycled material aggregates probably result in better particle interlock and higher cohesion levels. The increased particle friction increases the stress levels at which sliding and rolling occurs. At the same time, the shear and crushing strength of the concrete and masonry particles is lower in comparison to the G2. Together with this, the recycled materials are more susceptible to particle abrasion. It is now believed that the interaction between inter particle friction and particle strength is such that the latter is governing. Crushing and breaking of particles results in the development of a shear plane and relatively little energy is required to slide the two obtained bodies over each other. Interestingly, within the recycled materials, the ratio between 5% residual dissipated energy and failure dissipated energy appears to be fairly constant with respect to the confinement stress.

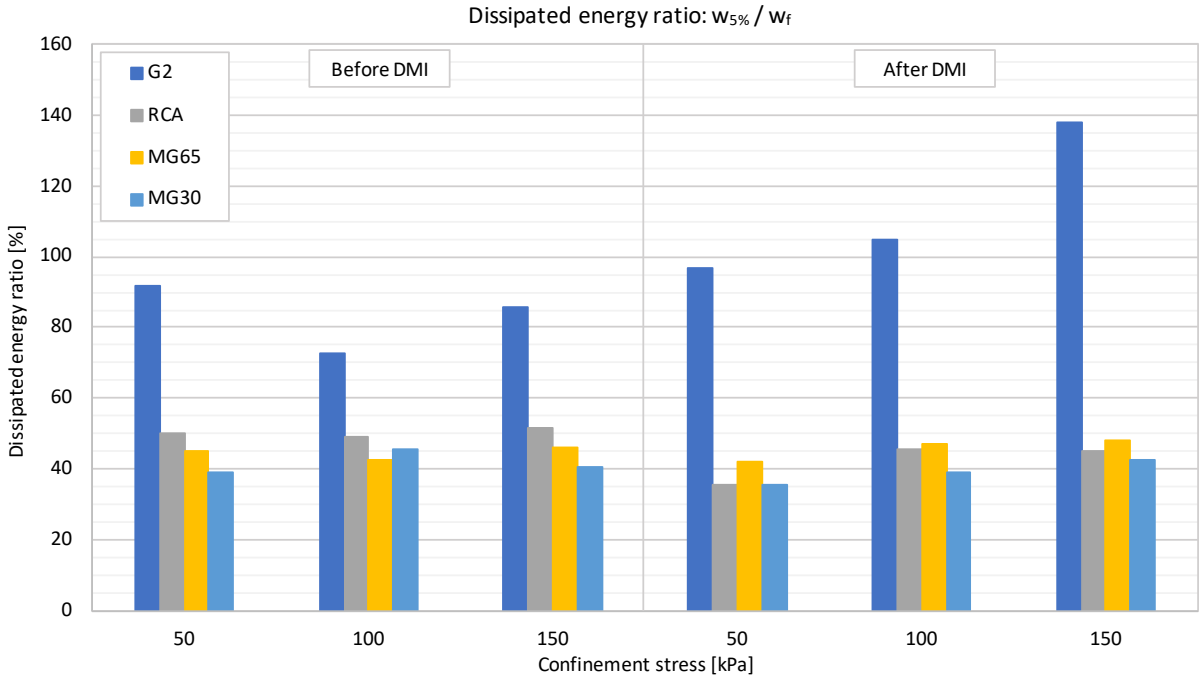

Figure 5.16: Dissipated energy ratio ($w_{5\%}$ / w_f) after monotonic triaxial testing

Table 5.9: Dissipated energy ratio ($w_{5\%}$ / w_f) after monotonic triaxial testing

		Before DMI			After DMI		
Confinement stress	[kPa]	50	100	150	50	100	150
G2	[%]	92	73	86	97	105	138
RCA	[%]	50	49	51	36	46	45
MG65	[%]	45	43	46	42	47	48
MG30	[%]	39	45	41	36	39	43

In general, the plastic failure mechanism of the G2 materials is favorable. However, when considering the energy dissipation with respect to displacements instead of strength (ratios), the recycled materials outperform the G2

materials. The recycled materials experience a significant drop in strength after reaching the maximum, but the dissipated energy and resisting force at a given displacement are always higher in comparison with their G2 counterparts. It is only after considerable strains ($\epsilon > 5\%$) that this is the other way around.

5.3. PAVEMENT ANALYSIS

In the previous chapter, it is concluded that the DSR of the recycled granulates should not exceed 30% to ensure stable behavior up to 250,000 load cycles. The stiffer (recycled) materials have higher shear parameters but also attract more stresses. To obtain a first impression of the occurring stress levels in a base layer, a small static multilayer pavement analysis is performed. WESLEA, a simple but user friendly software tool which calculates stresses and strains in multilayer systems, is used. WESLEA is based on linear elastic theory, and considers all layers to be purely elastic, isotropic and homogenous. As a result of this, tensile stresses may occur at the bottom of unbound layers. This is of course not in line with reality, and therefore the outcomes only serve as a rough approximation of what stress levels can be expected. Together with this, the results in the bottom parts of unbound layers should be ignored. The considered structure in this analysis is the South African N1 around Cape Town. It consists of a 40 mm asphalt layer on top of a 150 mm unbound granular base. The top layers are supported by a 300 mm C4 cemented subbase and a 300 mm G8 selected subgrade[2]. An in situ subgrade with a quality of G10 is assumed. Figure 5.17 shows the pavement structure for two cases. In the first case, the structure is loaded by a standard 80 kN axle with dual tires. In the second case, the structure is loaded by standard 80 kN axle with super single tires.

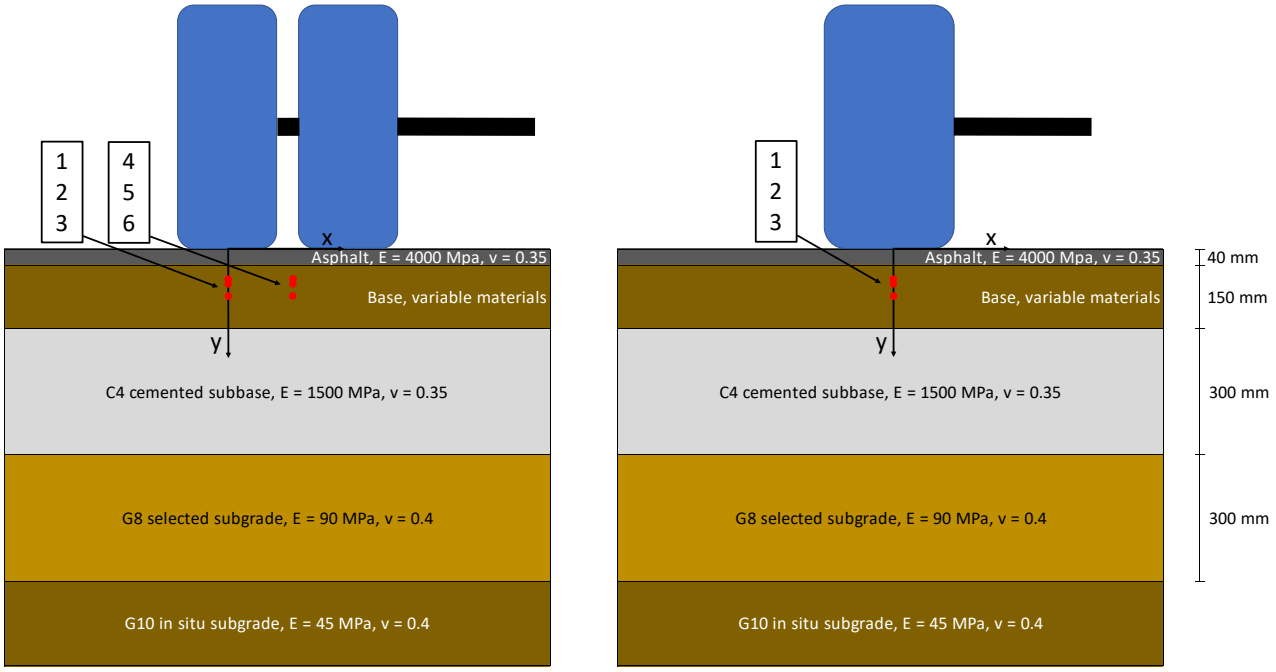

Figure 5.17: Pavement structure and loading situation **Left:** Dual tire **Right:** Super single tire

The material in the basecourse serves as variable (i.e. G2, RCA, MG65 and MG30, both milled and unmilled). The corresponding stiffness and shear parameters are based on the monotonic triaxial test results, and listed in Table 5.11. Since the stiffness found for the G2 is on the low side, a theoretical G2 is used instead of the unmilled G2

[2]Actually, the selected subgrade consists of 150 mm G7 and 150 mm G9. Since the maximum number of layers to be entered in WESLEA is 5, the selected subgrade is chosen as one 300 mm G8 layer.

material [11]. The material parameters of this theoretical G2 are chosen as E = 400 MPa, ϕ = 52° and c = 55 kPa. The stiffness of the other layers are common design values according to the South African Pavement Engineering Manual (SAPEM) [21]. As an alternative, the N1 in rural areas is considered as well. This structure is similar as the structure presented in Figure 5.17, except that the asphalt surface layer is replaced by a 19 mm cape seal. In total, four different situations are analyzed:

- 40 mm asphalt surface loaded with a standard dual tire (2 x 20 kN);
- 40 mm asphalt surface loaded with a standard super single tire (1 x 40 kN);
- Seal surface loaded with a standard dual tire (2 x 20 kN);
- Seal surface loaded with a standard super single tire (1 x 40 kN).

It is assumed that the structural capacity of the seal is negligible and that there exists full bond between the layers. The tire pressures of the dual and super single tires are set on 700 kPa and 825 kPa, respectively. This is conform with what can nowadays be found on South African roads [3]. The evaluated points are located in the basecourse layer directly under, at depths of 0.25, 0.33 and 0.5 times the layer height. In case of the dual tire, three extra points between the two wheels are evaluated as well. See also Figure 5.17. The corresponding coordinates are listed in Table 5.10.

Table 5.10: Coordinates of evaluated points

Tire	Location	Surface: 40 mm asphalt		Surface: seal	
		x [mm]	y [mm]	x [mm]	y [mm]
Dual 2 x 20 kN	1	0	78	0	38
	2	0	90	0	50
	3	0	115	0	75
	4	172	78	172	38
	5	172	90	172	50
	6	172	115	172	75
Super single 1 x 40 kN	1	0	78	0	38
	2	0	90	0	50
	3	0	115	0	75

WESLEA now calculates the stresses and strains at each point. The corresponding deviator stress ratios are calculated according to Equation 5.7. In here, the minimum occuring stress is regarded as the confinement stress (σ_3) and the maximum occuring stress is regarded as the vertical stress (σ_1). Doing so is only legitimate if the shear stresses are zero and thus directions of the calculated normal stresses correspond with the principal stress directions. For all four situations it is checked whether a combination between shear and normal stresses at the edges of the wheel load forms a more critical stress state, but this appears not to be the case. An overview of the results can be found in Appendix I. Table 5.18 and Figure 5.18 present the results at the governing locations. These are the locations at which the deviator stress ratio is maximum.

$$DSR = \frac{\sigma_d}{\sigma_{d,f}} \cdot 100\% = \frac{\sigma_1 - \sigma_3}{\sigma_{1,f} - \sigma_3} \cdot 100\% = \frac{(\sigma_1 - \sigma_3)(1 - \sin\phi)}{2\sigma_3 \sin\phi + 2c\cos\phi} \cdot 100\% \tag{5.7}$$

The results show that in all situations, the occuring deviator stress ratios are the highest in the G2. After durability milling, the stiffness and the cohesion of the recycled materials have decreased. The occurring deviator stress ratios however increased, implying that the decrease of cohesion forms the governing contribution. In all situations, it can be seen that the stresses in the RCA and the MG65 do not exceed 30% DSR. Long term behavior has to be researched more intensively, but based on the first results it appears that deviator stresses caused by standard axles are low and stay within reasonable limits. This also holds for their milled counterparts. The super single tire increases the

vertical and radial stress levels considerably. The latter has a beneficial influence on the deviator stress ratio, but this does not weigh up against the rise in vertical stress. In case of the sealed structure, the absolute stress levels in all materials rises as well. It should be noted that all radial stresses found in this case fall outside the tested range ($\sigma_{3,max}$ = 150 kPa). The Mohr-Coulomb theory assumes linearity of the failure envelope, but the exact response of the materials at these stress levels is unknown. In general, the lowest deviator stress ratios occur in the MG30. However, since no permanent deformation tests are conducted at these materials, it is unknown at what stress ratios unstable behavior can be expected. At first sight, it seems that MG65 and RCA, even after mechanical breakdown, are suitable base course materials in both structures.

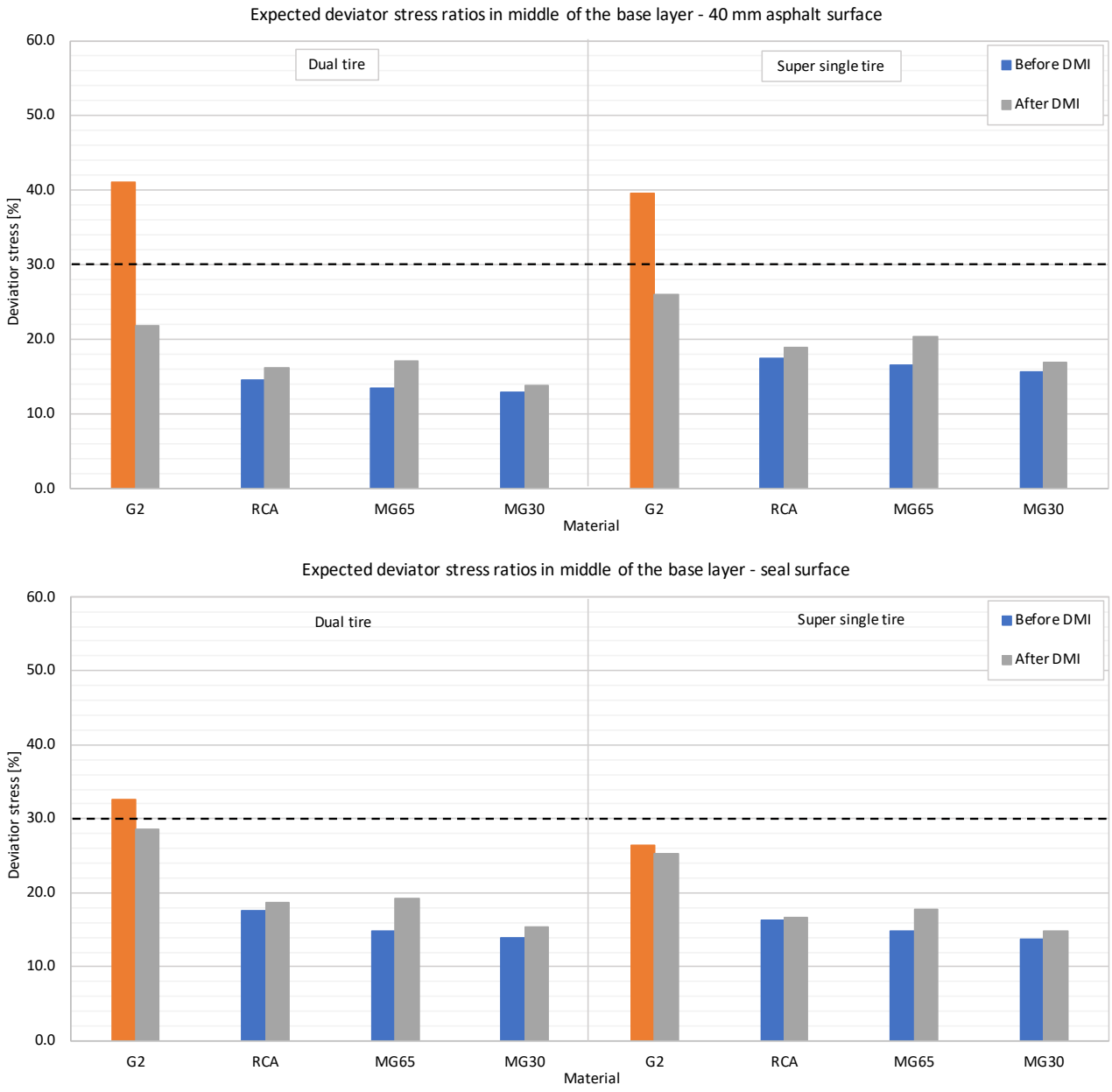

Figure 5.18: Predicted deviator stress ratios of the governing points **Top:** 40 mm asphalt surface **Bottom:** Seal surface

Table 5.11: Predicted deviator stress ratios of the governing points

Governing stress points: 40 mm asphalt surface & dual tire

	Governing location	Stiffness [MPa]	Friction angle [°]	Cohesion [kPa]	Confinement stress [kPa]	Vertical stress [kPa]	Deviator failure stress [kPa]	Deviator stress ratio [%]
G2 theory	2	400	52.0	55	62	382	780	41.1
G2 after DMI	1	165	51.2	142	67	347	1281	21.9
RCA before DMI	1	230	55.1	233	69	375	2112	14.5
RCA after DMI	1	230	56.6	178	69	375	1884	16.2
MG65 before DMI	1	365	51.2	354	73	411	2524	13.4
MG65 after DMI	1	280	53.5	214	70	391	1875	17.1
MG30 before DMI	1	360	53.9	328	73	410	2624	12.8
MG30 after DMI	1	320	54.1	285	71	401	2369	13.9

Governing stress points: 40 mm asphalt surface & super single tire

	Governing location	Stiffness [MPa]	Friction angle [°]	Cohesion [kPa]	Confinement stress [kPa]	Vertical stress [kPa]	Deviator failure stress [kPa]	Deviator stress ratio [%]
G2 theory	2	400	52.0	55	119	598	1208	39.6
G2 after DMI	2	165	51.2	142	115	536	1619	26.0
RCA before DMI	2	230	55.1	233	117	563	2546	17.5
RCA after DMI	2	230	56.6	178	117	563	2366	18.9
MG65 before DMI	2	365	51.2	354	119	593	2850	16.6
MG65 after DMI	2	280	53.5	214	118	578	2261	20.3
MG30 before DMI	2	360	53.9	328	119	593	3013	15.7
MG30 after DMI	2	320	54.1	285	118	586	2768	16.9

Governing stress points: Seal surface & dual tire

	Governing location	Stiffness [MPa]	Friction angle [°]	Cohesion [kPa]	Confinement stress [kPa]	Vertical stress [kPa]	Deviator failure stress [kPa]	Deviator stress ratio [%]
G2 theory	3	400	52.0	55	135	568	1325	32.6
G2 after DMI	3	165	51.2	142	115	579	1619	28.7
RCA before DMI	3	230	55.1	233	122	575	2591	17.5
RCA after DMI	3	230	56.6	178	122	575	2416	18.8
MG65 before DMI	3	365	51.2	354	133	569	2949	14.8
MG65 after DMI	3	280	53.5	214	126	573	2331	19.2
MG30 before DMI	3	360	53.9	328	132	569	3128	14.0
MG30 after DMI	3	320	54.1	285	129	571	2863	15.4

Governing stress points: Seal surface & super single tire

	Governing location	Stiffness [MPa]	Friction angle [°]	Cohesion [kPa]	Confinement stress [kPa]	Vertical stress [kPa]	Deviator failure stress [kPa]	Deviator stress ratio [%]
G2 theory	3	400	52.0	55	227	758	2009	26.4
G2 after DMI	3	165	51.2	142	205	775	2255	25.3
RCA before DMI	3	230	55.1	233	212	770	3419	16.3
RCA after DMI	3	230	56.6	178	212	770	3333	16.7
MG65 before DMI	3	365	51.2	354	225	761	3597	14.9
MG65 after DMI	3	280	53.5	214	217	766	3079	17.8
MG30 before DMI	3	360	53.9	328	224	761	3900	13.8
MG30 after DMI	3	320	54.1	285	221	764	3643	14.9

5.4. RESULT ANALYSIS OVERVIEW

During this chapter, several result analysation steps are applied to gain understanding in permanent deformation behavior of the recycled materials. This section provides a summary of the most important findings. Table 5.12 and Table 5.13 present an overview of the results for RCA and MG65, respectively. The influence of durability milling is expressed as percentage difference with respect to the unmilled materials. In the unstable specimens, the onset of instability can be identified from the strain rate, the dissipated energy and the stiffness response. The number of load cycles after which this happens are recorded in the tables. Although the exact conditions to identify the onset of instability from the stiffness response still need to be verified, it is reasonable that a progressive decrease of stiffness (i.e. both the slope and the curvature of the stiffness response curve are negative) indicates failure. Observing the curvature condition in the beginning stages of the test may not always be easy, but it appears in both unstable specimens that the stiffness response is the first indicator for delayed shear failure.

Regarding the influence of durability milling, it can be seen that the MG65 appears to be more affected than the RCA. Expecially the cohesion, permanent deformation (N = 250,000) and the strain rate (N = 250,000) are considerably different. A moderate reduction of stiffness can be noticed as well. For the RCA, the differences are less clear. Specimen RCA-DMIT-PD3, tested at 34.8% DSR, is severly affected as it failed before the end of the test (N =

153,000). The corresponding permanent deformation, strain rate and dissipated energy values at cycle 100,000 indicate that a progressive increase of permanent strain has already settled in at this point. Specimen RCA-DMIT-PD1 and RCA-DMIT-PD2, on the other hand, appear to beform better than their unmilled counterparts. In the former case, the permanent strain, strain rate, dissipated energy and stiffness have all improved. In the latter case, the permanent strain, dissipated energy and the stiffness have improved, but the strain not. It is believed that specimen variability in the unmilled materials coincidently plays a large role, and that specimens RCA-PERM-PD1 and RCA-PERM-PD2 perform better (i.e. less accumulation of permanent strains and less strain rate) in case these tests are repeated. When considering the monotonic triaxial tests, it can be seen that in both cases the cohesion and dissipated energy levels are decreased after durability milling. The stiffness in the RCA stays more or less equal while in the stiffness of the MG65 significantly decreases. A final remark on the summary tables is that the stiffness measured in the monotonic triaxial tests is in all cases lower than the resilient stiffness. This is most likely due to the difference in definition. The monotonic stiffness considers the relationship between stress and strain in the loading phase, while the resilient stiffness considers the relationship between stress and strain in the unloading / reloading phase. The latter is usually larger, hence the higher measured stiffness values.

Table 5.12: Summary of results for RCA - before and after durability milling

	RCA before DMI			Percentage difference			RCA after DMI		
	PD1	PD2	PD3	PD1	PD2	PD3	PD1	PD2	PD3
Loading									
Vertical stress [kPa]	546	656	765	0%	0%	0%	546	656	765
Confinement stress [kPa]	100	100	100	0%	0%	0%	100	100	100
DSR [%]	22.8	27.4	32.0	2.1%	2.5%	2.9%	24.9	29.9	34.8
Shakedown range									
Werkmeister	B	B	B	-	-	-	B	B	B
Tao	B	B	B	-	-	-	B	B	C
Instability	No	No	No	-	-	-	No	No	Yes
Permanent strain [%]									
100,000 cycles	0.31	0.47	0.48	-5%	-29%	62%	0.30	0.34	0.78
250,000 cycles	0.36	0.54	0.60	-9%	-24%	-	0.33	0.41	Failed
Strain rate [%]									
100,000 cycles	7.5E-07	6.3E-07	9.9E-07	-48%	4%	1652%	3.9E-07	6.6E-07	1.7E-05
250,000 cycles	1.9E-07	3.4E-07	6.5E-07	-4%	14%	-	1.8E-07	3.9E-07	Failed
Dissipated energy [kPa]									
100,000 cycles	4.2E-02	6.9E-02	7.8E-02	-6%	-15%	80%	4.0E-02	5.9E-02	1.4E-01
250,000 cycles	3.7E-02	6.6E-02	7.3E-02	-14%	-17%	-	3.2E-02	5.5E-02	Failed
Stiffness response [MPa]									
Mr^*_{10000}	319	384	391	12%	2%	-3%	358	391	378
$Mr^*_{average}$	316	380	388	12%	2%	-2%	354	389	379
Instability onset [cycles]									
Identified from strain rate	-	-	-	-	-	-	-	-	53,000
Identified from dissipated energy	-	-	-	-	-	-	-	-	30,000
Identified from stiffness response	-	-	-	-	-	-	-	-	4,000
Monotic triaxial testing									
Friction angle [°]		55.1			3%			56.6	
Cohesion [kPa]		233			-24%			178	
Dissipated energy - failure [kPa]		30			-19%			24	
Dissipated energy - 4% strain [kPa]		75			-14%			65	
Stiffness [kPa]		229			1%			231	
Pavement analysis (DSR [%])									
Asphalt & dual tire		14.5			1.7%			16.2	
Asphalt & super single tire		17.5			1.4%			18.9	
Seal & dual tire		17.5			1.3%			18.8	
Seal & super single tire		16.3			0.4%			16.7	

Table 5.13: Summary of results for MG65 - before and after durability milling

	MG65 before DMI			Percentage difference			MG65 after DMI		
	PD1	PD2	PD3	PD1	PD2	PD3	PD1	PD2	PD3
Loading									
Vertical stress [kPa]	544	650	760	0%	0%	0%	544	650	760
Confinement stress [kPa]	100	100	100	0%	0%	0%	100	100	100
DSR [%]	20.0	23.9	28.0	5.7%	6.8%	7.9%	25.7	30.7	35.9
Shakedown range									
Werkmeister	B	B	B	-	-	-	B	B	B
Tao	B	B	B	-	-	-	B	B	B
Instability	No	No	No	-	-	-	No	No	Yes
Permanent strain [%]									
100,000 cycles	0.24	0.31	0.37	26%	21%	34%	0.30	0.38	0.49
250,000 cycles	0.29	0.40	0.44	43%	19%	82%	0.42	0.48	0.81
Strain rate [%]									
100,000 cycles	6.3E-07	1.2E-06	1.0E-06	70%	-31%	-2%	1.1E-06	8.0E-07	1.0E-06
250,000 cycles	1.7E-07	2.8E-07	2.5E-07	236%	104%	2642%	5.6E-07	5.7E-07	6.8E-06
Dissipated energy [kPa]									
100,000 cycles	3.95E-02	6.52E-02	7.12E-02	24%	-3%	19%	4.90E-02	6.35E-02	8.50E-02
250,000 cycles	3.46E-02	6.18E-02	6.65E-02	35%	4%	109%	4.65E-02	6.42E-02	1.39E-01
Stiffness response [MPa]									
Mr^*_{10000}	349	359	368	-8%	-3%	-3%	321	349	357
$Mr^*_{average}$	359	366	379	-10%	-5%	-6%	324	346	357
Instability onset [cycles]									
Identified from strain rate	-	-	-	-	-	-	-	-	120,000
Identified from dissipated energy	-	-	-	-	-	-	-	-	78,000
Identified from stiffness response	-	-	-	-	-	-	-	-	20,000
Monotic triaxial testing									
Friction angle [°]		51.2			5%			53.5	
Cohesion [kPa]		354			-40%			214	
Dissipated energy - failure [kPa]		21			-10%			19	
Dissipated energy - 4% strain [kPa]		76			-18%			63	
Stiffness [kPa]		365			-24%			278	
Pavement analysis (DSR [%])									
Asphalt & dual tire		13.4			3.7%			17.1	
Asphalt & super single tire		16.6			3.7%			20.3	
Seal & dual tire		14.8			4.4%			19.2	
Seal & super single tire		14.9			2.9%			17.8	

5.5. CHAPTER SUMMARY AND CONCLUSIONS

This section finalizes the chapter with some final remarks and conclusions. Based on the analysis of the results and the linear elastic pavement assesment, it is likely that the recycled materials (pure RCA as well as blends of RCA and RCM) perform well within South African pavements. Although material breakdown in recycled materials is more severe than conventional base course materials (i.e. G1 or G2), the absolute bearing strength even after durability milling is higher than the G2 specimens. It is recognized that this research just proves the potential of the recycled materials and that more intensive research, especially into long term behavior, is required to establish actual guidelines for pavement design. Based on the findings in chapter, the following conclusions can made:

- In both the permanent deformation as the monotonic triaxial test, the MG65 materials perform better initially, but experience a bigger reduction of performance due to durability milling in comparison with the pure RCA.

- All twelve permanent deformation test results classify as shakedown range B according to the limits proposed by Werkmeister [28]. Based on the definitions of different ranges, it is concluded that the classification is made correctly and that shakedown range B can embrace a wide variety of responses.
- An alternative method to obtain the shakedown limits, based on dissipated energy, did not lead to satisfactory results. Besides difficulties with the repeatability of the method, it is not less subjective than the limits proposed by Werkmeister [28]. The added value of this approach is therefore questioned.
- Huurman's equations to model permanent deformations can also be used to describe the energy dissipation. Doing so may be of interest for obtaining trends and identify instable behavior.
- The strain rate, dissipated energy and stiffness response curves (with respect to the number of load cycles) all indicate the onset of instability. The latter appears to identify instability earlier than the former two, but the corresponding onset might also be less easy to derive if tests are only conducted to a limited number of load cycles.
- The results of a simple linear-elastic pavement analysis show that the DSR levels of the tested materials stay below the derived limit of 30%. The DSR levels of the recycled materials even stay below 20%. Although these outcomes serve only as a first indication, they show the potential of recycled granulates for practical use. Durability milling causes the DSR levels in a reference pavement to increase slighty. This is mainly the result of the loss of cohesion.

6

CONCLUSIONS AND RECOMMENDATIONS

In this research, peformance testing of recycled granulates is combined with a durability simulation. The primary aim is to gain understanding in the extent of (mechanical) breakdown and the way this affects performance. Monotonic and permanent deformation triaxial tests are carried out before and after durability milling. This chapter summarizes the most important conclusions and recommendations. The conclusions are categorized per testing type. Firstly, the outcomes of the durability mill are discussed. Then, the most important results of monotonic and permanent deformation triaxial testing are addressed. Finaly, recommendations for further studies are given at the end of the chapter.

6.1. CONCLUSIONS

6.1.1. DURABILITY

In the durability mill, test are carried out on G2, RCA, RCM, MG65 and MG30. The materials are subjected to three different types of milling, i.e. the dry ball mill, the wet ball mill and the wet mill. Per testing type, three specimens are tested. All specimens started with the same grading and are sieved out afterwards. The fines are collected for PI determination. Based on the obtained results, the following conclusions can be made:

- Both the RCA and the RCM are found to be non-plastic (PI = 1). The blends consist of a mixture of RCA and RCM and are concluded to be non-plastic as well (PI = 1). The G2 only carries a low amount of plasticy (PI = 3).
- Durability milling mostly affects the RCA materials. Increasing the masonry content results in a general decrease of total breakdown. It is believed that the mortar bound to the RCA aggregates is weaker than the masonry particles and most prone to damage. As predicted, the G2 materials suffer significantly less damage than the recycled materials.
- For the RCA and the G2, wet ball milling results in the most severe breakdown. For the materials containing masonry, wet ball milling and dry ball milling causes comparable damage. Wet milling is in all cases the least destructive test. For non-plastic materials, performing this test seems unnecessary.
- Considering the change of individual particle fractions, the most change is observed in the largest 14 mm fraction. Other fractions break down as well, but recieve 'new' particles from sieves above. The change of the largest fraction in combination with the increase of fines may adress material breakdown better than the fines alone.
- The Durability Mill Index as currently prescribed by the standards is not a good measure to quantify durability of non-plastic materials. According to the definition, the recycled materials rank higher than the G2 because PI = 1. The degradation of these materials however is much more severe. The weakness is found to be in the calculation of the DMI, not in the procedure itself.

- Substantial breakdown is observed in the sieved out monotonic triaxial samples. This implies that the vibratory compactor significantly damages the material. In contrast the durability milled specimens, the distribution of broken down particles concentrates mainly on the second largest sieve. Since the smaller particle fractions are hardly increased, it is concluded that the vibratory hammer primary affects the largest fraction.

6.1.2. MONOTONIC TRIAXIAL TESTING

Monotonic triaxial tests are performed on G2, RCA, MG65 and MG30. Test are conducted on initial materials and on durability milled materials, to study the effect of durability milling on shear strength. The obtained shear parameters are based on six tests per material. According to the results, the following conclusions can be made:

- The shear parameters of the recycled materials (both the friction angle and the cohesion) are in all cases higher than the shear parameters of the G2. Substantial cohesion levels are measured in the recycled materials. The highest angles of internal friction are related to the RCA, while the highest cohesion levels are found in mixed granulates. In general, an increase of compressive strength is measured in the materials containing more masonry. The shear parameters of both the G2 and the recycled materials fall in comparable ranges with respect to other work performed at Stellenbosch University.
- In the recycled materials, durability milling causes a small increase of the angle of internal friction and a moderate decrease of cohesion. The latter is the most significant, as in all cases the absolute compressive strength is reduced. In accordance with the findings in the durability mill, the shear parameters of the G2 materials are hardly influenced.
- Different failure types can be observed between the recycled materials and the G2. In the G2, a plastic failure type occurs. After reaching the peak strength, the specimens show dilatant behavior with only little reduction of strength as the displacement increases. The recycled materials show a more brittle type of failure, and develop a shear plane. A significant reduction of strength is measured as displacement further increases. Although plastic failure is preferable, it is only after considerable displacements ($\epsilon > 5\%$) that the compressive strength of the G2 is higher than the compressive strength of the recycled materials.
- In all cases, the results of the milled specimens are more consistent in comparison with their unmilled counterparts. It is likely that the relatively high amount of 14 mm particles (due to the scalped and added grading of the unmilled specimens) in combination with the mold diameter, reduces the packing and increases the variability. In the milled specimens, the 14 mm fraction is partly broken down. This results in easier to compact specimens, and probably also in an increased consistency. In addition to this, the quality of the results depends greatly on the sample preparation process. Paying attention to details is crucial and may significantly improve specimen coherence.

6.1.3. PERMANENT DEFORMATION TRIAXIAL TESTING

Permanent deformation triaxial tests are performed on RCA and MG65. Similar as in the monotonic triaxial tests, tests have been carried out on initial materials and on durability milled materials. For each material, three specimens are tested at ranging stress levels. Confinement stress is maintained constant (100 kPa), as well as the stress levels between materials. The results are analyzed with respect to strain rate, stiffness response and dissipated energy. Based on the obtained results and analysis, the following can be concluded:

- A stable response is found in all materials loaded under 30% DSR. The corresponding permanent deformation values after 250,000 load cycles are limited to less than 1%. Unstable behavior is measured in both milled RCA and milled MG65, tested at 35% DSR.

- Monotonic triaxial testing alone is not sufficient for an adequate material characterisation. Although the shear parameters are high in all cases, significant differences are measured between milled and unmilled specimens.
- Durability milling increases variability and weakens the specimens. Especially the MG65 materials are significantly affected. Increasing strain rate and unstable behavior are observed in both milled specimen groups.
- All specimens, including the unstable ones, classify as shakedown range B according to the criteria formulated by Werkmeister. It is believed that, based on the long term results and the definition of the shakedown ranges, the materials are categorized correctly. Subsequently, this implies that shakedown range B can embrace a wide variety of responses, including sound behavior.
- The application of the dissipated energy concept to identify shakedown limits showed potential but is still very subjective. Repeating the excersize proposed by Tao appeared troublesome and did not lead to workable results. For these two reasons, the added value of this method is questioned.
- The evolution of the strain rate, dissipated energy and approximated resilient modulus all point out the onset of eventual instability. The latter appears to be highly indicative for the rate of damage, and shows in case of instability a change of response in a very early stage of the test. The onset of this change however might be hard to identify. Both dissipated energy and stiffness response curves could be of interest for further studies into the prediction of long term instability.
- A small linear-elastic pavement analysis is carried out on a reference pavement to gain first insights in the occurring stress levels. The analysis considers a 80 kN standard axle load, provided with a dual or super single tire. It is found that in all situations, the recycled materials are loaded below 25% DSR. Although this analysis incorporates simplifications, it indicates that recycled granulates have substantial potential to be used in South African base layers.

Overall, this research mainly focusses on the use of recycled materials in base course layers. The performance in subbase layers is not extensively addressed. Considering the predicted stress levels from the multilayer analysis and obtained stress limits however, it is highly probable that these materials will perform well within subbase layers. Nevertheless, it is advisable to study the permanent deformation behavior at (lower) subbase stress conditions. Furthermore, the presence of masonry shows two different aspects. Based on the monotonic triaxial tests, increasing the masonry content results in higher cohesion levels. At the same time, less breakdown is observed in specimens containing more masonry. In contrast to this, the permanent deformation behavior of the MG65 seems much more affected by durability milling than the RCA. It is yet unclear if this is an accurate representation of reality or that it is caused by specimen variability. The type of material breakdown, i.e. chemical or mechanical, could also be of influence. More permanent deformation testing in combination with durability milling should rule out what is exactly happening, and may possibly explain the observed contradiction.

6.2. RECOMMENDATIONS

During the course of this research, some limitations are encountered which might be of interest for further studies. Besides new research possibilities, some overall improvements and additions related to this work are enlisted. The most important recommendations are listed below:

- In addition to this research, it is worthwile to perform durability milling on the full graded materials. The full grading includes all particle fractions and is a better representation of what would be applied in the field. In this case, only dry ball milling and wet ball milling should be considered. Wet milling of non-plastic materials causes only little breakdown and seems less relevant.

- Although the potential of the durability mill as a convenient durability simulator is recognized, the procedure should be expanded for non-plastic materials. A validation of the durability mill for non-plastic materials and a revision of the corresponding Durability Mill Index is therefore advised. Doing so may lead to a better understanding of the in-field breakdown and how this is best simulated with the durability mill. Subsequently, durability guidelines related to field performance might be derived. In the case of recycled materials, it is recognized that no field validation can be carried out yet. In a later stage, when test lanes are constructed, the durability properties of the recycled granulates can be addressed properly and validated against the results obtained in this research.
- It is believed that permanent deformation testing is currently the most accurate way to describe the behavior of unbound granulates in the field. In following research, the main focus should concentrate on long term behavior and finding stress limits at which the risk of instability is significant. Due to high variability in the permanent deformation tests, more tests are required to gain confidence in the results. Furthermore, important influence factors such as confinement stress and moisture conditions should be varied to obtain a complete picture of the material response. With sufficient data available, transfer functions for recycled materials could be derived to predict pavement service life.
- The variability in the RCA and RCM should be addressed by testing different material resources. Especially the latter might vary significantly when originated from manually processed bricks.
- In addition to the above, different types of processing (i.e. crushing or even dry ball milling) can be tried to find the optimal performance. Initially breaking the weak (mortar) bonds might improve the overal quality of the materials. Although undesirable in terms of testing time and workability, the most representative results are found in full scale triaxial tests (i.e. a specimen size of 600 x 300 mm), when tested up to 1,000,000 or more load cycles.
- The MATLAB scripts developed for this research can be of further use to analyse older permanent deformation data. Doing so may validate whether the dissipated energy and stiffness response curves are indeed early indicators for instability. Comparisons with older test results are also more accurate with all data similary processed.
- Pavement analysis should be extended by the use of more accurate models. Especially the ability to incorporate stress dependent stiffness is of interest. In this research, the resilient properties are not addressed. Performing resilient modulus triaxial tests should provide the required input for these models. At the same time, the resilient modulus can be put into perspective against the approximated resilient modulus acquired from permanent deformation testing.
- Finally, the best way to gain practical experience is by constructing test lanes. Local parallel lanes can be a possibility if traffic may not be hindered. Test lanes are the next step in bringing recycled materials into practice and provide numerous oppurtunities for performance and durability related research.

BIBLIOGRAPHY

[1] Alemgena A.A., "*Characterization of Unbound Materials for Pavements*", PhD dissertation, Delft University of Technology, Delft, The Netherlands, 2011.

[2] Barisanga F., "*Material characterisation and response modelling of recycled concrete and masonry in pavements*", MSc Thesis, Stellenbosch University, Stellenbosch, South Africa, 2014.

[3] Bredenkamp Z., "*The Performance Properties of Recycled Concrete in Road Pavement Materials*", MSc Thesis, Stellenbosch University, Stellenbosch, South Africa, 2018.

[4] Counsil for Scientific and Industrial Research (CSIR), "*Proposed protocol for resilient modulus and permanent deformation characteristics of unbound and bound granular materials*", Version: 1^{st} draft, 2011.

[5] CROW Information and Technology Centre for Transport and Infrastructure, "*RAW2000 Standard conditions of contract for works of civil engineering construction*, Ede, The Netherlands, 2000.

[6] CROW Information and Technology Centre for Transport and Infrastructure, "*Resten zijn géén afval (meer)*, Ede, The Netherlands, 1988.

[7] CROW Information and Technology Centre for Transport and Infrastructure, "*Steenfunderingen beter gefundeerd*, Ede, The Netherlands, 1988.

[8] Green R.A., "*Energy-Based Evaluation and Remediation of Liquifiable Soils*", PhD Dissertation, Virginia Polytechnic Institute and State University, Blackburg, Virginia, United States of America, 2001.

[9] Houben L.J.M., "*Soil and Granular (Sub-)Base Materials*", Course notes, Delft University of Technology, Delft, The Netherlands, 2013.

[10] Huurman M., "*Permanent deformation in concrete block pavements*", PhD dissertation, Delft University of Technology, Delft, The Netherlands, 1997.

[11] Jenkins K.J., Rudman C.E., "*Hitchhikers guide to pavement engineering*", Course notes, Stellenbosch University, Stellenbosch, South Africa, 2018.

[12] Kotzé N., "*Toets van Granulêre Materiale*", BSc Thesis, Stellenbosch University, Stellenbosch, South Africa, 2014.

[13] Molenaar A.A.A., Houben L.J.M., "*Wegen en spoorwegen*", Course notes, Delft University of Technology, Delft, The Netherlands, 2011.

[14] van Niekerk A.A., "*Mechanical behaviour and performance of granular bases and sub-bases in pavements*", PhD dissertation, Delft University of Technology, Delft, The Netherlands, 2002.

[15] van Niekerk A.A., van Scheers J., Galjaard P.J., "*De invloed van de gradering op het elastisch gedrag van menggranulaat - Een vergelijking van het gedrag van 0/40 mm en 0/22.4 mm graderingen*", Report, Delft University of Technology, Delft, The Netherlands, 1998.

[16] Paige-Green, P "*Durability testing of basic crystalline rocks and specification for use as road base aggregate*", Paper, CSIR Built Environment, (no date).

[17] Paige-Green P., "*Durability - granular materials & testing*", Presentation slides regarding the course "*Pavement materials 1 - granular and cemented materials*", Stellenbosch University, Stellenbosch, South Africa, 2016.

[18] Ride2Roam motorbike tours, "*South Africa: Ocean to ocean*", Cover image, www.ride2roam.com

[19] Rudman C.E., Jenkins K.J., "*Self-cementing Mechanisms of Recycled Concrete and Masonry Aggregate*", Unpublished paper, Stellenbosch University, Stellenbosch, South Africa, 2015.

[20] Sampson L.R, Netterberg F. "*The Durability Mill: A new performance-related durability test for basecourse aggregates*", Paper, The Civil Engineer, 1989.

[21] South African National Roads Agency (SANRAL), "*South African pavement engineering manual*", Second edition, 2014.

[22] South African National Standard SANS 3001-AG1, "*Particle size analysis of aggregates by sieving*", South African National Standard, Edition 1.2, 2014.

[23] South African National Standard SANS 3001-AG16, "*Determination of the durability mill index values for aggregates*", South African National Standard, Edition 1, 2013.

[24] South African National Standard SANS 3001-GR10, "*Determination of the one-point liquid limit, plastic limit, plasticity index and linear shrinkage*", South African National Standard, Edition 1.2, 2013.

[25] Sweere G.T.H., "*Unbound granular bases for roads*", PhD dissertation, Delft University of Technology, Delft, The Netherlands, 1990.

[26] Tao M., Mohammad L.N., Nazzal M.D., Zhang Z., Wu Z., "*Application of Shakedown Theory in Characterizing Traditional and Recycled Pavement Base Materials*", Paper, Journal of Transportation Engineering, 2010.

[27] Verruijt A., Broere W., "*Grondmechanica*", Course notes, Delft University of Technology, Delft, The Netherlands, 2012.

[28] Werkmeister S., "*Permanent Deformation Behaviour of Unbound Granular Materials in Pavement Constructions*", PhD dissertation, Dresden University of Technology, Dresden, Germany, 2003.

[29] van Zyl E.B., "*Influence of grading scale and specimen geometry on the performance of an unbound material*", MSc Thesis, Stellenbosch University, Stellenbosch, South Africa, 2015.

A

APPENDIX A: SOUTH AFRICAN GRANULAR CLASSIFICATION SYSTEM

Table A.1: Summary of TRH14 Classification System for Granular Materials, Gravels and Soils. G1 up and including G6 [21]

Groups	**G1, G2, G3: Graded Crushed Stone**			**G4, G5, G6: Natural Gravels**		
Description	G1 Crushed unweathered rock	G2, G3 Crushed rock, boulders or coarse gravel		Natural gravel; may be mixed with crushed rock such as boulders. May be cementitiously or mechanically modified.		
Material Class	**G1**	**G2**	**G3**	**G4**	**G5**	**G6**
GRADING						
Sieve Size (mm)	Nominal max size 37.5 mm[1]	Nominal max size **28** (26.5) mm[1]			Max size 64 mm or two-thirds of compacted layer thickness, whichever is smaller.	
50 / 53	100			100		
37.5	100			85 – 100		
28 / 26.5	84 – 94	100		–		
20 / 19	71 – 84	85 – 95		60 – 90		
14 / 13.2	59 – 75	71 – 84		–		
5 / 4.75	36 – 53	42 – 60		30 – 65		
2	23 – 40	27 – 45		20 – 50		
0.425	11 – 24	13 – 27		10 – 30		
0.075	4 – 12	5 – 12		5 – 15		
Grading Modulus (min)	n/a			n/a	1.5	1.2
Flakiness Index	Max 35% on weighted average of -28 (26.5) and -20 (19) mm fractions		n/a	n/a		
Crushing Strength	10% FACT (min) 110 kN or ACV (max) 29%		n/a	n/a		
ATTERBERG LIMITS						
Liquid Limit (max)	25	25		25	30	n/a
Plasticity Index, PI (max)	4	6		6	10	12 or 3 GM[2] + 10
Linear shrinkage, % (max)	4	3		3	5	n/a
Linear shrinkage x -0.425 mm sieve (max)[3]	n/a			170	170	n/a
BEARING STRENGTH AND SWELL						
CBR, % (min) at MDD[4]	n/a	80 at 98%		80 at 98%	45 at 95%[5]	25 at 93%
Swell, % (max) at MDD	n/a	0.2 at 100%		0.2 at 100%	0.5 at 100%	1.0%
Material Class	**G1**	**G2**	**G3**	**G4**	**G5**	**G6**

B

APPENDIX B: GRADINGS

B.1. GRADINGS TESTED BY ANDRES VAN NIEKERK

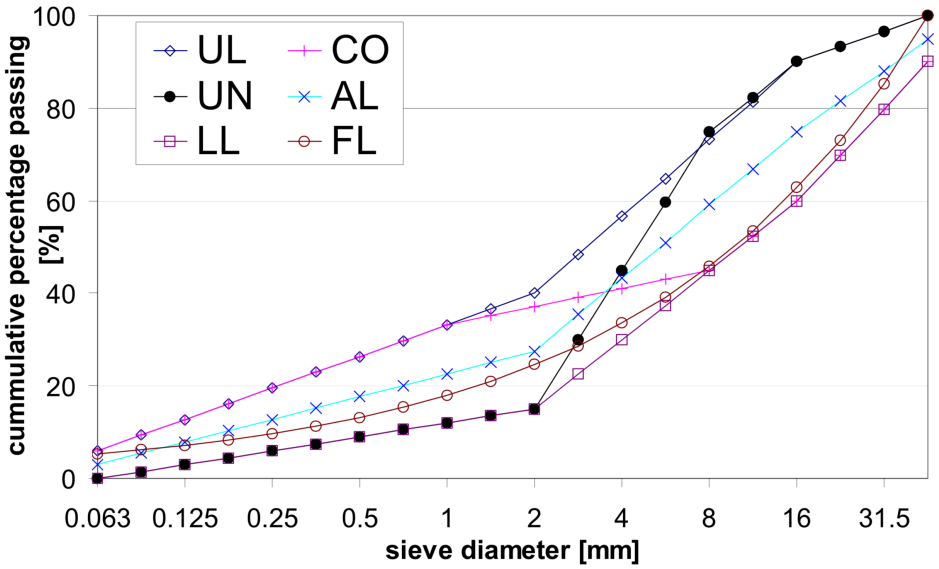

Figure B.1: Gradings used by Van Niekerk [14]

The gradings tested by Van Niekerk are based on limits prescribed by the Dutch RAW standards 2000 [5] and are listed as follows:

- LL (Lower Limit), the coursest allowable grading.
- UL (Upper Limit), the finest allowable grading.
- AL (Average Limit), the average of the upper and the lower limit.
- CO (Continuous), contains a high amount of fines (0 - 2 mm) and course material (8 - 40 mm).
- UN (Uniform), the opposite of CO, contains a high amount of the fraction 2 - 8 mm.
- FL (Füller), theoretically ideal grading curve with n = 0.45 (see Equation F.1).

B.2. SOUTH AFRICAN AND DUTCH GRADING STANDARDS

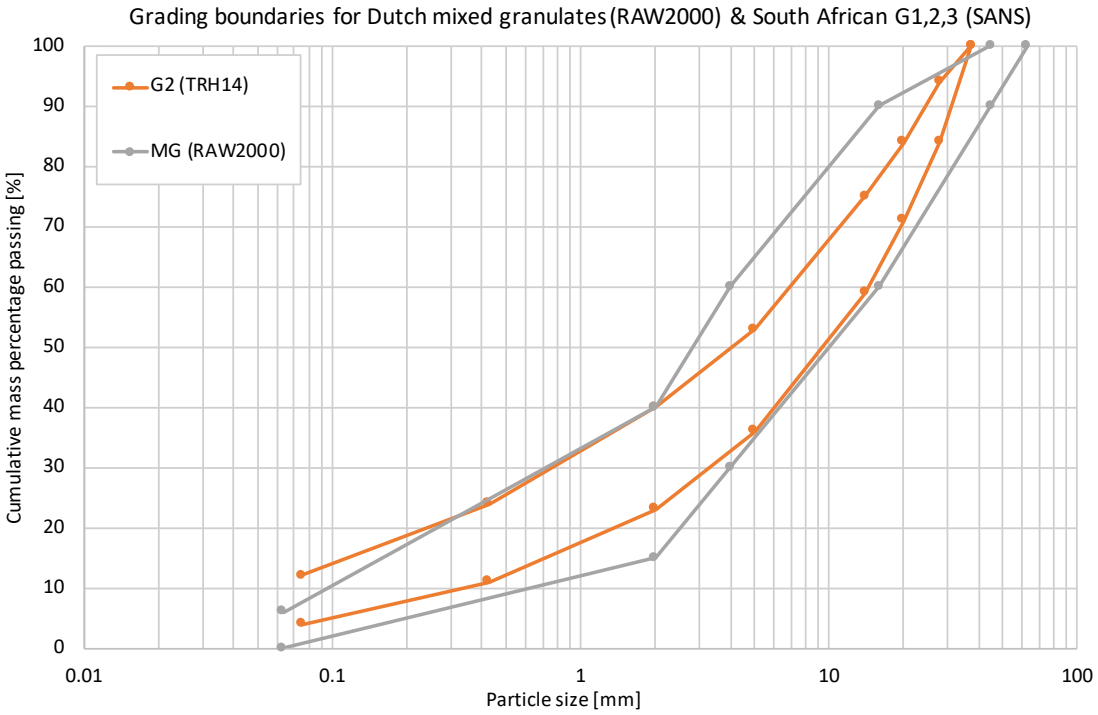

Figure B.2: Granding standards for South African G2 and Dutch mixed granulates [21][5]

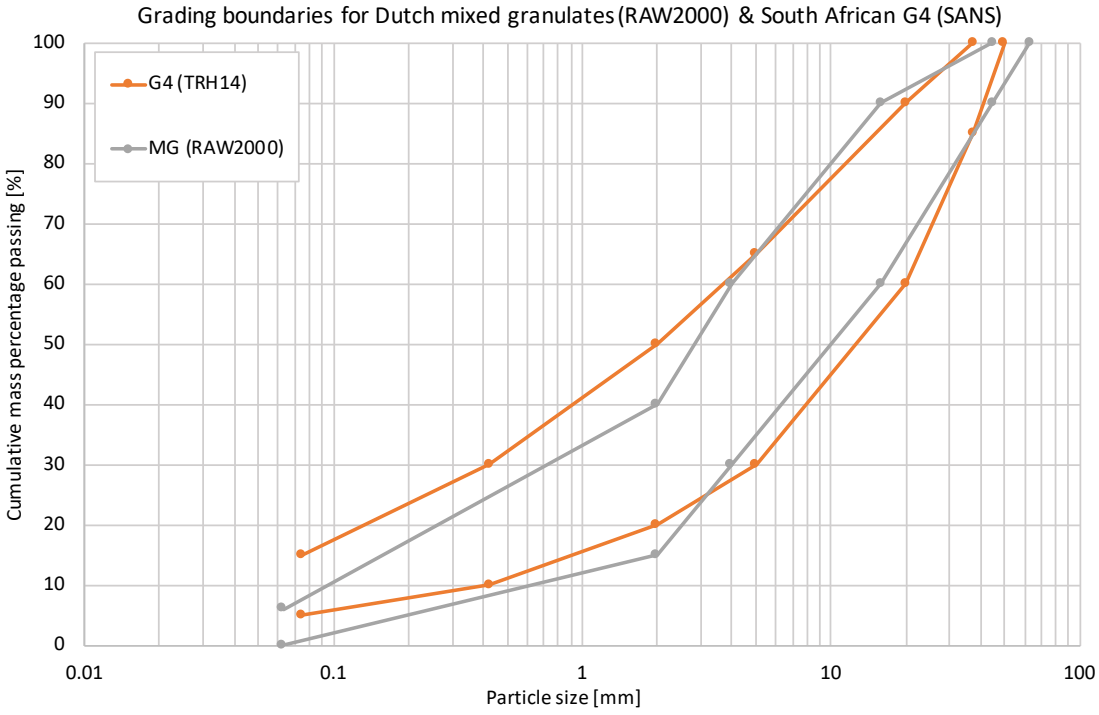

Figure B.3: Grading standards for South African G4 and Dutch mixed granulates [21][5]

C

APPENDIX C: OPTIMUM MOISTURE CONTENT TEST RESULTS

Table C.1: Optimum moisture content test results

Specimen	ID	Target MC [%]	Height [mm]	Wet mass [g]	Dry mass [g]	Mass water [g]	Actual MC [%]	Dry density [kg/m^2]
G2	G2-VMOD-2%	2	108	4593	4502	91	**2.02**	**2274**
	G2-VMOD-3%	3	104	4620	4483	136	**3.04**	**2366**
	G2-VMOD-4%	4	103	4669	4494	175	**3.88**	**2389**
	G2-VMOD-5%	5	101	4519	4325	194	**4.48**	**2349**
RCA	RCA-VMOD-8%	8	137	5222	4832	390	**8.08**	**1927**
	RCA-VMOD-9%	9	135	5315	4875	440	**9.03**	**1973**
	RCA-VMOD-10%	10	133	5363	4872	491	**10.07**	**2009**
	RCA-VMOD-11%	11	132	5378	4865	513	**10.55**	**2022**
	RCA-VMOD-12%	12	130	5269	4740	529	**11.17**	**2004**
MG65	MG65-VMOD-9%	9	144	5341	4919	422	**8.58**	**1873**
	MG65-VMOD-10%	10	140	5437	4975	462	**9.29**	**1949**
	MG65-VMOD-11%	11	138	5432	4921	511	**10.38**	**1956**
	MG65-VMOD-12%	12	137	5387	4857	530	**10.91**	**1941**
MG30	MG65-VMOD-10%	10	137	4973	4566	407	**8.91**	**1825**
	MG65-VMOD-11%	11	134	4975	4531	444	**9.80**	**1855**
	MG65-VMOD-12%	12	131	4962	4488	474	**10.56**	**1876**
	MG65-VMOD-13%	13	128	4939	4397	542	**12.33**	**1888**

Table C.2: Design moisture content and dry density

Material	Optimum moisture content [%]	Maximum dry density [kg/m^2]	Design degree of compaction [%]	Design moisture content [%]	Design dry density [kg/m^2]
G2	3.72	2390	97	3.70	2318
RCA	10.52	2018	100	10.00	2018
MG65	9.86	1964	97	10.00	1905
MG30	11.50	1890	97	10.50	1833

D

Appendix D: Recipes

Table D.1: Specimen mixture tables for G2, RCA & RCM

Specimen recepy for G2

Fraction [mm]	On Sieve [mm]	OMC test [kg]	DMI Full [kg]	DMI G20C [kg]	Triaxial [kg]
> 37.5	37.5	0.000	0.000	0.000	0.000
37.5 - 28	28	0.000	0.413	0.000	0.000
28 - 20	20	0.000	0.431	0.000	0.000
20 - 14	14	1.650	0.394	1.238	4.864
14 - 5	5	1.125	0.844	0.844	3.316
5 - 2	2	0.650	0.488	0.488	1.916
2 - 0.425	0.425	0.700	0.525	0.525	2.063
0.425 - 0.075	0.075	0.475	0.356	0.356	1.400
< 0.075 (pan)	Pan	0.400	0.300	0.300	1.179
	Total	**5.000**	**3.750**	**3.750**	**14.739**

Specimen recepy for RCM

DMI Full [kg]	DMI S&A [kg]
0.000	0.000
0.413	0.000
0.431	0.000
0.394	1.238
0.844	0.844
0.488	0.488
0.525	0.525
0.356	0.356
0.300	0.300
3.750	**3.750**

Specimen recepy for RCA

Fraction [mm]	On Sieve [mm]	OMC test [kg]	DMI Full [kg]	DMI G20C [kg]	Triaxial [kg]
> 37.5	37.5	0.000	0.000	0.000	0.000
37.5 - 28	28	0.000	0.413	0.000	0.000
28 - 20	20	0.000	0.431	0.000	0.000
20 - 14	14	1.650	0.394	1.238	4.398
14 - 5	5	1.125	0.844	0.844	2.998
5 - 2	2	0.650	0.488	0.488	1.732
2 - 0.425	0.425	0.700	0.525	0.525	1.866
0.425 - 0.075	0.075	0.475	0.356	0.356	1.266
< 0.075 (pan)	Pan	0.400	0.300	0.300	1.066
	Total	**5.000**	**3.750**	**3.750**	**13.326**

Table D.2: Specimen mixture tables for MG65 & MG30

Specimen recepy for MG65

Fraction	On Sieve	OMC test		DMI Full		DMI G20C		Triaxial	
[mm]	[mm]	RCA [kg]	RCM [kg]	RCA [kg]	RCM [kg]	RCA [kg]	RCM [kg]	RCA [kg]	RCM [kg]
> 37.5	37.5	0.000	0.000	0.000	0.000	0.000	0.000	0.000	0.000
37.5 - 28	28	0.000	0.000	0.268	0.144	0.000	0.000	0.000	0.000
28 - 20	20	0.000	0.000	0.280	0.151	0.000	0.000	0.000	0.000
20 - 14	14	1.073	0.578	0.256	0.138	0.804	0.433	2.700	1.454
14 - 5	5	0.731	0.394	0.548	0.295	0.548	0.295	1.841	0.991
5 - 2	2	0.423	0.228	0.317	0.171	0.317	0.171	1.064	0.573
2 - 0.425	0.425	0.455	0.245	0.341	0.184	0.341	0.184	1.146	0.617
0.425 - 0.075	0.075	0.309	0.166	0.232	0.125	0.232	0.125	0.777	0.419
< 0.075 (pan)	Pan	0.260	0.140	0.195	0.105	0.195	0.105	0.655	0.352
	Total	**3.250**	**1.750**	**2.438**	**1.313**	**2.438**	**1.313**	**8.182**	**4.406**
	Total	**5.000**		**3.750**		**3.750**		**12.588**	

Specimen recepy for MG30

Fraction	On Sieve	OMC test		DMI Full		DMI G20C		Triaxial	
[mm]	[mm]	RCA [kg]	RCM [kg]	RCA [kg]	RCM [kg]	RCA [kg]	RCM [kg]	RCA [kg]	RCM [kg]
> 37.5	37.5	0.000	0.000	0.000	0.000	0.000	0.000	0.000	0.000
37.5 - 28	28	0.000	0.000	0.124	0.289	0.000	0.000	0.000	0.000
28 - 20	20	0.000	0.000	0.129	0.302	0.000	0.000	0.000	0.000
20 - 14	14	0.495	1.155	0.118	0.276	0.371	0.866	1.204	2.810
14 - 5	5	0.338	0.788	0.253	0.591	0.253	0.591	0.821	1.916
5 - 2	2	0.195	0.455	0.146	0.341	0.146	0.341	0.474	1.107
2 - 0.425	0.425	0.210	0.490	0.158	0.368	0.158	0.368	0.511	1.192
0.425 - 0.075	0.075	0.143	0.333	0.107	0.249	0.107	0.249	0.347	0.809
< 0.075 (pan)	Pan	0.120	0.280	0.090	0.210	0.090	0.210	0.292	0.681
	Total	**1.500**	**3.500**	**1.125**	**2.625**	**1.125**	**2.625**	**3.649**	**8.514**
	Total	**5.000**		**3.750**		**3.750**		**12.163**	

Table D.3: Triaxial specimen recepy table

Triaxial specimen design		G2	RCA	MG65	MG30
Maximum dry density	[kg/m^3]	2390	2018	1964	1890
OMC	[%]	3.70	10.50	9.90	11.50
Design specimen dry density	[kg/m^3]	2318	2018	1905	1833
Design specimen MC	[%]	3.70	10.00	10.00	10.50
Design specimen dry mass	[kg]	12.703	11.058	10.439	10.047
Design specimen water mass	[kg]	0.470	1.106	1.044	1.055
Design specimen bulk density	[kg/m^3]	2404	2220	2096	2026
Total specimen mass	**[kg]**	**13.173**	**12.164**	**11.483**	**11.102**
Divide in 5 bags of:	**[kg]**	**2.635**	**2.433**	**2.297**	**2.220**

Triaxial specimen composition		G2	RCA	MG65	MG30
Composition dry mass	[kg]	14.703	13.058	12.439	12.047
Composition water mass	[kg]	0.544	1.306	1.244	1.265
Material air-dry MC	[%]	0.24	2.05	1.2	0.97
Mass water to be added	[kg]	0.509	1.038	1.095	1.148
Composition air-dry mass	[kg]	**14.739**	**13.326**	**12.588**	**12.163**
Total composition mass	[kg]	**15.247**	**14.364**	**13.683**	**13.312**

DMI Specimen air-dry mass	[kg]	3.750
OMC specimen air-dry mass	[kg]	5
Extra triaxial oven-dry mass	[kg]	2

E

APPENDIX E: SIEVE RESULTS

E.1. G2 SIEVE RESULTS

Table E.1: G2 sieve results: G20C initial grading, full initial grading & grading after monotonic triaxial testing

Particle size distribution - Fractions		G2 G20C graded - Initial			G2 full graded - Initial			G2 G20C graded - After monotonic triaxial test		
Sieve	Particle fraction	G2-INITIAL-S1	G2-INITIAL-S2	G2-INITIAL-S3	G2-INITIAL-F1	G2-INITIAL-F2	G2-INITIAL-F3	G2-MONO-M1	G2-MONO-M2	G2-MONO-M3
[mm]	[mm]	[%]	[%]	[%]	[%]	[%]	[%]	[%]	[%]	[%]
37.5	> 37.5	0.0	0.0	0.0	0.0	0.0	0.0	0.0	0.0	0.0
28	37.5 - 28	0.0	0.0	0.0	11.0	10.0	8.3	0.0	0.0	0.0
20	28 - 20	0.0	0.0	0.0	10.6	12.1	13.9	0.0	0.0	0.0
14	20 - 14	32.0	30.7	31.8	11.2	11.2	10.6	29.9	29.8	27.1
10	14 - 10	10.5	11.5	9.2	7.5	6.2	8.9	11.4	11.2	12.6
7.1	10 - 7.1	6.9	6.5	6.7	5.9	6.3	6.2	6.2	6.8	7.3
5	7.1 - 5	5.9	6.4	7.2	8.3	9.0	6.7	7.1	7.0	6.8
2	5 - 2	12.5	12.7	12.8	12.6	12.7	12.4	12.7	12.5	13.0
1	2 - 1	5.6	5.1	5.8	5.4	5.7	5.7	5.5	5.5	5.8
0.6	1 - 0.6	3.0	3.1	2.9	3.5	3.4	3.4	3.1	3.1	3.2
0.425	0.6 - 0.425	2.0	2.3	1.8	2.2	2.0	2.0	1.9	1.9	2.0
0.3	0.425 - 0.3	2.3	2.5	2.4	2.2	2.4	2.4	2.3	2.3	2.3
0.15	0.3 - 0.15	4.9	5.0	5.0	5.0	4.8	4.9	4.9	5.3	5.0
0.075	0.15 - 0.075	3.0	3.0	3.0	3.1	2.9	3.1	3.0	2.4	3.1
Pan	< 0.075 (pan)	11.4	11.2	11.3	11.4	11.4	11.4	12.0	12.1	11.9
	Total	**100.0**	**100.0**	**100.0**	**100.0**	**100.0**	**100.0**	**100.0**	**100.0**	**100.0**

Particle size distribution - Average		Fractions			Standard deviation			Passing		
Sieve	Particle fraction	G2-INITIAL-S	G2-INITIAL-F	G2-MONO	G2-INITIAL-S	G2-INITIAL-F	G2-MONO	G2-INITIAL-S	G2-INITIAL-F	G2-MONO
[mm]	[mm]	[%]	[%]	[%]	[%]	[%]	[%]	[%]	[%]	[%]
37.5	> 37.5	0.0	0.0	0.0	0.0	0.0	0.0	100.0	100.0	100.0
28	37.5 - 28	0.0	9.8	0.0	0.0	1.4	0.0	100.0	90.2	100.0
20	28 - 20	0.0	12.2	0.0	0.0	1.7	0.0	100.0	78.0	100.0
14	20 - 14	31.5	11.0	28.9	0.7	0.4	1.6	68.5	67.0	71.1
10	14 - 10	10.4	7.5	11.7	1.2	1.4	0.8	58.1	59.4	59.4
7.1	10 - 7.1	6.7	6.1	6.8	0.2	0.2	0.5	51.4	53.3	52.6
5	7.1 - 5	6.5	8.0	7.0	0.6	1.2	0.2	44.9	45.3	45.6
2	5 - 2	12.7	12.6	12.7	0.1	0.2	0.2	32.3	32.7	32.9
1	2 - 1	5.5	5.6	5.6	0.4	0.2	0.2	26.7	27.2	27.3
0.6	1 - 0.6	3.0	3.4	3.1	0.1	0.0	0.0	23.7	23.7	24.1
0.425	0.6 - 0.425	2.0	2.1	1.9	0.2	0.1	0.0	21.7	21.7	22.2
0.3	0.425 - 0.3	2.4	2.3	2.3	0.1	0.1	0.0	19.3	19.3	19.9
0.15	0.3 - 0.15	5.0	4.9	5.1	0.1	0.1	0.2	14.3	14.4	14.8
0.075	0.15 - 0.075	3.0	3.0	2.8	0.0	0.1	0.4	11.3	11.4	12.0
Pan	< 0.075 (pan)	11.3	11.4	12.0	0.1	0.0	0.1	0.0	0.0	0.0
	Total	**100.0**	**100.0**	**100.0**	**0.3**	**0.3**	**0.3**			
					Mean standard deviation					

Table E.2: G2 sieve results: G20C graded after durability milling

Particle size distribution - Fractions		DMI G20C graded - Dry ball mill			DMI G20C graded - Wet ball mill			DMI G20C graded - Wet mill		
Sieve	Particle fraction	G2-DMIS-DB1	G2-DMIS-DB2	G2-DMIS-DB3	G2-DMIS-WB1	G2-DMIS-WB2	G2-DMIS-WB3	G2-DMIS-W1	G2-DMIS-W2	G2-DMIS-W3
[mm]	[mm]	[%]	[%]	[%]	[%]	[%]	[%]	[%]	[%]	[%]
37.5	> 37.5	0.0	0.0	0.0	0.0	0.0	0.0	0.0	0.0	0.0
28	37.5 - 28	0.0	0.0	0.0	0.0	0.0	0.0	0.0	0.0	0.0
20	28 - 20	0.0	0.0	0.0	0.0	0.0	0.0	0.0	0.0	0.0
14	20 - 14	30.5	31.2	30.5	27.8	29.1	28.6	31.2	30.7	29.8
10	14 - 10	8.3	8.3	8.2	7.7	9.2	6.7	8.4	8.3	8.7
7.1	10 - 7.1	5.9	6.0	5.9	6.2	6.2	5.6	6.0	6.3	6.1
5	7.1 - 5	6.7	6.4	6.7	7.9	6.3	8.3	8.7	9.0	9.1
2	5 - 2	13.1	12.5	13.4	13.7	12.7	14.4	12.5	12.7	12.7
1	2 - 1	6.0	5.7	6.6	6.5	6.1	6.1	5.2	5.3	5.4
0.6	1 - 0.6	3.5	3.4	3.4	3.4	3.4	3.5	3.3	3.2	3.1
0.425	0.6 - 0.425	2.1	2.3	1.8	2.0	2.2	2.1	1.9	1.9	1.9
0.3	0.425 - 0.3	2.4	2.7	2.3	2.3	2.4	2.2	2.2	2.2	2.3
0.15	0.3 - 0.15	5.6	5.5	5.3	5.6	5.7	5.4	4.9	4.9	4.9
0.075	0.15 - 0.075	3.5	3.3	3.3	3.3	3.3	3.8	3.4	3.3	3.2
Pan	< 0.075 (pan)	12.6	12.7	12.6	13.5	13.5	13.3	12.2	12.4	12.7
	Total	**100.0**	**100.0**	**100.0**	**100.0**	**100.0**	**100.0**	**100.0**	**100.0**	**100.0**

Particle size distribution - Average		DMI G20C graded - Fractions			DMI G20C graded - Standard deviation			DMI G20C graded - Passing		
Sieve	Particle fraction	G2-DMIS-DB	G2-DMIS-WB	G2-DMIS-W	G2-DMIS-DB	G2-DMIS-WB	G2-DMIS-W	G2-DMIS-DB	G2-DMIS-WB	G2-DMIS-W
[mm]	[mm]	[%]	[%]	[%]	[%]	[%]	[%]	[%]	[%]	[%]
37.5	> 37.5	0.0	0.0	0.0	0.0	0.0	0.0	100.0	100.0	100.0
28	37.5 - 28	0.0	0.0	0.0	0.0	0.0	0.0	100.0	100.0	100.0
20	28 - 20	0.0	0.0	0.0	0.0	0.0	0.0	100.0	100.0	100.0
14	20 - 14	30.7	28.5	30.6	0.4	0.6	0.7	69.3	71.5	69.4
10	14 - 10	8.2	7.9	8.5	0.0	1.3	0.2	61.0	63.6	61.0
7.1	10 - 7.1	5.9	6.0	6.1	0.0	0.4	0.2	55.1	57.6	54.8
5	7.1 - 5	6.6	7.5	8.9	0.2	1.1	0.2	48.5	50.1	45.9
2	5 - 2	13.0	13.6	12.7	0.4	0.9	0.1	35.5	36.5	33.2
1	2 - 1	6.1	6.2	5.3	0.4	0.2	0.1	29.4	30.3	27.9
0.6	1 - 0.6	3.4	3.4	3.2	0.0	0.1	0.1	26.0	26.8	24.8
0.425	0.6 - 0.425	2.1	2.1	1.9	0.2	0.1	0.0	23.9	24.8	22.9
0.3	0.425 - 0.3	2.5	2.3	2.3	0.2	0.1	0.1	21.5	22.5	20.6
0.15	0.3 - 0.15	5.5	5.6	4.9	0.1	0.1	0.0	16.0	16.9	15.7
0.075	0.15 - 0.075	3.4	3.5	3.3	0.1	0.3	0.1	12.6	13.4	12.4
Pan	< 0.075 (pan)	12.6	13.4	12.4	0.1	0.1	0.2	0.0	0.0	0.0
	Total	**100.0**	**100.0**	**100.0**	**0.2**	**0.4**	**0.2**			
					Mean standard deviation					

Table E.3: G2 sieve results: Full graded after durability milling

Particle size distribution - Fractions		DMI Full graded - Dry Ball Mill			DMI Full graded - Wet Ball Mill			DMI Full graded - Wet Mill		
Sieve	Particle fraction	G2-DMIF-DB1	G2-DMIF-DB2	G2-DMIF-DB3	G2-DMIF-WB1	G2-DMIF-WB2	G2-DMIF-WB3	G2-DMIF-W1	G2-DMIF-W2	G2-DMIF-W3
[mm]	[mm]	[%]	[%]	[%]	[%]	[%]	[%]	[%]	[%]	[%]
37.5	> 37.5	0.0	0.0	0.0	0.0	0.0	0.0	0.0	0.0	0.0
28	37.5 - 28	10.8	9.7	10.7	10.4	10.2	11.0	11.5	11.0	10.1
20	28 - 20	10.9	11.6	11.6	11.9	11.7	9.7	9.6	11.3	11.8
14	20 - 14	9.0	10.6	9.4	8.9	9.7	9.5	11.4	10.2	10.8
10	14 - 10	8.4	7.9	8.5	7.1	7.0	8.1	6.6	7.0	6.5
7.1	10 - 7.1	5.9	6.1	6.1	5.7	5.4	5.5	6.6	5.5	5.5
5	7.1 - 5	6.2	6.1	5.7	6.3	5.8	6.2	8.5	8.6	9.4
2	5 - 2	12.5	12.3	12.5	12.8	13.2	12.8	12.3	12.6	12.6
1	2 - 1	6.0	6.0	6.0	6.3	6.5	6.2	5.5	5.8	5.4
0.6	1 - 0.6	3.5	3.5	3.5	3.5	3.5	3.5	3.1	3.1	3.0
0.425	0.6 - 0.425	2.3	2.2	2.2	2.2	2.1	2.1	1.9	1.8	1.9
0.3	0.425 - 0.3	2.6	2.6	2.6	2.4	2.5	2.6	2.4	2.3	2.4
0.15	0.3 - 0.15	5.3	5.5	5.3	5.7	5.4	5.4	4.9	5.0	5.1
0.075	0.15 - 0.075	3.6	3.3	3.5	3.5	3.7	3.8	3.1	3.3	3.1
Pan	< 0.075 (pan)	12.7	12.7	12.6	13.4	13.4	13.5	12.5	12.5	12.4
	Total	**100.0**	**100.0**	**100.0**	**100.0**	**100.0**	**100.0**	**100.0**	**100.0**	**100.0**

Particle size distribution - Average		DMI Full graded - Fractions			DMI G20C graded - Standard deviation			DMI Full graded - Passing		
Sieve	Particle fraction	G2-DMIF-DB	G2-DMIF-WB	G2-DMIF-W	G2-DMIF-DB	G2-DMIF-WB	G2-DMIF-W	G2-DMIF-DB	G2-DMIF-WB	G2-DMIF-W
[mm]	[mm]	[%]	[%]	[%]	[%]	[%]	[%]	[%]	[%]	[%]
37.5	> 37.5	0.0	0.0	0.0	0.0	0.0	0.0	100.0	100.0	100.0
28	37.5 - 28	10.4	10.5	10.9	0.6	0.4	0.7	89.6	89.5	89.1
20	28 - 20	11.4	11.1	10.9	0.4	1.2	1.1	78.2	78.4	78.3
14	20 - 14	9.7	9.4	10.8	0.8	0.4	0.6	68.6	69.0	67.4
10	14 - 10	8.3	7.4	6.7	0.3	0.6	0.3	60.3	61.6	60.7
7.1	10 - 7.1	6.0	5.5	5.9	0.1	0.1	0.6	54.3	56.1	54.9
5	7.1 - 5	6.0	6.1	8.8	0.3	0.2	0.5	48.3	50.0	46.0
2	5 - 2	12.4	12.9	12.5	0.2	0.2	0.2	35.8	37.1	33.5
1	2 - 1	6.0	6.3	5.6	0.0	0.1	0.2	29.8	30.7	27.9
0.6	1 - 0.6	3.5	3.5	3.1	0.0	0.0	0.0	26.3	27.2	24.9
0.425	0.6 - 0.425	2.2	2.1	1.9	0.1	0.1	0.0	24.1	25.1	23.0
0.3	0.425 - 0.3	2.6	2.5	2.4	0.0	0.1	0.1	21.5	22.6	20.6
0.15	0.3 - 0.15	5.4	5.5	5.0	0.1	0.2	0.1	16.1	17.1	15.6
0.075	0.15 - 0.075	3.5	3.7	3.2	0.2	0.1	0.1	12.7	13.4	12.5
Pan	< 0.075 (pan)	12.7	13.4	12.5	0.1	0.1	0.0	0.0	0.0	0.0
	Total	**100.0**	**100.0**	**100.0**	**0.2**	**0.2**	**0.2**	**0.0**	**0.0**	**0.0**
					Mean standard deviation					

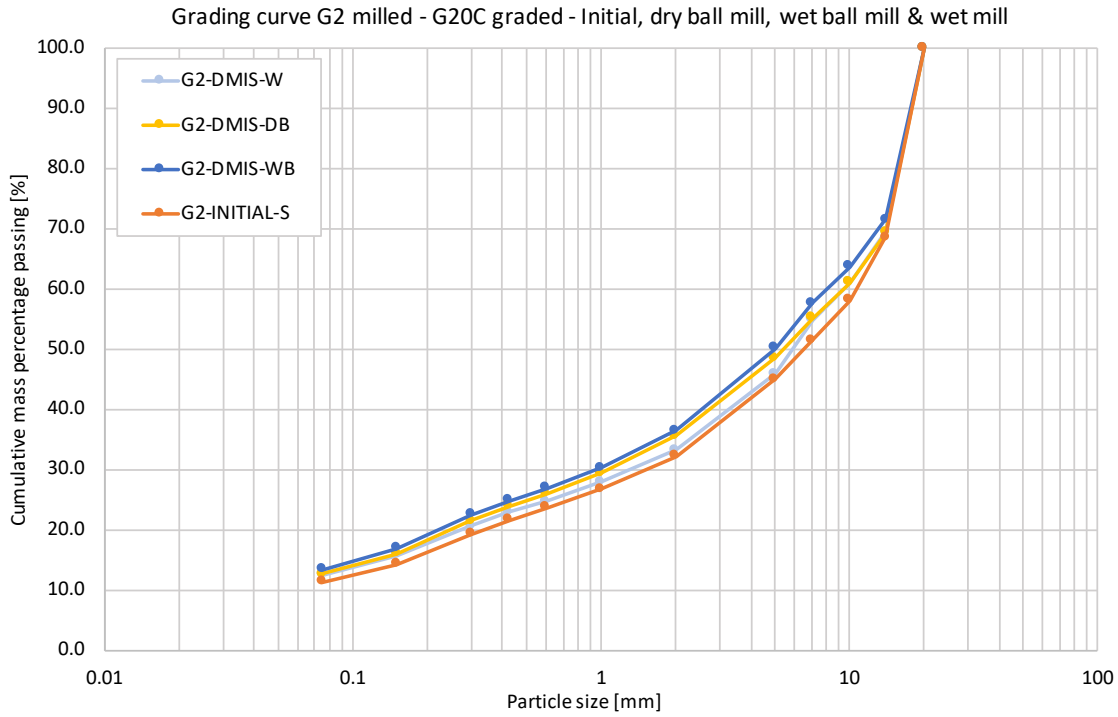

Figure E.1: G2: Gradings curves after durability milling (average of 3)

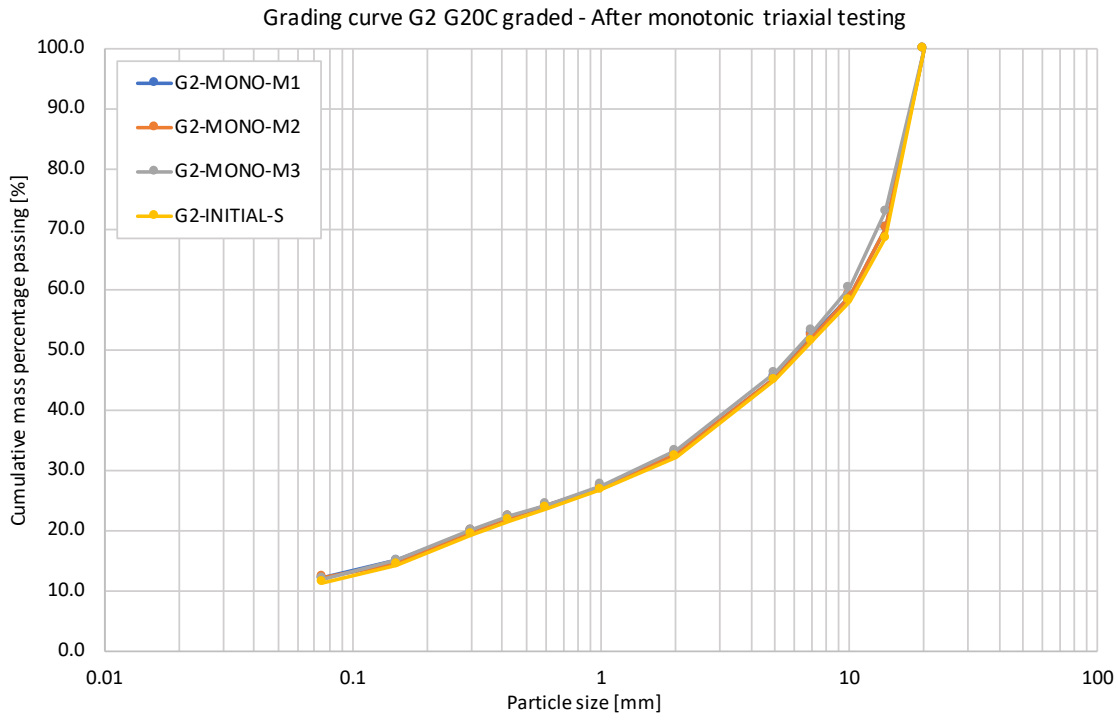

Figure E.2: G2: Grading curves after monotonic triaxial testing

E.2. RCA SIEVE RESULTS

Table E.4: RCA sieve results: G20C initial grading, after monotonic triaxial testing & after permanent deformation triaxial testing

Particle size distribution - Fractions		RCA G20C graded - Initial			RCA G20C graded - After monotonic triaxial test			RCA G20C graded - After permanent deformation test		
Sieve	Particle fraction	RCA-INITIAL-S1	RCA-INITIAL-S2	RCA-INITIAL-S3	RCA-MONO-M1	RCA-MONO-M2	RCA-MONO-M3	RCA-PERM-PD1	RCA-PERM-PD2	RCA-PERM-PD3
[mm]	[mm]	[%]	[%]	[%]	[%]	[%]	[%]	[%]	[%]	[%]
37.5	> 37.5	0.0	0.0	0.0	0.0	0.0	0.0	0.0	0.0	0.0
28	37.5 - 28	0.0	0.0	0.0	0.0	0.0	0.0	0.0	0.0	0.0
20	28 - 20	0.0	0.0	0.0	0.0	0.0	0.0	0.0	0.0	0.0
14	20 - 14	30.8	31.2	31.4	17.8	16.8	14.5	15.5	17.0	17.3
10	14 - 10	11.5	10.9	13.0	17.7	17.7	18.3	16.5	17.2	17.1
7.1	10 - 7.1	8.7	9.1	8.2	8.5	8.4	8.5	13.4	9.1	9.5
5	7.1 - 5	4.2	3.9	3.8	4.7	4.4	4.6	3.7	4.5	5.1
2	5 - 2	12.6	12.8	12.4	13.2	11.7	12.0	12.5	11.9	12.8
1	2 - 1	6.5	6.4	6.2	6.6	7.1	7.7	6.9	7.3	6.1
0.6	1 - 0.6	4.4	4.3	4.2	4.5	4.8	5.3	4.8	5.3	4.4
0.425	0.6 - 0.425	3.1	3.0	3.2	4.6	4.6	4.1	4.1	3.8	4.9
0.3	0.425 - 0.3	2.4	2.3	2.7	4.0	4.1	4.3	3.5	4.2	3.5
0.15	0.3 - 0.15	5.0	4.9	5.0	6.7	7.1	7.4	6.7	7.1	6.6
0.075	0.15 - 0.075	1.9	1.8	1.6	2.2	2.7	2.5	2.4	2.8	2.6
Pan	< 0.075 (pan)	9.0	9.3	8.3	9.6	10.4	10.9	10.1	9.9	10.1
	Total	**100.0**	**100.0**	**100.0**	**100.0**	**100.0**	**100.0**	**100.0**	**100.0**	**100.0**

Particle size distribution - Average		Fractions			Standard deviation			Passing		
Sieve	Particle fraction	RCA-INITIAL-S	RCA-MONO	RCA-PERM	RCA-INITIAL-S	RCA-MONO	RCA-PERM	RCA-INITIAL-S	RCA-MONO	RCA-PERM
[mm]	[mm]	[%]	[%]	[%]	[%]	[%]	[%]	[%]	[%]	[%]
37.5	> 37.5	0.0	0.0	0.0	0.0	0.0	0.0	100.0	100.0	100.0
28	37.5 - 28	0.0	0.0	0.0	0.0	0.0	0.0	100.0	100.0	100.0
20	28 - 20	0.0	0.0	0.0	0.0	0.0	0.0	100.0	100.0	100.0
14	20 - 14	31.1	16.4	16.6	0.3	1.7	1.2	68.9	83.6	83.4
10	14 - 10	11.8	17.9	16.9	1.1	0.3	0.9	57.0	65.7	66.5
7.1	10 - 7.1	8.7	8.5	10.7	0.4	0.1	2.8	48.4	57.2	55.8
5	7.1 - 5	3.9	4.5	4.4	0.2	0.1	0.5	44.4	52.7	51.4
2	5 - 2	12.6	12.3	12.4	0.2	0.8	0.4	31.8	40.4	39.0
1	2 - 1	6.4	7.1	6.8	0.1	0.6	0.4	25.4	33.3	32.2
0.6	1 - 0.6	4.3	4.8	4.8	0.1	0.4	0.3	21.1	28.4	27.4
0.425	0.6 - 0.425	3.1	4.4	4.2	0.1	0.3	0.3	18.0	24.0	23.1
0.3	0.425 - 0.3	2.5	4.1	3.7	0.2	0.1	0.4	15.6	19.8	19.4
0.15	0.3 - 0.15	4.9	7.0	6.8	0.0	0.3	0.4	10.6	12.8	12.6
0.075	0.15 - 0.075	1.8	2.5	2.6	0.1	0.3	0.2	8.9	10.3	10.0
Pan	< 0.075 (pan)	8.9	10.3	10.0	0.5	0.7	0.4	0.0	0.0	0.0
	Total	**100.0**	**100.0**	**100.0**	**0.3**	**0.5**	**0.5**			
					Mean standard deviation					

Table E.5: RCA sieve results: G20C graded after durability milling

Particle size distribution - Fractions		DMI G20C graded - Dry ball mill			DMI G20C graded - Wet ball mill			DMI G20C graded - Wet mill		
Sieve	Particle fraction	RCA-DMIS-DB1	RCA-DMIS-DB2	RCA-DMIS-DB3	RCA-DMIS-WB1	RCA-DMIS-WB2	RCA-DMIS-WB3	RCA-DMIS-W1	RCA-DMIS-W2	RCA-DMIS-W3
[mm]	[mm]	[%]	[%]	[%]	[%]	[%]	[%]	[%]	[%]	[%]
37.5	> 37.5	-	0.0	0.0	0.0	0.0	0.0	-	0.0	0.0
28	37.5 - 28	-	0.0	0.0	0.0	0.0	0.0	-	0.0	0.0
20	28 - 20	-	0.0	0.0	0.0	0.0	0.0	-	0.0	0.0
14	20 - 14	-	12.5	13.9	8.2	12.2	11.9	-	29.6	27.6
10	14 - 10	-	15.7	16.5	17.6	16.2	16.2	-	14.6	16.2
7.1	10 - 7.1	-	8.4	7.9	9.3	7.8	8.3	-	5.7	5.8
5	7.1 - 5	-	4.2	4.3	3.9	3.9	3.2	-	3.7	3.4
2	5 - 2	-	11.1	11.1	11.1	10.3	10.6	-	10.9	10.8
1	2 - 1	-	7.2	7.5	7.3	7.3	7.3	-	4.9	4.2
0.6	1 - 0.6	-	6.0	5.9	6.0	6.6	6.3	-	4.1	3.9
0.425	0.6 - 0.425	-	5.5	4.1	5.6	5.8	5.2	-	4.1	4.4
0.3	0.425 - 0.3	-	5.7	4.5	5.4	4.6	4.9	-	3.2	3.4
0.15	0.3 - 0.15	-	8.7	9.3	9.2	8.8	9.6	-	5.9	6.7
0.075	0.15 - 0.075	-	3.3	3.5	3.9	2.9	3.9	-	2.5	2.7
Pan	< 0.075 (pan)	-	11.8	11.7	12.4	13.5	12.7	-	10.7	10.9
	Total	**-**	**100.0**	**100.0**	**100.0**	**100.0**	**100.0**	**-**	**100.0**	**100.0**

Particle size distribution - Average		DMI G20C graded - Fractions			DMI G20C graded - Standard deviation			DMI G20C graded - Passing		
Sieve	Particle fraction	RCA-DMIS-DB	RCA-DMIS-WB	RCA-DMIS-W	RCA-DMIS-DB	RCA-DMIS-WB	RCA-DMIS-W	RCA-DMIS-DB	RCA-DMIS-WB	RCA-DMIS-W
[mm]	[mm]	[%]	[%]	[%]	[%]	[%]	[%]	[%]	[%]	[%]
37.5	> 37.5	0.0	0.0	0.0	0.0	0.0	0.0	100.0	100.0	100.0
28	37.5 - 28	0.0	0.0	0.0	0.0	0.0	0.0	100.0	100.0	100.0
20	28 - 20	0.0	0.0	0.0	0.0	0.0	0.0	100.0	100.0	100.0
14	20 - 14	13.2	10.8	28.6	1.0	2.2	1.4	86.8	89.2	71.4
10	14 - 10	16.1	16.7	15.4	0.6	0.8	1.1	70.7	72.6	56.0
7.1	10 - 7.1	8.2	8.4	5.8	0.4	0.8	0.0	62.5	64.1	50.3
5	7.1 - 5	4.3	3.7	3.6	0.1	0.4	0.2	58.3	60.4	46.7
2	5 - 2	11.1	10.7	10.8	0.0	0.4	0.1	47.2	49.8	35.9
1	2 - 1	7.3	7.3	4.6	0.2	0.0	0.4	39.9	42.5	31.3
0.6	1 - 0.6	5.9	6.3	4.0	0.1	0.3	0.2	33.9	36.2	27.3
0.425	0.6 - 0.425	4.8	5.5	4.3	1.0	0.3	0.2	29.2	30.6	23.1
0.3	0.425 - 0.3	5.1	5.0	3.3	0.8	0.4	0.1	24.1	25.7	19.8
0.15	0.3 - 0.15	9.0	9.2	6.3	0.4	0.4	0.6	15.1	16.5	13.4
0.075	0.15 - 0.075	3.4	3.6	2.6	0.1	0.6	0.2	11.7	12.9	10.8
Pan	< 0.075 (pan)	11.7	12.9	10.8	0.1	0.6	0.2	0.0	0.0	0.0
	Total	**100.0**	**100.0**	**100.0**	**0.4**	**0.6**	**0.4**			
					Mean standard deviation					

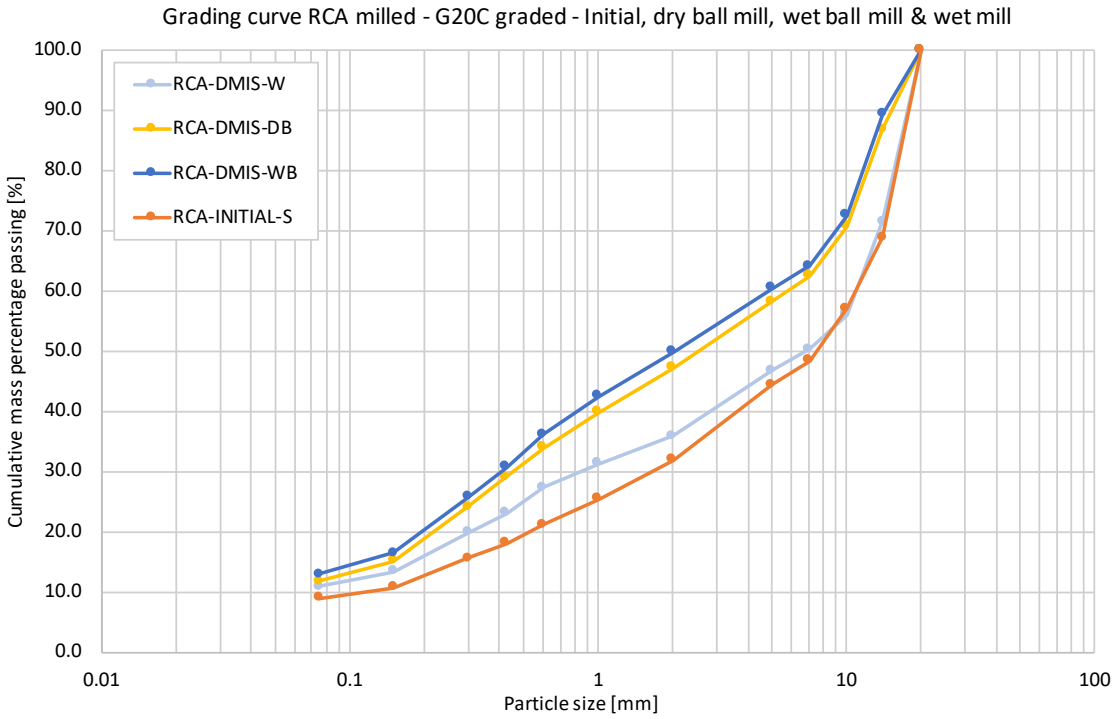

Figure E.3: RCA: Grading curves after durability milling (average of 3)

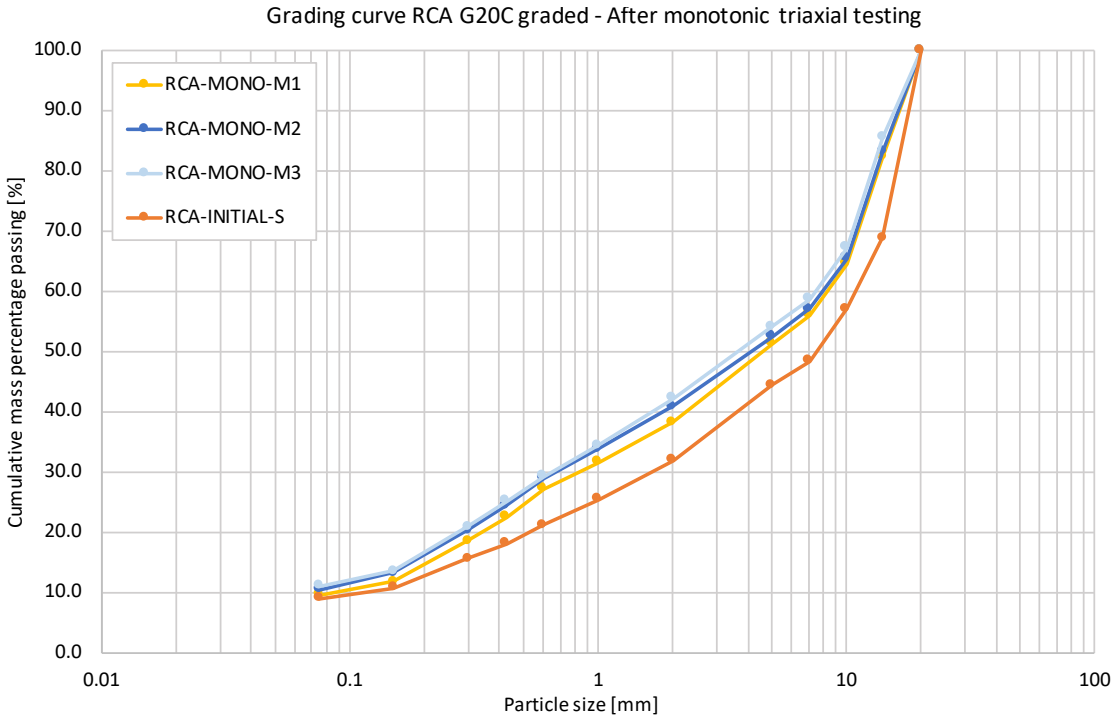

Figure E.4: RCA: Grading curves after monotonic triaxial testing

E.3. RCM SIEVE RESULTS

Table E.6: RCM sieve results: G20C initial grading & full initial grading

Particle size distribution - Fractions		RCM G20C graded - Initial			RCM full graded - Initial		
Sieve	Particle fraction	RCM-INITIAL-S1	RCM-INITIAL-S2	RCM-INITIAL-S3	RCM-INITIAL-F1	RCM-INITIAL-F2	RCM-INITIAL-F3
[mm]	[mm]	[%]	[%]	[%]	[%]	[%]	[%]
37.5	> 37.5	0.0	0.0	0.0	0.0	0.0	0.0
28	37.5 - 28	0.0	0.0	0.0	7.2	10.7	9.0
20	28 - 20	0.0	0.0	0.0	15.1	11.0	12.7
14	20 - 14	31.5	32.3	32.1	10.5	10.9	10.8
10	14 - 10	8.9	7.6	6.7	8.0	7.1	6.6
7.1	10 - 7.1	7.4	7.7	7.2	8.0	7.4	8.0
5	7.1 - 5	6.9	7.2	8.8	6.3	7.9	8.0
2	5 - 2	13.0	13.0	13.3	12.8	13.0	13.1
1	2 - 1	6.8	7.4	7.5	7.0	7.8	7.3
0.6	1 - 0.6	4.4	4.5	4.1	4.3	4.1	4.2
0.425	0.6 - 0.425	2.5	2.2	2.2	2.5	2.0	2.2
0.3	0.425 - 0.3	2.4	2.3	2.5	2.5	2.3	2.5
0.15	0.3 - 0.15	4.2	4.1	4.3	4.0	4.3	4.0
0.075	0.15 - 0.075	2.5	2.9	2.7	2.7	2.6	2.5
Pan	< 0.075 (pan)	9.4	8.9	8.7	9.0	9.0	9.0
	Total	**100.0**	**100.0**	**100.0**	**100.0**	**100.0**	**100.0**

Particle size distribution - Average		Fractions		Standard deviation		Passing	
Sieve	Particle fraction	RCM-INITIAL-S	RCM-INITIAL-F	RCM-INITIAL-S	RCM-INITIAL-F	RCM-INITIAL-S	RCM-INITIAL-F
[mm]	[mm]	[%]	[%]	[%]	[%]	[%]	[%]
37.5	> 37.5	0.0	0.0	0.0	0.0	100.0	100.0
28	37.5 - 28	0.0	9.0	0.0	1.8	100.0	91.0
20	28 - 20	0.0	12.9	0.0	2.1	100.0	78.1
14	20 - 14	31.9	10.7	0.4	0.2	68.1	67.4
10	14 - 10	7.7	7.2	1.1	0.7	60.3	60.1
7.1	10 - 7.1	7.5	7.8	0.3	0.4	52.9	52.3
5	7.1 - 5	7.6	7.4	1.0	0.9	45.2	44.9
2	5 - 2	13.1	13.0	0.2	0.2	32.1	31.9
1	2 - 1	7.2	7.4	0.3	0.4	24.9	24.5
0.6	1 - 0.6	4.3	4.2	0.2	0.1	20.6	20.3
0.425	0.6 - 0.425	2.3	2.2	0.1	0.3	18.3	18.1
0.3	0.425 - 0.3	2.4	2.4	0.1	0.1	15.9	15.6
0.15	0.3 - 0.15	4.2	4.1	0.1	0.2	11.7	11.6
0.075	0.15 - 0.075	2.7	2.6	0.2	0.1	9.0	9.0
Pan	< 0.075 (pan)	9.0	9.0	0.4	0.0	0.0	0.0
	Total	**100.0**	**100.0**	**0.4**	**0.3**	**0**	**0**
				Mean standard deviation			

Table E.7: RCM sieve results: G20C graded after durability milling

Particle size distribution - Fractions		DMI G20C graded - Dry ball mill			DMI G20C graded - Wet ball mill			DMI G20C graded - Wet mill		
Sieve	Particle fraction	RCM-DMIS-DB1	RCM-DMIS-DB2	RCM-DMIS-DB3	RCM-DMIS-WB1	RCM-DMIS-WB2	RCM-DMIS-WB3	RCM-DMIS-W1	RCM-DMIS-W2	RCM-DMIS-W3
[mm]	[mm]	[%]	[%]	[%]	[%]	[%]	[%]	[%]	[%]	[%]
37.5	> 37.5	-	0.0	0.0	0.0	0.0	0.0	0.0	0.0	0.0
28	37.5 - 28	-	0.0	0.0	0.0	0.0	0.0	0.0	0.0	0.0
20	28 - 20	-	0.0	0.0	0.0	0.0	0.0	0.0	0.0	0.0
14	20 - 14	-	19.8	20.3	24.0	23.3	22.8	31.1	31.4	30.0
10	14 - 10	-	9.4	8.6	7.4	8.0	7.3	6.6	7.8	7.7
7.1	10 - 7.1	-	6.6	5.6	5.0	5.0	5.4	6.9	7.3	7.1
5	7.1 - 5	-	7.0	7.1	6.3	6.0	6.3	8.7	6.6	8.4
2	5 - 2	-	13.8	14.7	13.4	13.2	14.1	12.3	11.8	12.3
1	2 - 1	-	8.1	9.0	8.7	8.6	8.9	6.4	7.1	7.3
0.6	1 - 0.6	-	5.7	5.7	5.5	5.6	5.6	4.1	3.8	3.8
0.425	0.6 - 0.425	-	3.5	3.1	3.0	3.2	3.0	2.4	1.9	2.2
0.3	0.425 - 0.3	-	3.6	3.5	3.4	3.6	3.3	2.5	2.5	3.0
0.15	0.3 - 0.15	-	6.0	6.1	6.2	6.2	5.9	4.5	4.7	4.4
0.075	0.15 - 0.075	-	4.1	4.4	4.1	4.6	4.2	3.5	3.0	2.7
Pan	< 0.075 (pan)	-	12.3	11.9	13.1	12.6	13.0	11.0	12.0	11.2
	Total	**100.0**	**100.0**	**100.0**	**100.0**	**100.0**	**100.0**	**100.0**	**100.0**	**100.0**

Particle size distribution - Average		DMI G20C graded - Fractions			DMI G20C graded - Standard deviation			DMI G20C graded - Passing		
Sieve	Particle fraction	RCM-DMIS-DB	RCM-DMIS-WB	RCM-DMIS-W	RCM-DMIS-DB	RCM-DMIS-WB	RCM-DMIS-W	RCM-DMIS-DB	RCM-DMIS-WB	RCM-DMIS-W
[mm]	[mm]	[%]	[%]	[%]	[%]	[%]	[%]	[%]	[%]	[%]
37.5	> 37.5	0.0	0.0	0.0	0.0	0.0	0.0	100.0	100.0	100.0
28	37.5 - 28	0.0	0.0	0.0	0.0	0.0	0.0	100.0	100.0	100.0
20	28 - 20	0.0	0.0	0.0	0.0	0.0	0.0	100.0	100.0	100.0
14	20 - 14	20.0	23.4	30.9	0.3	0.6	0.7	80.0	76.6	69.1
10	14 - 10	9.0	7.6	7.4	0.6	0.4	0.6	71.0	69.0	61.8
7.1	10 - 7.1	6.1	5.1	7.1	0.7	0.2	0.2	64.8	63.9	54.7
5	7.1 - 5	7.0	6.2	7.9	0.1	0.2	1.1	57.8	57.7	46.8
2	5 - 2	14.3	13.6	12.1	0.6	0.5	0.3	43.5	44.1	34.6
1	2 - 1	8.5	8.7	6.9	0.6	0.2	0.5	35.0	35.4	27.7
0.6	1 - 0.6	5.7	5.6	3.9	0.0	0.1	0.2	29.3	29.8	23.8
0.425	0.6 - 0.425	3.3	3.1	2.2	0.2	0.1	0.2	26.0	26.8	21.6
0.3	0.425 - 0.3	3.6	3.4	2.7	0.1	0.1	0.3	22.4	23.3	19.0
0.15	0.3 - 0.15	6.1	6.1	4.5	0.1	0.1	0.2	16.4	17.2	14.4
0.075	0.15 - 0.075	4.3	4.3	3.0	0.2	0.3	0.4	12.1	12.9	11.4
Pan	< 0.075 (pan)	12.1	12.9	11.4	0.3	0.3	0.5	0.0	0.0	0.0
	Total	**100.0**	**100.0**	**100.0**	**0.3**	**0.3**	**0.4**			
					Mean standard deviation					

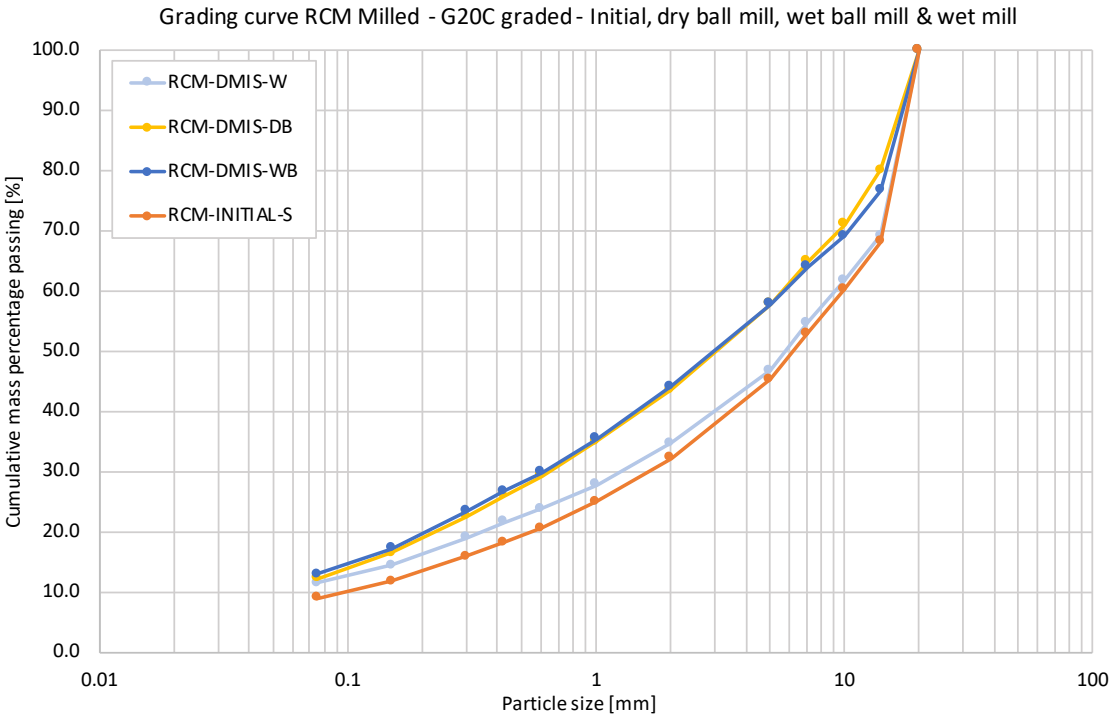

Figure E.5: RCM: Grading curves after durability milling (average of 3)

E.4. MG65 SIEVE RESULTS

Table E.8: MG65 sieve results: G20C initial grading, after monotonic triaxial testing & after permanent deformation triaxial testing

Particle size distribution - Fractions		MG65 G20C graded - Initial			MG65 G20C graded - After monotonic triaxial test			MG65 G20C graded - After permanent deformation test		
Sieve	Particle fraction	MG65-INITIAL-S1	MG65-INITIAL-S2	MG65-INITIAL-S3	MG65-MONO-1	MG65-MONO-2	MG65-MONO-3	MG65-PERM-PD1	MG65-PERM-PD2	MG65-PERM-PD3
[mm]	[mm]	[%]	[%]	[%]	[%]	[%]	[%]	[%]	[%]	[%]
37.5	> 37.5	0.0	0.0	0.0	0.0	0.0	0.0	-	-	0.0
28	37.5 - 28	0.0	0.0	0.0	0.0	0.0	0.0	-	-	0.0
20	28 - 20	0.0	0.0	0.0	0.0	0.0	0.0	-	-	0.0
14	20 - 14	32.4	32.2	33.2	18.3	17.8	17.0	-	-	16.1
10	14 - 10	9.0	7.2	7.0	13.7	14.0	12.2	-	-	13.7
7.1	10 - 7.1	7.7	7.4	7.8	10.2	9.1	9.9	-	-	9.7
5	7.1 - 5	6.6	9.3	8.0	8.7	8.0	9.4	-	-	8.2
2	5 - 2	12.8	13.5	13.1	13.7	14.0	14.3	-	-	13.7
1	2 - 1	7.1	6.5	6.5	7.4	7.7	7.5	-	-	8.1
0.6	1 - 0.6	4.2	4.3	4.5	5.1	5.5	5.5	-	-	4.9
0.425	0.6 - 0.425	2.4	2.1	2.6	4.2	3.5	3.2	-	-	2.8
0.3	0.425 - 0.3	2.9	2.5	2.5	4.5	3.2	3.8	-	-	3.4
0.15	0.3 - 0.15	4.1	4.1	4.1	3.8	4.7	5.0	-	-	5.9
0.075	0.15 - 0.075	2.0	2.2	2.0	1.2	2.4	1.7	-	-	3.1
Pan	< 0.075 (pan)	8.9	8.8	8.6	9.2	9.8	10.2	-	-	10.5
	Total	**100.0**	**100.0**	**100.0**	**100.0**	**100.0**	**100.0**	**-**	**-**	**100.0**

Particle size distribution - Average		Fractions			Standard deviation			Passing		
Sieve	Particle fraction	MG65-INITIAL-S	MG65-MONO	MG65-PERM	MG65-INITIAL-S	MG65-MONO	MG65-PERM	MG65-INITIAL-S	MG65-MONO	MG65-PERM
[mm]	[mm]	[%]	[%]	[%]	[%]	[%]	[%]	[%]	[%]	[%]
37.5	> 37.5	0.0	0.0	0.0	0.0	0.0	-	100.0	100.0	100.0
28	37.5 - 28	0.0	0.0	0.0	0.0	0.0	-	100.0	100.0	100.0
20	28 - 20	0.0	0.0	0.0	0.0	0.0	-	100.0	100.0	100.0
14	20 - 14	32.6	17.7	16.1	0.6	0.6	-	67.4	82.3	83.9
10	14 - 10	7.7	13.3	13.7	1.1	1.0	-	59.7	69.0	70.2
7.1	10 - 7.1	7.6	9.8	9.7	0.2	0.6	-	52.1	59.2	60.5
5	7.1 - 5	8.0	8.7	8.2	1.3	0.7	-	44.1	50.5	52.3
2	5 - 2	13.1	14.0	13.7	0.4	0.3	-	31.0	36.5	38.6
1	2 - 1	6.7	7.5	8.1	0.4	0.2	-	24.3	29.0	30.5
0.6	1 - 0.6	4.4	5.4	4.9	0.1	0.3	-	19.9	23.6	25.6
0.425	0.6 - 0.425	2.3	3.6	2.8	0.2	0.5	-	17.6	19.9	22.8
0.3	0.425 - 0.3	2.7	3.8	3.4	0.2	0.6	-	14.9	16.1	19.4
0.15	0.3 - 0.15	4.1	4.5	5.9	0.0	0.6	-	10.8	11.6	13.6
0.075	0.15 - 0.075	2.1	1.8	3.1	0.1	0.6	-	8.8	9.8	10.5
Pan	< 0.075 (pan)	8.8	9.8	10.5	0.1	0.5	-	0.0	0.0	0.0
	Total	**100.0**	**100.0**	**100.0**	**0.4**	**0.5**	**-**	**0**	**0**	**0**
					Mean standard deviation					

Table E.9: MG65 sieve results: G20C graded after durability milling

Particle size distribution - Fractions		DMI G20C graded - Dry ball mill			DMI G20C graded - Wet ball mill			DMI G20C graded - Wet mill		
Sieve	Particle fraction	MG65-DMIS-DB1	MG65-DMIS-DB2	MG65-DMIS-DB3	MG65-DMIS-WB1	MG65-DMIS-WB2	MG65-DMIS-W3	MG65-DMIS-W1	MG65-DMIS-W2	MG65-DMIS-W3
[mm]	[mm]	[%]	[%]	[%]	[%]	[%]	[%]	[%]	[%]	[%]
37.5	> 37.5	0.0	0.0	0.0	0.0	0.0	0.0	0.0	0.0	0.0
28	37.5 - 28	0.0	0.0	0.0	0.0	0.0	0.0	0.0	0.0	0.0
20	28 - 20	0.0	0.0	0.0	0.0	0.0	0.0	0.0	0.0	0.0
14	20 - 14	16.7	15.6	18.4	18.8	19.7	19.1	29.4	30.7	30.8
10	14 - 10	12.1	13.3	10.4	10.9	10.9	10.9	9.4	8.4	8.3
7.1	10 - 7.1	7.3	7.6	7.5	6.8	6.4	7.4	7.6	7.9	7.7
5	7.1 - 5	7.2	6.5	7.6	6.1	6.0	6.1	7.8	6.9	7.4
2	5 - 2	13.5	13.7	13.4	13.3	12.8	13.5	11.9	12.1	12.1
1	2 - 1	8.0	7.7	8.0	8.4	7.6	4.7	6.1	5.5	6.1
0.6	1 - 0.6	5.4	5.6	6.7	5.6	6.2	5.7	3.9	3.9	4.0
0.425	0.6 - 0.425	3.4	3.5	4.1	4.2	3.5	3.7	2.3	2.7	2.8
0.3	0.425 - 0.3	4.2	4.9	3.1	4.0	4.8	4.9	3.2	3.2	3.0
0.15	0.3 - 0.15	7.3	6.4	6.6	6.4	6.1	7.0	4.8	5.3	4.6
0.075	0.15 - 0.075	3.2	3.1	2.6	2.9	3.3	3.7	2.6	2.6	2.4
Pan	< 0.075 (pan)	11.7	12.1	11.6	12.6	12.6	13.4	11.0	10.9	10.9
	Total	**100.0**	**100.0**	**100.0**	**100.0**	**100.0**	**100.0**	**100.0**	**100.0**	**100.0**

Particle size distribution - Average		DMI G20C graded - Fractions			DMI G20C graded - Standard deviation			DMI G20C graded - Passing		
Sieve	Particle fraction	MG65-DMIS-DB	MG65-DMIS-WB	MG65-DMIS-W	MG65-DMIS-DB	MG65-DMIS-WB	MG65-DMIS-W	MG65-DMIS-DB	MG65-DMIS-WB	MG65-DMIS-W
[mm]	[mm]	[%]	[%]	[%]	[%]	[%]	[%]	[%]	[%]	[%]
37.5	> 37.5	0.0	0.0	0.0	0.0	0.0	0.0	100.0	100.0	100.0
28	37.5 - 28	0.0	0.0	0.0	0.0	0.0	0.0	100.0	100.0	100.0
20	28 - 20	0.0	0.0	0.0	0.0	0.0	0.0	100.0	100.0	100.0
14	20 - 14	16.9	19.2	30.3	1.4	0.7	0.8	83.1	80.8	69.7
10	14 - 10	11.9	10.9	8.7	1.5	0.0	0.6	71.2	69.9	61.0
7.1	10 - 7.1	7.5	6.6	7.7	0.2	0.2	0.2	63.7	63.3	53.3
5	7.1 - 5	7.1	6.0	7.3	0.5	0.1	0.4	56.6	57.2	45.9
2	5 - 2	13.5	13.1	12.0	0.2	0.3	0.1	43.1	44.2	33.9
1	2 - 1	7.9	8.0	5.9	0.2	0.6	0.4	35.2	36.2	28.0
0.6	1 - 0.6	5.9	5.9	3.9	0.7	0.4	0.1	29.3	30.3	24.1
0.425	0.6 - 0.425	3.7	3.9	2.6	0.3	0.5	0.2	25.6	26.4	21.5
0.3	0.425 - 0.3	4.1	4.4	3.1	0.9	0.6	0.1	21.5	22.0	18.4
0.15	0.3 - 0.15	6.8	6.3	4.9	0.5	0.2	0.4	14.8	15.7	13.5
0.075	0.15 - 0.075	3.0	3.1	2.5	0.3	0.3	0.1	11.8	12.6	10.9
Pan	< 0.075 (pan)	11.8	12.6	10.9	0.3	0.0	0.1	0.0	0.0	0.0
	Total	**100.0**	**100.0**	**100.0**	**0.6**	**0.3**	**0.3**	**0**	**0**	**0**
					Mean standard deviation					

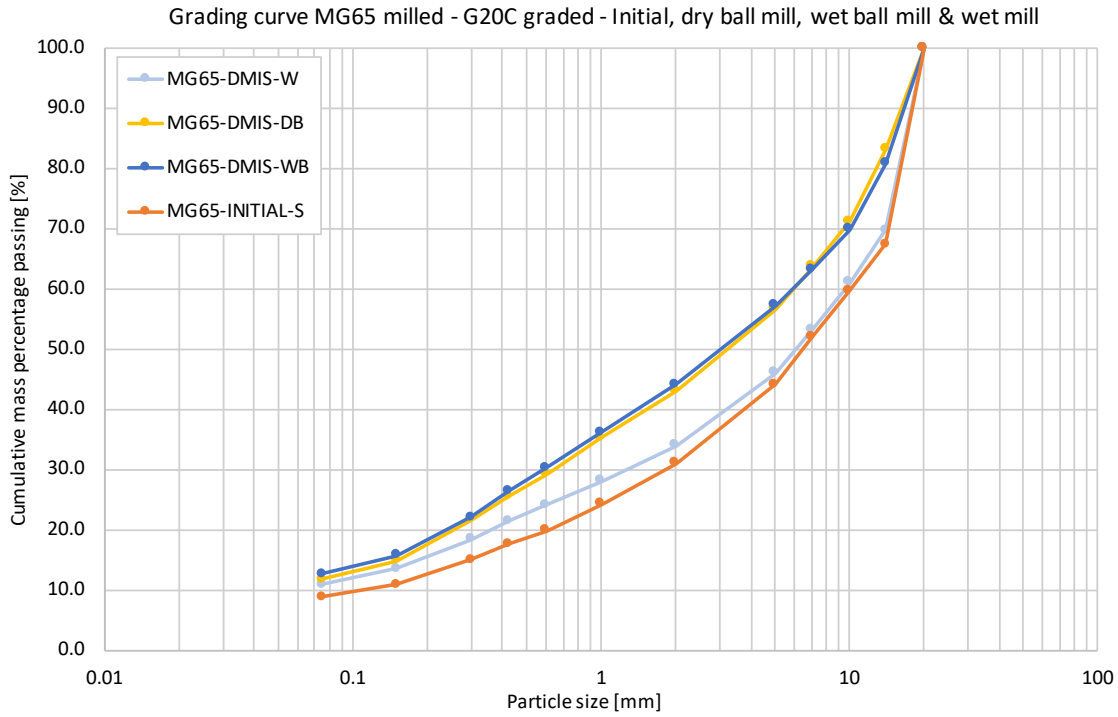

Figure E.6: MG65: Grading curves after durability milling (average of 3)

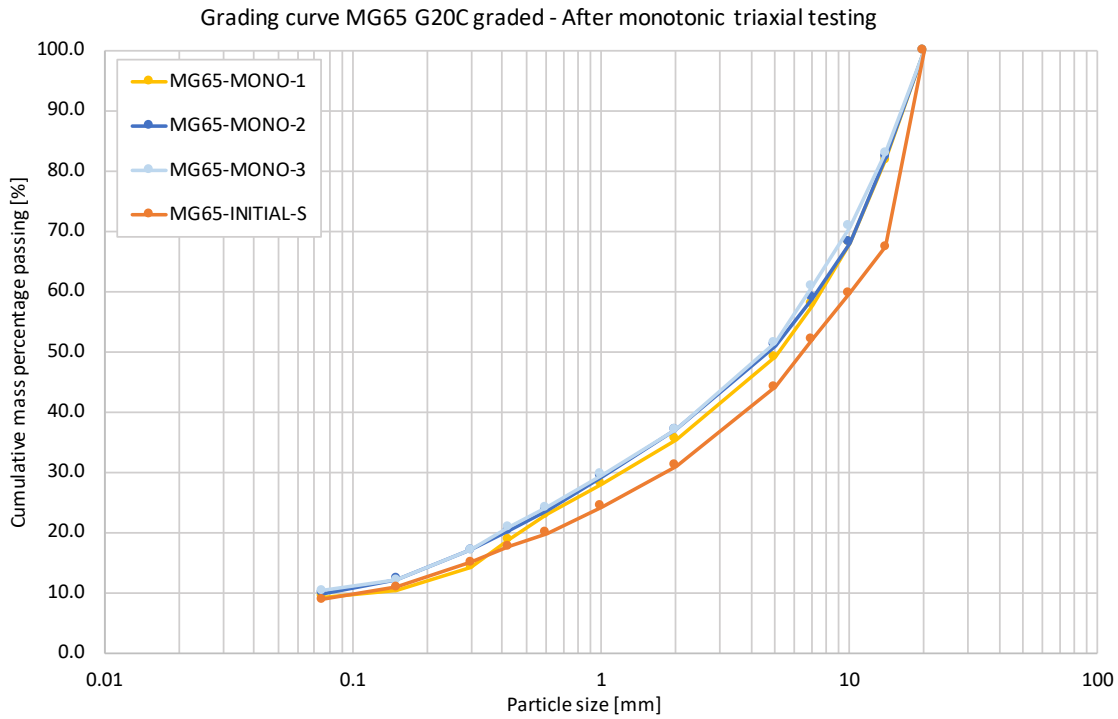

Figure E.7: MG65: Grading curves after monotonic triaxial testing

E.5. MG30 SIEVE RESULTS

Table E.10: MG30 sieve results: G20C initial grading, after monotonic triaxial testing & after permanent deformation triaxial testing

Particle size distribution - Fractions		MG30 G20C graded - Initial			MG30 G20C graded - After monotonic triaxial test		
Sieve	Particle fraction	MG30-INITIAL-S1	MG30-INITIAL-S2	MG30-INITIAL-S3	MG30-MONO-M1	MG30-MONO-M2	MG30-MONO-M3
[mm]	[mm]	[%]	[%]	[%]	[%]	[%]	[%]
37.5	> 37.5	0.0	0.0	0.0	-	0.0	0.0
28	37.5 - 28	0.0	0.0	0.0	-	0.0	0.0
20	28 - 20	0.0	0.0	0.0	-	0.0	0.0
14	20 - 14	29.5	30.9	28.6	-	19.6	17.4
10	14 - 10	6.7	8.3	8.9	-	11.9	11.8
7.1	10 - 7.1	9.6	8.4	10.2	-	10.1	9.1
5	7.1 - 5	8.7	7.4	7.1	-	9.2	9.6
2	5 - 2	12.9	12.8	13.0	-	13.4	14.2
1	2 - 1	7.4	7.2	7.3	-	7.4	7.9
0.6	1 - 0.6	4.1	4.3	4.0	-	4.7	5.0
0.425	0.6 - 0.425	2.3	2.4	2.3	-	2.8	3.1
0.3	0.425 - 0.3	2.4	2.4	2.3	-	2.8	3.0
0.15	0.3 - 0.15	4.1	4.0	4.1	-	5.0	5.1
0.075	0.15 - 0.075	2.5	2.5	2.5	-	3.0	3.1
Pan	< 0.075 (pan)	9.7	9.4	9.6	-	10.2	10.5
	Total	**100.0**	**100.0**	**100.0**	**-**	**100.0**	**100.0**

Particle size distribution - Average		Fractions		Standard deviation		Passing	
Sieve	Particle fraction	MG30-INITIAL-S	MG30-MONO	MG30-INITIAL-S	MG30-MONO	MG30-INITIAL-S	MG30-MONO
[mm]	[mm]	[%]	[%]	[%]	[%]	[%]	[%]
37.5	> 37.5	0.0	0.0	0.0	0.0	100.0	100.0
28	37.5 - 28	0.0	0.0	0.0	0.0	100.0	100.0
20	28 - 20	0.0	0.0	0.0	0.0	100.0	100.0
14	20 - 14	29.6	18.5	1.2	1.5	70.4	81.5
10	14 - 10	8.0	11.9	1.2	0.0	62.4	69.6
7.1	10 - 7.1	9.4	9.6	0.9	0.7	53.0	60.0
5	7.1 - 5	7.7	9.4	0.9	0.3	45.2	50.6
2	5 - 2	12.9	13.8	0.1	0.6	32.3	36.7
1	2 - 1	7.3	7.6	0.1	0.4	25.0	29.1
0.6	1 - 0.6	4.1	4.8	0.2	0.2	20.9	24.3
0.425	0.6 - 0.425	2.3	3.0	0.1	0.2	18.5	21.3
0.3	0.425 - 0.3	2.4	2.9	0.0	0.2	16.2	18.4
0.15	0.3 - 0.15	4.1	5.0	0.0	0.1	12.1	13.4
0.075	0.15 - 0.075	2.5	3.0	0.0	0.0	9.6	10.3
Pan	< 0.075 (pan)	9.6	10.3	0.1	0.2	0.0	0.0
	Total	**100.0**	**100.0**	**0.4**	**0.4**		
				Mean standard deviation			

Table E.11: MG30 sieve results: G20C graded after durability milling

Particle size distribution - Fractions		DMI G20C graded - Dry ball mill			DMI G20C graded - Wet ball mill			DMI G20C graded - Wet mill		
Sieve	Particle fraction	MG30-DMIS-DB1	MG30-DMIS-DB2	MG30-DMIS-DB3	MG30-DMIS-WB1	MG30-DMIS-WB2	MG30-DMIS-W3	MG30-DMIS-W1	MG30-DMIS-W2	MG30-DMIS-W3
[mm]	[mm]	[%]	[%]	[%]	[%]	[%]	[%]	[%]	[%]	[%]
37.5	> 37.5	0.0	0.0	0.0	0.0	0.0	0.0	0.0	0.0	0.0
28	37.5 - 28	0.0	0.0	0.0	0.0	0.0	0.0	0.0	0.0	0.0
20	28 - 20	0.0	0.0	0.0	0.0	0.0	0.0	0.0	0.0	0.0
14	20 - 14	16.6	18.6	18.4	20.4	17.8	19.9	30.4	31.4	29.9
10	14 - 10	8.8	8.7	8.0	7.7	8.4	7.9	6.8	5.8	7.1
7.1	10 - 7.1	7.3	7.4	8.4	5.9	6.9	6.9	8.4	7.5	8.9
5	7.1 - 5	9.3	8.5	8.4	8.3	8.6	7.7	8.7	9.9	8.2
2	5 - 2	15.4	15.2	15.6	15.0	14.8	14.1	11.9	12.5	12.9
1	2 - 1	8.2	7.8	7.8	8.0	8.5	8.6	6.6	6.0	6.4
0.6	1 - 0.6	6.3	5.1	5.9	7.2	6.1	5.7	4.2	4.3	4.4
0.425	0.6 - 0.425	3.3	3.7	3.8	5.1	3.6	3.7	2.3	2.5	2.1
0.3	0.425 - 0.3	3.8	3.3	3.7	2.3	4.2	3.8	2.8	3.3	2.5
0.15	0.3 - 0.15	5.7	6.0	5.5	5.5	5.6	5.7	4.4	3.6	4.2
0.075	0.15 - 0.075	3.2	3.4	2.4	2.2	2.8	3.4	2.6	2.3	2.3
Pan	< 0.075 (pan)	12.2	12.3	12.0	12.4	12.7	12.6	10.9	10.9	11.1
	Total	**100.0**	**100.0**	**100.0**	**100.0**	**100.0**	**100.0**	**100.0**	**100.0**	**100.0**

Particle size distribution - Average		DMI G20C graded - Fractions			DMI G20C graded - Standard deviation			DMI G20C graded - Passing		
Sieve	Particle fraction	MG30-DMIS-DB	MG30-DMIS-WB	MG30-DMIS-W	MG30-DMIS-DB	MG30-DMIS-WB	MG30-DMIS-W	MG30-DMIS-DB	MG30-DMIS-WB	MG30-DMIS-W
[mm]	[mm]	[%]	[%]	[%]	[%]	[%]	[%]	[%]	[%]	[%]
37.5	> 37.5	0.0	0.0	0.0	0.0	0.0	0.0	100.0	100.0	100.0
28	37.5 - 28	0.0	0.0	0.0	0.0	0.0	0.0	100.0	100.0	100.0
20	28 - 20	0.0	0.0	0.0	0.0	0.0	0.0	100.0	100.0	100.0
14	20 - 14	17.9	19.4	30.6	1.1	1.4	0.8	82.1	80.6	69.4
10	14 - 10	8.5	8.0	6.6	0.4	0.3	0.7	73.6	72.6	62.9
7.1	10 - 7.1	7.7	6.6	8.3	0.6	0.6	0.7	65.9	66.1	54.6
5	7.1 - 5	8.7	8.2	9.0	0.5	0.5	0.9	57.2	57.9	45.6
2	5 - 2	15.4	14.6	12.4	0.2	0.4	0.5	41.8	43.2	33.2
1	2 - 1	7.9	8.4	6.3	0.2	0.3	0.3	33.9	34.9	26.9
0.6	1 - 0.6	5.8	6.3	4.3	0.6	0.8	0.1	28.1	28.6	22.6
0.425	0.6 - 0.425	3.6	4.1	2.3	0.3	0.8	0.2	24.5	24.4	20.3
0.3	0.425 - 0.3	3.6	3.5	2.9	0.3	1.0	0.4	20.9	21.0	17.4
0.15	0.3 - 0.15	5.7	5.6	4.1	0.2	0.1	0.5	15.2	15.4	13.3
0.075	0.15 - 0.075	3.0	2.8	2.4	0.5	0.6	0.2	12.2	12.6	11.0
Pan	< 0.075 (pan)	12.2	12.6	11.0	0.2	0.2	0.1	0.0	0.0	0.0
	Total	**100.0**	**100.0**	**100.0**	**0.4**	**0.6**	**0.4**	**0**	**0**	**0**
					Mean standard deviation					

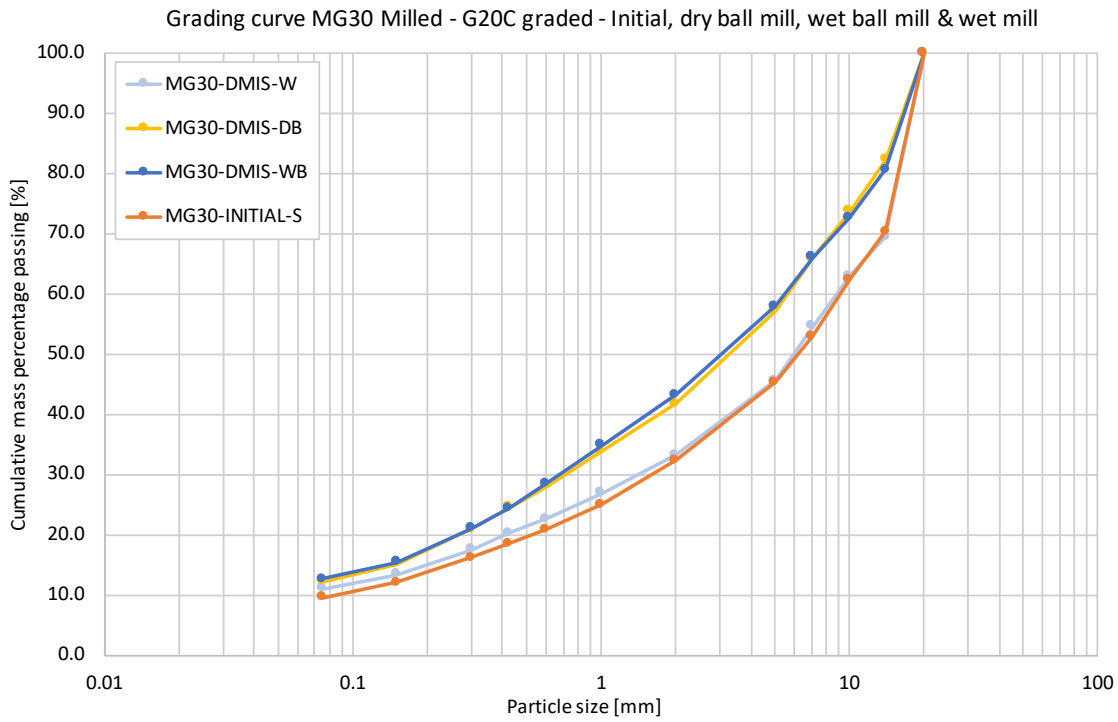

Figure E.8: MG30: Grading curves after durability milling (average of 3)

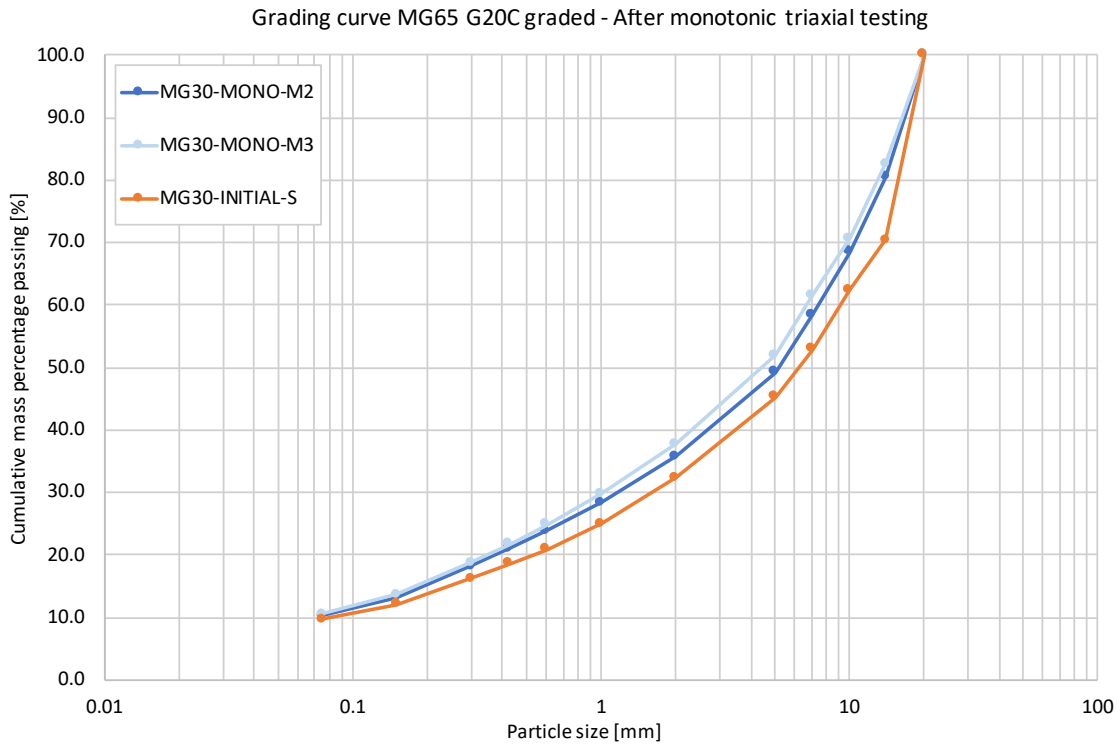

Figure E.9: MG30: Grading curves after monotonic triaxial testing

E.6. COMPARISONS: AFTER MONOTONIC TRIAXIAL TESTING

Table E.12: Gradings after monotonic triaxial testing for all compositions (average of 3)

			Mass percentage passing			
Sieve [mm]	Particle fraction [mm]	Design grading [%]	G2-MONO [%]	RCA-MONO [%]	MG65-MONO [%]	MG30-MONO [%]
37.5	> 37.5	[%]	100.0	100.0	100.0	100.0
28	37.5 - 28	100	100.0	100.0	100.0	100.0
20	28 - 20	100	100.0	100.0	100.0	100.0
14	20 - 14	100	71.1	83.6	82.3	81.5
10	14 - 10	67	59.4	65.7	69.0	69.6
7.1	10 - 7.1	Not defined	52.6	57.2	59.2	60.0
5	7.1 - 5	Not defined	45.6	52.7	50.5	50.6
2	5 - 2	45	32.9	40.4	36.5	36.7
1	2 - 1	32	27.3	33.3	29.0	29.1
0.6	1 - 0.6	Not defined	24.1	28.4	23.6	24.3
0.425	0.6 - 0.425	Not defined	22.2	24.0	19.9	21.3
0.3	0.425 - 0.3	18	19.9	19.8	16.1	18.4
0.15	0.3 - 0.15	Not defined	14.8	12.8	11.6	13.4
0.075	0.15 - 0.075	Not defined	12.0	10.3	9.8	10.3
Pan	< 0.075 (pan)	8	0.0	0.0	0.0	0.0

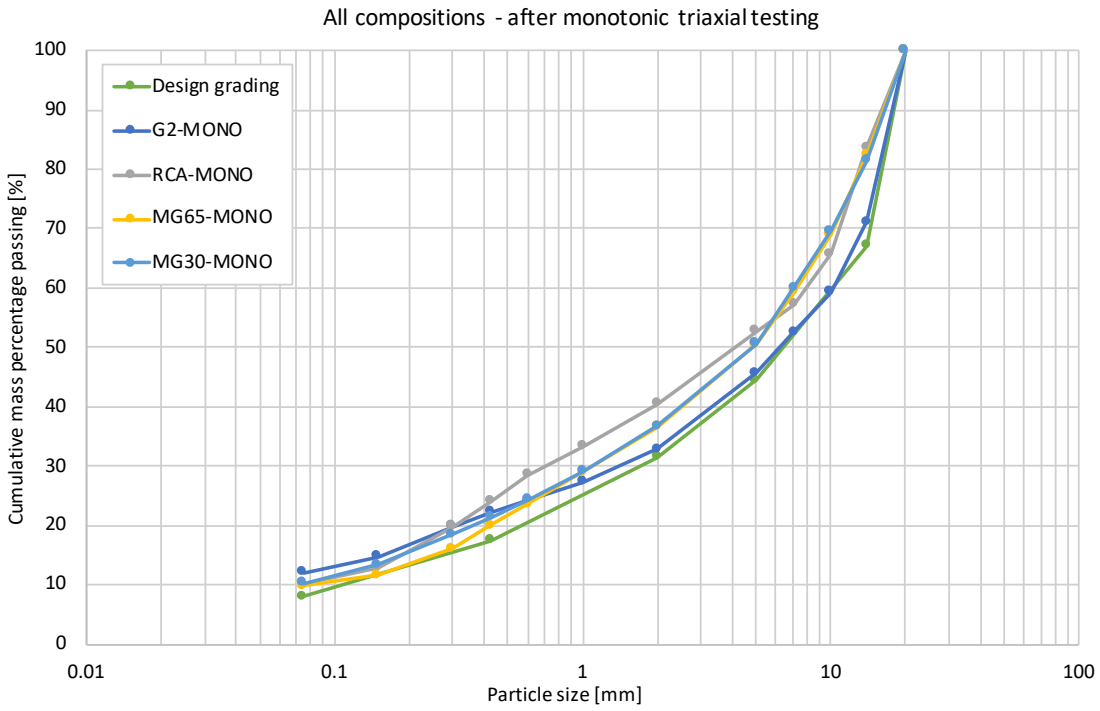

Figure E.10: Grading curves after monotonic triaxial testing for all compositions (average of 3)

E.7. COMPARISONS: DRY BALL MILL

Table E.13: Gradings after dry ball milling for all compositions (average of 3)

		Mass percentage passing					
Sieve [mm]	Particle fraction [mm]	Design grading [%]	G2-DMIS-DB [%]	RCA-DMIS-DB [%]	RCM-DMIS-DB [%]	MG65-DMIS-DB [%]	MG30-DMIS-DB [%]
37.5	> 37.5	100	100.0	100.0	100.0	100.0	100.0
28	37.5 - 28	100	100.0	100.0	100.0	100.0	100.0
20	28 - 20	100	100.0	100.0	100.0	100.0	100.0
14	20 - 14	67	69.3	86.8	80.0	83.1	82.1
10	14 - 10	Not defined	61.0	70.7	71.0	71.2	73.6
7.1	10 - 7.1	Not defined	55.1	62.5	64.8	63.7	65.9
5	7.1 - 5	45	48.5	58.3	57.8	56.6	57.2
2	5 - 2	32	35.5	47.2	43.5	43.1	41.8
1	2 - 1	Not defined	29.4	39.9	35.0	35.2	33.9
0.6	1 - 0.6	Not defined	26.0	33.9	29.3	29.3	28.1
0.425	0.6 - 0.425	18	23.9	29.2	26.0	25.6	24.5
0.3	0.425 - 0.3	Not defined	21.5	24.1	22.4	21.5	20.9
0.15	0.3 - 0.15	Not defined	16.0	15.1	16.4	14.8	15.2
0.075	0.15 - 0.075	8	12.6	11.7	12.1	11.8	12.2
Pan	< 0.075 (pan)	0	0.0	0.0	0.0	0.0	0.0

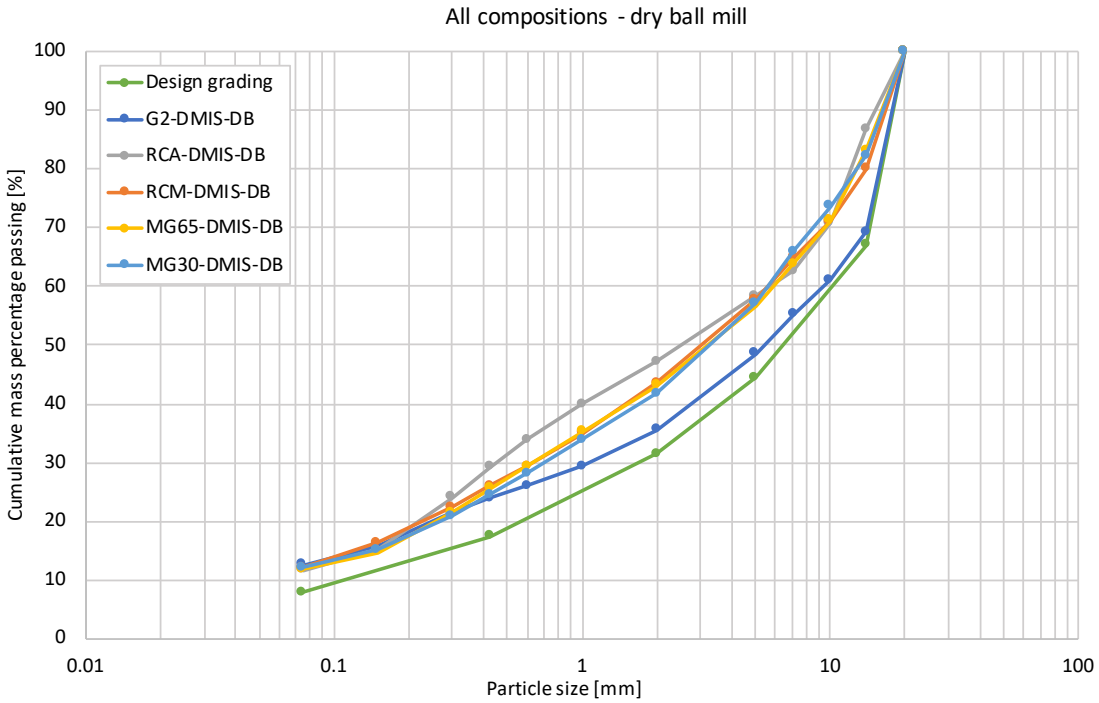

Figure E.11: Grading curves after dry ball milling for all compositions (average of 3)

E.8. COMPARISONS: WET BALL MILL

Table E.14: Gradings after wet ball milling for all compositions (average of 3)

			Mass percentage passing				
Sieve [mm]	Particle fraction [mm]	Design grading [%]	G2-DMIS-WB [%]	RCA-DMIS-WB [%]	RCM-DMIS-WB [%]	MG65-DMIS-WB [%]	MG30-DMIS-WB [%]
37.5	> 37.5	100	100.0	100.0	100.0	100.0	100.0
28	37.5 - 28	100	100.0	100.0	100.0	100.0	100.0
20	28 - 20	100	100.0	100.0	100.0	100.0	100.0
14	20 - 14	67	71.5	89.2	76.6	80.8	80.6
10	14 - 10	Not defined	63.6	72.6	69.0	69.9	72.6
7.1	10 - 7.1	Not defined	57.6	64.1	63.9	63.3	66.1
5	7.1 - 5	45	50.1	60.4	57.7	57.2	57.9
2	5 - 2	32	36.5	49.8	44.1	44.2	43.2
1	2 - 1	Not defined	30.3	42.5	35.4	36.2	34.9
0.6	1 - 0.6	Not defined	26.8	36.2	29.8	30.3	28.6
0.425	0.6 - 0.425	18	24.8	30.6	26.8	26.4	24.4
0.3	0.425 - 0.3	Not defined	22.5	25.7	23.3	22.0	21.0
0.15	0.3 - 0.15	Not defined	16.9	16.5	17.2	15.7	15.4
0.075	0.15 - 0.075	8	13.4	12.9	12.9	12.6	12.6
Pan	< 0.075 (pan)	0	0.0	0.0	0.0	0.0	0.0

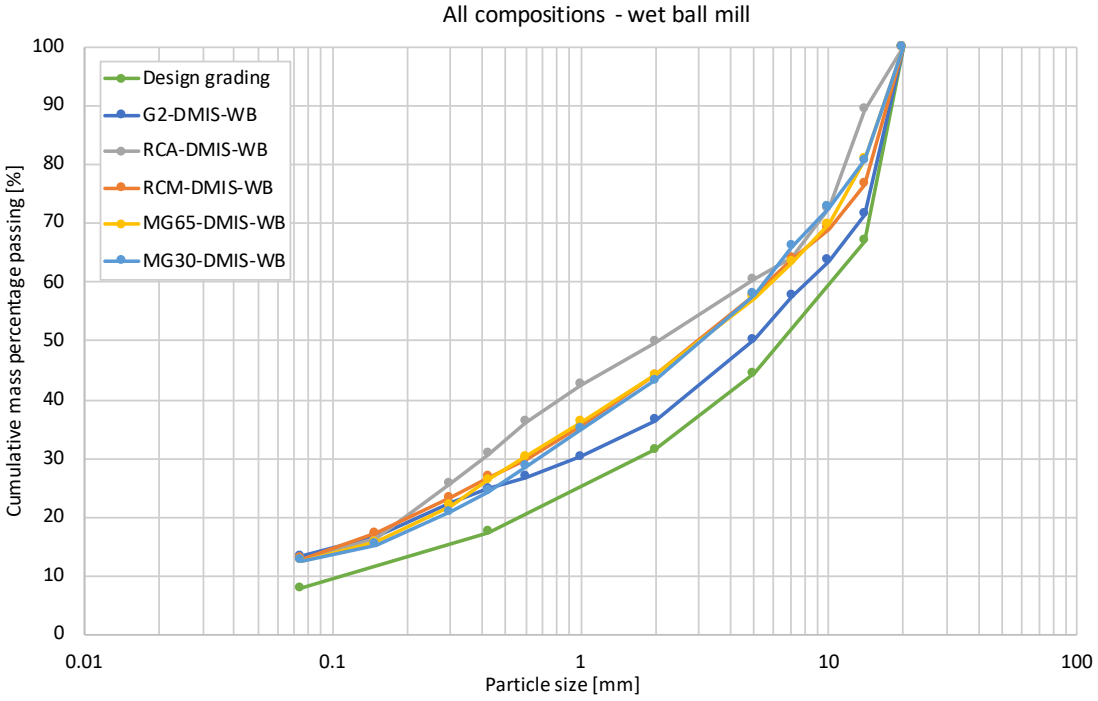

Figure E.12: Grading curves after wet ball milling for all compositions (average of 3)

E.9. COMPARISONS: WET MILL

Table E.15: Gradings after wet milling for all compositions (average of 3)

		Mass percentage passing					
Sieve [mm]	Particle fraction [mm]	Design grading [%]	G2-DMIS-W [%]	RCA-DMIS-W [%]	RCM-DMIS-W [%]	MG65-DMIS-W [%]	MG30-DMIS-W [%]
37.5	> 37.5	100	100.0	100.0	100.0	100.0	100.0
28	37.5 - 28	100	100.0	100.0	100.0	100.0	100.0
20	28 - 20	100	100.0	100.0	100.0	100.0	100.0
14	20 - 14	67	69.4	71.4	69.1	69.7	69.4
10	14 - 10	Not defined	61.0	56.0	61.8	61.0	62.9
7.1	10 - 7.1	Not defined	54.8	50.3	54.7	53.3	54.6
5	7.1 - 5	45	45.9	46.7	46.8	45.9	45.6
2	5 - 2	32	33.2	35.9	34.6	33.9	33.2
1	2 - 1	Not defined	27.9	31.3	27.7	28.0	26.9
0.6	1 - 0.6	Not defined	24.8	27.3	23.8	24.1	22.6
0.425	0.6 - 0.425	18	22.9	23.1	21.6	21.5	20.3
0.3	0.425 - 0.3	Not defined	20.6	19.8	19.0	18.4	17.4
0.15	0.3 - 0.15	Not defined	15.7	13.4	14.4	13.5	13.3
0.075	0.15 - 0.075	8	12.4	10.8	11.4	10.9	11.0
Pan	< 0.075 (pan)	0	0.0	0.0	0.0	0.0	0.0

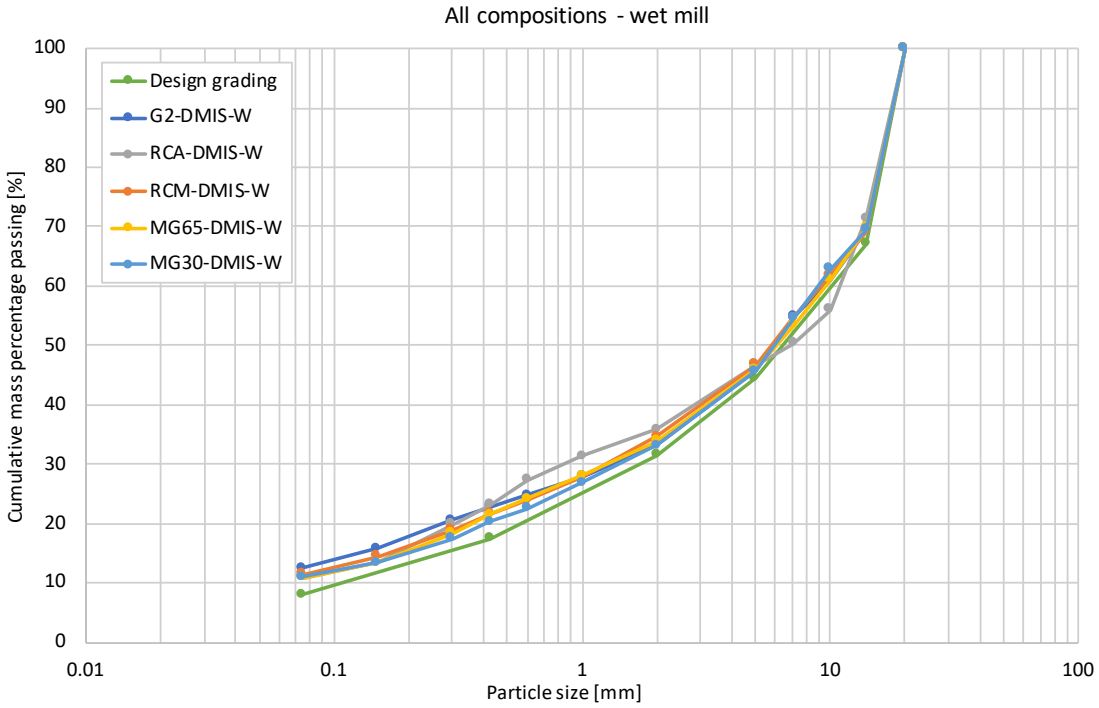

Figure E.13: Grading curves after wet milling for all compositions (average of 3)

E.10. SIEVING LOSSES

Table E.16: Recorded sieving losses. Excluded samples are displayed in red

G2 Sieving losses

Sample	Oven dry mass before sieving [g]	Oven dry mass after sieving [g]	Losses [g]	Percentage losses [%]
G2-INITIAL-S1	3742	3724	18	0.48
G2-INITIAL-S2	3742	3730	12	0.32
G2-INITIAL-S3	3742	3733	9	0.24
G2-INITIAL-F1	3746	3750	-4	-0.11
G2-INITIAL-F2	3746	3737	9	0.24
G2-INITIAL-F3	3746	3750	-4	-0.11
G2-MONO-M1	12656	12639	17	0.13
G2-MONO-M2	12698	12690	8	0.06
G2-MONO-M3	12701	12698	3	0.02
G2-DMIS-DB1	3745	3747	-2	-0.05
G2-DMIS-DB2	3741	3744	-3	-0.08
G2-DMIS-DB3	3743	3748	-5	-0.13
G2-DMIS-WB1	3743	3741	2	0.05
G2-DMIS-WB2	3743	3741	2	0.05
G2-DMIS-WB3	3743	3746	-3	-0.08
G2-DMIS-W1	3745	3743	2	0.05
G2-DMIS-W2	3744	3743	1	0.03
G2-DMIS-W3	3745	3746	-1	-0.03
G2-DMIF-DB1	3752	3754	-2	-0.05
G2-DMIF-DB2	3752	3753	-1	-0.03
G2-DMIF-DB3	3751	3755	-4	-0.11
G2-DMIF-WB1	3751	3750	1	0.03
G2-DMIF-WB2	3750	3750	0	0.00
G2-DMIF-WB3	3751	3747	4	0.11
G2-DMIF-W1	3752	3749	3	0.08
G2-DMIF-W2	3751	3750	1	0.03
G2-DMIF-W3	3752	3748	4	0.11

RCA sieving losses

Sample	Oven dry mass before sieving [g]	Oven dry mass after sieving [g]	Losses [g]	Percentage losses [%]
RCA-INITIAL-S1	3695	3697	-2	-0.05
RCA-INITIAL-S2	3693	3646	47	1.27
RCA-INITIAL-S3	3689	3652	37	1.00
RCA-MONO-M4	5494	5497	-3	-0.05
RCA-MONO-M5	5502	5503	-1	-0.02
RCA-MONO-M6	5505	5513	-8	-0.15
RCA-PERM-PD1	11019	11014	5	0.05
RCA-PERM-PD2	5530	5538	-8	-0.14
RCA-PERM-PD3	5492	5479	13	0.24
RCA-DMIS-DB1	Lost: Not sieved out			
RCA-DMIS-DB2	3677	3675	2	0.05
RCA-DMIS-DB3	3675	3677	-2	-0.05
RCA-DMIS-WB1	3676	3676	0	0.00
RCA-DMIS-WB2	3675	3677	-2	-0.05
RCA-DMIS-WB3	3677	3677	0	0.00
RCA-DMIS-W1	3676	4125	-449	-12.22
RCA-DMIS-W2	3676	3673	3	0.08
RCA-DMIS-W3	3676	3679	-3	-0.08

RCM sieving losses

Sample	Oven dry mass before sieving [g]	Oven dry mass after sieving [g]	Losses [g]	Percentage losses [%]
RCM-INITIAL-S1	3738	3740	-2	-0.05
RCM-INITIAL-S2	3738	3760	-22	-0.59
RCM-INITIAL-S3	3736	3740	-4	-0.11
RCM-INITIAL-F1	3736	3740	-4	-0.11
RCM-INITIAL-F2	3736	3740	-4	-0.11
RCM-INITIAL-F3	3738	3736	2	0.05
RCM-DMIS-DB1	3736	3613	123	3.29
RCM-DMIS-DB2	3735	3731	4	0.11
RCM-DMIS-DB3	3736	3736	0	0.00
RCM-DMIS-WB1	3737	3737	0	0.00
RCM-DMIS-WB2	3736	3736	0	0.00
RCM-DMIS-WB3	3737	3734	3	0.08
RCM-DMIS-W1	3736	3734	2	0.05
RCM-DMIS-W2	3736	3769	-33	-0.88
RCM-DMIS-W3	3736	3735	1	0.03

MG65 Sieving losses

Sample	Oven dry mass before sieving [g]	Oven dry mass after sieving [g]	Losses [g]	Percentage losses [%]
MG65-INITIAL-S1	3695	3697	-2	-0.05
MG65-INITIAL-S2	3694	3690	4	0.11
MG65-INITIAL-S3	3696	3694	2	0.05
MG65-MONO-M1	5216	5217	-1	-0.02
MG65-MONO-M2	5200	5199	1	0.02
MG65-MONO-M3	5208	5211	-3	-0.06
MG65-PERM-PD1	Lost: Not sieved out			
MG65-PERM-PD2	Lost: Not sieved out			
MG65-PERM-PD3	5199	5199	Unknown	Unknown
MG65-DMIS-DB1	3694	3699	-5	-0.14
MG65-DMIS-DB2	3696	3701	-5	-0.14
MG65-DMIS-DB3	3693	3698	-5	-0.14
MG65-DMIS-WB1	3695	3703	-8	-0.22
MG65-DMIS-WB2	3696	3696	0	0.00
MG65-DMIS-WB3	3695	3567	128	3.46
MG65-DMIS-W1	3694	3698	-4	-0.11
MG65-DMIS-W2	3694	3695	-1	-0.03
MG65-DMIS-W3	3692	3698	-6	-0.16

MG30 sieving losses

Sample	Oven dry mass before sieving [g]	Oven dry mass after sieving [g]	Losses [g]	Percentage losses [%]
MG30-INITIAL-S1	3716	3716	Unknown	Unknown
MG30-INITIAL-S2	3717	3717	Unknown	Unknown
MG30-INITIAL-S3	3719	3719	Unknown	Unknown
MG30-MONO-M1	Lost: Not sieved out			
MG30-MONO-M2	5029	5029	Unknown	Unknown
MG30-MONO-M3	5033	5033	Unknown	Unknown
MG30-DMIS-DB1	3717	3719	-2	-0.05
MG30-DMIS-DB2	3716	3721	-5	-0.13
MG30-DMIS-DB3	3716	3717	-1	-0.03
MG30-DMIS-WB1	3716	3724	-8	-0.22
MG30-DMIS-WB2	3716	3719	-3	-0.08
MG30-DMIS-WB3	3716	3718	-2	-0.05
MG30-DMIS-W1	3715	3719	-4	-0.11
MG30-DMIS-W2	3715	3717	-2	-0.05
MG30-DMIS-W3	3716	3710	6	0.16

F

APPENDIX F: MATERIAL BREAKDOWN

F.1. SUMMARY: ALL COMPOSITIONS

Table F.1: Material breakdown & fines increase per DMI testing type

	Breakdown [%]			
	Dry ball mill	Wet ball mill	Wet mill	After monotonics
G2	3.7	6.3	4.0	3.0
RCA	20.0	22.8	9.8	15.3
MG65	16.7	16.4	5.3	15.2
MG30	13.5	13.1	4.2	11.1
RCM	13.8	12.5	3.6	-

	Fines increase [%]			
	Dry ball mill	Wet ball mill	Wet mill	After monotonics
G2	2.3	3.1	1.2	0.5
RCA	11.1	12.6	3.4	5.9
MG65	8.1	8.8	3.9	2.4
MG30	6.0	5.9	1.7	2.8
RCM	7.8	8.5	3.4	-

	Breakdown severity [%]			
	Dry ball mill	Wet ball mill	Wet mill	After monotonics
G2	27	42	17	10
RCA	129	150	36	78
MG65	106	108	30	57
MG30	90	92	12	50
RCM	99	98	26	-

Table F.2: Durability Mill Index of all compositions

Material	Milling type [-]	Passing 0.425mm [%]	Increase 0.425mm [%]	Plasticity Index [%]	DMI 0.425mm [-]
G2	Dry ball	23.9	2.3	3	**74**
	Wet ball	24.8	3.1	3	
	Wet ball	22.9	1.2	3	
RCA	Dry ball	29.2	11.1	1	**31**
	Wet ball	30.6	12.6	1	
	Wet ball	23.1	5.0	1	
RCM	Dry ball	26.0	7.8	1	**27**
	Wet ball	26.8	8.5	1	
	Wet ball	21.6	3.4	1	
MG65	Dry ball	25.6	8.1	1	**26**
	Wet ball	26.4	8.8	1	
	Wet ball	21.5	3.9	1	
MG30	Dry ball	24.5	6.0	1	**25**
	Wet ball	24.4	5.9	1	
	Wet ball	20.3	1.7	1	

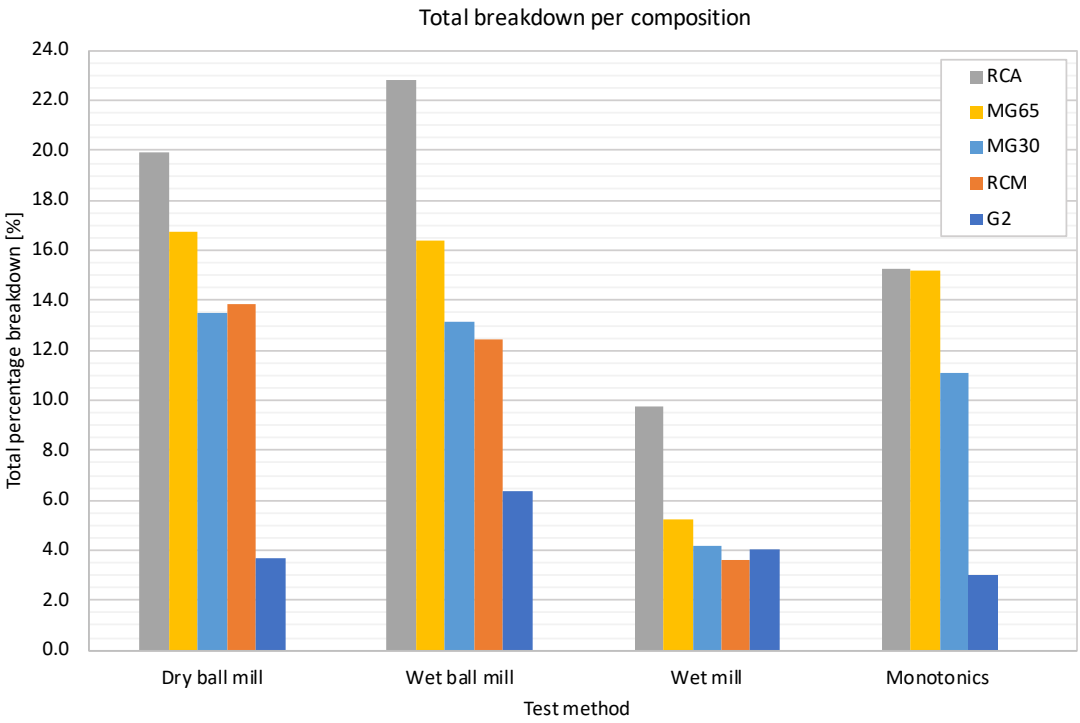

Figure F.1: Material breakdown per DMI testing type and after monotonic triaxial testing

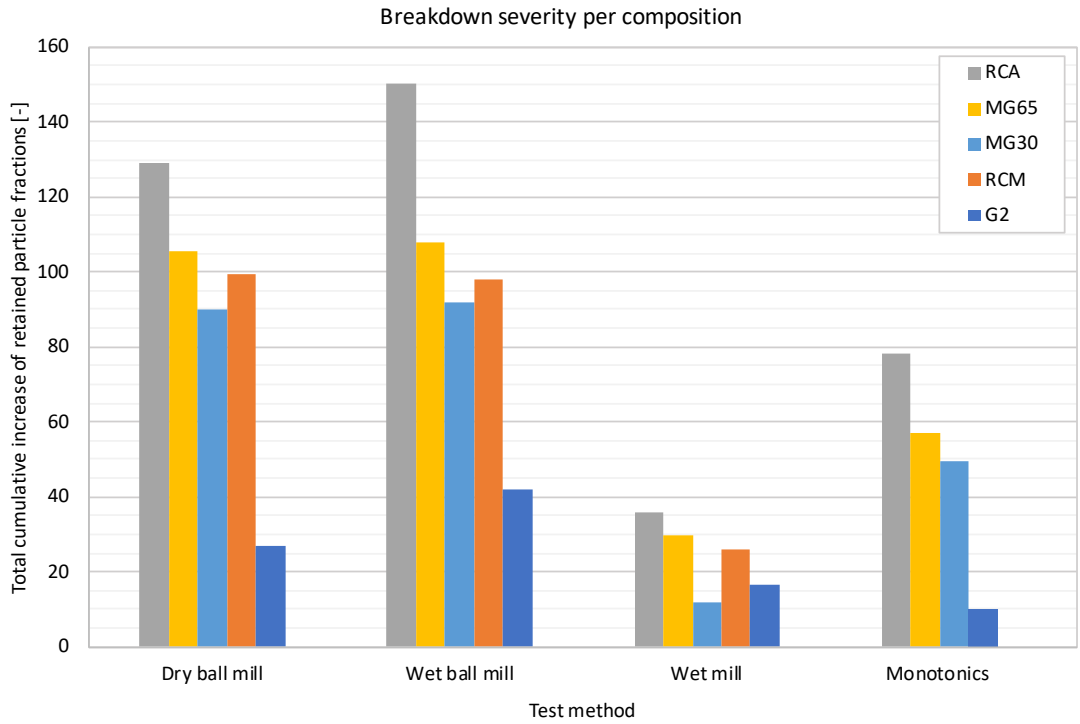

Figure F.2: Breakdown severity per DMI testing type and after monotonic triaxial testing

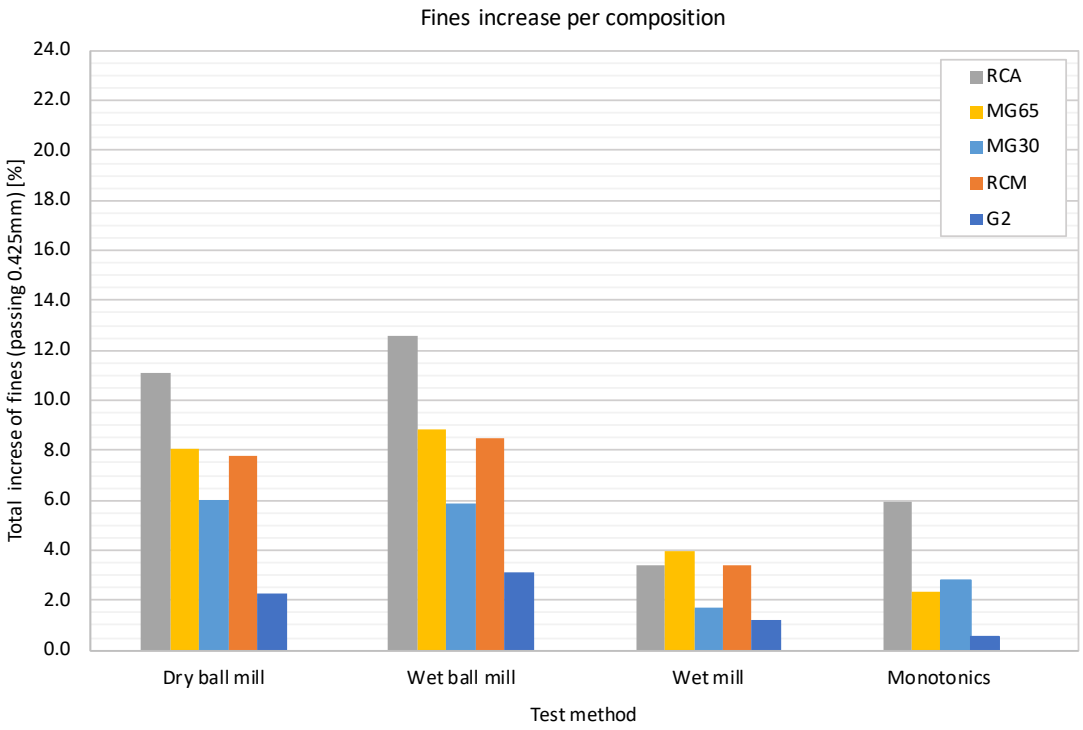

Figure F.3: Fines increase per DMI testing type and after monotonic triaxial testing

F.2. G2 MATERIAL BREAKDOWN

Table F.3: G2: grading change per fraction (average of 3) for all testing types

G2		Initial and milled particle distributions				Mass change per fraction		
Retained	Particle fraction	G2-INITIAL-S	G2-DMIS-DB	G2-DMIS-WB	G2-DMIS-W	G2-DMIS-DB	G2-DMIS-WB	G2-DMIS-W
[mm]	[mm]	[%]	[%]	[%]	[%]	[%]	[%]	[%]
37.5	> 37.5	0.0	0.0	0.0	0.0	0.0	0.0	0.0
28	37.5 - 28	0.0	0.0	0.0	0.0	0.0	0.0	0.0
20	28 - 20	0.0	0.0	0.0	0.0	0.0	0.0	0.0
14	20 - 14	31.5	30.7	28.5	30.6	-0.8	-3.0	-0.9
10	14 - 10	10.4	8.2	7.9	8.5	-2.2	-2.5	-1.9
7.1	10 - 7.1	6.7	5.9	6.0	6.1	-0.8	-0.7	-0.6
5	7.1 - 5	6.5	6.6	7.5	8.9	0.1	1.0	2.4
2	5 - 2	12.7	13.0	13.6	12.7	0.3	1.0	0.0
1	2 - 1	5.5	6.1	6.2	5.3	0.6	0.7	-0.2
0.6	1 - 0.6	3.0	3.4	3.4	3.2	0.4	0.4	0.1
0.425	0.6 - 0.425	2.0	2.1	2.1	1.9	0.0	0.0	-0.2
0.3	0.425 - 0.3	2.4	2.5	2.3	2.3	0.1	-0.1	-0.2
0.15	0.3 - 0.15	5.0	5.5	5.6	4.9	0.5	0.6	-0.1
0.075	0.15 - 0.075	3.0	3.4	3.5	3.3	0.4	0.5	0.3
Pan	< 0.075 (pan)	11.3	12.6	13.4	12.4	1.3	2.1	1.1
	Total	**100.0**	**100.0**	**100.0**	**100.0**	**0.0**	**0.0**	**0.0**
					Breakdown	**3.7**	**6.3**	**4.0**
					Fines increase	**2.3**	**3.1**	**1.2**

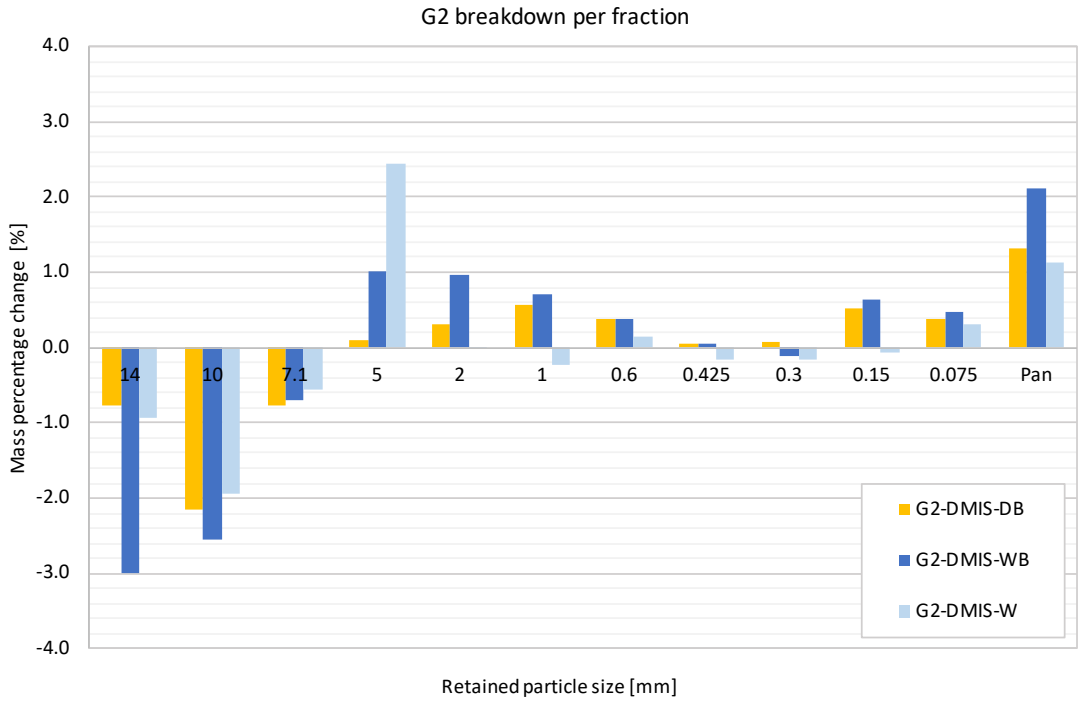

Figure F.4: G2: grading change per fraction (average of 3) for all testing types

F.3. RCA MATERIAL BREAKDOWN

Table F.4: RCA: grading change per fraction (average of 3) for all testing types

RCA		Initial and milled particle distributions				Mass change per fraction		
Retained [mm]	Particle fraction [mm]	RCA-INITIAL-S [%]	RCA-DMIS-DB [%]	RCA-DMIS-WB [%]	RCA-DMIS-W [%]	RCA-DMIS-DB [%]	RCA-DMIS-WB [%]	RCA-DMIS-W [%]
37.5	> 37.5	0.0	0.0	0.0	0.0	0.0	0.0	0.0
28	37.5 - 28	0.0	0.0	0.0	0.0	0.0	0.0	0.0
20	28 - 20	0.0	0.0	0.0	0.0	0.0	0.0	0.0
14	20 - 14	31.1	13.2	10.8	28.6	-17.9	-20.4	-2.6
10	14 - 10	11.8	16.1	16.7	15.4	4.3	4.8	3.6
7.1	10 - 7.1	8.7	8.2	8.4	5.8	-0.5	-0.2	-2.9
5	7.1 - 5	3.9	4.3	3.7	3.6	0.3	-0.3	-0.4
2	5 - 2	12.6	11.1	10.7	10.8	-1.5	-1.9	-1.8
1	2 - 1	6.4	7.3	7.3	4.6	0.9	0.9	-1.8
0.6	1 - 0.6	4.3	5.9	6.3	4.0	1.6	2.0	-0.3
0.425	0.6 - 0.425	3.1	4.8	5.5	4.3	1.7	2.5	1.2
0.3	0.425 - 0.3	2.5	5.1	5.0	3.3	2.6	2.5	0.8
0.15	0.3 - 0.15	4.9	9.0	9.2	6.3	4.0	4.3	1.4
0.075	0.15 - 0.075	1.8	3.4	3.6	2.6	1.6	1.8	0.8
Pan	< 0.075 (pan)	8.9	11.7	12.9	10.8	2.9	4.0	1.9
	Total	**100.0**	**100.0**	**100.0**	**100.0**	**0.0**	**0.0**	**0.0**
					Breakdown	**20.0**	**22.8**	**9.8**
					Fines increase	**11.1**	**12.6**	**5.0**

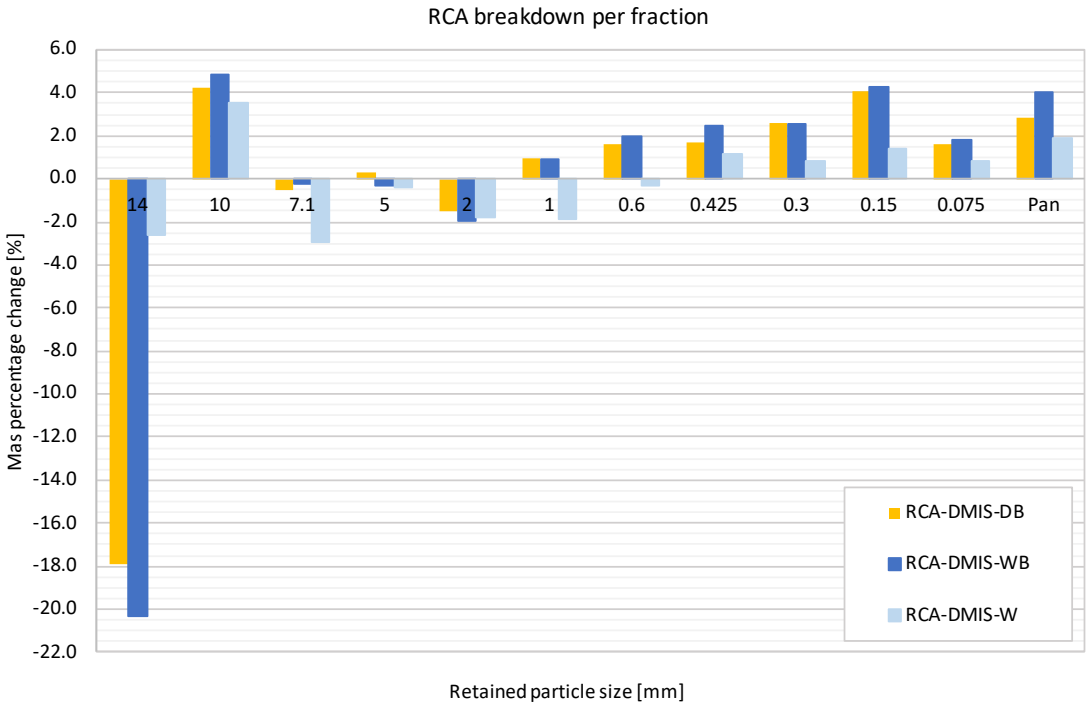

Figure F.5: RCA: grading change per fraction (average of 3) for all testing types

F.4. RCM MATERIAL BREAKDOWN

Table F.5: RCM: grading change per fraction (average of 3) for all testing types

RCM		Initial and milled particle distributions				Mass change per fraction		
Retained [mm]	Particle fraction [mm]	RCM-INITIAL-S [%]	RCM-DMIS-DB [%]	RCM-DMIS-WB [%]	RCM-DMIS-W [%]	RCM-DMIS-DB [%]	RCM-DMIS-WB [%]	RCM-DMIS-W [%]
37.5	> 37.5	0.0	0.0	0.0	0.0	0.0	0.0	0.0
28	37.5 - 28	0.0	0.0	0.0	0.0	0.0	0.0	0.0
20	28 - 20	0.0	0.0	0.0	0.0	0.0	0.0	0.0
14	20 - 14	31.9	20.0	23.4	30.9	-11.9	-8.6	-1.1
10	14 - 10	7.7	9.0	7.6	7.4	1.3	-0.1	-0.4
7.1	10 - 7.1	7.5	6.1	5.1	7.1	-1.3	-2.3	-0.3
5	7.1 - 5	7.6	7.0	6.2	7.9	-0.6	-1.4	0.3
2	5 - 2	13.1	14.3	13.6	12.1	1.2	0.5	-1.0
1	2 - 1	7.2	8.5	8.7	6.9	1.3	1.5	-0.3
0.6	1 - 0.6	4.3	5.7	5.6	3.9	1.3	1.2	-0.4
0.425	0.6 - 0.425	2.3	3.3	3.1	2.2	1.0	0.8	-0.1
0.3	0.425 - 0.3	2.4	3.6	3.4	2.7	1.2	1.0	0.3
0.15	0.3 - 0.15	4.2	6.1	6.1	4.5	1.9	1.9	0.4
0.075	0.15 - 0.075	2.7	4.3	4.3	3.0	1.6	1.6	0.3
Pan	< 0.075 (pan)	9.0	12.1	12.9	11.4	3.1	3.9	2.4
	Total	**100.0**	**100.0**	**100.0**	**100.0**	**0.0**	**0.0**	**0.0**
					Breakdown	**13.8**	**12.5**	**3.6**
					Fines increase	**7.8**	**8.5**	**3.4**

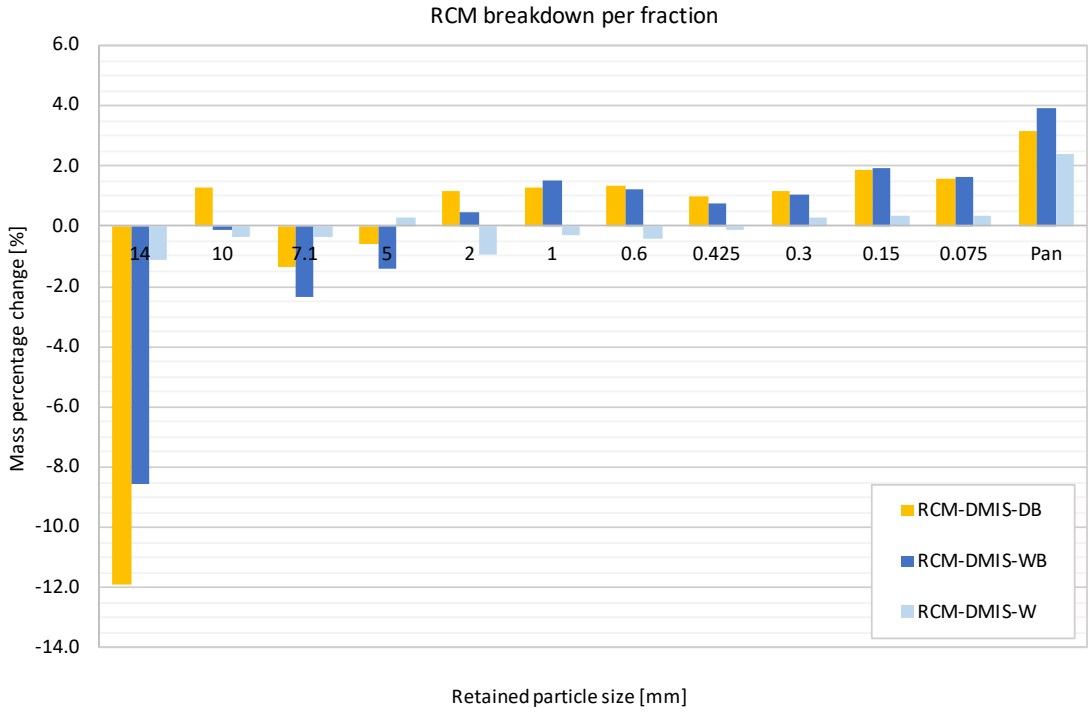

Figure F.6: RCM: grading change per fraction (average of 3) for all testing types

F.5. MG65 MATERIAL BREAKDOWN

Table F.6: MG65: grading change per fraction (average of 3) for all testing types

MG65		Initial and milled particle distributions				Mass change per fraction		
Retained	Particle fraction	MG65-INITIAL-S	MG65-DMIS-DB	MG65-DMIS-WB	MG65-DMIS-W	MG65-DMIS-DB	MG65-DMIS-WB	MG65-DMIS-W
[mm]	[mm]	[%]	[%]	[%]	[%]	[%]	[%]	[%]
37.5	> 37.5	0.0	0.0	0.0	0.0	0.0	0.0	0.0
28	37.5 - 28	0.0	0.0	0.0	0.0	0.0	0.0	0.0
20	28 - 20	0.0	0.0	0.0	0.0	0.0	0.0	0.0
14	20 - 14	32.6	16.9	19.2	30.3	-15.7	-13.4	-2.3
10	14 - 10	7.7	11.9	10.9	8.7	4.2	3.2	1.0
7.1	10 - 7.1	7.6	7.5	6.6	7.7	-0.2	-1.0	0.1
5	7.1 - 5	8.0	7.1	6.0	7.3	-0.9	-1.9	-0.6
2	5 - 2	13.1	13.5	13.1	12.0	0.4	-0.1	-1.1
1	2 - 1	6.7	7.9	8.0	5.9	1.2	1.3	-0.8
0.6	1 - 0.6	4.4	5.9	5.9	3.9	1.5	1.6	-0.4
0.425	0.6 - 0.425	2.3	3.7	3.9	2.6	1.3	1.5	0.3
0.3	0.425 - 0.3	2.7	4.1	4.4	3.1	1.4	1.8	0.5
0.15	0.3 - 0.15	4.1	6.8	6.3	4.9	2.7	2.2	0.8
0.075	0.15 - 0.075	2.1	3.0	3.1	2.5	0.9	1.0	0.5
Pan	< 0.075 (pan)	8.8	11.8	12.6	10.9	3.0	3.9	2.2
	Total	**100.0**	**100.0**	**100.0**	**100.0**	**0.0**	**0.0**	**0.0**
					Breakdown	**16.7**	**16.4**	**5.3**
					Fines increase	**8.1**	**8.8**	**3.9**

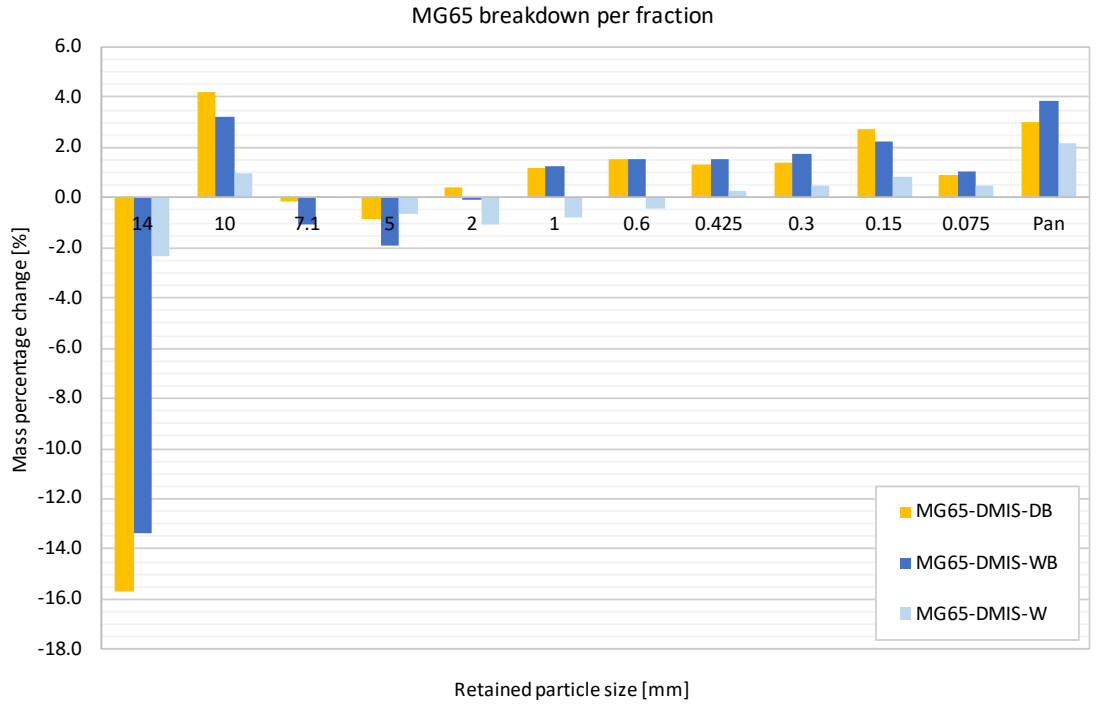

Figure F.7: MG65: grading change per fraction (average of 3) for all testing types

F.6. MG30 MATERIAL BREAKDOWN

Table F.7: MG30: grading change per fraction (average of 3) for all testing types

MG30		Initial and milled particle distributions				Mass change per fraction		
Retained [mm]	Particle fraction [mm]	MG30-INITIAL-S [%]	MG30-DMIS-DB [%]	MG30-DMIS-WB [%]	MG30-DMIS-W [%]	MG30-DMIS-DB [%]	MG30-DMIS-WB [%]	MG30-DMIS-W [%]
37.5	> 37.5	0.0	0.0	0.0	0.0	0.0	0.0	0.0
28	37.5 - 28	0.0	0.0	0.0	0.0	0.0	0.0	0.0
20	28 - 20	0.0	0.0	0.0	0.0	0.0	0.0	0.0
14	20 - 14	29.6	17.9	19.4	30.6	-11.8	-10.3	0.9
10	14 - 10	8.0	8.5	8.0	6.6	0.5	0.0	-1.4
7.1	10 - 7.1	9.4	7.7	6.6	8.3	-1.7	-2.9	-1.1
5	7.1 - 5	7.7	8.7	8.2	9.0	1.0	0.5	1.2
2	5 - 2	12.9	15.4	14.6	12.4	2.5	1.7	-0.5
1	2 - 1	7.3	7.9	8.4	6.3	0.6	1.1	-1.0
0.6	1 - 0.6	4.1	5.8	6.3	4.3	1.6	2.2	0.2
0.425	0.6 - 0.425	2.3	3.6	4.1	2.3	1.3	1.8	0.0
0.3	0.425 - 0.3	2.4	3.6	3.5	2.9	1.2	1.1	0.5
0.15	0.3 - 0.15	4.1	5.7	5.6	4.1	1.7	1.5	0.0
0.075	0.15 - 0.075	2.5	3.0	2.8	2.4	0.5	0.3	-0.1
Pan	< 0.075 (pan)	9.6	12.2	12.6	11.0	2.6	3.0	1.4
	Total	**100.0**	**100.0**	**100.0**	**100.0**	**0.0**	**0.0**	**0.0**
					Breakdown	**13.5**	**13.1**	**4.2**
					Fines increase	**6.0**	**5.9**	**1.7**

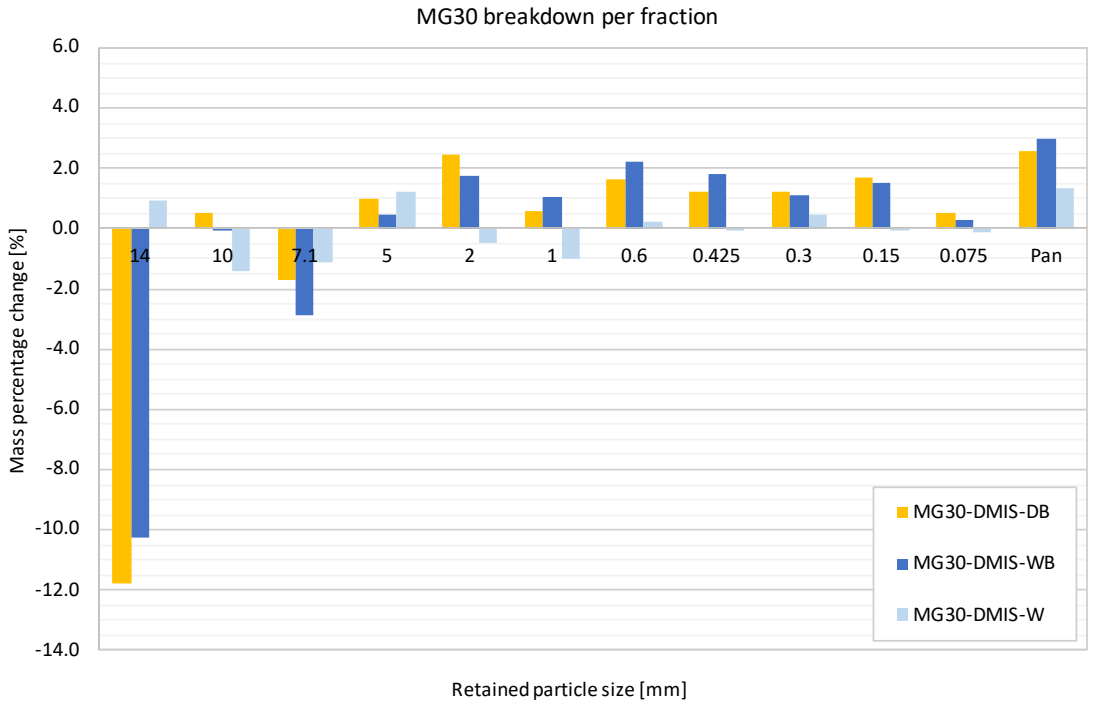

Figure F.8: MG30: grading change per fraction (average of 3) for all testing types

F.7. COMPARISONS: AFTER MONOTONIC TRIAXIAL TESTING

Table F.8: All compositions: Grading change per fraction after monotonic triaxial testing

G2		Particle distribution after monotonic triaxial testing				Mass change per fraction			
Retained [mm]	Particle fraction [mm]	G2-MONO [%]	RCA-MONO [%]	MG65-MONO [%]	MG30-MONO [%]	G2-MONO [%]	RCA-MONO [%]	MG65-MONO [%]	MG30-MONO
37.5	> 37.5	0.0	0.0	0.0	0.0	0.0	0.0	0.0	0.0
28	37.5 - 28	0.0	0.0	0.0	0.0	0.0	0.0	0.0	0.0
20	28 - 20	0.0	0.0	0.0	0.0	0.0	0.0	0.0	0.0
14	20 - 14	28.9	16.4	17.7	18.5	-2.6	-14.8	-14.9	-11.1
10	14 - 10	11.7	17.9	13.3	11.9	1.3	6.1	5.6	3.9
7.1	10 - 7.1	6.8	8.5	9.8	9.6	0.1	-0.2	2.1	0.2
5	7.1 - 5	7.0	4.5	8.7	9.4	0.5	0.6	0.8	1.7
2	5 - 2	12.7	12.3	14.0	13.8	0.1	-0.3	0.9	0.9
1	2 - 1	5.6	7.1	7.5	7.6	0.1	0.7	0.8	0.3
0.6	1 - 0.6	3.1	4.8	5.4	4.8	0.1	0.5	1.0	0.7
0.425	0.6 - 0.425	1.9	4.4	3.6	3.0	-0.1	1.4	1.3	0.6
0.3	0.425 - 0.3	2.3	4.1	3.8	2.9	-0.1	1.7	1.2	0.5
0.15	0.3 - 0.15	5.1	7.0	4.5	5.0	0.1	2.1	0.4	1.0
0.075	0.15 - 0.075	2.8	2.5	1.8	3.0	-0.2	0.7	-0.3	0.5
Pan	< 0.075 (pan)	12.0	10.3	9.8	10.3	0.7	1.5	1.0	0.7
	Total	**100.0**	**100.0**	**100.0**	**100.0**	**0.0**	**0.0**	**0.0**	**0.0**
					Breakdown	**3.0**	**15.3**	**15.2**	**11.1**
					Fines increase	**0.5**	**5.9**	**2.4**	**2.8**

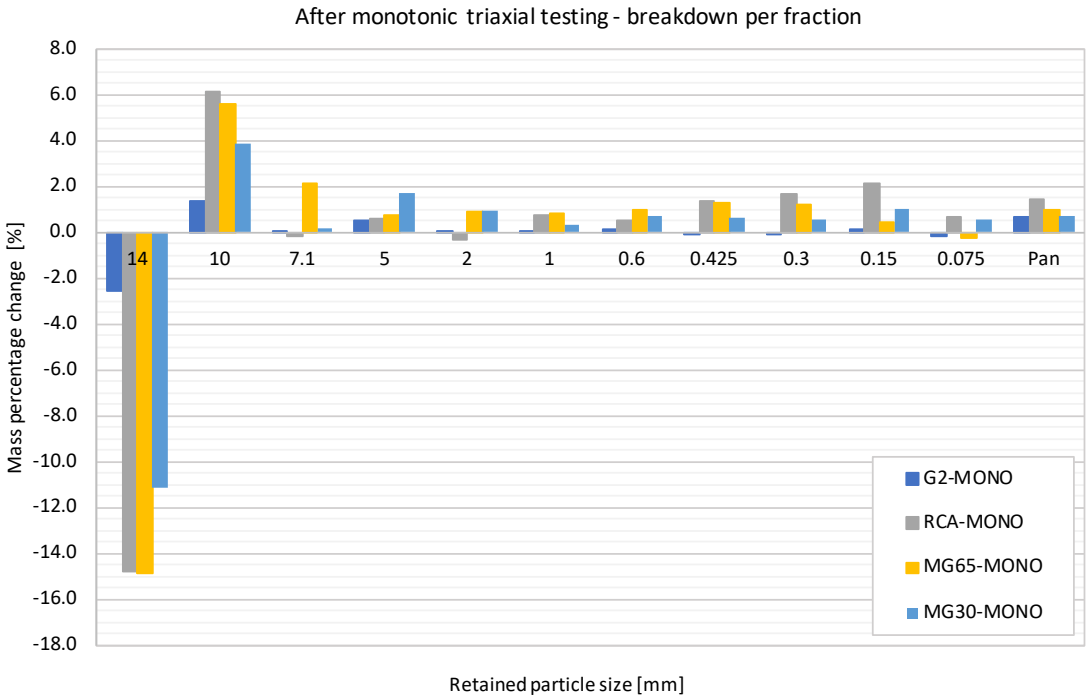

Figure F.9: All compositions: Grading change per fraction after monotonic triaxial testing

F.8. COMPARISONS: DRY BALL MILL

Table F.9: Material breakdown after dry ball milling for all compositions

Sieve [mm]	Particle fraction [mm]	G2-DMIS-DB [%]	RCA-DMIS-DB [%]	RCM-DMIS-DB [%]	MG65-DMIS-DB [%]	MG30-DMIS-DB [%]
37.5	> 37.5	0.0	0.0	0.0	0.0	0.0
28	37.5 - 28	0.0	0.0	0.0	0.0	0.0
20	28 - 20	0.0	0.0	0.0	0.0	0.0
14	20 - 14	-0.8	-17.9	-11.9	-15.7	-11.8
10	14 - 10	-2.2	4.3	1.3	4.2	0.5
7.1	10 - 7.1	-0.8	-0.5	-1.3	-0.2	-1.7
5	7.1 - 5	0.1	0.3	-0.6	-0.9	1.0
2	5 - 2	0.3	-1.5	1.2	0.4	2.5
1	2 - 1	0.6	0.9	1.3	1.2	0.6
0.6	1 - 0.6	0.4	1.6	1.3	1.5	1.6
0.425	0.6 - 0.425	0.0	1.7	1.0	1.3	1.3
0.3	0.425 - 0.3	0.1	2.6	1.2	1.4	1.2
0.15	0.3 - 0.15	0.5	4.0	1.9	2.7	1.7
0.075	0.15 - 0.075	0.4	1.6	1.6	0.9	0.5
Pan	< 0.075 (pan)	1.3	2.9	3.1	3.0	2.6
	Breakdown	**3.7**	**20.0**	**13.8**	**16.7**	**13.5**
	Fines increase	**2.3**	**11.1**	**7.8**	**8.1**	**6.0**

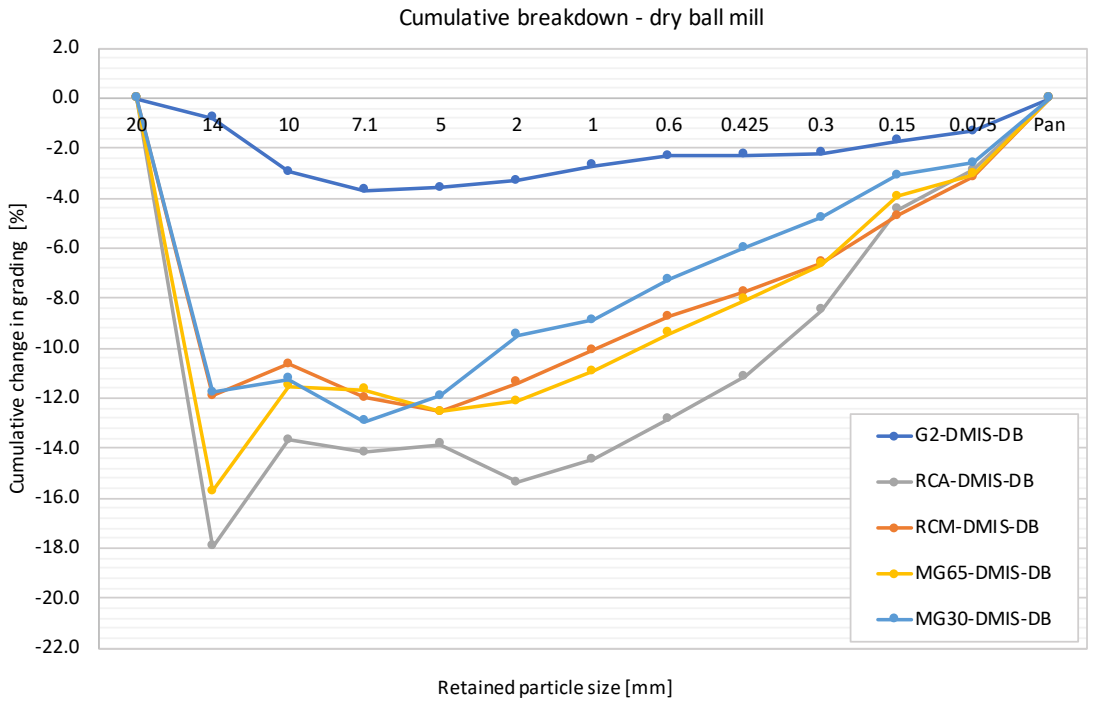

Figure F.10: Cumulative change in grading after dry ball milling for all compositions

F.9. COMPARISONS: WET BALL MILL

Table F.10: Grading change after wet ball milling for all compositions

Sieve [mm]	Particle fraction [mm]	G2-DMIS-WB [%]	RCA-DMIS-WB [%]	RCM-DMIS-WB [%]	MG65-DMIS-WB [%]	MG30-DMIS-WB [%]
37.5	> 37.5	0.0	0.0	0.0	0.0	0.0
28	37.5 - 28	0.0	0.0	0.0	0.0	0.0
20	28 - 20	0.0	0.0	0.0	0.0	0.0
14	20 - 14	-3.0	-20.4	-8.6	-13.4	-10.3
10	14 - 10	-2.5	4.8	-0.1	3.2	0.0
7.1	10 - 7.1	-0.7	-0.2	-2.3	-1.0	-2.9
5	7.1 - 5	1.0	-0.3	-1.4	-1.9	0.5
2	5 - 2	1.0	-1.9	0.5	-0.1	1.7
1	2 - 1	0.7	0.9	1.5	1.3	1.1
0.6	1 - 0.6	0.4	2.0	1.2	1.6	2.2
0.425	0.6 - 0.425	0.0	2.5	0.8	1.5	1.8
0.3	0.425 - 0.3	-0.1	2.5	1.0	1.8	1.1
0.15	0.3 - 0.15	0.6	4.3	1.9	2.2	1.5
0.075	0.15 - 0.075	0.5	1.8	1.6	1.0	0.3
Pan	< 0.075 (pan)	2.1	4.0	3.9	3.9	3.0
	Breakdown	**6.3**	**22.8**	**12.5**	**16.4**	**13.1**
	Fines increase	**3.1**	**12.6**	**8.5**	**8.8**	**5.9**

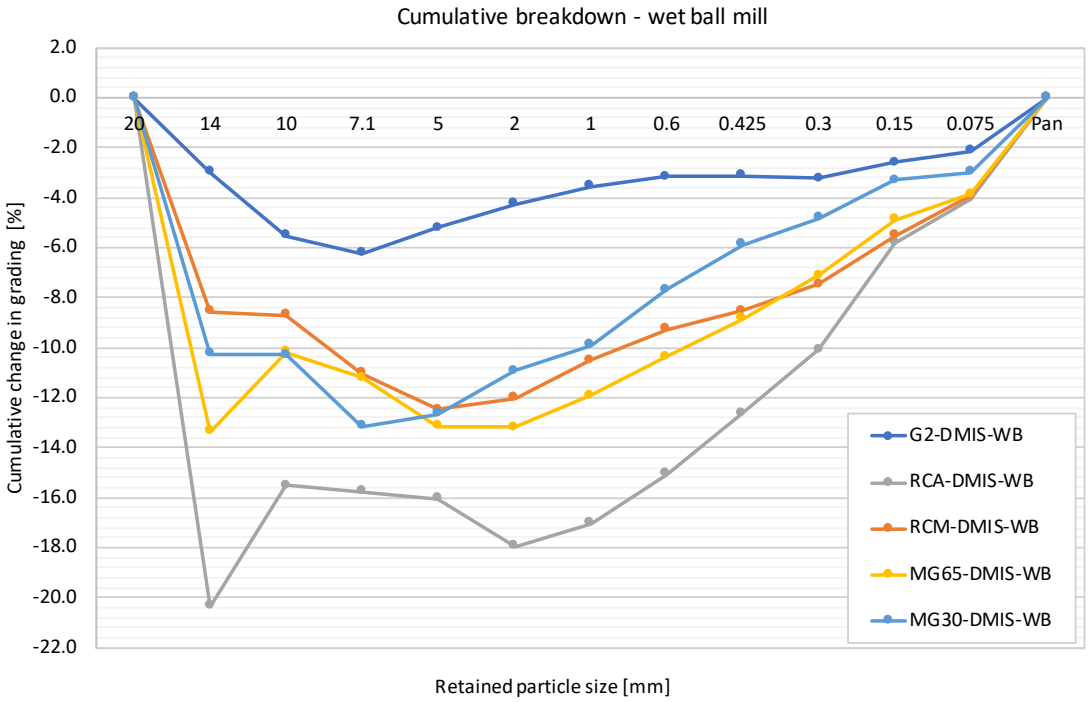

Figure F.11: Cumulative change in grading after wet ball milling for all compositions

F.10. COMPARISONS: WET MILL

Table F.11: Grading after wet milling for all compositions

Sieve [mm]	Particle fraction [mm]	G2-DMIS-W [%]	RCA-DMIS-W [%]	RCM-DMIS-W [%]	MG65-DMIS-W [%]	MG30-DMIS-W [%]
37.5	> 37.5	0.0	0.0	0.0	0.0	0.0
28	37.5 - 28	0.0	0.0	0.0	0.0	0.0
20	28 - 20	0.0	0.0	0.0	0.0	0.0
14	20 - 14	-0.9	-2.6	-1.1	-2.3	0.9
10	14 - 10	-1.9	3.6	-0.4	1.0	-1.4
7.1	10 - 7.1	-0.6	-2.9	-0.3	0.1	-1.1
5	7.1 - 5	2.4	-0.4	0.3	-0.6	1.2
2	5 - 2	0.0	-1.8	-1.0	-1.1	-0.5
1	2 - 1	-0.2	-1.8	-0.3	-0.8	-1.0
0.6	1 - 0.6	0.1	-0.3	-0.4	-0.4	0.2
0.425	0.6 - 0.425	-0.2	1.2	-0.1	0.3	0.0
0.3	0.425 - 0.3	-0.2	0.8	0.3	0.5	0.5
0.15	0.3 - 0.15	-0.1	1.4	0.4	0.8	0.0
0.075	0.15 - 0.075	0.3	0.8	0.3	0.5	-0.1
Pan	< 0.075 (pan)	1.1	1.9	2.4	2.2	1.4
	Breakdown	**4.0**	**9.8**	**3.6**	**5.3**	**4.2**
	Fines increase	**1.2**	**5.0**	**3.4**	**3.9**	**1.7**

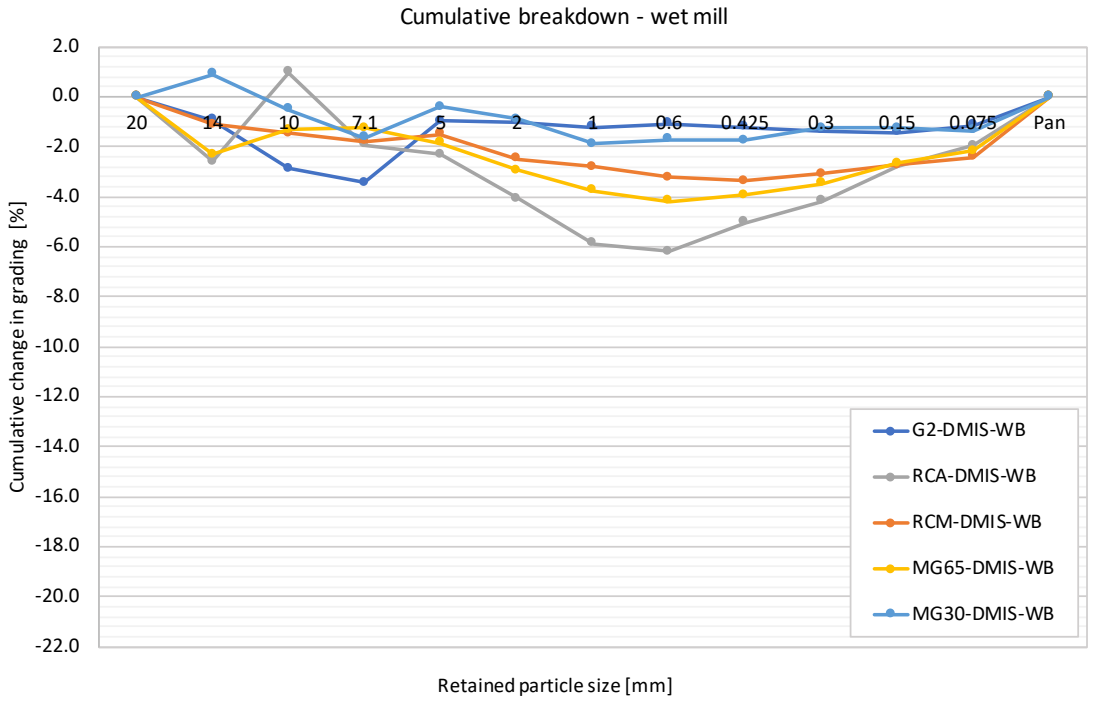

Figure F.12: Cumulative change in grading after wet milling for all compositions[1]

[1] Note that positive values of cumulative change in grading are theoretically impossible. The positive values recorded here might have been caused by slight differences between the reference grading and the actual initial grading of the sample.

F.11. UNIFORMITY AND CURVE COEFFICIENTS

Table F.12: Uniformity and Curve Coefficients of the milled materials

G2	Initial grading [mm, -]	Dry ball mill [mm, -]	Wet ball mill [mm, -]	Wet mill [mm, -]
D60	10.7	9.5	8.2	9.5
D10	0.1	0.1	0.1	0.1
D30	1.6	1.1	1.0	1.4
C_u	162	160	147	158
C_c	3.6	2.1	2.0	3.4

Uniformity Coefficient	Initial grading [-]	Dry ball mill [-]	Wet ball mill [-]	Wet mill [-]
G2	162	160	147	158
RCA	90	92	84	159
MG65	84	94	100	140
MG30	106	92	93	131
RCM	96	130	99	141

RCA	Initial grading [mm, -]	Dry ball mill [mm, -]	Wet ball mill [mm, -]	Wet mill [mm, -]
D60	11.0	5.8	4.9	11.0
D10	0.1	0.1	0.1	0.1
D30	1.7	0.5	0.4	0.9
C_u	90	92	84	159
C_c	2.2	0.6	0.6	1.0

Curve Coefficient	Initial grading [-]	Dry ball mill [-]	Wet ball mill [-]	Wet mill [-]
G2	3.6	2.1	2.0	3.4
RCA	2.2	0.6	0.6	1.0
MG65	2.8	1.1	1.0	2.7
MG30	3.5	1.5	1.4	3.6
RCM	2.9	0.8	1.1	2.9

MG65	Initial grading [mm, -]	Dry ball mill [mm, -]	Wet ball mill [mm, -]	Wet mill [mm, -]
D60	10.2	6.0	6.0	9.6
D10	0.1	0.1	0.1	0.1
D30	1.9	0.6	0.6	1.3
C_u	84	94	100	140
C_c	2.8	1.1	1.0	2.7

Change after wet ball mill	Breakdown [%]	C_u change [-]	C_c change [-]	Cohesion change [kPa]
G2	6.3	-14.2	-1.5	1
RCA	22.8	-5.9	-1.6	-55
MG65	16.4	15.8	-1.8	-140
MG30	13.1	-13.1	-2.0	-43
RCM	12.5	3.7	-1.7	-

MG30	Initial grading [mm, -]	Dry ball mill [mm, -]	Wet ball mill [mm, -]	Wet mill [mm, -]
D60	9.3	5.7	5.5	9.0
D10	0.1	0.1	0.1	0.1
D30	1.7	0.7	0.7	1.5
C_u	106	92	93	131
C_c	3.5	1.5	1.4	3.6

	Fuller curve [-]
D60	7.2
D10	0.2
D30	1.8
C_u	36
C_c	2.3

RCM	Initial grading [mm, -]	Dry ball mill [mm, -]	Wet ball mill [mm, -]	Wet mill [mm, -]
D60	9.9	8.0	5.8	9.3
D10	0.1	0.1	0.1	0.1
D30	1.7	0.6	0.6	1.3
C_u	96	130	99	141
C_c	2.9	0.8	1.1	2.9

The Uniformity coeficcient, Curve coeficcient and Fuller curve are defined as follows:

$$C_u = \frac{D_{60}}{D_{10}} \qquad C_c = \frac{D_{30}^2}{D_{60} \cdot D_{10}} \qquad P(d) = \left(\frac{d}{D_{max}}\right)^{0.5} \cdot 100\% \tag{F.1}$$

Where:

C_u = Uniformity coefficient [-]

C_c = Curve coefficient [-]

P = Mass percentage passing [%]

D_n = Particle diameter for which n% is smaller [mm]

d = Particle diameter under consideration [mm]

G

APPENDIX G: MONOTONIC TRIAXIAL TESTING

G.1. MONOTONIC TRIAXIAL TEST RESULTS

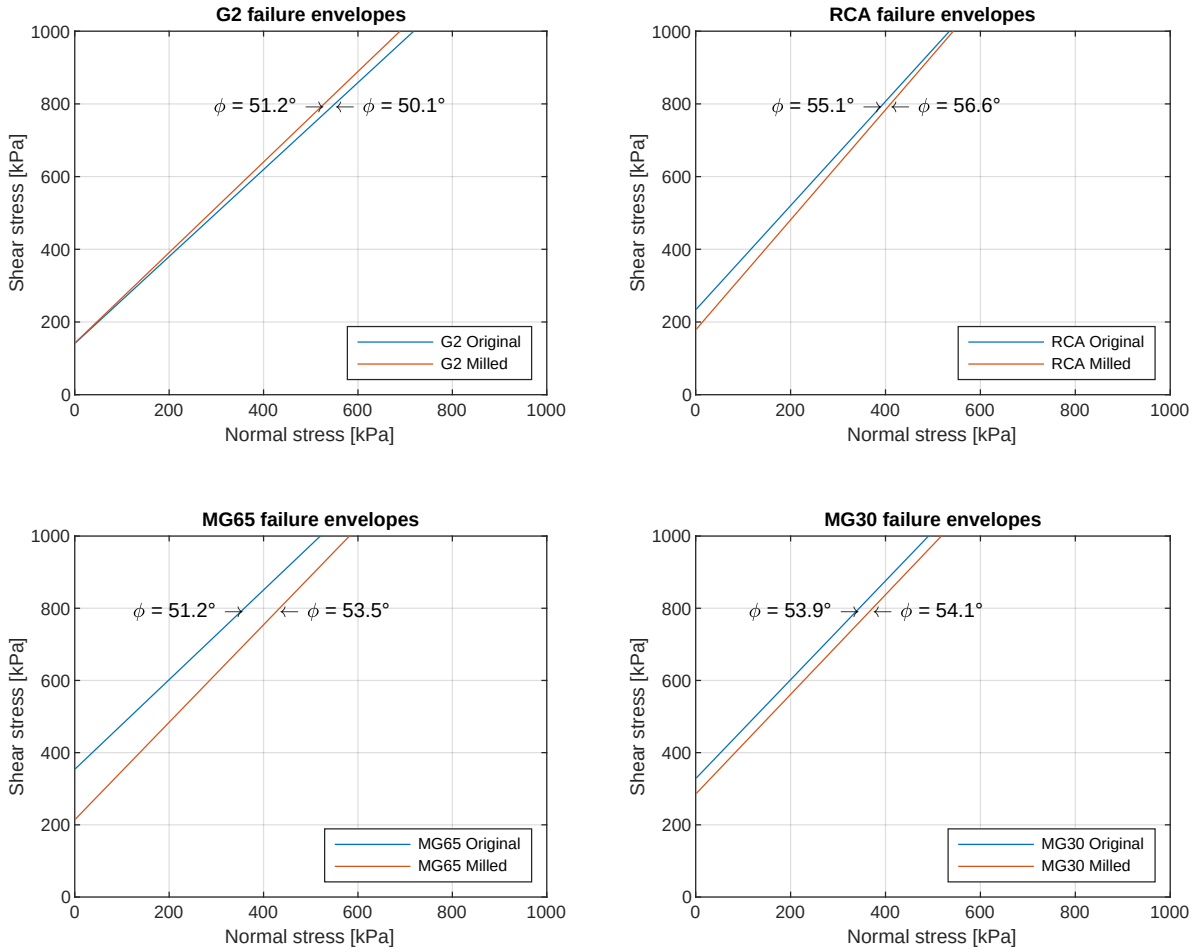

Figure G.1: Comparison of failure envelopes within materials

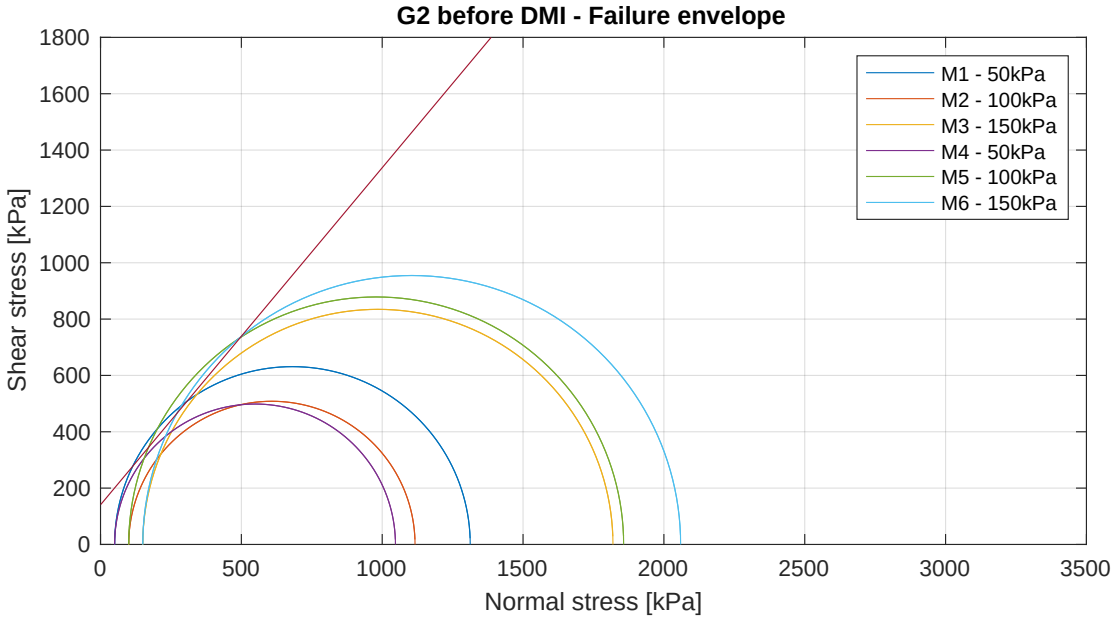

Friction angle = 50.1 degrees
Cohesion = 141 kPa
r-squared = 0.63

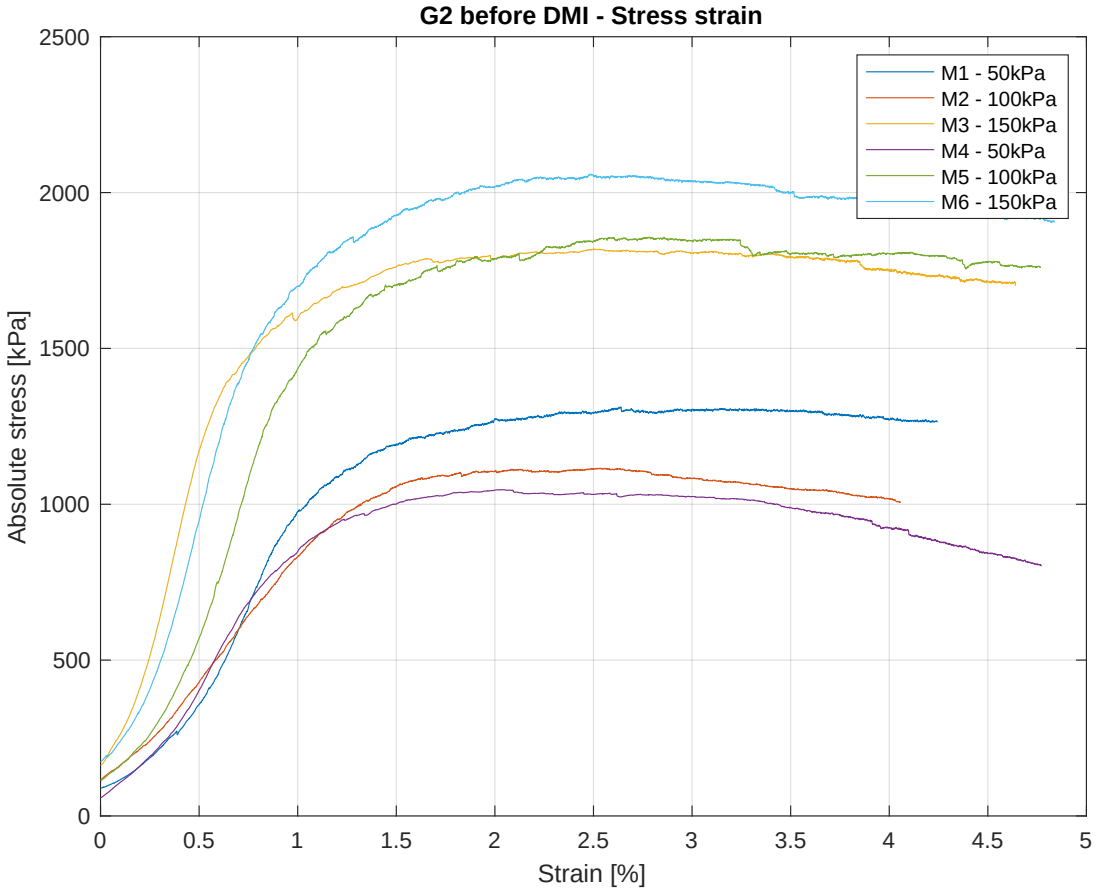

Figure G.2: Monotonic triaxial test results for G2 before durability milling

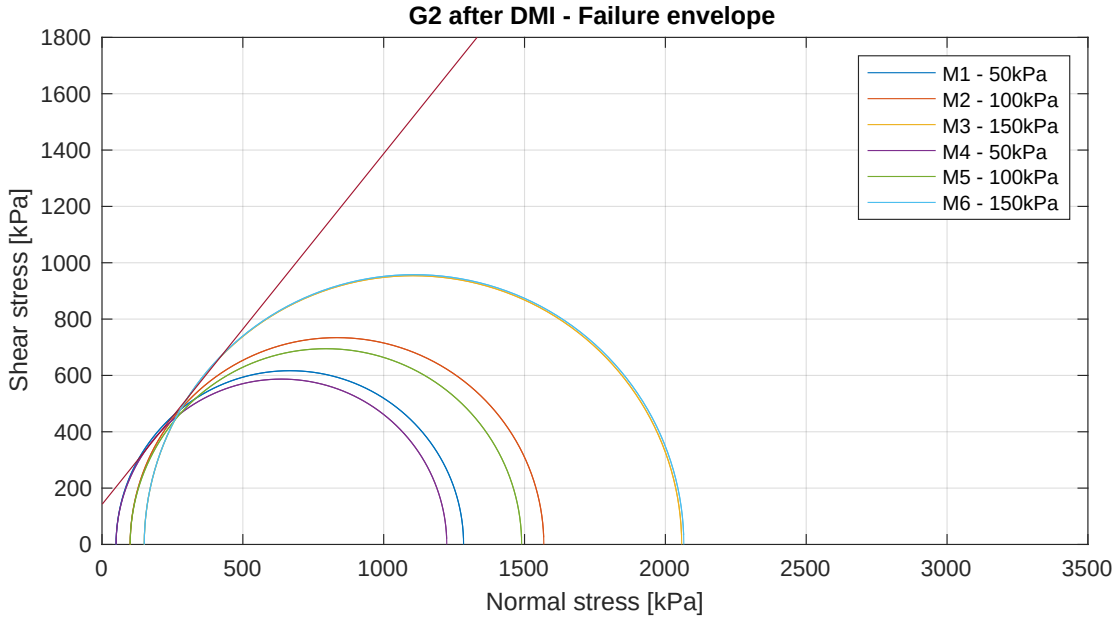

Friction angle = 51.2 degrees
Cohesion = 142 kPa
r-squared = 0.96

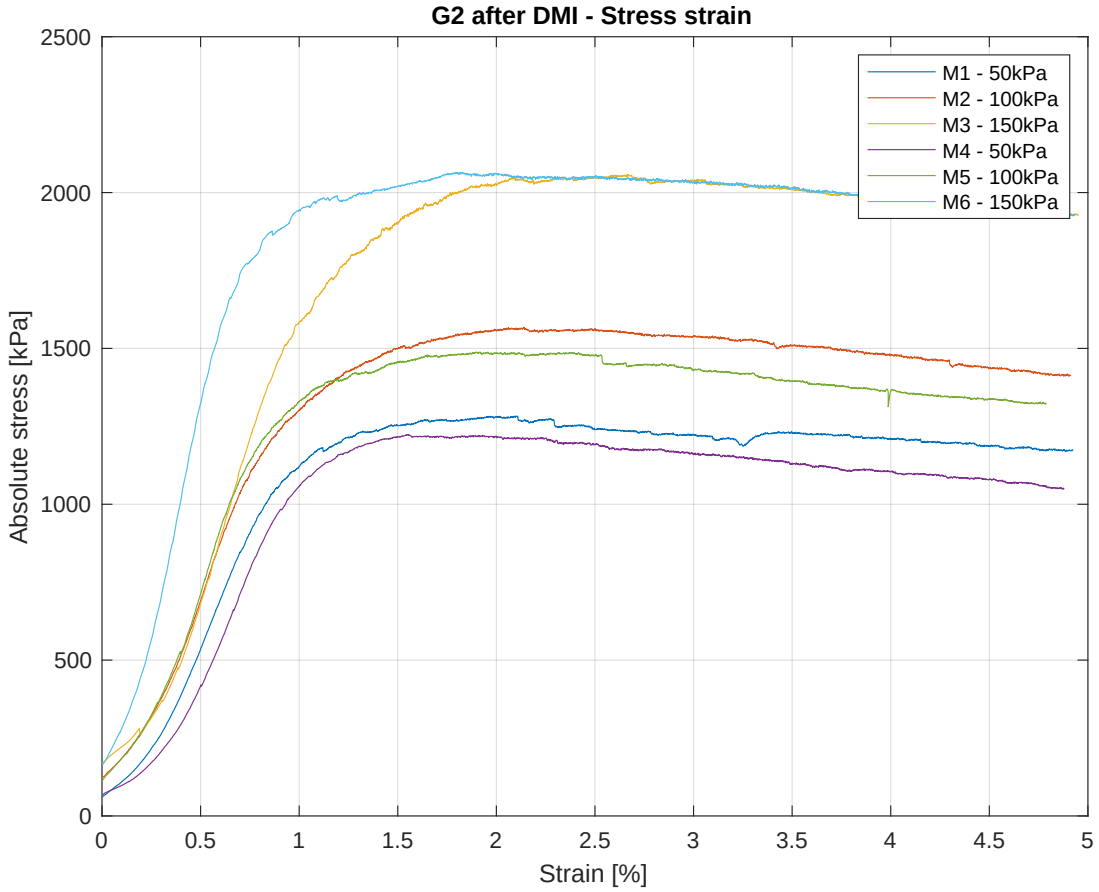

Figure G.3: Monotonic triaxial test results for G2 after durability milling

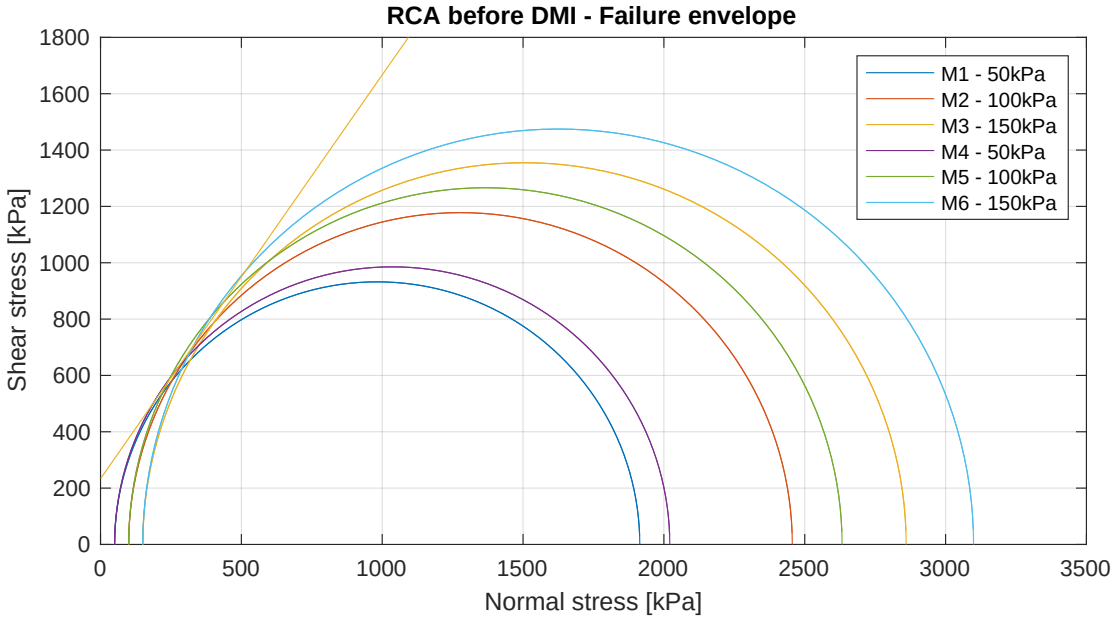

Friction angle = 55.1 degrees
Cohesion = 233 kPa
r-squared = 0.95

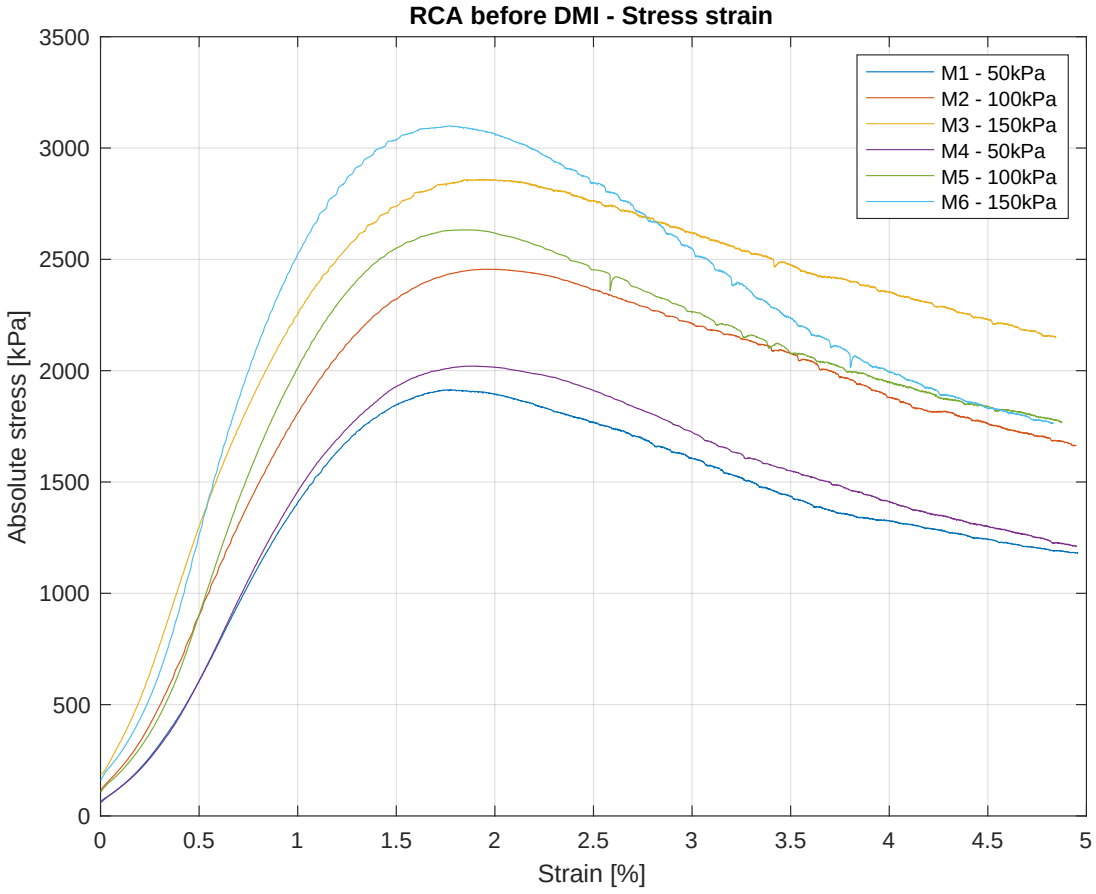

Figure G.4: Monotonic triaxial test results for RCA before durability milling

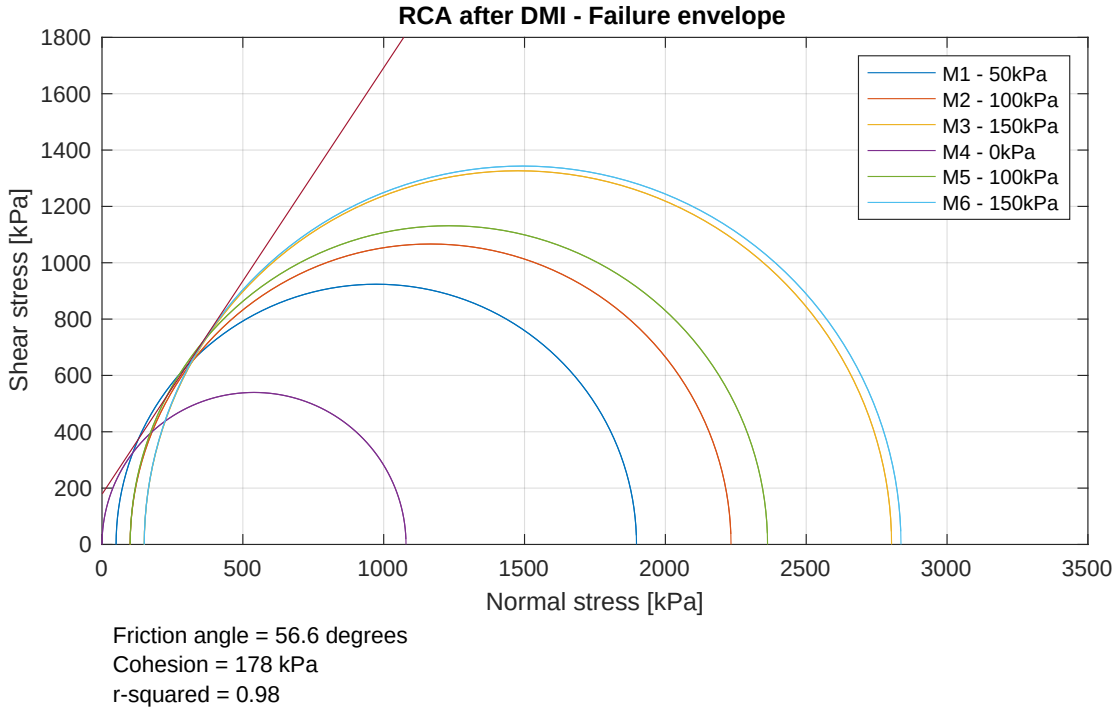

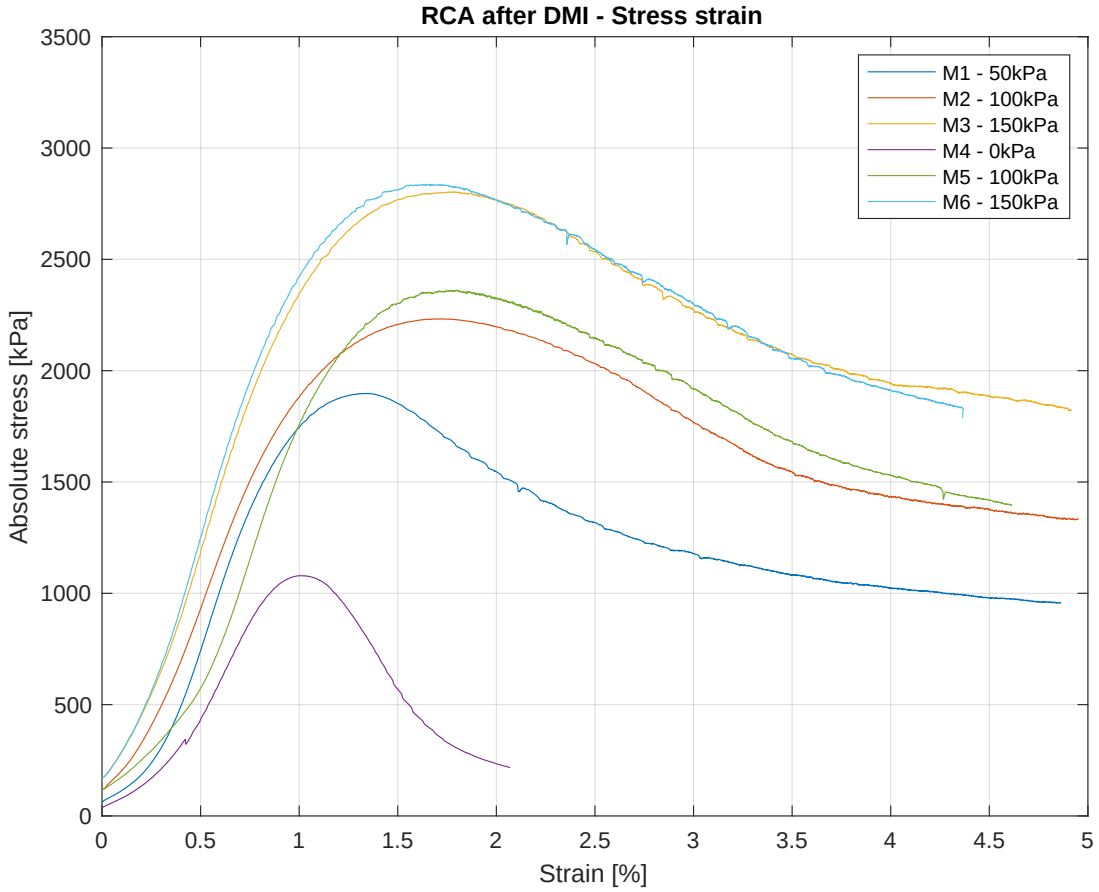

Figure G.5: Monotonic triaxial test results for RCA after durability milling

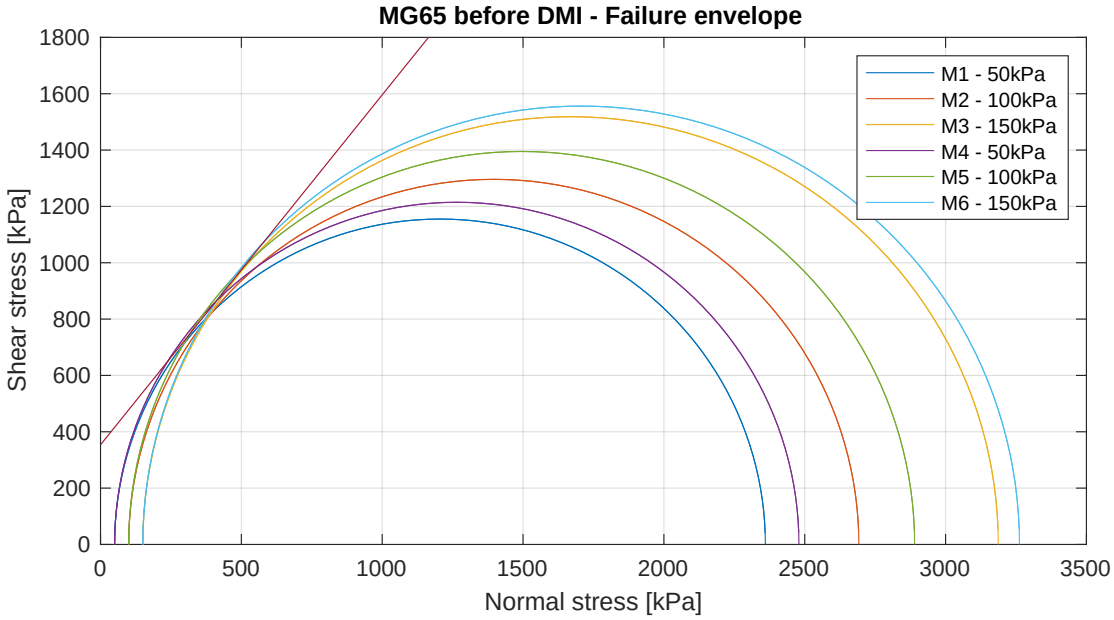

Friction angle = 51.2 degrees
Cohesion = 354 kPa
r-squared = 0.95

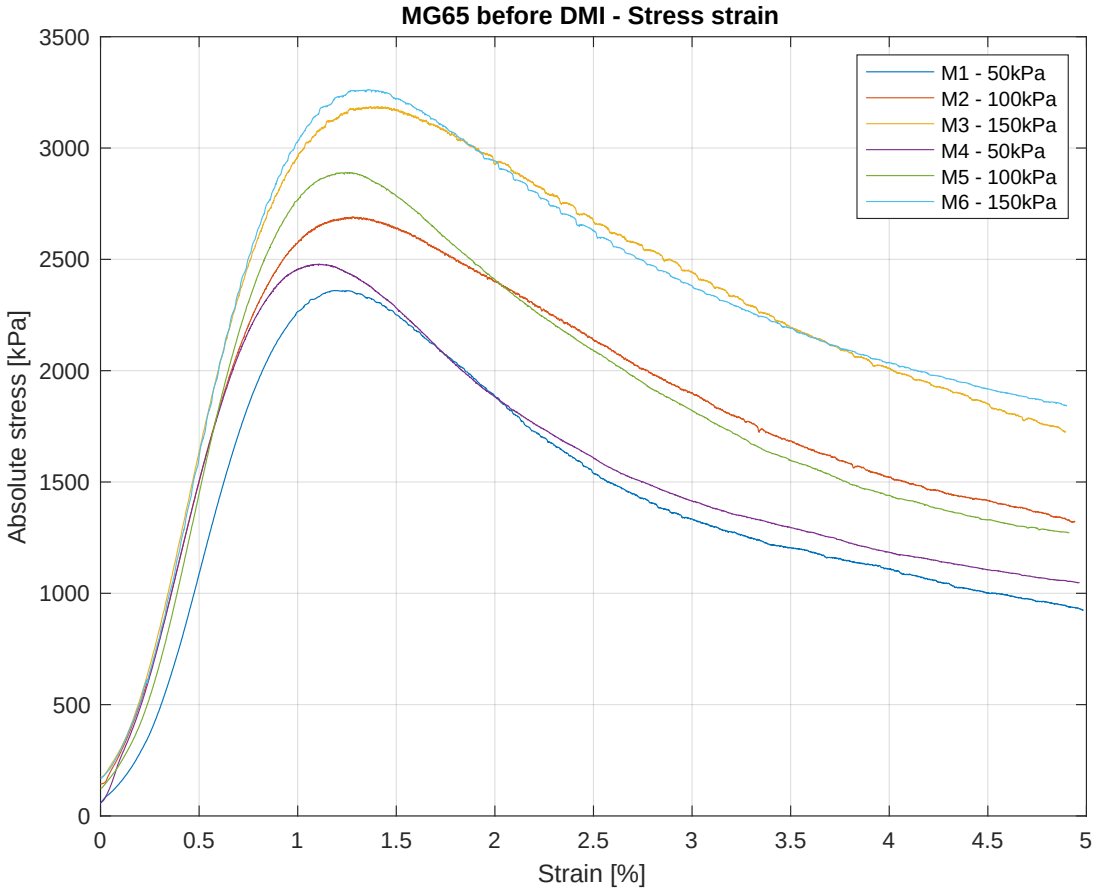

Figure G.6: Monotonic triaxial test results for MG65 before durability milling

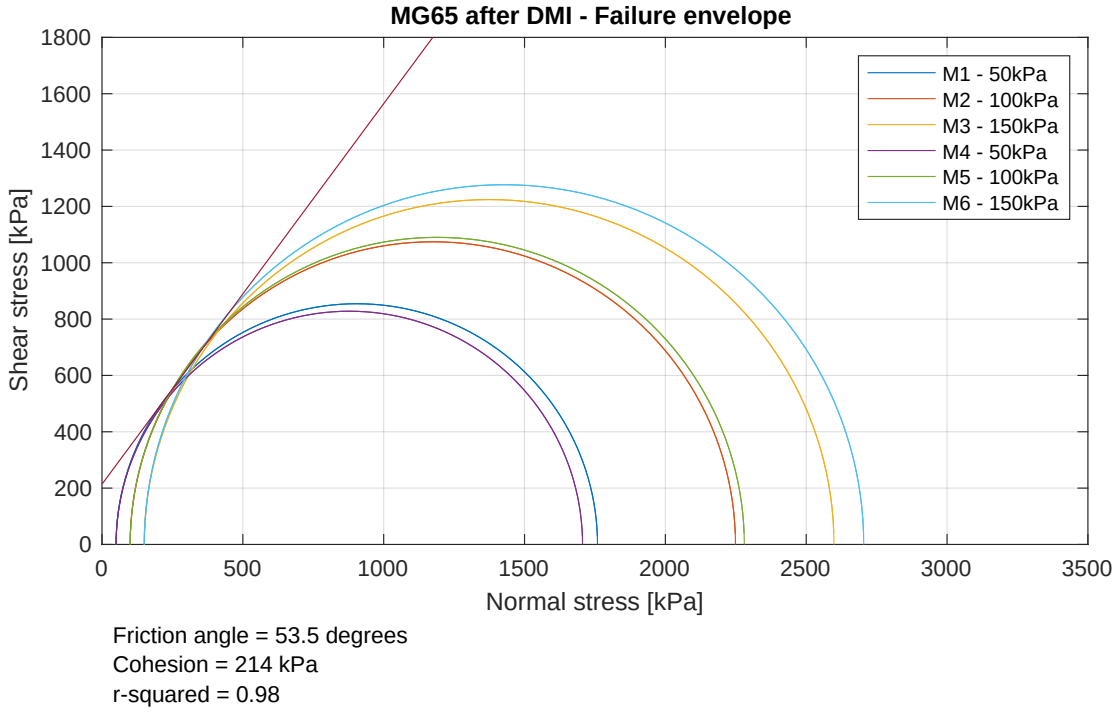

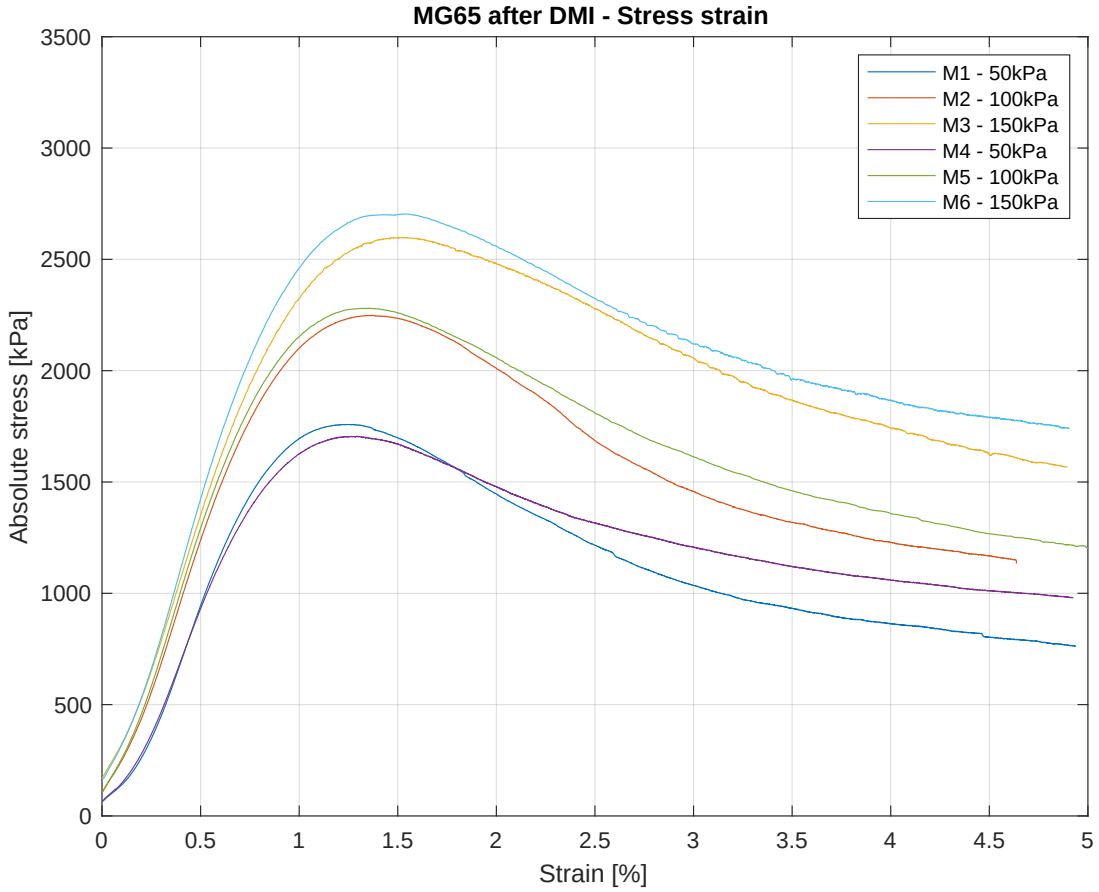

Figure G.7: Monotonic triaxial test results for MG65 after durability milling

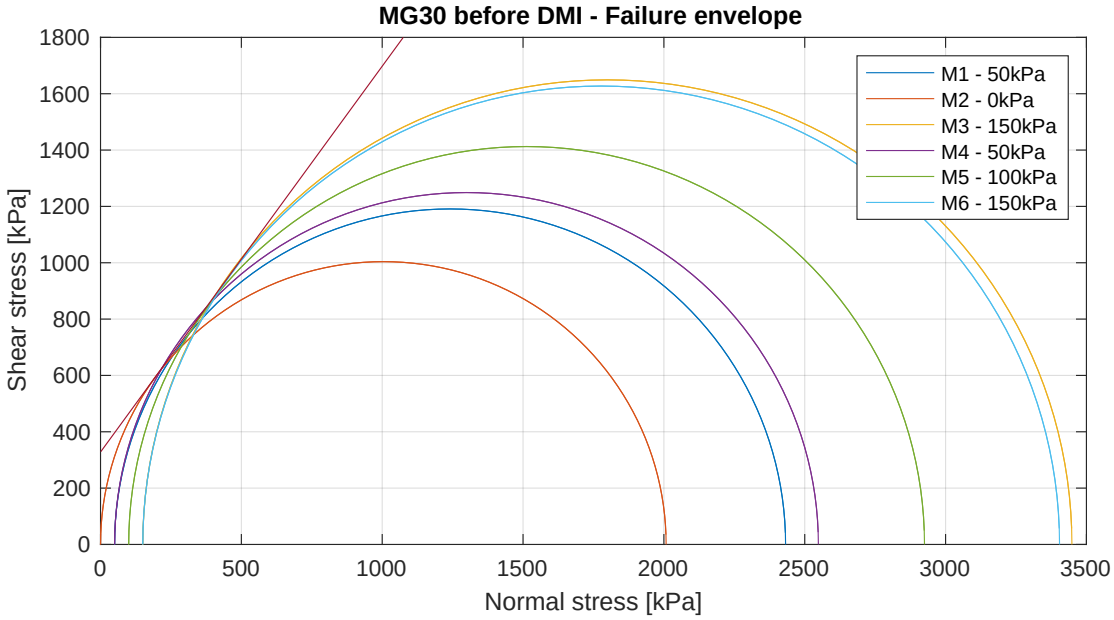

Friction angle = 53.9 degrees
Cohesion = 328 kPa
r-squared = 0.99

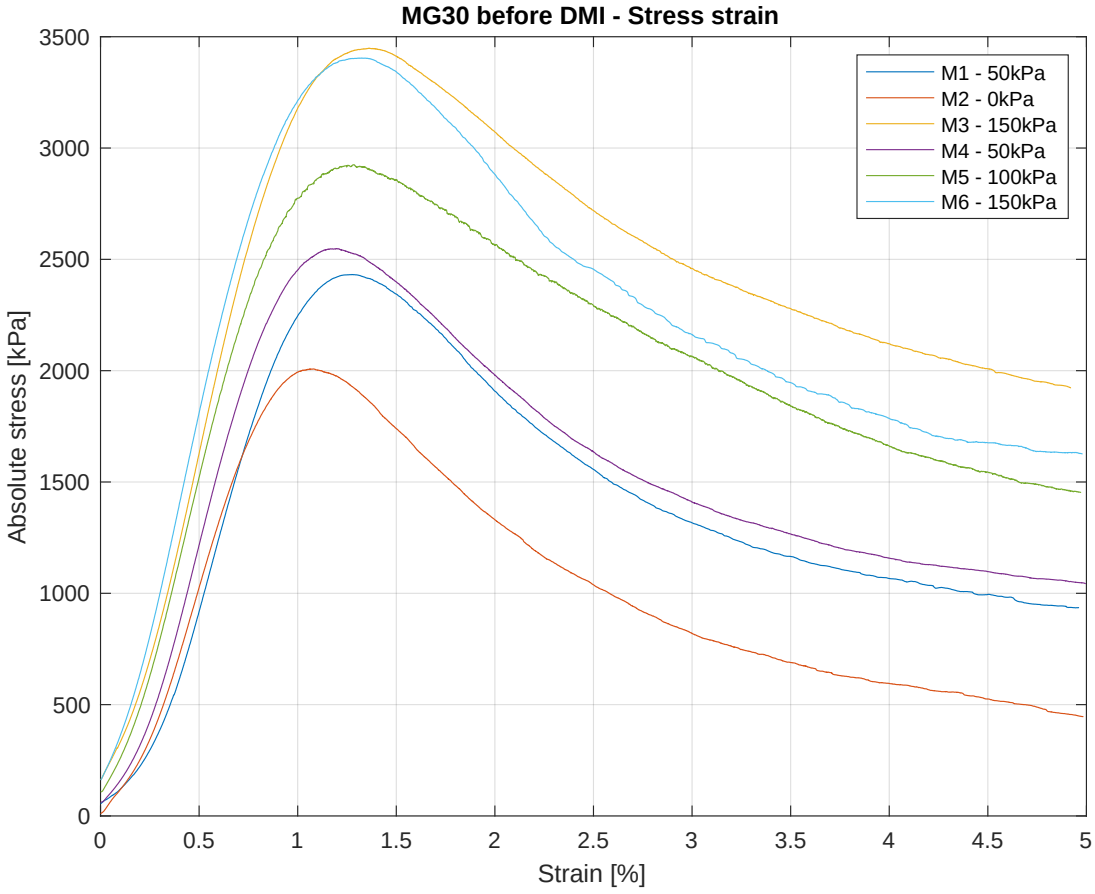

Figure G.8: Monotonic triaxial test results for MG30 before durability milling

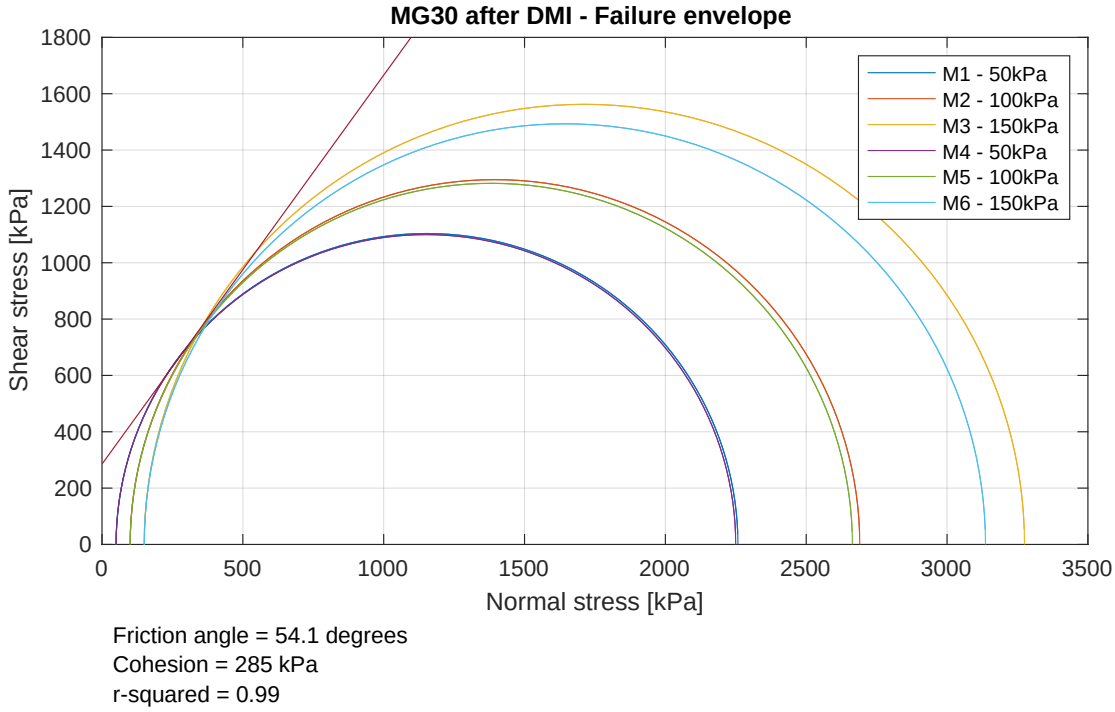

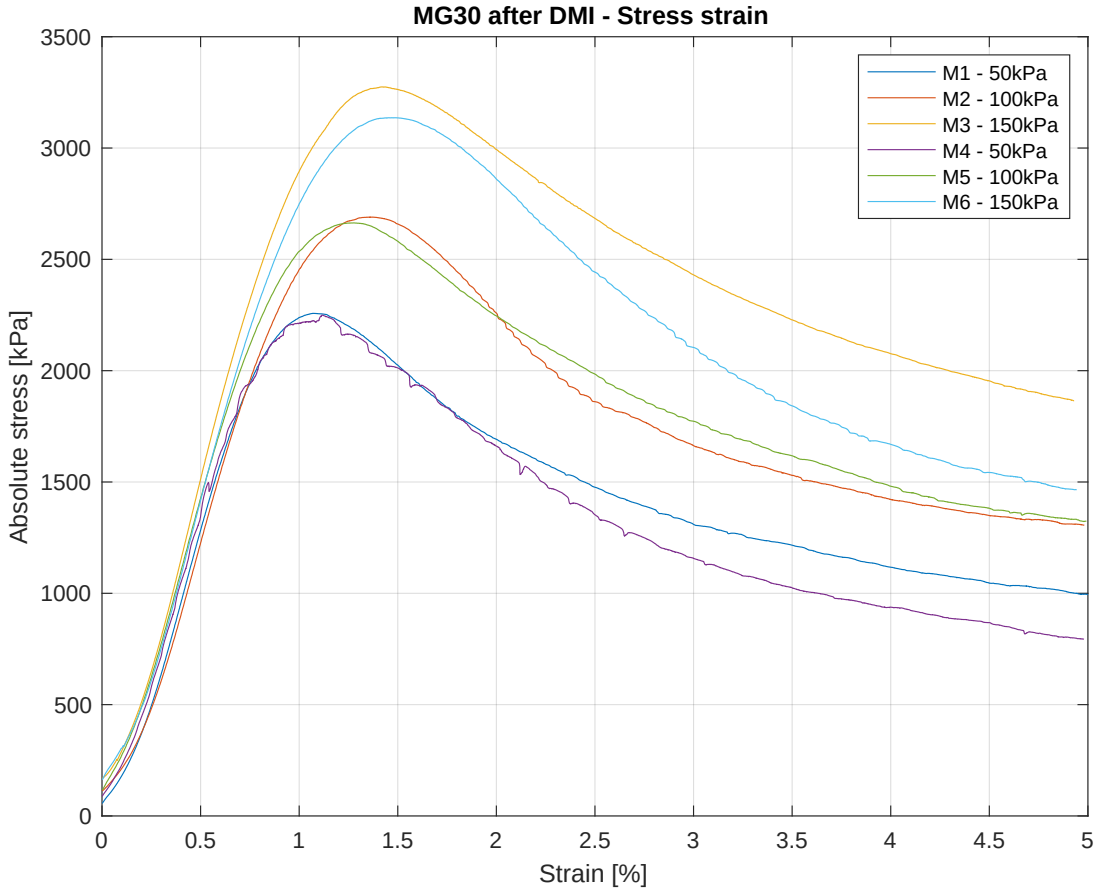

Figure G.9: Monotonic triaxial test results for MG30 after durability milling

Table G.1: Monotonic triaxial test results

Test	Specimen ID	Target MC [%]	Target DD [kg/m^2]	Mixing MC [%]	Specimen MC [%]	Dry density [kg/m^2]	Confinement stress [kPa]	Absolute failure load [kN]	Absolute failure stress [kPa]
G2 before DMI	G2-MONO-M1	3.7	2318	-	3.23	2310	50	23.97	1312
	G2-MONO-M2			-	3.29	2321	100	20.39	1117
	G2-MONO-M3			-	3.31	2322	150	33.23	1819
	G2-MONO-M4			-	3.20	2320	50	19.12	1047
	G2-MONO-M5			-	3.22	2315	100	33.92	1857
	G2-MONO-M6			-	3.23	2324	150	37.62	2059
G2 after DMI	G2-DMIT-M1	3.7	2318	4.07	3.07	2317	50	23.45	1284
	G2-DMIT-M2			3.84	3.15	2319	100	28.65	1568
	G2-DMIT-M3			3.80	3.04	2329	150	37.59	2058
	G2-DMIT-M4			3.66	3.09	2318	50	22.36	1224
	G2-DMIT-M5			3.99	3.20	2335	100	27.21	1490
	G2-DMIT-M6			4.34	3.09	2345	150	37.73	2065
RCA before DMI	RCA-MONO-M1	10	2018	10.16	9.95	2015	50	34.97	1914
	RCA-MONO-M2			10.51	9.95	2023	100	44.86	2456
	RCA-MONO-M3			10.65	10.19	2009	150	52.24	2860
	RCA-MONO-M4			10.56	10.16	2007	50	36.91	2021
	RCA-MONO-M5			10.62	10.16	2013	100	48.09	2633
	RCA-MONO-M6			9.92	10.03	2011	150	56.61	3099
RCA after DMI	RCA-DMIT-M1	10	2018	10.56	8.87	2015	50	34.66	1897
	RCA-DMIT-M2			10.31	9.83	2010	100	40.79	2233
	RCA-DMIT-M3			10.51	9.47	2019	150	51.20	2803
	RCA-DMIT-M4			10.57	9.56	2020	0	19.71	1079
	RCA-DMIT-M5			9.96	9.56	2013	100	43.16	2363
	RCA-DMIT-M6			10.57	9.29	2023	150	51.81	2836
MG65 before DMI	MG65-MONO-M1	10	1905	10.70	9.09	1915	50	43.11	2360
	MG65-MONO-M2			10.49	9.48	1904	100	49.17	2692
	MG65-MONO-M3			10.52	9.33	1909	150	58.21	3187
	MG65-MONO-M4			10.42	9.26	1910	50	45.29	2479
	MG65-MONO-M5			10.23	9.20	1909	100	52.79	2890
	MG65-MONO-M6			10.29	9.29	1909	150	59.59	3262
MG65 after DMI	MG65-DMIT-M1	10	1905	10.13	9.41	1897	50	32.13	1759
	MG65-DMIT-M2			10.22	9.53	1905	100	41.08	2249
	MG65-DMIT-M3			10.45	9.41	1907	150	47.46	2599
	MG65-DMIT-M4			10.08	9.41	1895	50	31.16	1706
	MG65-DMIT-M5			10.01	9.50	1906	100	41.65	2280
	MG65-DMIT-M6			10.17	Unknown	Unknown	150	49.39	2704
MG30 before DMI	MG30-MONO-M1	10.5	1833	11.06	10.09	1842	50	44.42	2432
	MG30-MONO-M2			11.00	9.92	1845	0	36.68	2008
	MG30-MONO-M3			11.03	9.93	1845	150	62.99	3448
	MG30-MONO-M4			10.67	9.98	1847	50	46.55	2548
	MG30-MONO-M5			10.84	9.98	1842	100	53.43	2925
	MG30-MONO-M6			10.72	9.68	1849	150	62.19	3405
MG30 after DMI	MG30-DMIT-M1	10.5	1833	10.70	9.35	1856	50	41.24	2258
	MG30-DMIT-M2			10.77	9.86	1849	100	49.14	2690
	MG30-DMIT-M3			10.85	9.68	1852	150	59.82	3275
	MG30-DMIT-M4			10.79	9.95	1847	50	41.09	2250
	MG30-DMIT-M5			10.72	Unknown	Unknown	100	48.66	2664
	MG30-DMIT-M6			10.87	Unknown	Unknown	150	57.29	3136

Table G.2: Shear properties of the tested materials

Material	Friction angle [°]	Cohesion [kPa]	R^2 [-]
G2 before DMI	50.1	141	0.63
G2 after DMI	51.2	142	0.96
RCA before DMI	55.1	233	0.95
RCA after DMI	56.6	178	0.98
MG65 before DMI	51.2	354	0.95
MG65 after DMI	53.5	214	0.98
MG30 before DMI	53.9	328	0.99
MG30 after DMI	54.1	285	0.99

G.2. MONOTONIC TRIAXIAL TEST ANALYSIS

Table G.3: Monotonic triaxial test analysis: Youngs modulus estimation and dissipated energy calculations

	Confinement [kPa]	Absolute failure stress [kPa]	Estimated Youngs modulus [MPa]	Dissipated energy 4% strain [kPa]	Dissipated energy up to failure [kPa]	Dissipated energy 5% fracture [kPa]
G2-MONO-M1	50	1312	121	40	23	20
G2-MONO-M2	100	1116	81	33	19	8
G2-MONO-M3	150	1819	257	59	34	30
G2-MONO-M4	50	1047	106	33	14	14
G2-MONO-M5	100	1857	183	57	36	32
G2-MONO-M6	150	2060	236	65	36	30
G2-DMIT-M1	50	1284	148	41	19	12
G2-DMIT-M2	100	1569	165	50	22	25
G2-DMIT-M3	150	2058	203	63	37	38
G2-DMIT-M4	50	1224	135	39	11	17
G2-DMIT-M5	100	1490	166	47	20	19
G2-DMIT-M6	150	2066	294	68	26	49
RCA-MONO-M1	50	1915	167	55	19	10
RCA-MONO-M2	100	2456	204	73	29	16
RCA-MONO-M3	150	2860	252	87	35	20
RCA-MONO-M4	50	2021	178	58	23	11
RCA-MONO-M5	100	2633	254	77	30	13
RCA-MONO-M6	150	3099	317	89	33	15
RCA-DMIT-M1	50	1898	259	49	14	5
RCA-DMIT-M2	100	2233	231	64	24	11
RCA-DMIT-M3	150	2803	278	81	31	13
RCA-DMIT-M4	0	1079	134	11	5	2
RCA-DMIT-M5	100	2363	231	65	24	11
RCA-DMIT-M6	150	2837	294	82	29	14
MG65-MONO-M1	50	2360	319	59	15	7
MG65-MONO-M2	100	2692	346	76	21	10
MG65-MONO-M3	150	3187	392	92	28	13
MG65-MONO-M4	50	2480	348	64	16	7
MG65-MONO-M5	100	2890	385	76	21	8
MG65-MONO-M6	150	3262	400	91	26	12
MG65-DMIT-M1	50	1759	246	46	13	5
MG65-DMIT-M2	100	2249	273	61	19	9
MG65-DMIT-M3	150	2598	278	76	24	13
MG65-DMIT-M4	50	1706	229	48	13	6
MG65-DMIT-M5	100	2280	283	64	19	9
MG65-DMIT-M6	150	2704	304	79	26	11
MG30-MONO-M1	50	2432	313	59	16	6
MG30-MONO-M2	0	2008	290	45	12	4
MG30-MONO-M3	150	3449	386	96	27	12
MG30-MONO-M4	50	2549	340	64	17	7
MG30-MONO-M5	100	2925	362	81	22	10
MG30-MONO-M6	150	3405	401	90	27	10
MG30-DMIT-M1	50	2258	319	58	13	6
MG30-DMIT-M2	100	2690	314	69	21	8
MG30-DMIT-M3	150	3275	353	92	27	12
MG30-DMIT-M4	50	2250	309	55	15	4
MG30-DMIT-M5	100	2664	321	72	20	8
MG30-DMIT-M6	150	3137	332	83	27	11

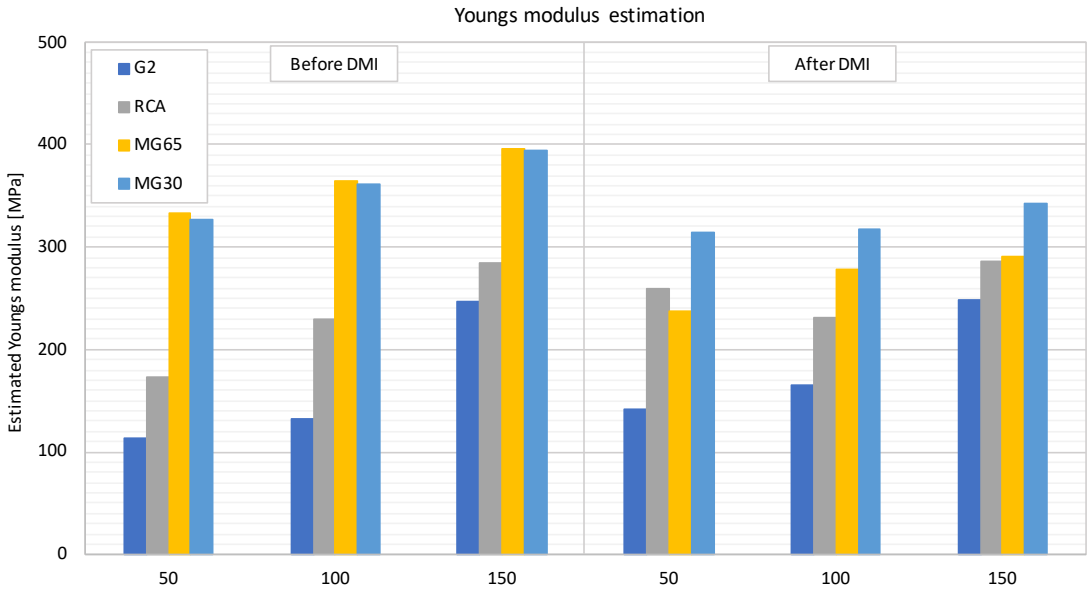

Figure G.10: Average linear estimated Youngs moduli obtained after monotonic triaxial testing

Table G.4: Average linear estimated Youngs moduli obtained after monotonic triaxial testing

		Before DMI			After DMI		
Confinement stress	[kPa]	50	100	150	50	100	150
G2	[MPa]	113	132	246	142	165	249
RCA	[MPa]	173	229	284	259	231	286
MG65	[MPa]	333	365	396	237	278	291
MG30	[MPa]	326	362	394	314	318	342

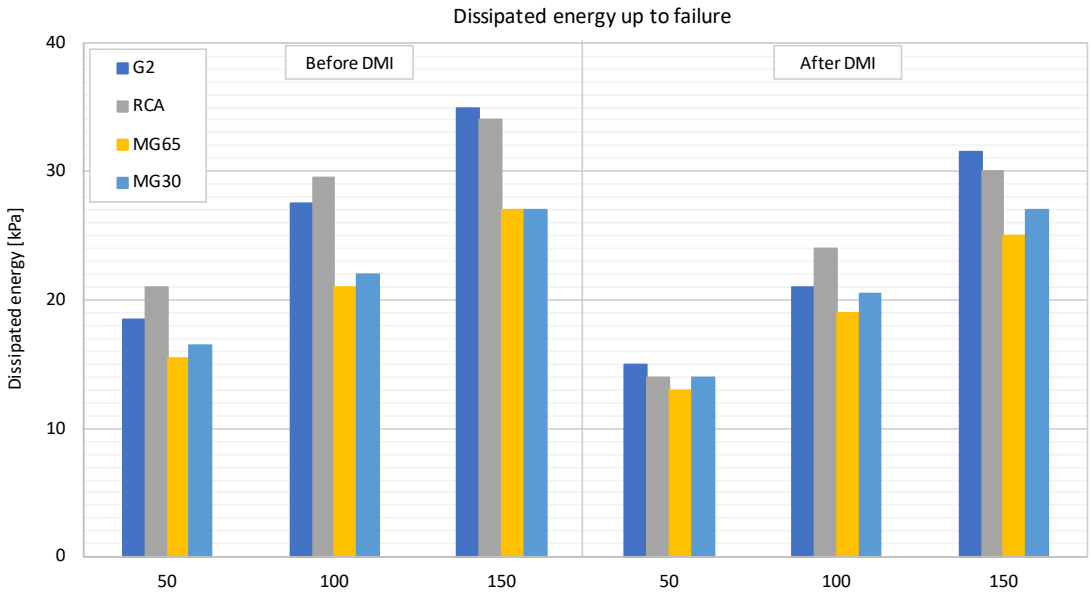

Figure G.11: Average energy dissipation up to failure after monotonic triaxial testing

Table G.5: Average energy dissipation up to failure after monotonic triaxial testing

		Before DMI			After DMI		
Confinement stress	[kPa]	50	100	150	50	100	150
G2	[kPa]	19	28	35	15	21	32
RCA	[kPa]	21	30	34	14	24	30
MG65	[kPa]	16	21	27	13	19	25
MG30	[kPa]	17	22	27	14	21	27

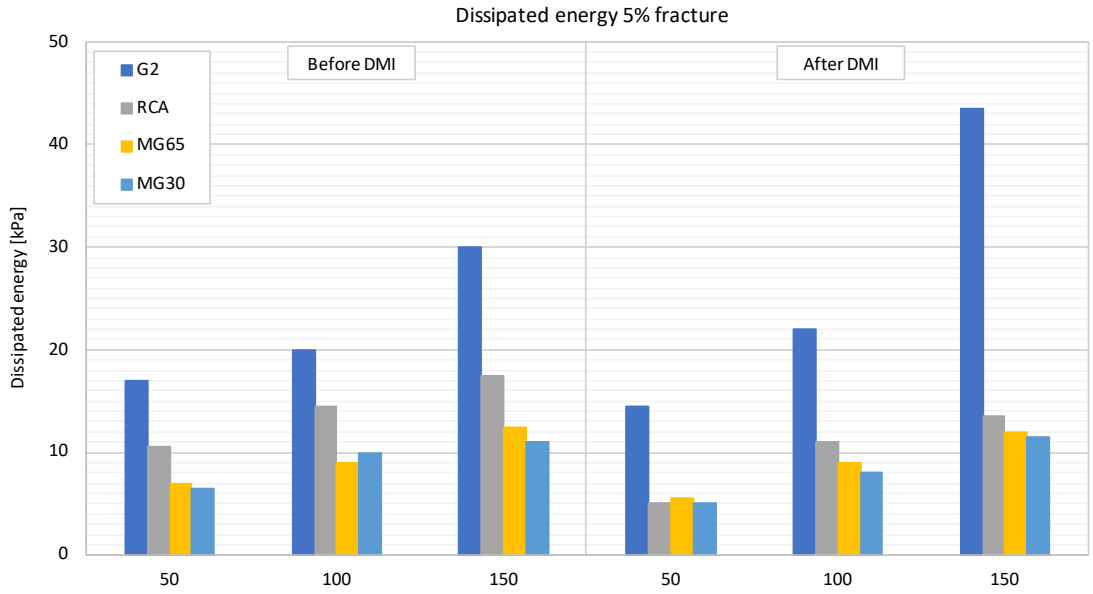

Figure G.12: Dissipated energy between failure and 5% fracture after monotonic triaxial testing

Table G.6: Dissipated energy between failure and 5% fracture after monotonic triaxial testing

		Before DMI			After DMI		
Confinement stress	[kPa]	50	100	150	50	100	150
G2	[kPa]	17	20	30	15	22	44
RCA	[kPa]	11	15	18	5	11	14
MG65	[kPa]	7	9	13	6	9	12
MG30	[kPa]	7	10	11	5	8	12

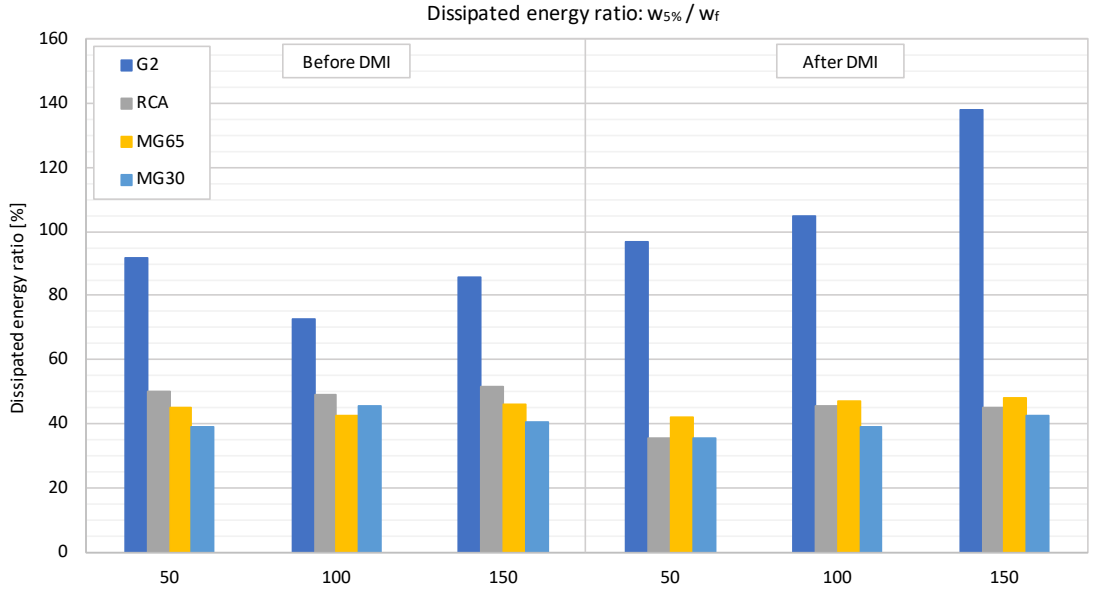

Figure G.13: Dissipated energy ratio ($w_{5\%}$ / w_f) after monotonic triaxial testing

Table G.7: Dissipated energy ratio ($w_{5\%}$ / w_f) after monotonic triaxial testing

		Before DMI			After DMI		
Confinement stress	[kPa]	50	100	150	50	100	150
G2	[%]	92	73	86	97	105	138
RCA	[%]	50	49	51	36	46	45
MG65	[%]	45	43	46	42	47	48
MG30	[%]	39	45	41	36	39	43

H

APPENDIX H: PERMANENT DEFORMATION TRIAXIAL TESTING

H.1. PERMANENT DEFORMATION SPECIMEN DETAILS

Table H.1: Permanent deformation triaxial test results at 100 kPa confinement

Triaxial test specimen details

Test	Specimen ID	Target MC [%]	Target DD [kg/m^2]	Mixing MC [%]	Specimen MC [%]	Dry mass [kg]	Height [mm]	Dry density [kg/m^2]
RCA before DMI	RCA-PERM-PD1	10	2018	10.59	9.87	11.019	302.00	1998
	RCA-PERM-PD2			10.64	9.83	11.023	298.00	2025
	RCA-PERM-PD3			10.60	9.49	11.060	299.50	2022
RCA after DMI	RCA-DMIT-PD1	10	2018	10.26	9.50	11.042	299.75	2017
	RCA-DMIT-PD2			10.64	9.14	11.083	300.25	2021
	RCA-DMIT-PD3			10.65	9.26	11.058	306.50	1975
MG65 before DMI	MG65-PERM-PD1	10	1905	10.59	9.31	10.402	297.75	1913
	MG65-PERM-PD2			10.24	8.93	10.435	298.25	1916
	MG65-PERM-PD3			10.19	9.29	10.398	298.00	1910
MG65 after DMI	MG65-DMIT-PD1	10	1905	10.31	9.35	10.395	298.25	1908
	MG65-DMIT-PD2			10.66	9.23	10.409	298.50	1909
	MG65-DMIT-PD3			10.34	9.32	10.394	300.25	1895

Triaxial test loading conditions

Test	Specimen ID	Confinement [kPa]	Target DSR [%]	Static deviator failure stress [kPa]	Applied deviator load [kN]	Applied deviator stress [kPa]	Actual DSR [%]	Absolute residual strength [kPa]
RCA before DMI	RCA-PERM-PD1	100	25	2395	9.98	546	22.82	2251
	RCA-PERM-PD2	100	30		11.98	656	27.39	2418
	RCA-PERM-PD3	100	35		13.98	765	31.96	2791
RCA after DMI	RCA-DMIT-PD1	100	25	2198	9.98	546	24.87	2360
	RCA-DMIT-PD2	100	30		11.98	656	29.85	2312
	RCA-DMIT-PD3	100	35		13.98	765	34.83	Failed in PD test
MG65 before DMI	MG65-PERM-PD1	100	25	2717	9.93	544	20.01	2268
	MG65-PERM-PD2	100	30		11.88	650	23.94	2239
	MG65-PERM-PD3	100	35		13.88	760	27.98	2674
MG65 after DMI	MG65-DMIT-PD1	100	25	2118	9.93	544	25.68	1814
	MG65-DMIT-PD2	100	30		11.88	650	30.72	2091
	MG65-DMIT-PD3	100	35		13.88	760	35.89	2075

H.2. RCA BEFORE DMI

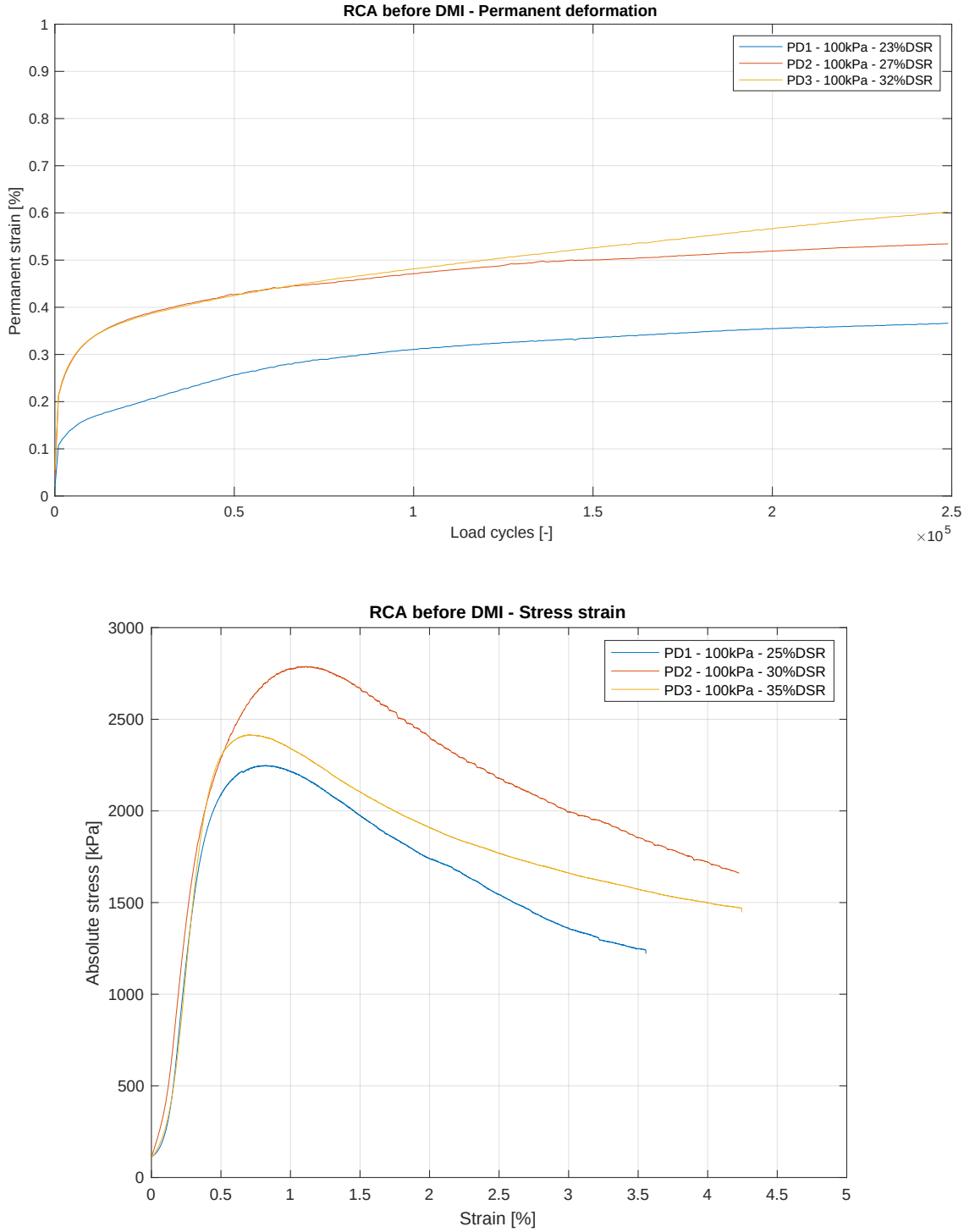

Figure H.1: Permanent deformation triaxial test results for unmilled RCA **Top:** Permanent strain versus the number of load cycles **Bottom:** Monotonic triaxial test results after permanent deformation triaxial testing

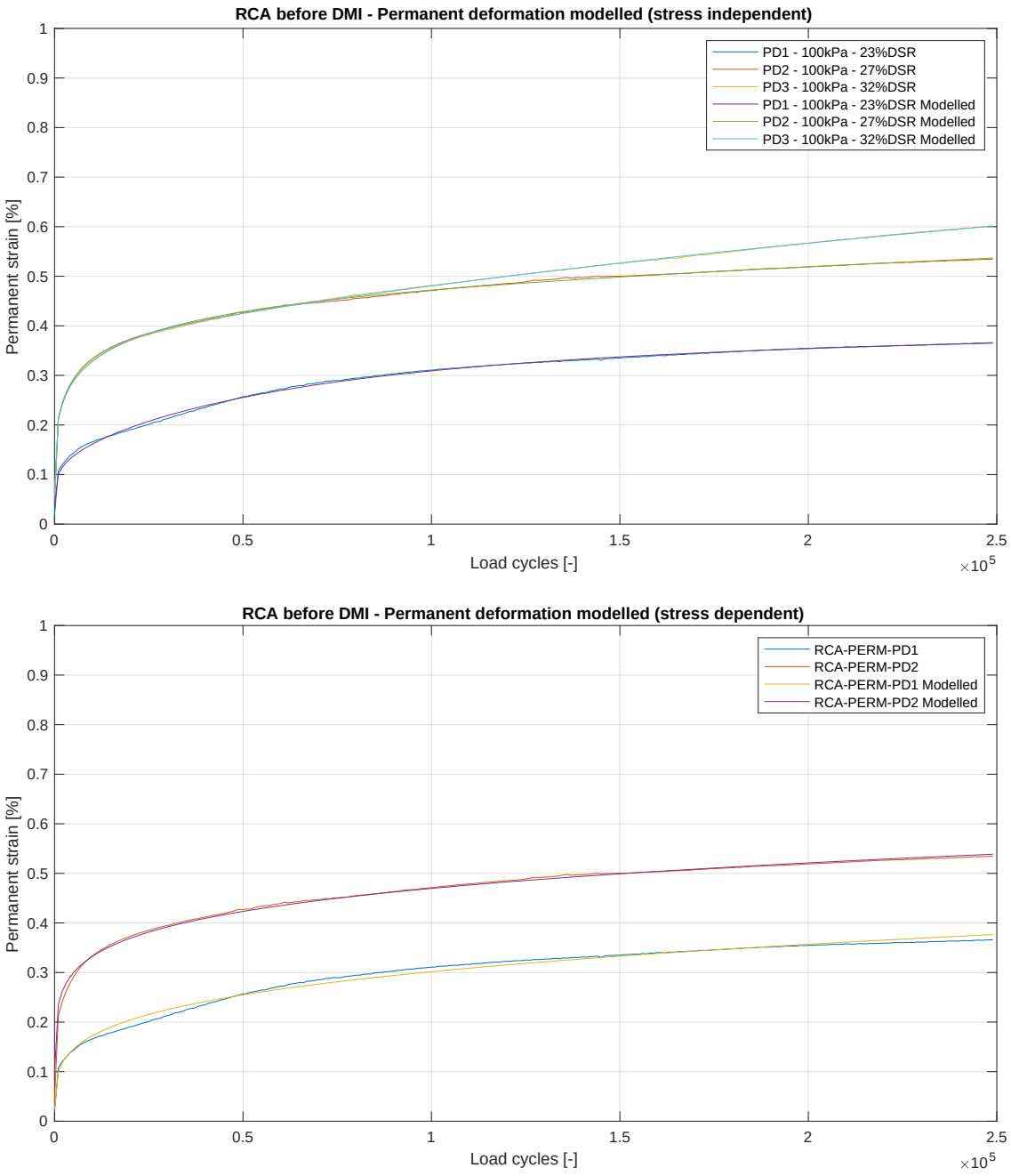

Figure H.2: Permanent deformation triaxial test models (Huurman) for unmilled RCA **Top:** Stress independent (4 coefficients including unstable behavior, different for all tests) **Bottom:** Stress dependent (4 coefficients excluding unstable behavior, based on two tests up to 30% DSR)

Table H.2: Permanent deformation model parameters for RCA before DMI

RCA before DMI	Actual DSR [%]	A [%]	B [-]	C [%]	D [-]	$\sum d^2$	R^2
RCA-PERM-PD1	22.82	0.0983	0.1595	-0.1305	-0.0161	0.0020	0.9979
RCA-PERM-PD2	27.39	0.2123	0.1990	0.1266	-0.0063	0.0018	0.9983
RCA-PERM-PD3	31.96	0.2127	0.2253	0.1372	-0.0207	0.0004	0.9998

RCA before DMI	Actual DSR [%]	a_1 [%]	a_2 [-]	b_1 [-]	b_2 [-]	$\sum d^2$	R^2
RCA-PERM-PD1	22.82	112.5222	4.7650	0.0049	-2.6362	0.0121	0.9878
RCA-PERM-PD2	27.39					0.0067	0.9938
					Full dataset match	**0.0188**	**0.9909**

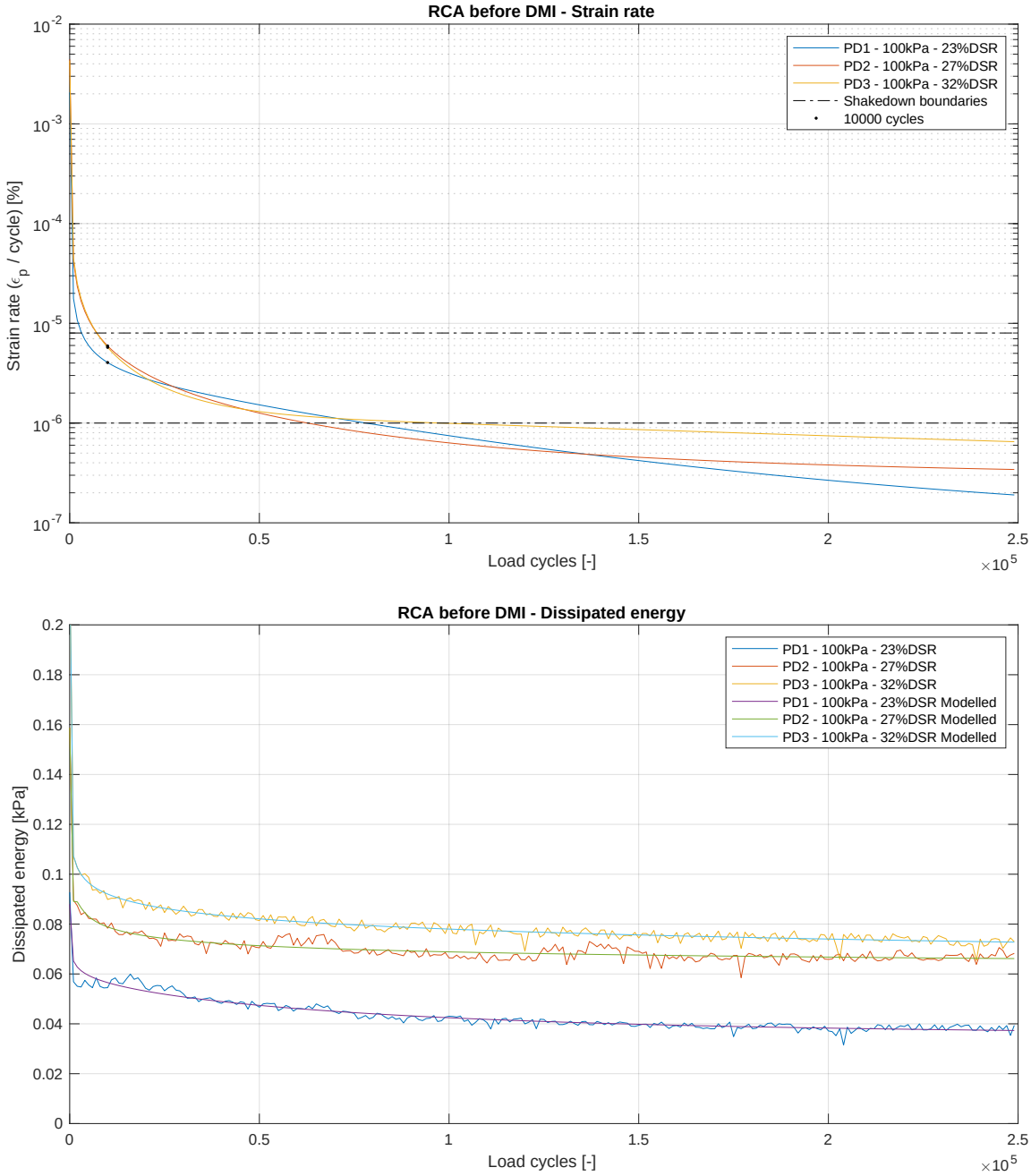

Figure H.3: Permanent deformation triaxial test calculations for unmilled RCA **Top:** Strain rate versus number of load cycles **Bottom:** Dissipated energy per load cycle (real and Huurman modelled)

Table H.3: Dissipated energy model parameters for RCA before DMI

RCA before DMI	Actual DSR [%]	A [kPa]	B [-]	C [kPa]	D [-]	$\sum d^2$	R^2
RCA-PERM-PD1	22.82	0.0654	-0.0511	0.0124	-0.0136	0.0007	0.9331
RCA-PERM-PD2	27.39	0.0412	-0.2317	-0.0547	-2.0811	0.0010	0.9188
RCA-PERM-PD3	31.96	0.1831	-0.0380	0.0757	-10.0000	0.0007	0.9774

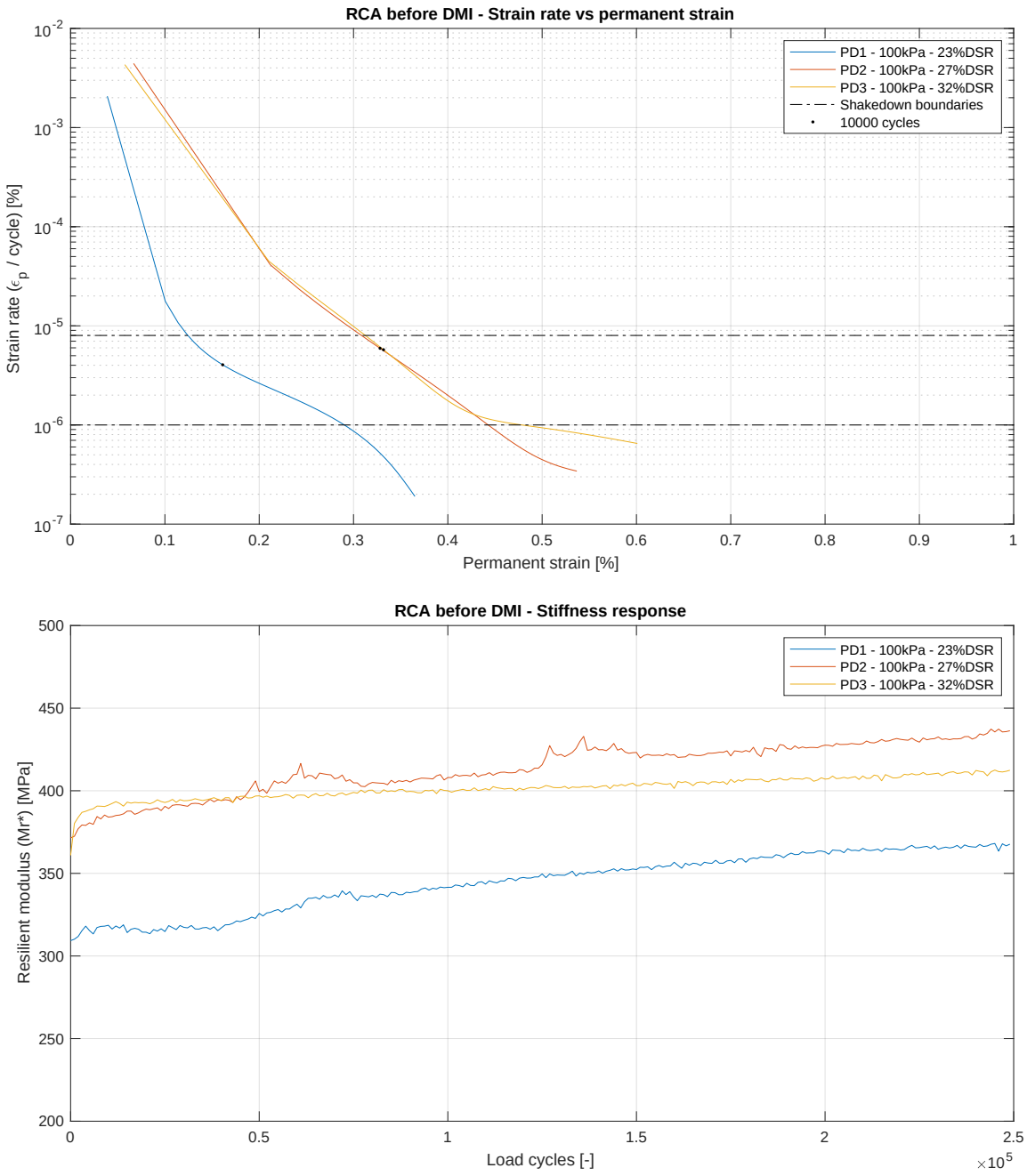

Figure H.4: Permanent deformation triaxial test calculations for unmilled RCA **Top:** Strain rate versus permanent deformation **Bottom:** Stiffness response

H.3. RCA AFTER DMI

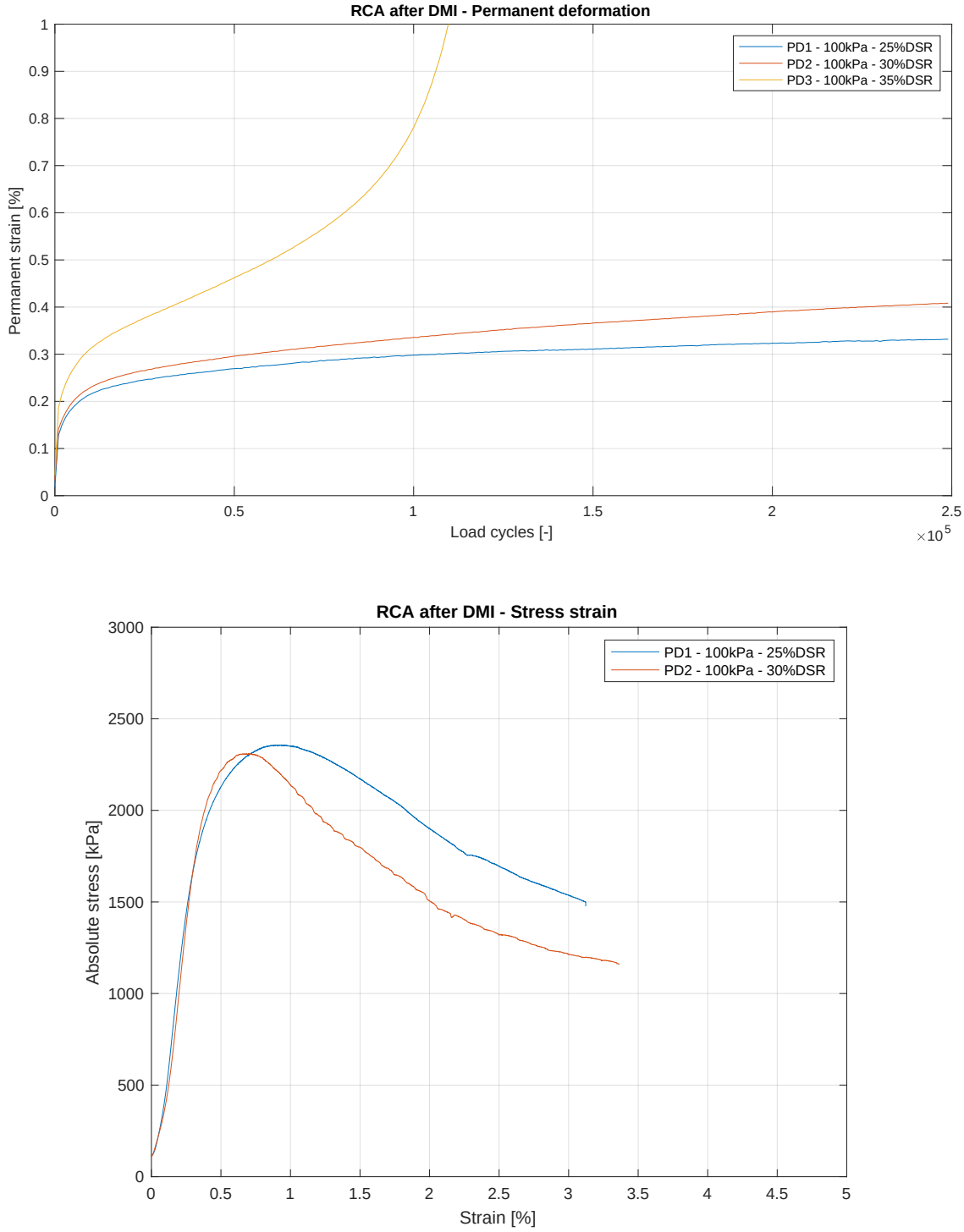

Figure H.5: Permanent deformation triaxial test results for milled RCA **Top:** Permanent strain versus the number of load cycles **Bottom:** Monotonic triaxial test results after permanent deformation triaxial testing

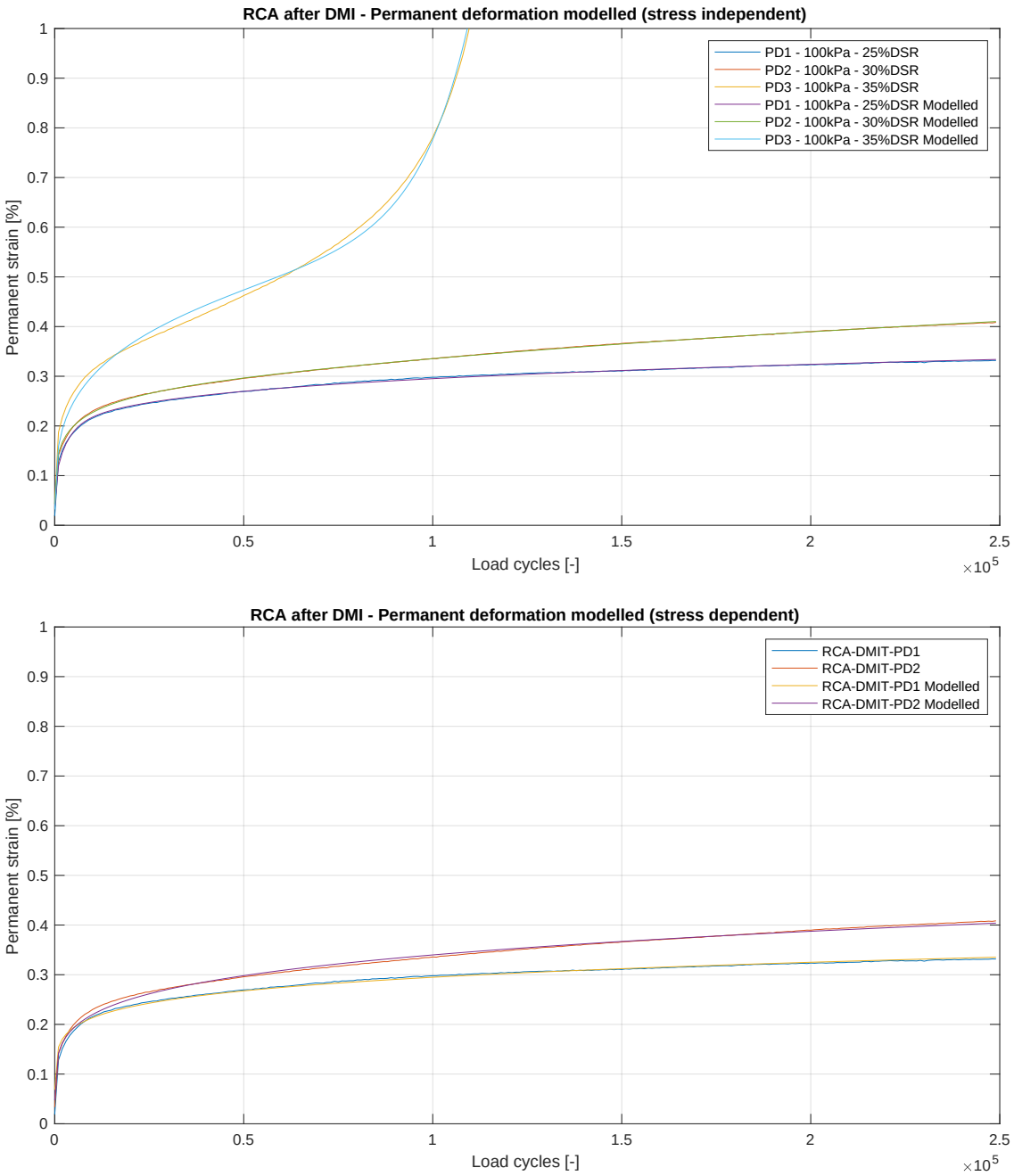

Figure H.6: Permanent deformation triaxial test models (Huurman) for milled RCA **Top:** Stress independent (4 coefficients including unstable behavior, different for all tests) **Bottom:** Stress dependent (4 coefficients excluding unstable behavior, based on two tests up to 30% DSR)

Table H.4: Permanent deformation model parameters for RCA after DMI

RCA after DMI	Actual DSR [%]	A [%]	B [-]	C [%]	D [-]	$\sum d^2$	R^2
RCA-DMIT-PD1	24.87	0.1014	0.1735	-0.0698	-0.3033	0.0011	0.9973
RCA-DMIT-PD2	29.85	0.1463	0.2109	0.0589	-0.0203	0.0004	0.9995
RCA-DMIT-PD3	34.83	0.1588	0.2769	0.0001	0.0760	0.0219	0.9985

RCA after DMI	Actual DSR [%]	a_1 [%]	a_2 [-]	b_1 [-]	b_2 [-]	$\sum d^2$	R^2
RCA-DMIT-PD1	24.87	0.0827	-0.4481	1.3505	1.6256	0.0051	0.9868
RCA-DMIT-PD2	29.85					0.0037	0.9954
					Full dataset match	**0.0089**	**0.9926**

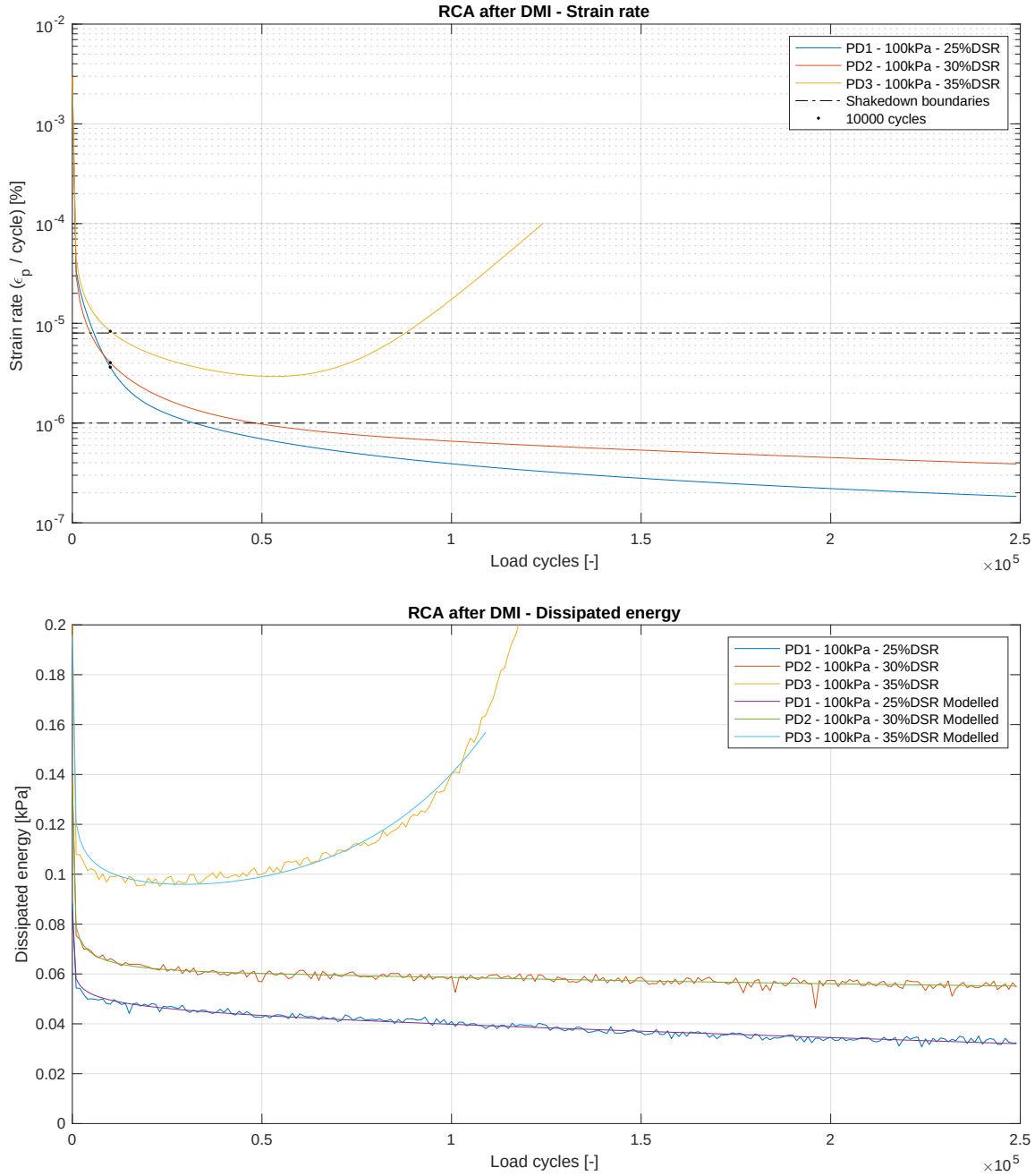

Figure H.7: Permanent deformation triaxial test calculations for milled RCA **Top:** Strain rate versus number of load cycles **Bottom:** Dissipated energy per load cycle (real and Huurman modelled)

Table H.5: Dissipated energy model parameters for RCA after DMI

RCA after DMI	Actual DSR [%]	A [kPa]	B [-]	C [kPa]	D [-]	$\sum d^2$	R^2
RCA-DMIT-PD1	24.87	0.0581	-0.0665	-0.0175	0.0015	0.0003	0.9668
RCA-DMIT-PD2	29.85	0.0787	-0.0955	-0.0087	-0.0237	0.0005	0.9494
RCA-DMIT-PD3	34.83	0.1204	-0.0835	0.0043	0.0268	0.0011	0.9706

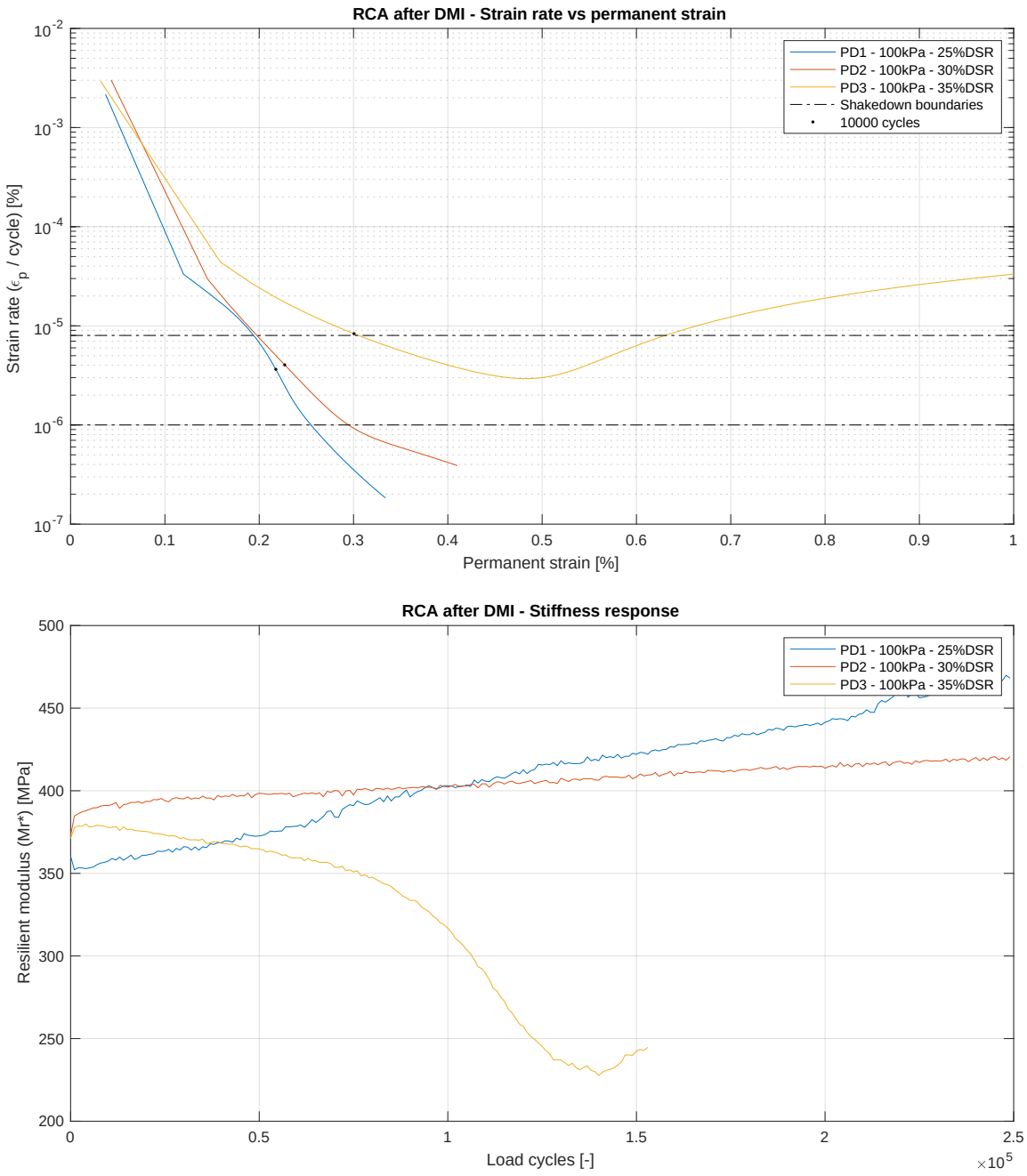

Figure H.8: Permanent deformation triaxial test calculations for milled RCA **Top:** Strain rate versus permanent deformation **Bottom:** Stiffness response

H.4. MG65 BEFORE DMI

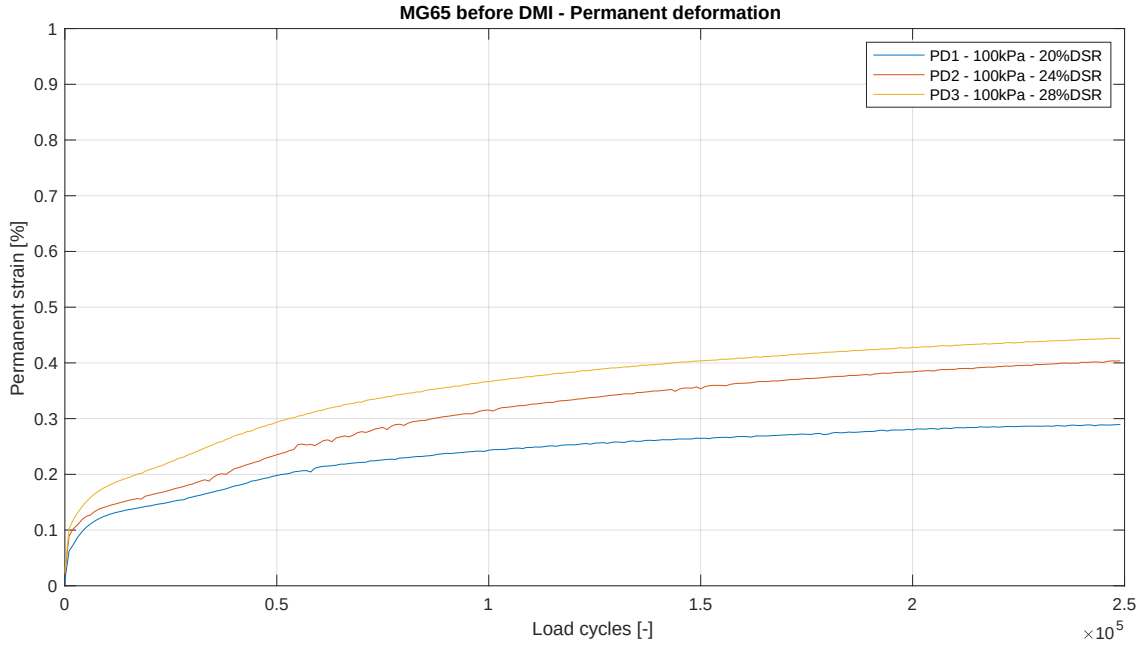

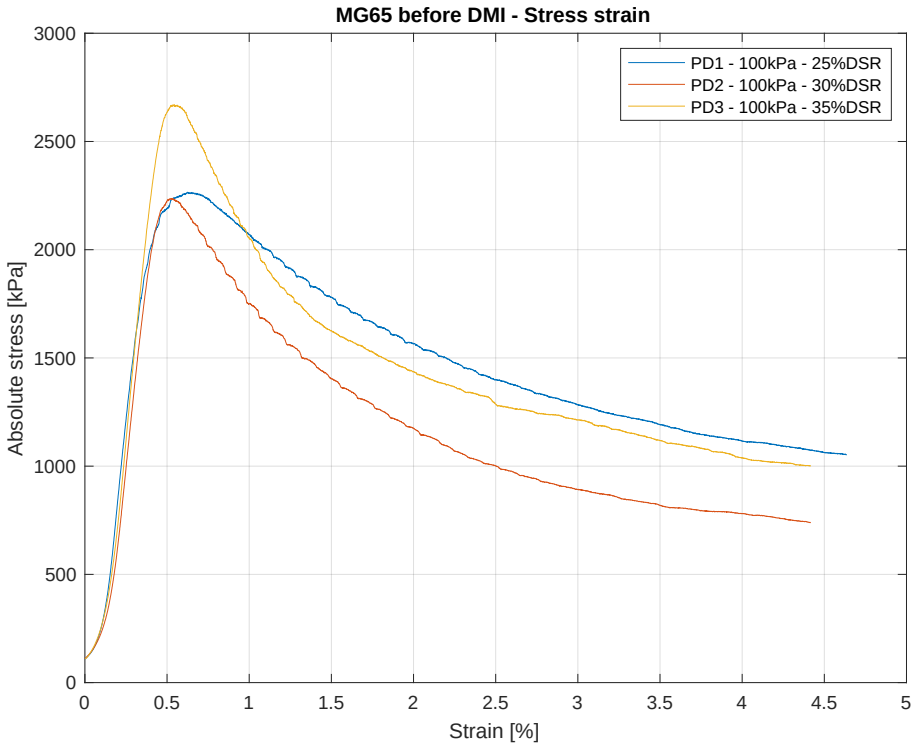

Figure H.9: Permanent deformation triaxial test results for unmilled MG65 **Top:** Permanent strain versus the number of load cycles **Bottom:** Monotonic triaxial test results after permanent deformation triaxial testing

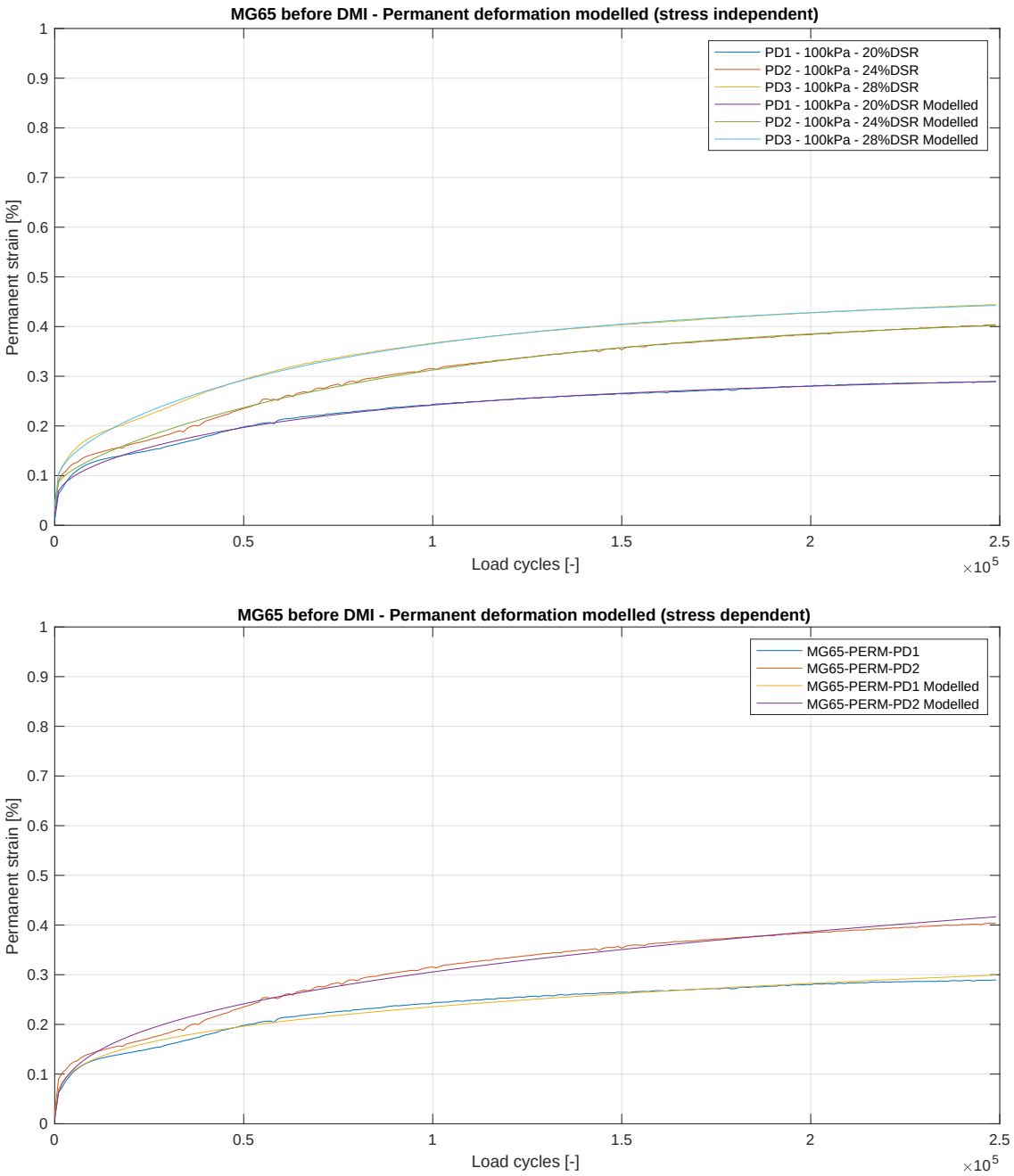

Figure H.10: Permanent deformation triaxial test models (Huurman) for unmilled MG65 **Top:** Stress independent (4 coefficients including unstable behavior, different for all tests) **Bottom:** Stress dependent (4 coefficients excluding unstable behavior, based on two tests up to 25% DSR)

Table H.6: Permanent deformation model parameters for MG65 before DMI

MG65 before DMI	Actual DSR [%]	A [%]	B [-]	C [%]	D [-]	$\sum d^2$	R^2
MG65-PERM-PD1	20.01	0.0670	0.1831	-0.1072	-0.0163	0.0021	0.9969
MG65-PERM-PD2	23.94	0.0836	0.1025	-0.2757	-0.0104	0.0043	0.9975
MG65-PERM-PD3	27.98	0.0997	0.1641	-0.2020	-0.0143	0.0018	0.9990

MG65 before DMI	Actual DSR [%]	a_1 [%]	a_2 [-]	b_1 [-]	b_2 [-]	$\sum d^2$	R^2
MG65-PERM-PD1	20.01	0.0304	-0.5187	2.6154	1.4274	0.0096	0.9862
MG65-PERM-PD2	23.94					0.0209	0.9879
					Full dataset match	**0.0305**	**0.9874**

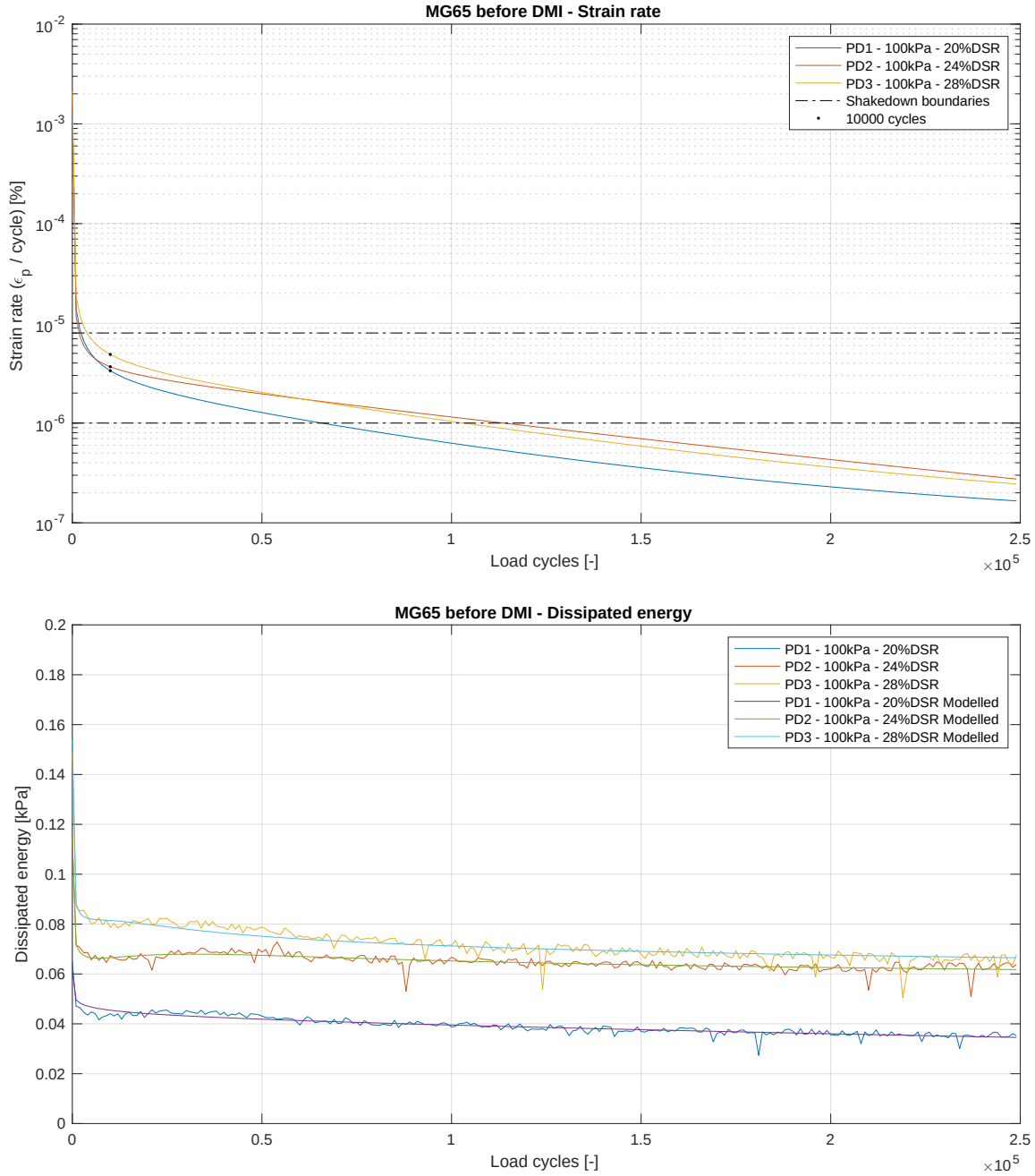

Figure H.11: Permanent deformation triaxial test calculations for unmilled MG65 **Top:** Strain rate versus number of load cycles **Bottom:** Dissipated energy per load cycle (real and Huurman modelled)

Table H.7: Dissipated energy model parameters for MG65 before DMI

MG65 before DMI	Actual DSR [%]	A [kPa]	B [-]	C [kPa]	D [-]	$\sum d^2$	R^2
MG65-PERM-PD1	20.01	0.0496	-0.0353	0.0421	-0.0006	0.0005	0.8589
MG65-PERM-PD2	23.94	0.0705	-0.0827	-0.0171	-0.0658	0.0008	0.8154
MG65-PERM-PD3	27.98	0.0856	-0.1010	-0.0174	-0.1506	0.0016	0.8896

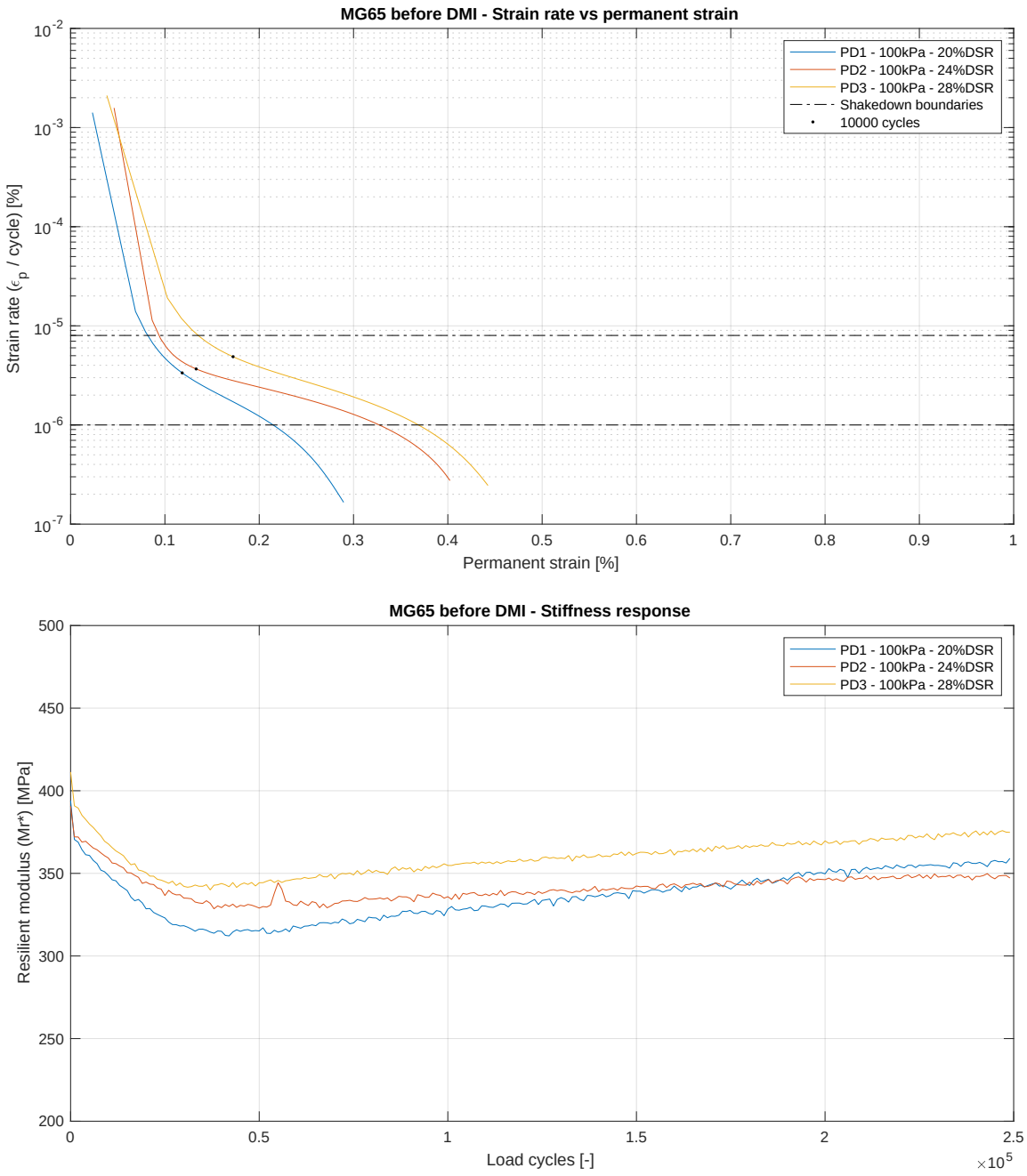

Figure H.12: Permanent deformation triaxial test calculations for unmilled MG65 **Top:** Strain rate versus permanent deformation **Bottom:** Stiffness response

H.5. MG65 AFTER DMI

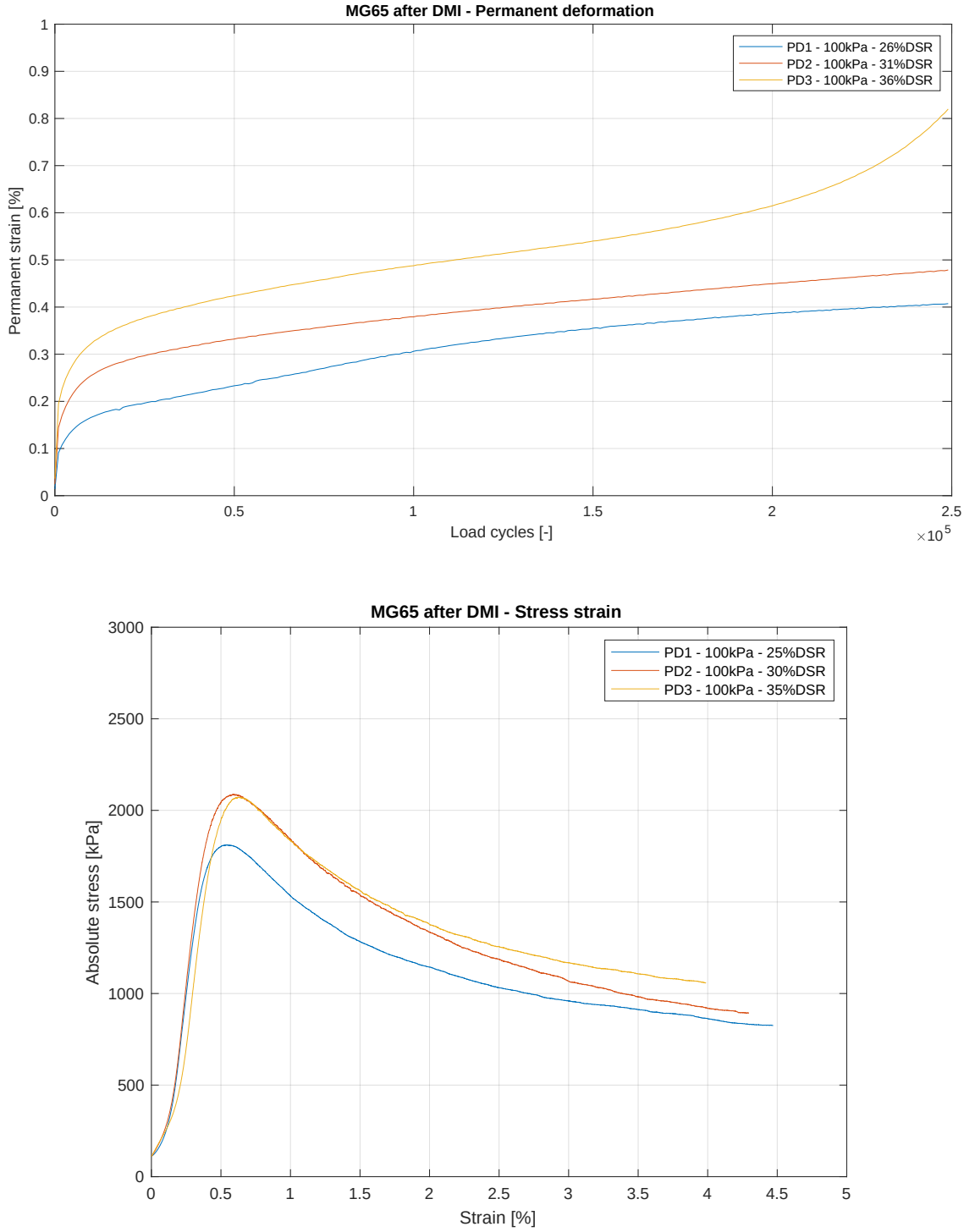

Figure H.13: Permanent deformation triaxial test results for milled MG65 **Top:** Permanent strain versus the number of load cycles **Bottom:** Monotonic triaxial test results after permanent deformation triaxial testing

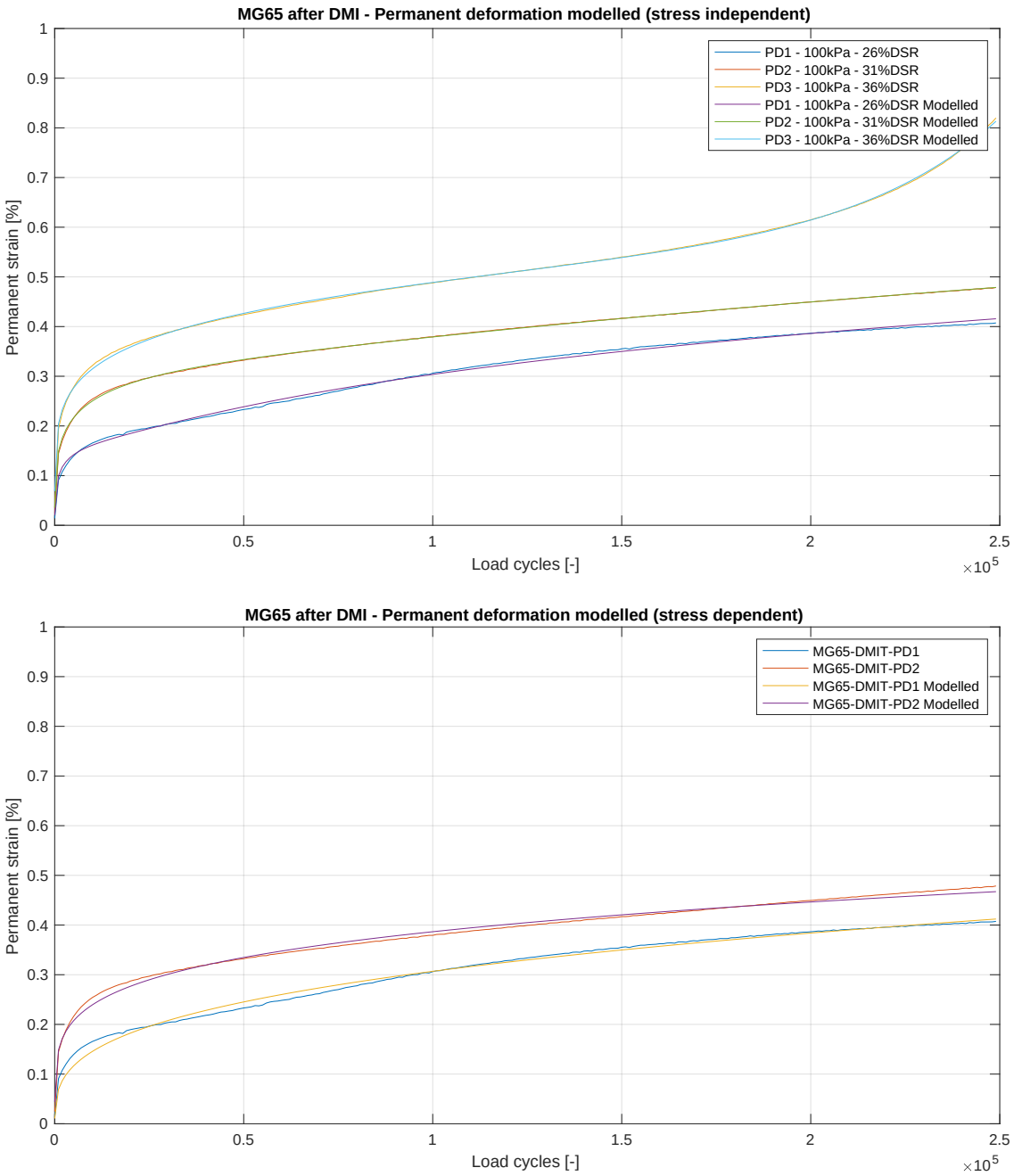

Figure H.14: Permanent deformation triaxial test models (Huurman) for milled MG65 **Top:** Stress independent (4 coefficients including unstable behavior, different for all tests) **Bottom:** Stress dependent (4 coefficients excluding unstable behavior, based on two tests up to 30% DSR)

Table H.8: Permanent deformation model parameters for MG65 after DMI

MG65 after DMI	Actual DSR [%]	A [%]	B [-]	C [%]	D [-]	$\sum d^2$	R^2
MG65-DMIT-PD1	25.68	0.1047	0.2815	0.0790	-0.0675	0.0046	0.9970
MG65-DMIT-PD2	30.72	0.1512	0.2497	0.1229	-0.0161	0.0005	0.9996
MG65-DMIT-PD3	35.89	0.2044	0.1877	0.0003	0.0273	0.0026	0.9993

MG65 after DMI	Actual DSR [%]	a_1 [%]	a_2 [-]	b_1 [-]	b_2 [-]	$\sum d^2$	R^2
MG65-DMIT-PD1	25.68	22.5390	4.2551	0.0113	-2.4659	0.0144	0.9908
MG65-DMIT-PD2	30.72					0.0100	0.9918
					Full dataset match	**0.0244**	**0.9912**

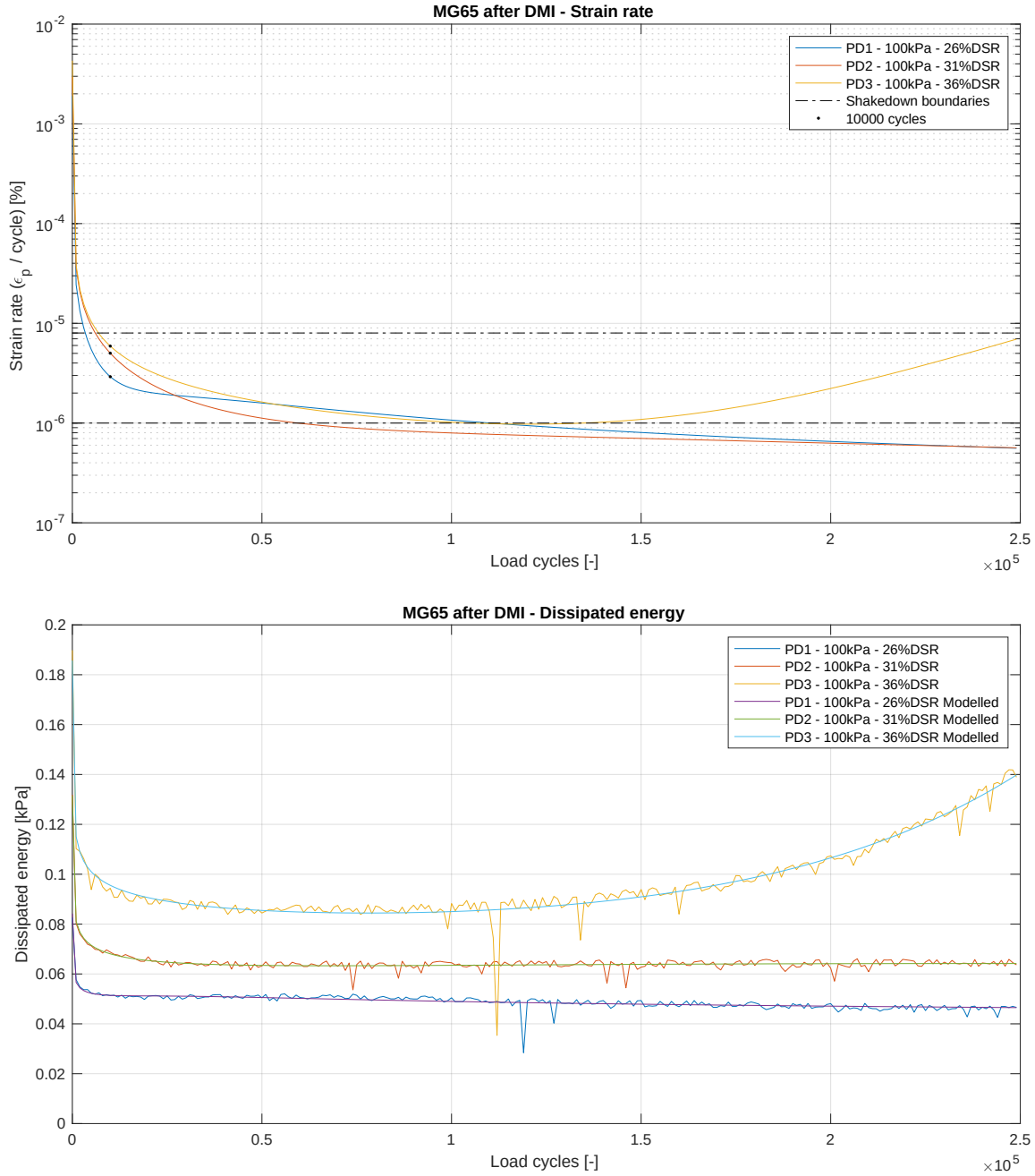

Figure H.15: Permanent deformation triaxial test calculations for milled MG65 **Top:** Strain rate versus number of load cycles **Bottom:** Dissipated energy per load cycle (real and Huurman modelled)

Table H.9: Dissipated energy model parameters for MG65 after DMI

MG65 after DMI	Actual DSR [%]	A [kPa]	B [-]	C [kPa]	D [-]	$\sum d^2$	R^2
MG65-DMIT-PD1	25.68	0.0562	-0.0697	-0.0083	-0.0567	0.0007	0.7450
MG65-DMIT-PD2	30.72	0.0811	-0.0832	-0.0151	-0.0078	0.0006	0.9015
MG65-DMIT-PD3	35.89	0.1151	-0.0823	0.0020	0.0143	0.0042	0.9337

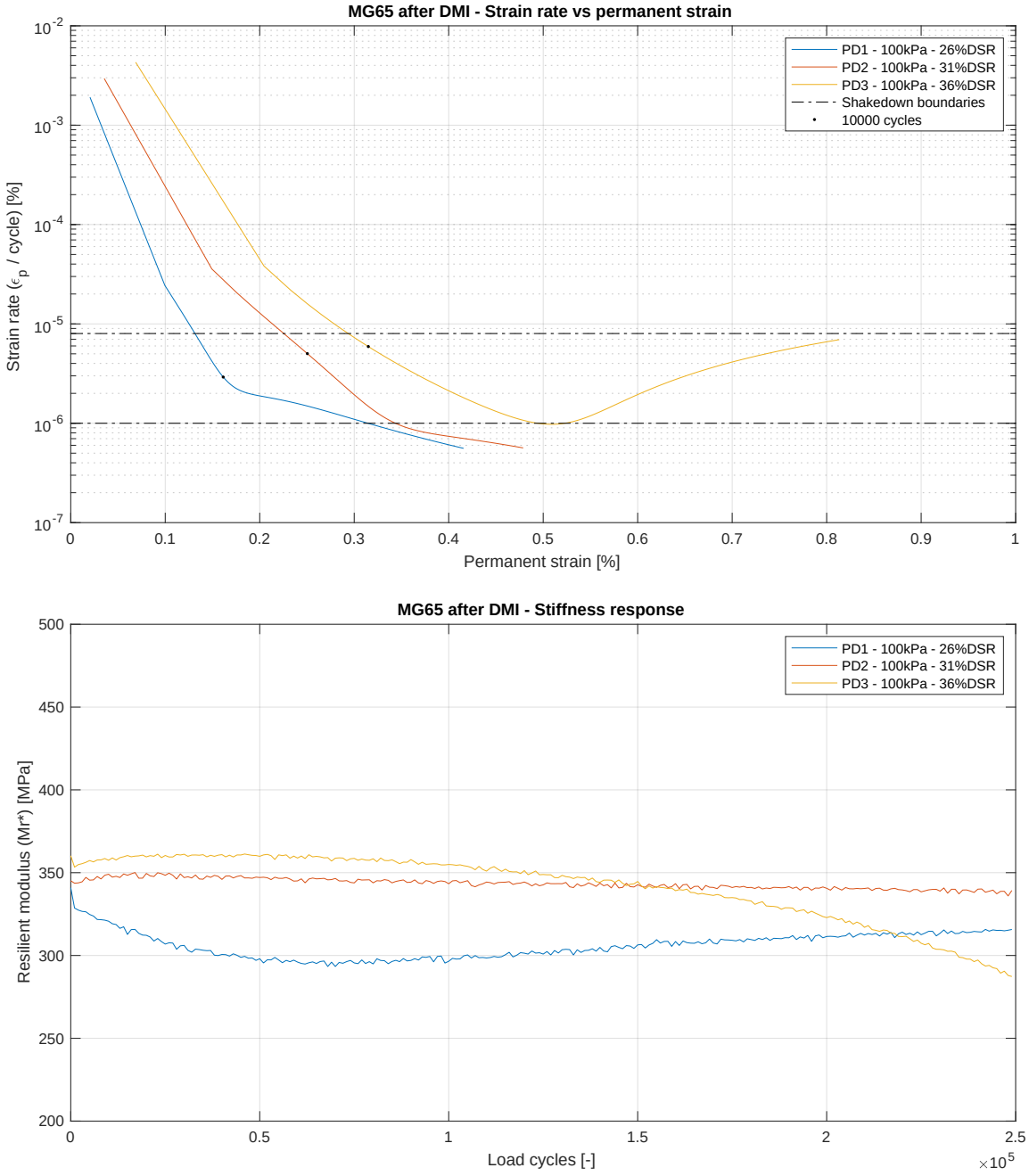

Figure H.16: Permanent deformation triaxial test calculations for milled MG65 **Top:** Strain rate versus permanent deformation **Bottom:** Stiffness response

H.6. COMPARISONS AT 545 KPA (10 KN) DEVIATOR STRESS

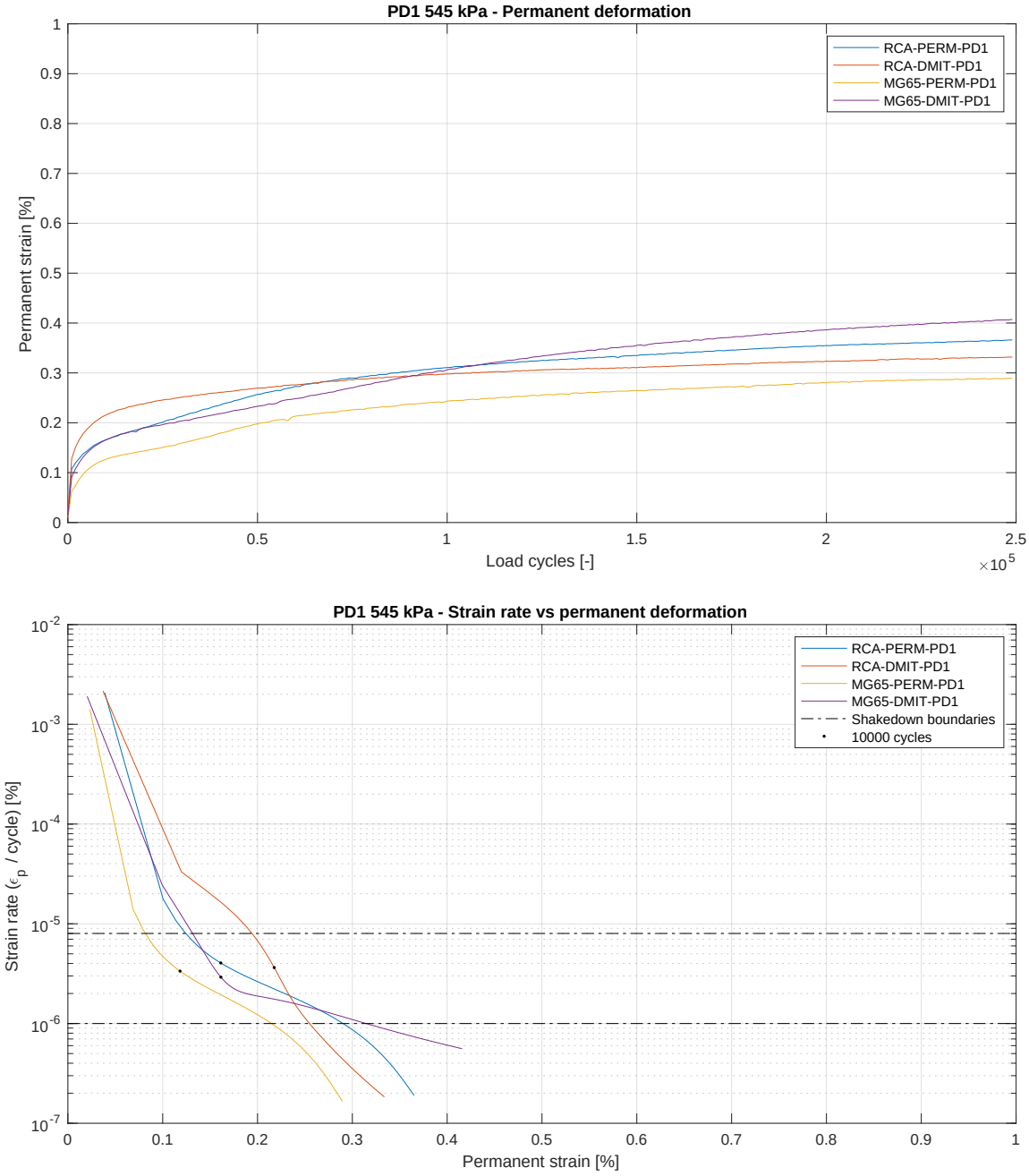

Figure H.17: Permanent deformation triaxial test comparisons at 545 kPa (10 kN) **Top:** Permanent deformation **Bottom:** Strain rate

Table H.10: Permanent deformation model parameters for all materials tested at 545 kPa (10 kN)

25% DSR	Actual DSR [%]	A [%]	B [-]	C [%]	D [-]	$\sum d^2$	R^2
RCA-PERM-PD1	22.82	0.0983	0.1595	-0.1305	-0.0161	0.0020	0.9979
RCA-DMIT-PD1	24.87	0.1014	0.1735	-0.0698	-0.3033	0.0011	0.9973
MG65-PERM-PD1	20.01	0.0670	0.1831	-0.1072	-0.0163	0.0021	0.9969
MG65-DMIT-PD1	25.68	0.1047	0.2815	0.0790	-0.0675	0.0046	0.9970

H.7. COMPARISONS AT 650 KPA (12 KN) DEVIATOR STRESS

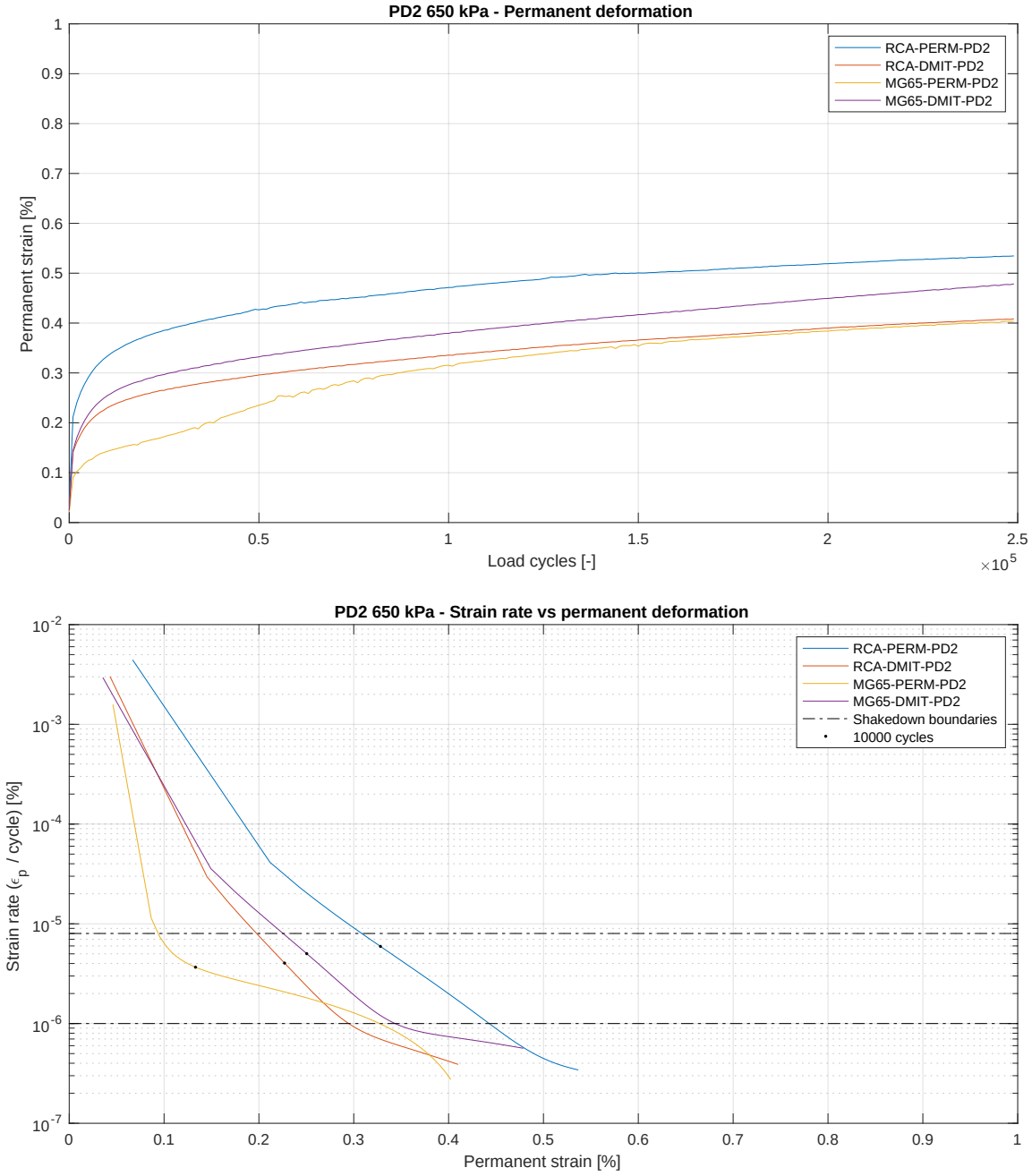

Figure H.18: Permanent deformation triaxial test comparisons at 650 kPa (12 kN) **Top:** Permanent deformation **Bottom:** Strain rate

Table H.11: Permanent deformation model parameters for all materials tested at 650 kPa (12 kN)

30% DSR	Actual DSR [%]	A [%]	B [-]	C [%]	D [-]	$\sum d^2$	R^2
RCA-PERM-PD2	27.39	0.2123	0.1990	0.1266	-0.0063	0.0018	0.9983
RCA-DMIT-PD2	29.85	0.1463	0.2109	0.0589	-0.0203	0.0004	0.9995
MG65-PERM-PD2	23.94	0.0836	0.1025	-0.2757	-0.0104	0.0043	0.9975
MG65-DMIT-PD2	30.72	0.1512	0.2497	0.1229	-0.0161	0.0005	0.9996

H.8. COMPARISONS AT 760 KPA (14 KN) DEVIATOR STRESS

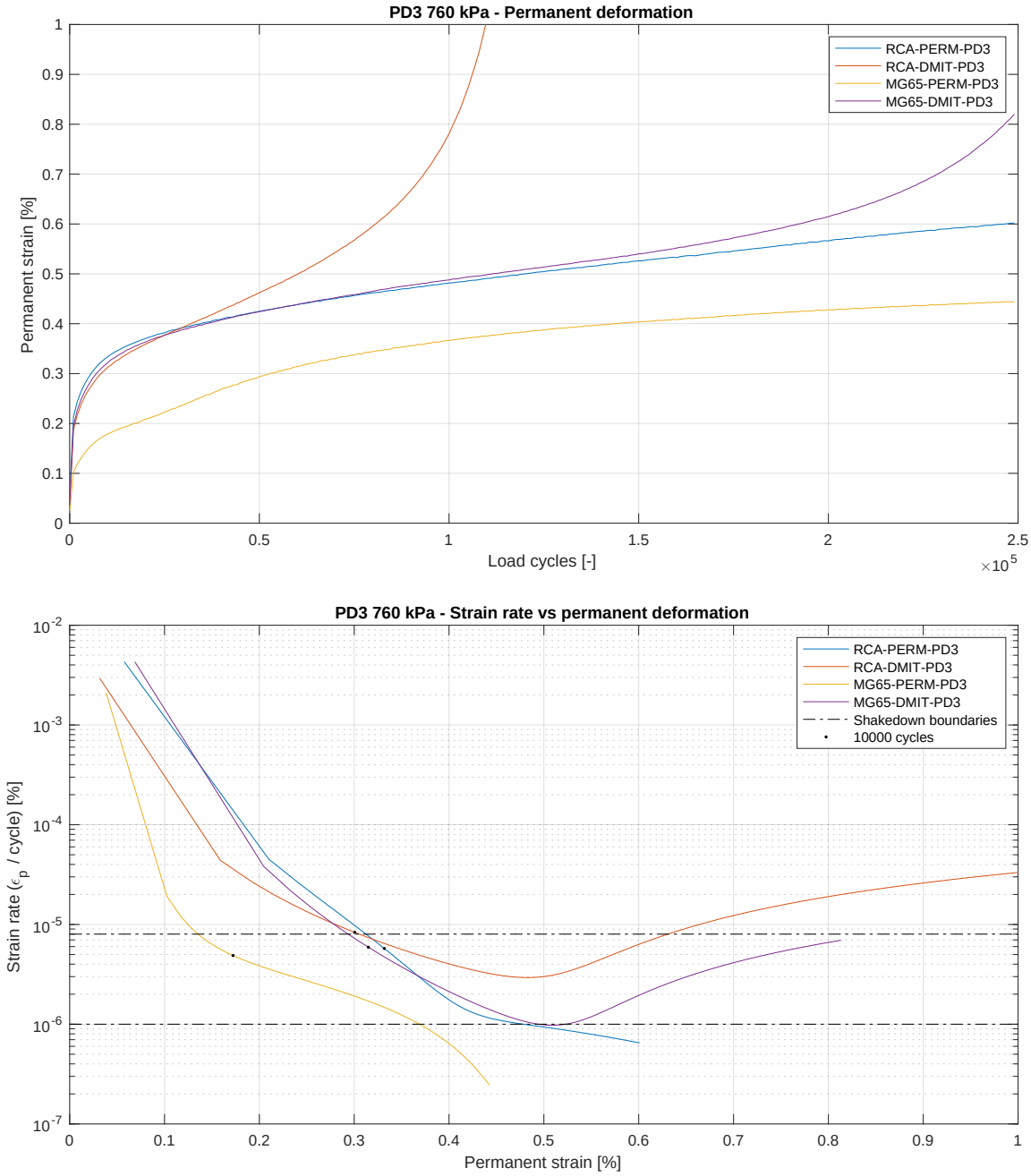

Figure H.19: Permanent deformation triaxial test comparisons at 760 kPa (14 kN) **Top:** Permanent deformation **Bottom:** Strain rate

Table H.12: Permanent deformation model parameters for all materials tested at 760 kPa (14 kN)

35% DSR	Actual DSR [%]	A [%]	B [-]	C [%]	D [-]	$\sum d^2$	R^2
RCA-PERM-PD3	31.96	0.2127	0.2253	0.1372	-0.0207	0.0004	0.9998
RCA-DMIT-PD3	34.83	0.1588	0.2769	0.0001	0.0760	0.0219	0.9985
MG65-PERM-PD3	27.98	0.0997	0.1641	-0.2020	-0.0143	0.0018	0.9990
MG65-DMIT-PD3	35.89	0.2044	0.1877	0.0003	0.0273	0.0026	0.9993

H.9. MODELLING SUMMARY

Table H.13: Summarized permanent deformation model parameters for stress independent Huurman modelling

Test	Specimen ID	A [%]	B [-]	C [%]	D [-]	$\sum d^2$	R^2
RCA before DMI	RCA-PERM-PD1	0.0983	0.1595	-0.1305	-0.0161	0.0020	0.9979
	RCA-PERM-PD2	0.2123	0.1990	0.1266	-0.0063	0.0018	0.9983
	RCA-PERM-PD3	0.2127	0.2253	0.1372	-0.0207	0.0004	0.9998
RCA after DMI	RCA-DMIT-PD1	0.1014	0.1735	-0.0698	-0.3033	0.0011	0.9973
	RCA-DMIT-PD2	0.1463	0.2109	0.0589	-0.0203	0.0004	0.9995
	RCA-DMIT-PD3	0.1588	0.2769	0.0001	0.0760	0.0219	0.9985
MG65 before DMI	MG65-PERM-PD1	0.0670	0.1831	-0.1072	-0.0163	0.0021	0.9969
	MG65-PERM-PD2	0.0836	0.1025	-0.2757	-0.0104	0.0043	0.9975
	MG65-PERM-PD3	0.0997	0.1641	-0.2020	-0.0143	0.0018	0.9990
MG65 after DMI	MG65-DMIT-PD1	0.1047	0.2815	0.0790	-0.0675	0.0046	0.9970
	MG65-DMIT-PD2	0.1512	0.2497	0.1229	-0.0161	0.0005	0.9996
	MG65-DMIT-PD3	0.2044	0.1877	0.0003	0.0273	0.0026	0.9993

Table H.14: Summarized dissipated energy model parameters for stress independent Huurman modelling

Test	Specimen ID	A [kPa]	B [-]	C [kPa]	D [-]	$\sum d^2$	R^2
RCA before DMI	RCA-PERM-PD1	0.0654	-0.0511	0.0124	-0.0136	0.0007	0.9331
	RCA-PERM-PD2	0.0412	-0.2317	-0.0547	-2.0811	0.0010	0.9188
	RCA-PERM-PD3	0.1831	-0.0380	0.0757	-10.0000	0.0007	0.9774
RCA after DMI	RCA-DMIT-PD1	0.0581	-0.0665	-0.0175	0.0015	0.0003	0.9668
	RCA-DMIT-PD2	0.0787	-0.0955	-0.0087	-0.0237	0.0005	0.9494
	RCA-DMIT-PD3	0.1204	-0.0835	0.0043	0.0268	0.0011	0.9706
MG65 before DMI	MG65-PERM-PD1	0.0496	-0.0353	0.0421	-0.0006	0.0005	0.8589
	MG65-PERM-PD2	0.0705	-0.0827	-0.0171	-0.0658	0.0008	0.8154
	MG65-PERM-PD3	0.0856	-0.1010	-0.0174	-0.1506	0.0016	0.8896
MG65 after DMI	MG65-DMIT-PD1	0.0562	-0.0697	-0.0083	-0.0567	0.0007	0.7450
	MG65-DMIT-PD2	0.0811	-0.0832	-0.0151	-0.0078	0.0006	0.9015
	MG65-DMIT-PD3	0.1151	-0.0823	0.0020	0.0143	0.0042	0.9337

Table H.15: Summarized permanent deformation model parameters for stress dependent Huurman modelling (up to 30% DSR)

Material	a_1 [%]	a_2 [-]	b_1 [-]	b_2 [-]	$\sum d^2$	R^2
RCA before DMI	112.5222	4.7650	0.0049	-2.6362	0.0188	0.9909
RCA after DMI	0.0827	-0.4481	1.3505	1.6256	0.0089	0.9926
MG65 before DMI	0.0304	-0.5187	2.6154	1.4274	0.0305	0.9874
MG65 after DMI	22.5390	4.2551	0.0113	-2.4659	0.0244	0.9912

Table H.16: Modelled permanent deformation triaxial test results: General, at 10,000, 50,000 and 100,000 load cycles

General	Final permanent deformation [%]	Shakedown limit Werkmeister	Shakedown limit Tao	Failure [-]	Instability [-]
RCA-PERM-PD1	0.37	B	B	No	No
RCA-PERM-PD2	0.53	B	B	No	No
RCA-PERM-PD3	0.60	B	B	No	No
RCA-DMIT-PD1	0.33	B	B	No	No
RCA-DMIT-PD2	0.41	B	B	No	No
RCA-DMIT-PD3	7.25	B	C	Yes	Yes
MG65-PERM-PD1	0.29	B	B	No	No
MG65-PERM-PD2	0.40	B	B	No	No
MG65-PERM-PD3	0.44	B	B	No	No
MG65-DMIT-PD1	0.41	B	B	No	No
MG65-DMIT-PD2	0.48	B	B	No	No
MG65-DMIT-PD3	0.82	B	B	No	Yes

10,000 load cycles	Permanent deformation [%]	Strain rate [%]	Strain rate change [%]	Dissipated energy [kPa]	Dissipated energy change [kPa / cycle]
RCA-PERM-PD1	0.16	4.05E-06	-5.44E-05	5.65E-02	-4.44E-07
RCA-PERM-PD2	0.33	5.94E-06	-8.99E-05	7.89E-02	-5.60E-07
RCA-PERM-PD3	0.33	5.74E-06	-1.01E-04	9.21E-02	-6.37E-07
RCA-DMIT-PD1	0.22	3.64E-06	-1.45E-04	4.95E-02	-3.58E-07
RCA-DMIT-PD2	0.23	4.04E-06	-9.36E-05	6.50E-02	-4.39E-07
RCA-DMIT-PD3	0.30	8.33E-06	-7.24E-05	1.01E-01	-6.78E-07
MG65-PERM-PD1	0.12	3.35E-06	-5.31E-05	4.55E-02	-1.89E-07
MG65-PERM-PD2	0.13	3.67E-06	-3.40E-05	6.65E-02	1.01E-07
MG65-PERM-PD3	0.17	4.88E-06	-4.84E-05	8.14E-02	-1.02E-07
MG65-DMIT-PD1	0.16	2.92E-06	-7.66E-05	5.14E-02	-6.73E-08
MG65-DMIT-PD2	0.25	5.02E-06	-9.53E-05	6.81E-02	-4.48E-07
MG65-DMIT-PD3	0.31	5.92E-06	-8.15E-05	9.55E-02	-7.51E-07

50,000 load cycles	Permanent deformation [%]	Strain rate [%]	Strain rate change [%]	Dissipated energy [kPa]	Dissipated energy change [kPa / cycle]
RCA-PERM-PD1	0.26	1.52E-06	-1.63E-05	4.74E-02	-1.40E-07
RCA-PERM-PD2	0.43	1.26E-06	-2.05E-05	7.13E-02	-7.71E-08
RCA-PERM-PD3	0.43	1.31E-06	-1.15E-05	8.21E-02	-1.20E-07
RCA-DMIT-PD1	0.27	6.93E-07	-1.65E-05	4.34E-02	-8.87E-08
RCA-DMIT-PD2	0.30	9.76E-07	-1.38E-05	6.02E-02	-4.01E-08
RCA-DMIT-PD3	0.47	2.95E-06	-3.61E-06	9.90E-02	2.95E-07
MG65-PERM-PD1	0.20	1.28E-06	-1.63E-05	4.19E-02	-5.69E-08
MG65-PERM-PD2	0.24	1.96E-06	-1.14E-05	6.75E-02	-4.25E-08
MG65-PERM-PD3	0.29	2.03E-06	-1.50E-05	7.51E-02	-1.15E-07
MG65-DMIT-PD1	0.24	1.59E-06	-8.28E-06	5.05E-02	-3.20E-08
MG65-DMIT-PD2	0.33	1.12E-06	-1.42E-05	6.34E-02	-1.77E-08
MG65-DMIT-PD3	0.43	1.63E-06	-1.55E-05	8.55E-02	-8.03E-08

100,000 load cycles	Permanent deformation [%]	Strain rate [%]	Strain rate change [%]	Dissipated energy [kPa]	Dissipated energy change [kPa / cycle]
RCA-PERM-PD1	0.31	7.48E-07	-1.27E-05	4.24E-02	-6.96E-08
RCA-PERM-PD2	0.47	6.33E-07	-9.17E-06	6.89E-02	-3.28E-08
RCA-PERM-PD3	0.48	9.94E-07	-3.08E-06	7.80E-02	-5.84E-08
RCA-DMIT-PD1	0.30	3.91E-07	-8.27E-06	3.98E-02	-6.00E-08
RCA-DMIT-PD2	0.34	6.59E-07	-4.93E-06	5.86E-02	-2.91E-08
RCA-DMIT-PD3	0.78	1.74E-05	6.85E-05	1.40E-01	1.61E-06
MG65-PERM-PD1	0.24	6.28E-07	-1.26E-05	3.95E-02	-4.05E-08
MG65-PERM-PD2	0.31	1.15E-06	-1.03E-05	6.52E-02	-3.83E-08
MG65-PERM-PD3	0.37	1.04E-06	-1.23E-05	7.12E-02	-5.43E-08
MG65-DMIT-PD1	0.30	1.07E-06	-6.83E-06	4.90E-02	-2.68E-08
MG65-DMIT-PD2	0.38	7.96E-07	-3.24E-06	6.35E-02	8.05E-09
MG65-DMIT-PD3	0.49	1.02E-06	-4.28E-06	8.50E-02	5.17E-08

Table H.17: Modelled permanent deformation triaxial test results: At 150,000 and 250,000 load cycles

150,000 load cycles	Permanent deformation [%]	Strain rate [%]	Strain rate change [%]	Dissipated energy [kPa]	Dissipated energy change [kPa / cycle]
RCA-PERM-PD1	0.34	4.21E-07	-1.03E-05	3.98E-02	-3.91E-08
RCA-PERM-PD2	0.50	4.54E-07	-4.70E-06	6.76E-02	-1.99E-08
RCA-PERM-PD3	0.53	8.60E-07	-2.86E-06	7.56E-02	-3.83E-08
RCA-DMIT-PD1	0.31	2.80E-07	-5.51E-06	3.70E-02	-5.25E-08
RCA-DMIT-PD2	0.36	5.35E-07	-3.66E-06	5.72E-02	-2.51E-08
RCA-DMIT-PD3	Failed	Failed	Failed	Failed	Failed
MG65-PERM-PD1	0.27	3.57E-07	-1.01E-05	3.77E-02	-3.45E-08
MG65-PERM-PD2	0.36	6.97E-07	-9.82E-06	6.37E-02	-2.56E-08
MG65-PERM-PD3	0.40	5.87E-07	-1.06E-05	6.91E-02	-3.47E-08
MG65-DMIT-PD1	0.35	8.05E-07	-4.77E-06	4.79E-02	-1.83E-08
MG65-DMIT-PD2	0.42	7.02E-07	-2.21E-06	6.39E-02	6.97E-09
MG65-DMIT-PD3	0.54	1.09E-06	7.65E-06	9.09E-02	1.97E-07

250,000 load cycles	Permanent deformation [%]	Strain rate [%]	Strain rate change [%]	Dissipated energy [kPa]	Dissipated energy change [kPa / cycle]
RCA-PERM-PD1	0.36	1.91E-07	-5.98E-06	3.73E-02	-1.59E-08
RCA-PERM-PD2	0.54	3.43E-07	-1.74E-06	6.62E-02	-1.07E-08
RCA-PERM-PD3	0.60	6.52E-07	-2.67E-06	7.28E-02	-2.28E-08
RCA-DMIT-PD1	0.33	1.85E-07	-3.33E-06	3.21E-02	-5.05E-08
RCA-DMIT-PD2	0.41	3.90E-07	-2.84E-06	5.52E-02	-1.73E-08
RCA-DMIT-PD3	Failed	Failed	Failed	Failed	Failed
MG65-PERM-PD1	0.29	1.67E-07	-5.70E-06	3.46E-02	-2.90E-08
MG65-PERM-PD2	0.40	2.77E-07	-8.93E-06	6.18E-02	-1.49E-08
MG65-PERM-PD3	0.44	2.47E-07	-7.07E-06	6.65E-02	-2.00E-08
MG65-DMIT-PD1	0.42	5.61E-07	-2.90E-06	4.65E-02	-1.07E-08
MG65-DMIT-PD2	0.48	5.66E-07	-2.18E-06	6.42E-02	-1.29E-10
MG65-DMIT-PD3	0.81	6.77E-06	2.54E-05	1.39E-01	9.44E-07

I

APPENDIX I: WESLEA RESULTS

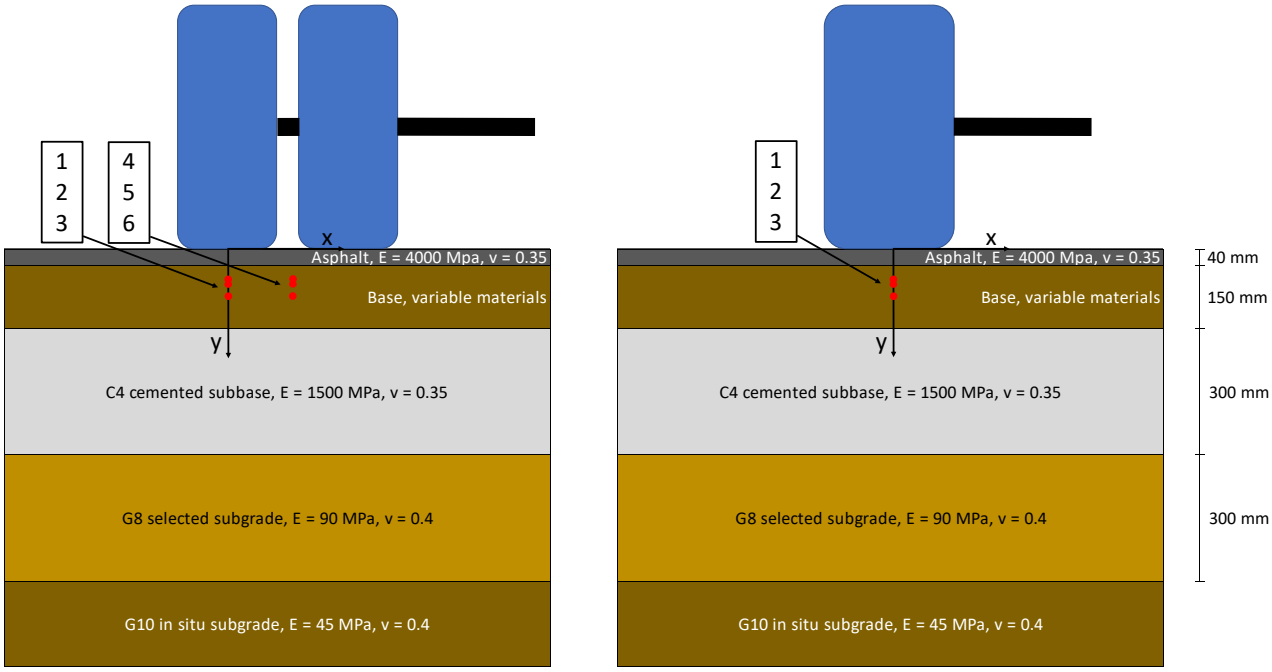

Figure I.1: Pavement structure and loading situation **Left:** Dual tire **Right:** Super single tire

I.1. ASPHALT STRUCTURE LOADED WITH A DUAL TIRE

Table I.1: Weslea results: Asphalt surface loaded with a dual tire (2 x 20 kN, 700 kPa, full layer bond)

	Data point	Coordinates			Normal stress			Shear stress		
	[-]	X [mm]	Y[mm]	Z [mm]	σ_{xx} [kPa]	σ_{yy} [kPa]	σ_{zz} [kPa]	σ_{yz} [kPa]	σ_{xz} [kPa]	σ_{xy} [kPa]
G2 theory	1	0	0	78	83	74	417	0	-7	0
	2	0	0	90	73	62	382	0	-9	0
	3	0	0	115	64	52	322	0	-12	0
	4	172	0	78	148	39	121	0	0	0
	5	172	0	90	142	38	129	0	0	0
	6	172	0	115	129	38	139	0	0	0
G2 after DMI	1	0	0	78	78	67	347	0	-4	0
	2	0	0	90	71	59	324	0	-6	0
	3	0	0	115	66	54	283	0	-9	0
	4	172	0	78	127	44	152	0	0	0
	5	172	0	90	123	42	157	0	0	0
	6	172	0	115	115	44	161	0	0	0
RCA (before and after DMI)	1	0	0	78	80	69	375	0	-5	0
	2	0	0	90	71	60	347	0	-7	0
	3	0	0	115	65	53	300	0	-10	0
	4	172	0	78	135	41	141	0	0	0
	5	172	0	90	130	40	147	0	0	0
	6	172	0	115	120	42	154	0	0	0
MG65 before DMI	1	0	0	78	82	73	411	0	-7	0
	2	0	0	90	72	61	377	0	-8	0
	3	0	0	115	64	52	319	0	-11	0
	4	172	0	78	146	39	124	0	0	0
	5	172	0	90	140	38	132	0	0	0
	6	172	0	115	127	39	142	0	0	0
MG65 after DMI	1	0	0	78	81	70	391	0	-6	0
	2	0	0	90	72	60	361	0	-7	0
	3	0	0	115	65	53	308	0	-10	0
	4	172	0	78	139	40	134	0	0	0
	5	172	0	90	135	39	141	0	0	0
	6	172	0	115	123	40	149	0	0	0
MG30 before DMI	1	0	0	78	82	73	410	0	-7	0
	2	0	0	90	72	61	376	0	-8	0
	3	0	0	115	64	52	318	0	-11	0
	4	172	0	78	145	39	125	0	0	0
	5	172	0	90	140	38	132	0	0	0
	6	172	0	115	127	39	142	0	0	0
MG30 after DMI	1	0	0	78	81	71	401	0	-6	0
	2	0	0	90	72	61	369	0	-8	0
	3	0	0	115	64	52	314	0	-11	0
	4	172	0	78	142	39	129	0	0	0
	5	172	0	90	137	38	136	0	0	0
	6	172	0	115	125	40	145	0	0	0

Table I.2: Weslea calculations - Asphalt surface loaded with a dual tire (2 x 20 kN, 700 kPa, full layer bond)

	Datapoint [-]	Stiffness [MPa]	Friction angle [°]	Cohesion [kPa]	σ_3 [kPa]	σ_1 [kPa]	$\sigma_{d,f}$ [kPa]	DSR [%]
G2 theory	1	400	52	55	74	417	867	39.6
	2				62	382	780	41.1
	3				52	323	704	38.5
	4				39	148	610	17.8
	5				38	142	600	17.4
	6				38	139	605	16.6
G2 after DMI	1	165	51.2	142	67	347	1281	21.9
	2				59	324	1223	21.7
	3				54	284	1185	19.4
	4				44	152	1116	9.7
	5				42	157	1106	10.3
	6				44	161	1117	10.5
RCA before DMI	1	230	55.1	233	69	375	2112	14.5
	2				60	348	2027	14.2
	3				53	300	1966	12.6
	4				41	141	1857	5.4
	5				40	147	1846	5.8
	6				42	154	1862	6.0
RCA after DMI	1	230	56.6	178	69	375	1884	16.3
	2				60	348	1790	16.1
	3				53	300	1722	14.3
	4				41	141	1602	6.2
	5				40	147	1590	6.7
	6				42	154	1607	7.0
MG65 before DMI	1	365	51.2	354	73	411	2524	13.4
	2				61	377	2444	12.9
	3				52	319	2378	11.2
	4				39	146	2287	4.7
	5				38	140	2278	4.5
	6				39	142	2285	4.5
MG65 after DMI	1	280	53.5	214	70	391	1875	17.1
	2				60	361	1792	16.8
	3				53	309	1729	14.8
	4				40	139	1625	6.1
	5				39	141	1616	6.3
	6				40	149	1629	6.7
MG30 before DMI	1	360	53.9	328	73	410	2624	12.9
	2				61	376	2529	12.5
	3				52	319	2451	10.9
	4				39	145	2342	4.5
	5				38	140	2332	4.4
	6				39	142	2341	4.4
MG30 after DMI	1	320	54.1	285	71	401	2369	13.9
	2				61	369	2278	13.5
	3				52	314	2205	11.9
	4				39	142	2095	4.9
	5				38	137	2085	4.8
	6				40	145	2097	5.0

I.2. ASPHALT STRUCTURE LOADED WITH A SUPER SINGLE TIRE

Table I.3: Weslea results - Asphalt surface loaded with a super single tire (1 x 40 kN), 825 kPa, full layer bond

	Data point	Coordinates			Normal stress			Shear stress		
	[-]	X [mm]	Y[mm]	Z [mm]	σ_{xx} [kPa]	σ_{yy} [kPa]	σ_{zz} [kPa]	σ_{yz} [kPa]	σ_{xz} [kPa]	σ_{xy} [kPa]
G2 theory E = 400 MPa	1	0	0	78	140	140	635	0	0	0
	2	0	0	90	119	119	598	0	0	0
	3	0	0	115	99	99	526	0	0	0
G2 after DMI E = 165 MPa	1	0	0	78	130	130	564	0	0	0
	2	0	0	90	115	115	536	0	0	0
	3	0	0	115	103	103	483	0	0	0
RCA (before and after DMI) E = 230 MPa	1	0	0	78	133	133	595	0	0	0
	2	0	0	90	117	117	563	0	0	0
	3	0	0	115	102	102	503	0	0	0
MG65 before DMI E = 365 MPa	1	0	0	78	139	139	630	0	0	0
	2	0	0	90	119	119	593	0	0	0
	3	0	0	115	100	100	523	0	0	0
MG65 after DMI E = 280 MPa	1	0	0	78	135	135	612	0	0	0
	2	0	0	90	118	118	578	0	0	0
	3	0	0	115	101	101	513	0	0	0
MG30 before DMI E = 360 MPa	1	0	0	78	138	138	629	0	0	0
	2	0	0	90	119	119	593	0	0	0
	3	0	0	115	100	100	523	0	0	0
MG30 after DMI E = 320 MPa	1	0	0	78	137	137	621	0	0	0
	2	0	0	90	118	118	586	0	0	0
	3	0	0	115	101	101	519	0	0	0

Table I.4: Weslea calculations - Asphalt surface loaded with a super single tire (1 x 40 kN), 825 kPa, full layer bond

	Data point	Stiffness	Friction angle	Cohesion	σ_3	σ_1	$\sigma_{d,f}$	DSR
	[-]	[MPa]	[°]	[kPa]	[kPa]	[kPa]	[kPa]	[%]
G2 theory	1	400	52	55	140	635	1359	36.5
	2				119	598	1208	39.6
	3				99	526	1057	40.4
G2 after DMI	1	165	51.2	142	130	564	1724	25.2
	2				115	536	1619	26.0
	3				103	483	1533	24.8
RCA before DMI	1	230	55.1	233	133	595	2698	17.1
	2				117	563	2546	17.5
	3				102	503	2414	16.6
RCA after DMI	1	230	56.6	178	133	595	2533	18.2
	2				117	563	2366	18.9
	3				102	503	2219	18.1
MG65 before DMI	1	365	51.2	354	139	630	2989	16.4
	2				119	593	2850	16.6
	3				100	523	2716	15.6
MG65 after DMI	1	280	53.5	214	135	612	2407	19.8
	2				118	578	2261	20.3
	3				101	513	2128	19.4
MG30 before DMI	1	360	53.9	328	138	629	3177	15.4
	2				119	593	3013	15.7
	3				100	523	2854	14.8
MG30 after DMI	1	320	54.1	285	137	621	2927	16.6
	2				118	586	2768	16.9
	3				101	519	2618	16.0

I.3. SEAL STRUCTURE LOADED WITH A DUAL TIRE

Table I.5: Weslea results - Seal surface loaded with a dual tire (2 x 20 kN), 700 kPa, full layer bond

	Data point	Coordinates			Normal stress			Shear stress		
	[-]	X [mm]	Y[mm]	Z [mm]	σ_{xx} [kPa]	σ_{yy} [kPa]	σ_{zz} [kPa]	σ_{yz} [kPa]	σ_{xz} [kPa]	σ_{xy} [kPa]
G2 theory E = 400 MPa	1	0	0	38	277	277	676	0	-2.31	0
	2	0	0	50	214	212	647	0	-3.43	0
	3	0	0	75	139	135	568	0	-6.12	0
	4	172	0	38	139	55	14	0	0	0
	5	172	0	50	168	55	28	0	0	0
	6	172	0	75	188	56	61	0	0	0
G2 after DMI E = 165 MPa	1	0	0	38	247	242	680	0	-1.14	0
	2	0	0	50	188	183	653	0	-1.89	0
	3	0	0	75	121	115	579	0	-3.9	0
	4	172	0	38	112	21	14	0	0	0
	5	172	0	50	144	25	28	0	0	0
	6	172	0	75	169	32	60	0	0	0
RCA (before and after DMI) E = 230 MPa	1	0	0	38	256	253	678	0	-1.51	0
	2	0	0	50	196	192	651	0	-2.38	0
	3	0	0	75	126	122	575	0	-4.61	0
	4	172	0	38	121	31	14	0	0	0
	5	172	0	50	151	34	28	0	0	0
	6	172	0	75	175	40	61	0	0	0
MG65 before DMI E = 365 MPa	1	0	0	38	273	272	676	0	-2.16	0
	2	0	0	50	211	209	648	0	-3.24	0
	3	0	0	75	137	133	569	0	-5.84	0
	4	172	0	38	135	51	14	0	0	0
	5	172	0	50	165	51	28	0	0	0
	6	172	0	75	186	53	61	0	0	0
MG65 after DMI E = 280 MPa	1	0	0	38	263	261	678	0	-1.77	0
	2	0	0	50	202	199	650	0	-2.72	0
	3	0	0	75	131	126	573	0	-5.1	0
	4	172	0	38	126	39	14	0	0	0
	5	172	0	50	157	41	28	0	0	0
	6	172	0	75	179	45	61	0	0	0
MG30 before DMI E = 360 MPa	1	0	0	38	273	272	677	0	-2.14	0
	2	0	0	50	210	208	648	0	-3.21	0
	3	0	0	75	136	132	569	0	-5.8	0
	4	172	0	38	135	50	14	0	0	0
	5	172	0	50	164	51	28	0	0	0
	6	172	0	75	186	53	61	0	0	0
MG30 after DMI E = 320 MPa	1	0	0	38	268	266	677	0	-1.96	0
	2	0	0	50	206	204	649	0	-2.97	0
	3	0	0	75	134	129	571	0	-5.46	0
	4	172	0	38	131	45	14	0	0	0
	5	172	0	50	161	46	28	0	0	0
	6	172	0	75	183	49	61	0	0	0

Table I.6: Weslea calculations - Seal surface loaded with a dual tire (2 x 20 kN), 700 kPa, full layer bond

	Datapoint [-]	Stiffness [MPa]	Friction angle [°]	Cohesion [kPa]	σ_3 [kPa]	σ_1 [kPa]	$\sigma_{d,f}$ [kPa]	DSR [%]
G2 theory	1	400	52	55	277	676	2378	16.8
	2				212	647	1899	22.9
	3				135	568	1325	32.6
	4				55	139	426	29.2
	5				55	168	531	26.3
	6				56	188	738	17.9
G2 after DMI	1	165	51.2	142	242	680	2518	17.4
	2				183	653	2098	22.4
	3				115	579	1619	28.7
	4				21	112	907	10.8
	5				25	144	980	12.1
	6				32	169	1035	13.2
RCA before DMI	1	230	55.1	233	253	678	3790	11.2
	2				192	651	3235	14.2
	3				122	576	2591	17.5
	4				31	121	1613	6.6
	5				34	151	1740	7.1
	6				40	175	1847	7.3
RCA after DMI	1	230	56.6	178	253	678	3745	11.4
	2				192	651	3129	14.7
	3				122	576	2416	18.8
	4				31	121	1331	8.0
	5				34	151	1472	8.4
	6				40	175	1591	8.5
MG65 before DMI	1	365	51.2	354	272	676	3935	10.3
	2				209	648	3485	12.6
	3				133	569	2949	14.8
	4				51	135	2112	5.7
	5				51	165	2211	6.2
	6				53	186	2387	5.6
MG65 after DMI	1	280	53.5	214	261	678	3434	12.1
	2				199	650	2926	15.4
	3				126	573	2331	19.2
	4				39	126	1415	7.9
	5				41	157	1530	8.4
	6				45	179	1669	8.0
MG30 before DMI	1	360	53.9	328	272	677	4300	9.4
	2				208	648	3765	11.7
	3				132	569	3128	14.0
	4				50	135	2134	5.6
	5				51	164	2252	6.0
	6				53	186	2458	5.4
MG30 after DMI	1	320	54.1	285	266	677	4031	10.2
	2				204	649	3495	12.7
	3				129	571	2863	15.4
	4				45	131	1882	6.2
	5				46	161	2001	6.6
	6				49	183	2179	6.1

I.4. SEAL STRUCTURE LOADED WITH A SUPER SINGLE TIRE

Table I.7: Weslea results - Seal surface loaded with a super single tire (1 x 40 kN), 825 kPa, full layer bond

	Data point	Coordinates			Normal stress			Shear stress		
	[-]	X [mm]	Y[mm]	Z [mm]	σ_{xx} [kPa]	σ_{yy} [kPa]	σ_{zz} [kPa]	σ_{yz} [kPa]	σ_{xz} [kPa]	σ_{xy} [kPa]
G2 theory E = 400 MPa	1	0	0	38	376	376	820	0	0	0
	2	0	0	50	313	313	807	0	0	0
	3	0	0	75	227	227	758	0	0	0
G2 after DMI E = 165 MPa	1	0	0	38	332	332	826	0	0	0
	2	0	0	50	277	277	816	0	0	0
	3	0	0	75	205	205	775	0	0	0
RCA (before and after DMI) E = 230 MPa	1	0	0	38	346	346	824	0	0	0
	2	0	0	50	288	288	813	0	0	0
	3	0	0	75	212	212	770	0	0	0
MG65 before DMI E = 365 MPa	1	0	0	38	370	370	821	0	0	0
	2	0	0	50	309	309	808	0	0	0
	3	0	0	75	225	225	761	0	0	0
MG65 after DMI E = 280 MPa	1	0	0	38	355	355	823	0	0	0
	2	0	0	50	296	296	811	0	0	0
	3	0	0	75	217	217	766	0	0	0
MG30 before DMI E = 360 MPa	1	0	0	38	369	369	821	0	0	0
	2	0	0	50	308	308	808	0	0	0
	3	0	0	75	224	224	761	0	0	0
MG30 after DMI E = 320 MPa	1	0	0	38	363	363	822	0	0	0
	2	0	0	50	302	302	810	0	0	0
	3	0	0	75	221	221	764	0	0	0

Table I.8: Weslea calculations - Seal surface loaded with a super single tire (1 x 40 kN), 825 kPa, full layer bond

	Data point	Stiffness	Friction angle	Cohesion	σ_3	σ_1	$\sigma_{d,f}$	DSR
	[-]	[MPa]	[°]	[kPa]	[kPa]	[kPa]	[kPa]	[%]
G2 theory	1	400	52	55	376	820	3115	14.3
	2				313	807	2649	18.6
	3				227	758	2009	26.4
G2 after DMI	1	165	51.2	142	332	826	3153	15.6
	2				277	816	2763	19.5
	3				205	775	2255	25.3
RCA before DMI	1	230	55.1	233	346	824	4636	10.3
	2				288	813	4112	12.8
	3				212	770	3419	16.3
RCA after DMI	1	230	56.6	178	346	824	4682	10.2
	2				288	813	4102	12.8
	3				212	770	3333	16.7
MG65 before DMI	1	365	51.2	354	370	821	4626	9.7
	2				309	808	4191	11.9
	3				225	761	3597	14.9
MG65 after DMI	1	280	53.5	214	355	823	4210	11.1
	2				296	811	3727	13.8
	3				217	766	3079	17.8
MG30 before DMI	1	360	53.9	328	369	821	5123	8.8
	2				308	808	4605	10.9
	3				224	761	3900	13.8
MG30 after DMI	1	320	54.1	285	363	822	4852	9.5
	2				302	810	4338	11.7
	3				221	764	3643	14.9